

Nanomaterials modified conducting paper sensors for biomedical applications

THESIS

Submitted to the Delhi Technological University for the award of the degree of

DOCTOR OF PHILOSOPHY

by

Niharika Gupta

(2K17/PHD/BT/02)

under the supervision of

Prof. D. Kumar
Professor,
Department of Applied Chemistry

Dr. Bansi D. Malhotra
Professor (Formerly),
Department of Biotechnology

Dr. Asmita Das
Assistant Professor
Department of Biotechnology



Department of Biotechnology
Delhi Technological University
(Formerly Delhi College of Engineering)
Shahbad Daulatpur, Main Bawana Road, Delhi-110042, INDIA

January 2024

Copyright ©Delhi Technological University-2024
All rights reserved.

To
My mother, Rajni
&
My mentor and friend, Shine

DECLARATION

I hereby declare that the thesis entitled “**Nanomaterials modified conducting paper sensors for biomedical applications**” submitted by me, for the award of the degree of *Doctor of Philosophy* to **Delhi Technological University (formerly DCE)** is a record of bona fide work carried out by me under the guidance of Prof. D. Kumar, Prof. (Retd.) Bansi D. Malhotra, and Dr. Asmita Das.

I further declare that the work reported in this thesis has not been submitted and will not be submitted, either in part or in full, for the award of any other degree or diploma in this Institute or any other Institute or University.

Name: Niharika Gupta
Reg No: 2K17/PHD/BT/02
Department of Biotechnology
Delhi Technological University (DTU)
Shahbad Daultapur, Bawana Road, Delhi-110042

Place: Delhi

Date:

CERTIFICATE

This is to certify that the thesis entitled “**Nanomaterials modified conducting paper sensors for biomedical applications**” submitted by **Ms. Niharika Gupta** to **Delhi Technological University (formerly DCE)**, for the award of the degree of “Doctor of Philosophy” in Biotechnology is a record of *bona fide* work carried out by her. Ms. Niharika Gupta has worked under our guidance and supervision and has fulfilled the requirements for the submission of this thesis, which to our knowledge has reached requisite standards.

The results contained in this thesis are original and have not been submitted to any other university or institute for the award of any degree or diploma.

Prof. D. Kumar Supervisor Department of Applied Chemistry	Prof. (formerly) Bansi D. Malhotra Joint Supervisor Department of Biotechnology	Dr. Asmita Das Joint Supervisor Department of Biotechnology
--	--	--

Place: Delhi

Date:

Prof. Yasha Hasija
Head & DRC Chairman,
Department of Biotechnology
Delhi Technological University

Place: Delhi

Date:

ACKNOWLEDGEMENTS

“Our greatest weakness lies in giving up. The most certain way to succeed is always to try just one more time.”

- Thomas A. Edison

This thesis is the culmination of 6 years of hard work and perseverance (2017-2023) at the Department of Biotechnology, Delhi Technological University, Delhi, India. I take this opportunity to acknowledge and express my gratitude towards the numerous people who contributed to my successful journey towards this PhD thesis.

I would like to acknowledge Prof. Prateek Sharma, Hon'ble Vice Chancellor, DTU for providing necessary facilities and infrastructure. I thank Prof. Yasha Hasija, Head and DRC Chairman, Department of Biotechnology, DTU, for her support and kindness throughout my journey as a PhD scholar.

I will never have enough words to acknowledge my three supervisors: Prof. D. Kumar (Applied Chemistry, DTU), Prof. Bansi D. Malhotra (formerly Professor, Department of Biotechnology, DTU), and Dr. Asmita Das (Assistant Professor, Department of Biotechnology, DTU). I express my profound sense of gratitude towards Prof. B. D. Malhotra for his support, guidance, and wise words throughout the course of my PhD. He encouraged me to pursue research and bestowed unconditional faith in me towards the end of this work. His presence in my life as a supervisor has helped shape the course of my life, academic or otherwise. He taught me to think big, to think out of the box, and to be a fearless visionary. The calm words of Prof. D. Kumar and his quiet sense of confidence in me always lifted my spirits in times of need, boosted my self-confidence, and helped me finish my PhD work on time. I shall strive to possess the same calm demeanor and positive attitude in all my future endeavors. I acknowledge Dr. Asmita Das for showing faith in me and supporting me when all else was failing in my academic life. I greatly acknowledge her support, administrative or otherwise, towards the completion of this thesis.

I also acknowledge Prof. Pravir Kumar, Professor and former Head, Department of Biotechnology, DTU for his support towards my work during his tenure as the Head (Biotechnology) (2020-23), and teaching me the values of kindness, humility, and quiet strength. I acknowledge the DRC and faculty members of the Department of Biotechnology: Prof. Jai Gopal Sharma (Professor and former Head), Dr. Navneeta Bharadwaja (Assistant Professor), Dr. Smita Rastogi, Dr. Kriti Bhandari, and Dr. Prakash Chandra (Assistant Professors) for bestowing their help, support, and appreciation towards my PhD work. I also thank all other DRC/SRC members: Prof. Sonika Bhatnagar (Head, Department of Biological Sciences and Engineering, NSUT, Delhi), Prof. A. K. Dubey (Department of Biological Sciences and Engineering, NSUT, Delhi), Prof. Prashant Mishra (Department of Biochemical Engineering and Biotechnology, IIT Delhi), and Prof. Seema Sood (Department of Microbiology, All India Institute of Medical Sciences (AIIMS), New Delhi) for their critical analysis and appreciation of my work. I thank Prof. Seema Sood especially for believing in my work, allowing me access to her laboratory resources (STD lab, Department of Microbiology, AIIMS, New Delhi), and lending bacterial DNA samples for analysis, which was crucial towards the fruition of my PhD work. I also acknowledge the staff of the Department of Biotechnology, DTU: Mr. Chhail Bihari Singh, Mr. Jitendra Singh, Mr. Lalit Kumar, and Mrs. Saumya Maurice for all the administrative help during the past 6 years.

There have been many people in my life, without whose help this thesis would not have been possible. First and foremost, I acknowledge Dr. Shine Augustine (Postdoctoral Fellow, SKKU University, Suwon, South Korea) who has always stood by me unconditionally in times of need. She inspired me to not quit and stand tall in the face of adversity. I shall always be grateful to her for all her help. I further acknowledge her for help in XPS analyses. I thank Dr. Suveen Kumar (Assistant Professor (Medical Devices), NIPER Ahmedabad, Gujarat) for helping me with many characterization studies mentioned in this thesis. I also thank him for his unclaimed mentorship to me throughout my PhD; his critique and timely suggestions for my work have greatly helped in improving the quality of this research work. I greatly acknowledge the help, suggestions, and

critique of Dr. Saurabh Kumar (Assistant Professor (Medical Devices), NIPER Guwahati, Assam). I strived to build upon his work on conducting paper and his suggestions have been invaluable towards both the quality of this work and my acumen as a researcher.

I acknowledge Mr. Tarun Narayan (PhD scholar and Research Assistant, Department of Nanotechnology, Tyndall National University, Cork, Ireland) for always providing honest opinions on my work and his expert help with AFM analysis. His confidence in my skills has always encouraged me to perform better every day. I also thank Dr. Shipra Solanki and Dr. Sharda Nara (formerly Postdoctoral Fellows, Department of Biotechnology, DTU) for their scientific suggestions towards my work, moral support, and friendship. The positive attitude of Dr. Solanki helped me overcome some of the most difficult times faced during the course of this work.

I acknowledge the different instrumentation centers I visited for various characterization studies discussed in this work: the Central Research Facility (CRF, IIT Delhi, New Delhi) for SEM, FESEM, AFM, and XPS analyses, the Central Instrumentation Facility (CIF, Department of Applied Chemistry, DTU) for rheological examinations, and the University Science Instrumentation Centre (USIC, Faculty of Science, Delhi University, New Delhi) for Raman spectroscopic studies. I would especially like to thank my dear friend Dr. Ashish Kalkal (Postdoctoral Fellow, University College London, UK) for his help with TEM studies at IIT Roorkee, Uttarakhand. I acknowledge Dr. Lakhan Kumar who endured the stress of PhD with me all these years and helped me with ultrasonication studies. I also thank Mr. Jawed Alam (Junior Mechanic, CIF, Department of Applied Chemistry, DTU) for his timely help with the rheological examinations. I thank all the staff of the STD lab (Department of Microbiology, AIIMS, New Delhi), especially Dr. Shilpi Malhotra, Mr. Rajendra Singh, and Dr. Rajni Mala for their help in sample acquisition and gel electrophoresis studies. Ms. Sammriddhi (PhD scholar, CSIR-National Physical Laboratory, CSIR-NPL, New Delhi) is acknowledged for access to contact angle goniometer. I also acknowledge Dr. Dipti Chauhan, Mr. Yogesh Gagneja, and Mr. Saurav Shankar

(PhD scholars, Department of Chemistry, Delhi University, New Delhi) for their help with various studies and moral support.

No journey has been completed without support from friends and family. I thank my fellow PhD scholar and roommate Ms. Neha Kumari (Department of Biotechnology, DTU) for being with me throughout the last two years of our companionship and bearing my rants over my work. I also acknowledge my PhD colleagues, Dr. Rajkumar Chakraborty (Junior Scientist-2, Aganitha, Hyderabad), Ms. Kanika Sharma and Mr. Yash Pathak (Department of Applied Physics, DTU), and Mrs. Sakshi Verma and Mr. Namit Dey (Department of Applied Chemistry, DTU) for helping me as a friend during my PhD. I thank my friends Pooja, Ashwini, and Rahul for keeping me away from spiraling into a negative mental space and helping me financially in the past two years. Most importantly, I acknowledge my parents, Mr. Brijesh Kishore Gupta and Mrs. Rajni Gupta, not only for their unconditional support and patience but also for financially supporting me during the last two years of my PhD. I express many thanks to my brothers, Shivam and Shubam, and my sister-in-law Tanya for their support, love, and encouragement throughout the duration of this work. I would especially mention Shivam for effortlessly navigating through our personal, familial problems on his own and not letting them affect me or my work during the last 6 years. The journey has been long and tiring, and I take this opportunity to thank any and every person, whose names I may have unintentionally forgotten to mention, and who helped or supported me in any way towards reaching my goal of this PhD thesis.

(Niharika Gupta)

ABSTRACT

Paper is a sustainable, flexible, affordable, and easy to use substrate for electrochemical biosensors. Recent advances in materials sciences have allowed researchers to incorporate nanomaterials into and modulate the porosity and surface roughness of paper to develop highly efficient paper-based biosensing devices. Such modified paper is referred to as conductive paper, owing to the conductivity imparted to it by nanomaterials. There are several ways of incorporating nanomaterials into paper and modulating its properties. One such method is the coating of paper by conductive inks. These specialized inks comprise conductive nanomaterials and binders, which can render the paper substrate conductive and ensure adherence of nanomaterials to it. These inks can be coated onto the paper either manually or using various printing techniques such as screen printing, which offer batch reproducibility and scalability to the fabrication process.

Different kinds of nanomaterials have been utilized for the development of conductive inks, such as silver nanoparticles, carbon nanomaterials (graphene, carbon nanotubes), PEDOT:PSS, etc. Multiwalled carbon nanotubes (MWCNTs) have good conductivity and dispersibility in solvents, intrinsic adherence to plastic and paper, and mechanical strength. These can be for development of conductive ink towards the applications of printed and flexible electronics.

Biosensors have sparked a renewed interest in the post-pandemic era. These fast, specific, sensitive, and reliable counterparts of the more traditional molecular assays can prove instrumental towards better access to health care and mass screening for several diseases. Electrochemical biosensors (that convert a biological signal into a current/resistance/voltage change) have proven more successful in terms of their quantitative nature, low power requirements, ease of use, and ability to be miniaturized. With an increasing focus on accessible health care and the rise of telemedicine, biosensing devices are being developed to be more

flexible, wearable, and even skin-conformal. Thus, there has been a shift from the conventional metallic/semiconductor biosensing substrates to more sustainable, flexible, and ‘wearable’ options such as paper. The emergence of printable conductive inks has especially brought more attention to paper-based electrochemical devices. Several different types of paper-based electrochemical biosensors have been demonstrated recently for the detection of different disease biomarkers and pathogens. Evidently, there is an increased attention on the development of paper-based electrochemical devices for the screening and detection of infectious diseases including sexually transmitted infections (STIs).

Neisseria gonorrhoeae is a bacterial pathogen in humans whose infection causes the STI, gonorrhea. It is a curable infection, however lack of awareness, absence of symptoms in most cases, and stigma associated with STIs have made it difficult to diagnose and treat this infection timely. There is urgent need to develop efficient point-of-care devices that are sensitive, easy to use, specific, and yield faster results as compared to the conventional techniques being utilized for *N. gonorrhoeae* detection.

This thesis on “Nanomaterials modified conducting paper sensors for biomedical applications” deals with the fabrication and characterization of MWCNT-modified conducting paper and its application towards the development of electrochemical DNA biosensors for *N. gonorrhoeae* detection. Conductive ink formulations were prepared by dispersing carboxylated MWCNTs in solvent bases. The conductive inks were optimized for conductivity, rheology, and adherence to the paper substrates. The solvent base(s) comprised terpineol (Tp) and deionized water as solvents, carboxymethylcellulose (CMC) as binder and rheology modifier, and polysorbate 80 (PS80) as a stabilizer/emulsifier. The advantage of using inks over other methods such as dip coating and *in situ* nanomaterial synthesis is that it can prevent nanomaterial leaching, allow change in the hydrophilicity of the paper substrate, and enable batch reproduction and scalability. The number of coats required for desirable conductivity

(without leaching) was optimized along with the annealing temperature and time. Magnetic bead-assisted DNA assays were designed for specific capture of the target DNA (*porA* pseudogene sequence of *N. gonorrhoeae*), and integrated to the cMWCNT@paper electrodes for electrochemical detection via CV and EIS. Screen printed electrodes (SPEs) were fabricated on paper using the conductive ink, which were further utilized for detection of gonorrheal target sequence as proof of concept.

This work demonstrated the development of paper-based biosensing assays with potential of point-of-care (PoC) application. It has attempted to bring STI diagnostics to the forefront and promote the development of sensitive and reliable PoC devices for STIs including gonorrhea.

CONTENTS

Title	Page No.
Acknowledgements	i
Abstract	v
Abbreviations and Symbols	xi
List of Figures	xiv
List of Schemes	xviii
List of Tables	xix
Chapter 1: Introduction and Literature Review	1-40
1.1 Paper: An overview	2
1.1.1 Structure and characteristic of paper	2
1.2 Conducting paper	6
1.2.1 Nanomaterials-modified conducting paper	6
a) Multi-walled carbon nanotubes	8
1.2.2 Methods of fabrication of conducting paper	10
1.3 Conductive inks	11
1.3.1 Components of conductive inks	12
1.3.2 Methods of coating of conductive inks	15
a) Screen printing	15
1.4 Biosensors	17
1.4.1 Bioreceptors	19
a) Sandwich hybridization-based DNA biosensors	21
b) Supersandwich hybridization-based DNA biosensors	22
1.4.2 Transducers	24
a) Electrochemical transducers	24
1.4.3 Immobilization matrix	26
1.5 <i>Neisseria gonorrhoeae</i>	30
1.5.1 Gonorrhea: Causes and symptoms	30
1.5.2 Conventional methods of NG detection	32
1.5.3 Recent advances in NG detection	33
1.6 Objectives of the study	36
Chapter 2: Materials and Experimental Techniques	41-81
2.1 Introduction	42
2.2 Chemicals, reagents, and buffers	42
2.3 Design of oligonucleotide probes	43
2.4 Formulation of conductive inks	44
2.5 Screen printing of conductive inks	45
2.6 Characterization Techniques	47
2.6.1 X-Ray diffraction	47
2.6.2 Transmission electron microscopy	50
2.6.3 Scanning electron microscopy	51
2.6.4 Field emission scanning electron microscopy	53
2.6.5 Atomic force microscopy	54
2.6.6 Raman spectroscopy	56
2.6.7 Contact angle studies	58

2.6.8 X-Ray photoelectron spectroscopy	59
2.6.9 Rheometry	61
2.6.10 Conductivity measurement studies	63
2.6.11 Agarose gel electrophoresis	65
2.6.12 Electrochemical techniques	68
(a) Cyclic voltammetry (CV)	69
(b) Electrochemical impedance spectroscopy (EIS)	71
2.7 Magnetic-bead assisted DNA hybridization assays	75
2.7.1 Significance of magnetic beads in assays	75
2.7.2 Immobilization of capture probes onto MBs	76
(a) Avidin-biotin affinity-based immobilization	76
(b) EDC-NHS chemistry-based immobilization	77
2.7.3 Electrochemical MB-assisted hybridization assay	78
2.8 Real sample analysis and specificity studies	79
Chapter 3: Carbon Nanomaterial-Modified Conductive Ink for Paper-Based Electrochemical Detection of <i>Neisseria gonorrhoeae</i>	81-101
3.1 Introduction	82
3.2 Experimental details	83
3.2.1 Conductive ink formulation	83
3.2.2 Fabrication of ink-coated paper electrodes	84
3.2.3 Electrochemical magnetic DNA hybridization assay	84
3.3 Results and discussion	87
3.3.1 XRD and TEM analysis	87
3.3.2 SEM and contact angle studies	87
3.3.3 Conductivity studies	89
3.3.4 Raman and XPS analysis	92
3.3.5 Electrochemical characterization studies	94
3.3.7 Electrochemical response studies	96
3.3.8 Real sample analysis and specificity studies	98
3.4 Conclusion	100
Chapter 4: Supersandwich DNA Assay-Integrated Paper Biosensor for Electrochemical Detection of <i>Neisseria gonorrhoeae</i>	102-123
4.1 Introduction	103
4.2 Experimental details	104
4.2.1 Design of oligonucleotide probes	104
4.2.2 Formulation of conductive ink	105
4.2.3 Rheological studies	105
4.2.4 Fabrication of C5@paper electrodes	106
4.2.5 Electrochemical magnetic bead-assisted DNA supersandwich assay	106
4.3 Results and discussion	108
4.3.1 Rheological optimization of the conductive ink	108
4.3.2 Morphological analysis of the C5@paper electrodes	111
a) SEM/FESEM analysis	111
b) AFM analysis	112
4.3.3 Conductivity studies	113
4.3.4 Electrochemical stability and reproducibility studies	115
4.3.5 Electrochemical response studies	117
4.3.6 Real sample analysis and specificity studies	121

4.4 Conclusion	122
Chapter 5: Screen Printing Of MWCNT-Modified Conductive Ink Towards Paper-Based Biosensor for <i>Neisseria gonorrhoeae</i> Detection	124-135
5.1 Introduction	125
5.2 Experimental details	127
5.2.1 Conductive ink formulation	127
5.2.2 Screen printing of the C5 conductive ink onto paper	127
5.2.3 Conductivity studies	127
5.2.4 Electrochemical studies	127
5.3 Results and discussion	128
5.3.1 Screen printing studies	128
5.3.2 SEM studies	129
5.3.3 Conductivity studies	130
5.3.4 Electrochemical characterization	131
5.3.5 Electrochemical response studies	132
5.4 Conclusion	134
Chapter 6: Summary and Future Prospects	136-143
6.1 Summary	137
6.2 Future prospects	141
References	144-160
Thesis Publications	161
Biodata	
Appendix: CD	

Abbreviations and Symbols

3iTt	3-interval thixotropy test
μA	Micro-ampere
μL	Microliter
μm	Micrometer
μPAD	Micro-paper analytical device
$\Omega.\text{cm}$	Ohm centimeter
ρ_0	Initial resistivity
ρ	Resistivity after correction
AFM	Atomic force microscopy
Ag/AgCl	Silver/Silver chloride
Ag NPs	Silver nanoparticles
aM	Attomolar
AMR	Antimicrobial resistance
Au	Gold
Av	Avidin
bp	Base pairs
BSA	Bovine serum albumin
C5	MWCNT-based conductive ink (5 % w/v)
CB	Carbon black
C_{dl}	Double layer capacitance
CE	Counter electrode
Ch	<i>Chlamydia trachomatis</i>
cMWCNT	Carboxylated multi-walled carbon nanotubes
CMC	Carboxymethyl cellulose
CNT	Carbon nanotubes
CNM	Carbon nanomaterials
CP	Capture probe
CPE	Constant phase element
CV	Cyclic voltammetry
DNA	Deoxyribonucleic acid
DP	Detector probe
EC	<i>Escherichia coli</i>
EDC	1-ethyl-3-(3-dimethyl aminopropyl) carbodiimide
EDTA	Ethylene diamine tetraacetic acid
EF	<i>Enterococcus faecalis</i>
EIS	Electrochemical impedance spectroscopy
EtBr	Ethidium bromide
FESEM	Field emission scanning electron microscopy
fM	Femtomolar
gsm	Grams per square meter
IoT	Internet of things
I_p	Peak current
J	Current density
k Ω	Kilo-ohms
KP	<i>Klebsiella pneumoniae</i>
LAMP	Loop-mediated isothermal amplification

LFA	Lateral flow assay
LFB	Lateral flow biosensor
LOD	Limit of detection
mM	Millimolar
MB	Magnetic beads
MCDA	Multiple cross displacement amplification
MetB	Methylene blue
miRNA	Micro-ribonucleic acid
MWCNT	Multi-walled carbon nanotubes
NA	Nucleic acid
NAAT	Nucleic acid amplification test
NC	Non complementary
NG	<i>Neisseria gonorrhoeae</i>
NHS	N-hydroxy succinimide
NM	<i>Neisseria meningitidis</i>
nM	Nanomolar
NMu	<i>Neisseria mucosa</i>
NP	Nanoparticles
NS	<i>Neisseria sicca</i>
PANI	Polyaniline
Pa.s	Pascal seconds
PBS	Phosphate buffered saline
PCR	Polymerase chain reaction
PEDOT:PSS	Poly(3,4-ethylenedioxythiophene)-poly(styrenesulfonate)
pM	Picomolar
PMNC	Polymorphonuclear cells
PNA	Peptide nucleic acid
PoC	Point-of-care
PS80	Polysorbate 80
PSA	Prostate specific antigen
Pt	Platinum
Q	Constant phase element
R _{ct}	Charge transfer resistance
RCA	Rolling circle amplification
RE	Reference electrode
rGO	Reduced graphene oxide
RNA	Ribonucleic acid
RPA	Recombinase polymerase amplification
R _s	Solution resistance
S cm ⁻¹	Siemens per centimeter
SA	<i>Staphylococcus aureus</i>
SCP	Supersandwich capture probe
SD	Standard deviation
SDP	Supersandwich detector probe
SELEX	Systematic evolution of ligands by exponential enrichment
SEM	Scanning electron microscopy
SERS	Surface enhanced Raman scattering
SHERLOCK	Specific high-sensitivity enzymatic reporter unlocking

SPE	Screen-printed electrode
ssDNA	Single stranded DNA
STI	Sexually transmitted infection
SWCNT	Single-walled carbon nanotubes
TBE	Tris borate EDTA
TE	Tris EDTA
TEM	Transmission electron microscopy
TMB	3,3',5,5'-Tetramethylbenzidine
TP	Target probe
Tp	Terpineol
UU	<i>Ureaplasma urealyticum</i>
w/v	Weight by volume
W	Warburg's impedance
WE	Working electrode
WHO	World Health Organization
XPS	X-ray photon spectroscopy
XRD	X-ray diffraction

List of Figures

S. No.	Figure Captions	Page No.
Figure 1.1	(A) Diagrammatic representation showing the structure of a plant cell wall, from where the cellulose fibers are separated and treated chemically to make paper sheets, and (B) Chemical structure of cellulose, showing the 1,4 β -linkages and hydrogen bonds (both intra- and intermolecular).	3
Figure 1.2	Pictorial representation of different characteristic features of paper that make it suitable for wide applications.	5
Figure 1.3	Different carbon nanomaterials and their morphologies.	7
Figure 1.4	Pictorial representation of different properties of MWCNTs.	9
Figure 1.5	Pictorial representation of constituents for the formulation of a conductive ink.	13
Figure 1.6	Principle and working mechanism of screen-printing method. (A) Diagrammatic representation of screen-printing process, (B) the mechanism of screen printing, wherein (a) fluid on the mesh, (b) force applied by squeegee leading to contact between screen and substrate and filling of cavities (patterns) in the screen by mesh, and (c) separation of the screen from the substrate and removal of ink, and (C) High speed image of the ink transfer by screen printing method and its illustration.	16
Figure 1.7	Flow chart depicting the various applications of biosensors.	18
Figure 1.8	Basic components of a biosensor.	19
Figure 1.9	Schematic representation of a sandwich DNA hybridization-based biosensor.	22
Figure 1.10	Schematic representation of a supersandwich DNA assay as compared to traditional hybridization method.	23
Figure 1.11	(A) Schematic of the 3-electrode assembly showing the WE, RE, and CE connected to a potentiostat, (B) the corresponding circuit diagram, (C) redox reaction at WE surface, and (D) image of a commercial screen-printed electrode (SPE).	25
Figure 1.12	Comparison of different types of immobilization techniques.	27
Figure 1.13	Schematic showing the reaction intermediates and final product formed by the EDC-NHS mediated formation of amide bond.	28
Figure 1.14	Avidin-biotin affinity interactions. Every avidin/streptavidin molecule can bind to four biotin molecules, leading to their role as signal amplification agents in molecular assays.	29
Figure 1.15	<i>Neisseria gonorrhoeae</i> (NG) is a Gram negative, diplococcus bacteria that causes gonorrhoea. It resides intracellularly in specialized white blood cells, known as polymorphonuclear cells (PMNC).	30
Figure 1.16	Pictorial representation of the different host adaptations of NG and its pathogenesis.	31
Figure 2.1	(A) Photograph of the Corel Draw sheet showing the patterns of the SPE designed for screen printing, and (B) A magnified view of the SPE showing the dimensions and length of the working electrode.	46
Figure 2.2	Diagram explaining Bragg's diffraction (principle of XRD).	48
Figure 2.3	(A) X-ray diffractometer (Bruker D-8 Advance model), and (B) XRD spectrum of nYZR with peaks corresponding to the lattice planes of tetragonal yttria-doped zirconia (JCPDS 48-0224).	49
Figure 2.4	(A) A simplified schematic displaying the various components of a TEM instrument, and (B) A photograph of the JEOL JEM 3200 FS model electron microscope.	51
Figure 2.5	(A) Simplified schematic of a SEM instrument, (B) A photograph of the	53

	Zeiss EVO 18 model SEM instrument, and (C) SEM image of CuO nanoparticles grown onto paper.	
Figure 2.6	(A) Photograph of the JEOL JSM-7800F Prime model electron microscope, and (B) FESEM image of a diagonal edge of the conductive ink-coated paper showing the different layers of ink coated sequentially onto the paper substrate.	54
Figure 2.7	(A) Schematic representing the basic AFM instrumentation and working principle, and (B) A photograph of the Asylum Research MFP3D-BIO-AFM instrument used in this study.	56
Figure 2.8	(A) Stokes and anti-Stokes Raman scattering as shown in an energy level diagram, and (B) A photograph of the Renishaw Invia II Raman spectrometer.	57
Figure 2.9	(A) Diagram illustrating the Young's equation and calculation of contact angle, (B) Image of a water droplet on an ITO electrode as taken by a contact angle goniometer. The shape of the droplet indicates that the electrode is hydrophilic in nature, and (C) Photograph of the Data Physics OCA15EC model contact angle measurement system.	59
Figure 2.10	Photograph of the AXIS Supra model XPS instrument.	60
Figure 2.11	Photograph of the Anton Paar MCR 302 rheometer used in the study.	62
Figure 2.12	(A) (i) Schematic diagram of the 4-probe (4P) conductivity meter, and (ii) the magnified view of the four probes showing the interprobe distance, S, (B) A V vs. I curve of the cMWCNT@paper electrode used for calculating resistance, R, of the electrode, and (C) A photograph of the conductivity meter (SES Instruments Pvt. Ltd.) used in the study.	65
Figure 2.13	Schematic diagram depicting (A) a typical gel electrophoresis unit, and (B) direction of movement of DNA molecules in the gel and their separation based on molecular size.	67
Figure 2.14	Photograph of a PGSTAT 302N Autolab (Metrohm, Netherlands) potentiostat/galvanostat.	69
Figure 2.15	Diagram depicting an electric double layer formed at the working electrode in an electrochemical system.	72
Figure 2.16	(A) (i) Representation of a Nyquist plot between $-Z_{imag}$ (capacitive Z) and Z_{real} (resistive Z) showing values of different parameters, including Z, R_s , R_{ct} , etc., and (ii) The corresponding electrical circuit explaining the different elements that contributed to the plot. (B) A Nyquist plot depicting the influence of Warburg impedance, W, and the corresponding equivalent circuit (known as the Randles' circuit).	73
Figure 3.1	(A) XRD spectrum, and (B, C) TEM images of the cMWCNTs used in the formulation of conductive ink.	87
Figure 3.2	SEM images of (A, B) bare paper, (C, D) cMWCNT ink-coated paper (cMWCNT@paper) (inset of (C) shows the photograph of the cMWCNT@paper electrode ($2 \times 2 \text{ cm}^2$)), and (E, F) Av/MB/cMWCNT@paper electrode. Contact angle measurements for (G) bare paper, and (H) cMWCNT@paper electrode.	88
Figure 3.3	(A) Resistivity of the cMWCNT@paper electrodes vs. annealing time at different annealing temperatures, (B) Change in resistivity of the cMWCNT@paper electrodes with temperature after annealing for 10 min., (C) Resistivity of the cMWCNT@paper electrodes vs. number of coats of the conductive ink, and (D) Viscosity of the cMWCNT ink vs. shear rate displaying thixotropic behavior.	90
Figure 3.4	(A) Raman spectrum, (B) XPS survey scan, (C) deconvoluted peaks of C1s, and (D) deconvoluted peaks of O1s.	93
Figure 3.5	(A) Continuous use stability as depicted by CV scans of change in current density with potential for the cMWCNT@paper electrodes, (B) storage	96

	stability as indicated by change in peak current density of the cMWCNT@paper electrodes over a period of 7-90 days, (C) Batch reproducibility as indicated by variability in the peak current density values of different cMWCNT@paper electrodes, and (D) CV scans showing the change in the current density of the cMWCNT@paper electrodes before and after deposition of MBs and other biomolecules.	
Figure 3.6	(A) Peak current density of the C-T-D/Av/MB/cMWCNT@paper electrodes (100 pM T concentration) with respect to different amounts of MB, (B) The peak current density of the C-T-D/Av/MB/cMWCNT@paper electrode for 1 pM target concentration (porA TP) with time, (C) Change in current density with increasing concentration of the C-T-D hybridization complex at the cMWCNT@paper electrode surface, and (D) the calibration graph showing net change in peak current density (ΔJ) vs. the log of TP concentration.	98
Figure 3.7	(A) Comparison of biosensing signal obtained for different of TP concentration with extracted gonococcal genomic DNA, and (B) the net current density change shown by the C5@paper electrodes when exposed to mixture of gonococcal DNA and non-gonococcal DNA.	99
Figure 4.1	(A) Viscometric analysis: change in viscosity of the CMC ₁ , CMC _{2.5} and CMC ₅ base emulsions with shear rate in the range 0.1-100 s ⁻¹ , (B) Results of the 3iTT for the CMC ₁ , CMC _{2.5} and CMC ₅ base emulsions (change in viscosity with abrupt change in the shear rate), (C) Change in viscosity of the CMC ₅ base emulsion and the C5 ink with shear rate (0.1-100 s ⁻¹), and (D) A comparison of the results of the 3iTT for CMC ₅ base emulsion and the C5 ink.	111
Figure 4.2	SEM images of (A, B) bare paper, and (C, D) C5@paper electrodes at different magnifications. (E) FESEM image of the C5@paper electrode, and (F) High magnification FESEM image showing cMWCNT in the ink matrix.	112
Figure 4.3	AFM images of the (A) bare paper, and (B) C5@paper electrode. The RMS roughness decreased upon ink coating from 168.2 nm for bare paper to 41.6 nm for C5@paper electrode.	113
Figure 4.4	Conductivity of the C5@paper electrode vs. (A) number of coats, and (B) bending angle.	115
Figure 4.5	(A) CV curves of the C5@paper electrode at 1 st , 25 th , and 50 th cycle displaying the continuous use stability. Inset shows a magnified view of the CV curves, (B) R _{ct} values of randomly selected C5@paper electrodes from different batches, (C) Equivalent circuit model fitted into the Nyquist plots, and (D) R _{ct} of the C5@paper electrodes measured at every 10 days of storage in dark, dry conditions at room temperature.	116
Figure 4.6	(A) Nyquist plots of the C5@paper, SCP/MB/C5@paper, and the BSA/SCP/MB/C5@paper electrodes. Inset shows the magnified view of the Nyquist plot of the C5@paper electrode, and (B) Gel electrophoresis results showing the formation of DNA supersandwich structures at different temperature and time. Lane 1, 14: DNA ladder (10-300 bp), Lanes 2-4: SCP and SDP without TP (negative control) incubated at 25 °C for 5, 10 and 15 min respectively, Lanes 5-7: Supersandwich structures formed by hybridization of SCP, TP and SDP at 25 °C for 5, 10 and 15 min, respectively, Lanes 8-10: SCP and SDP without TP incubated at 55 °C for 5, 10 and 15 min respectively, and Lanes 11-13: Supersandwich structures formed by hybridization of SCP, TP and SDP at 55 °C for 5, 10 and 15 min, respectively.	118
Figure 4.7	(A) Nyquist plots of the C5@paper electrodes for different concentrations	119

	of the TP, and (B) Corresponding calibration curve showing linear correlation between ΔR_{ct} and log of TP concentration.	
Figure 4.8	(A) Bar graph showing the ΔR_{ct} values of the C5@paper electrodes in response to synthetic TP and genomic DNA from NG (100 aM – 1 pM), and (B) the ΔR_{ct} values in response to NG DNA mixed with other bacterial DNA.	122
Figure 5.1	(A) Schematic showing the process of screen printing, and (B) A photograph of the screen-printing mask utilized in the study.	128
Figure 5.2	Photographic images of (A) rectangular pattern, and (B) SPE printed onto ivory paper by the C5 ink (without Ag/AgCl) (the images are not to scale).	129
Figure 5.3	SEM images of (A) the screen-printed paper showing the printed and nonprinted regions, and (B) the surface morphology of the printed patterns.	130
Figure 5.4	Change in the resistivity of the printed paper with number of coats.	131
Figure 5.5	(A) CV response of the SPEs at 1 st and 20 th CV cycle indicating the continuous use stability, and (B) Nyquist plot of the SPE with the equivalent model circuit in the inset.	132
Figure 5.6	(A) CV response of the SPE with change in concentration of CP-TP-DP complex in the range of 1 pM-10 nM, and (B) Magnified view of the CV curves obtained for 1 and 10 pM CP-TP-DP complexes.	133
Figure 5.7	Linear calibration curve between peak current obtained by the SPE biosensor and concentration of CP-TP-DP complex.	134

List of Schemes

S. No.	Title	Page No.
Scheme 3.1	Steps involved in the development of the conductive ink and the cMWCNT@paper electrodes.	84
Scheme 3.2	Schematic diagram depicting the various steps involved in the MB-assisted sandwich DNA hybridization assay.	86
Scheme 3.3	Schematic diagram depicting the integration of the MB-assisted DNA hybridization complex with the cMWCNT@paper electrodes for electrochemical analysis.	86
Scheme 4.1	Schematic diagram depicting (A) the steps in the formation of MB-assisted supersandwich hybridization assembly for N. gonorrhoeae detection, and (B) comparison between sandwich and supersandwich DNA hybridization.	107
Scheme 4.2	Integration of the MB-assisted DNA supersandwich assembly with the C5@paper electrodes for electrochemical detection of N. gonorrhoeae via EIS.	108

List of Tables

S. No.	Title	Page No.
Table 1.1	Comparison of some properties of different carbon nanomaterials.	8
Table 3.1	DNA sequences of the biosensor oligonucleotide probes.	85
Table 3.2	A comparative analysis of some recently reported MWCNT-based inks.	91
Table 3.3	Some recent studies on paper-based electrochemical biosensors for detection of pathogenic DNA.	100
Table 4.1	Details of DNA oligonucleotide probes used in this work.	105
Table 4.2	Apparent viscosities of the different emulsion bases at different shear rates as determined by 3iTT.	110
Table 4.3	Summary of recent reports on paper-based DNA biosensors for detection of pathogens.	120
Table 6.1.	Biosensing parameters of the cMWCNT@paper, C5@paper, and C5-based SPE biosensing platforms for detection of NG <i>porA</i> sequence.	140

Chapter 1

Introduction and Literature Review

1. Introduction

1.1 Paper: An overview

Paper is one of the most ubiquitous and successful man-made inventions. Invented roughly 2000 years ago, paper has been one of the greatest inventions by mankind [1]. It led to easier storage and transmission of information, which eventually paced up technological advances globally. It is still the most prominently used medium of storage and exchange of information worldwide. Historically used in the publishing industry, paper (and its derivatives thereof) has pervaded different strata of life, from monetary representation (currency notes, tickets, vouchers, etc.) and packaging material to more sophisticated scientific applications such as chromatography [2], pH indicator strips, lateral flow assays (LFAs) [3, 4], dipstick assays [5, 6], flexible electronics [1, 7-9], etc. These diverse applications of paper have been made possible due to its structure and distinctive properties, including flexibility, hydrophilicity, disposability, affordability, ease of availability, etc. This section details the structure of paper and its characteristic features that make it suitable for diverse scientific applications.

1.1.1 Structure and characteristics of paper

Structurally, paper consists of cellulose fibers, which are naturally present in a plant cell wall (**Figure 1.1(A)**). Cellulose is a biopolymer consisting of repeating units of β -linked D-glucose molecules in a linear fashion, and hence classified as a polysaccharide. Within a plant cell wall, microfibrils composed of crystalline cellulose chains are present, which are joined together with amorphous hemicellulose (a non-linear polysaccharide) and lignin. The cellulose chains within the microfibrils are held together by hydrogen bonds (**Figure 1.1(B)**). Paper is made by first separating the cellulose fibers from hemicellulose and lignin by chemical/mechanical treatment and diluting them with excess of water (known as ‘pulp’) [1]. The pulp is dewatered, pressed, and dried to form paper sheets consisting of long cellulose kept

together by mechanical force and hydrogen bonds.

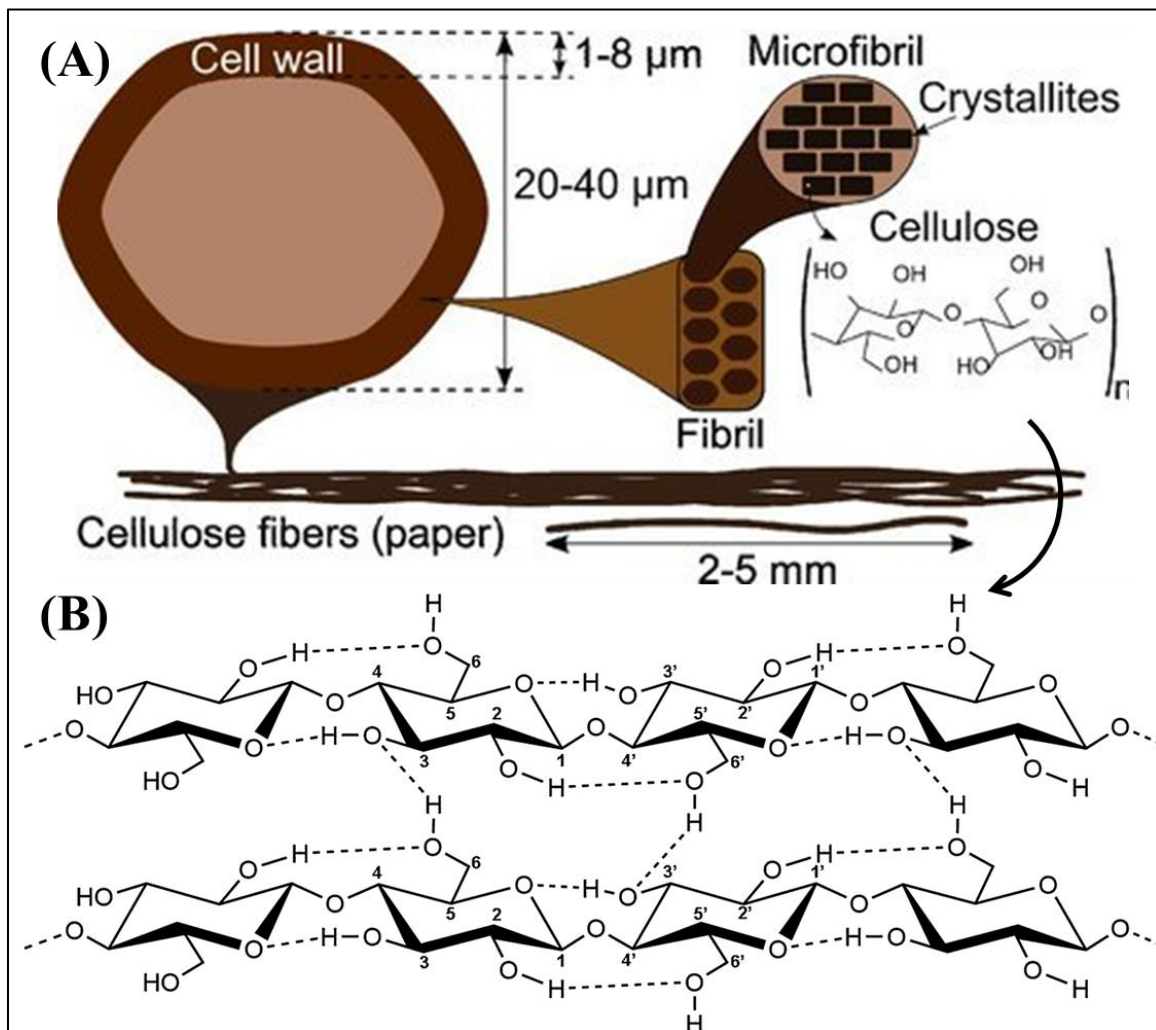


Figure 1.1. (A) Diagrammatic representation showing the structure of a plant cell wall, from where the cellulose fibers are separated and treated chemically to make paper sheets [1], and (B) Chemical structure of cellulose, showing the 1,4 β -linkages and hydrogen bonds (both intra- and intermolecular) [10].

The pore size of paper can be varied by reducing the length of cellulose fibers and by the addition of certain minerals such as clays, calcium carbonate, etc. These mineral fillers also enhance the smoothness and other properties of paper [1]. The thickness of a typical office paper is $\sim 100 \mu\text{m}$ with a grammage (mass per unit area) of $\sim 80 \text{ g m}^{-2}$ (or, gsm), while drawing paper specifically designed for applications such as painting, etc. have a thickness of 100-250 μm with grammage ranging from 200-300 gsm [1]. The choice of the type of paper substrates

depends upon the type of applications, e. g., LFAs require high adsorbent paper to load a high number of biomolecules for assessment [3]. The properties of paper that have made it suitable for different applications (**Figure 1.2**), include:

- (i) **Hydrophilicity and high adsorption:** Paper substrates are highly hydrophilic in nature. This allows them to retain high amounts of water and any constituents thereof within its matrix for long durations. Thus, in absence of aqueous environment, paper may provide a water-like environment for preservation of some biomolecules. These properties are often found suitable for applications such as pH strips, dipstick assays, and LFAs, as they rely on the immobilization of dyes/reagents (pH strips) and biomolecules (antibodies, enzymes, etc.) for proper results.
- (ii) **Porosity:** The microfibrillar structure of paper allows it to have a porous structure. The porosity of paper is inversely proportional to its grammage, i.e., the number of pores/pore size decrease upon increase in grammage. Porosity along with the hydrophilicity of paper allows wicking of liquids within its matrix without any external stimulus (capillary flow). Hence it is a desirable trait in applications where movement of buffers and liquids is required such as LFAs, dipstick assays, chromatography, etc. It is also a desirable trait for energy storage applications [11]. However, the porosity of paper is a hindrance in applications such as modifications of paper for high conductivity [12].
- (iii) **Environmental sustainability:** The rise in global pollution and climate change has led to an increased focus on environmentally sustainable substrates for devices. Since paper is composed of a naturally occurring biopolymer, cellulose, it is completely biodegradable and non-toxic. It does not leave any toxic residue after decomposition. Hence, it is being touted as a potential ‘green’ replacement of metallic/semiconducting substrates utilized in electronic/electrical industry [13]. It should be noted, however, that

the additives that make paper suitable for applications such as electrochemical biosensing may leave toxic residues after decomposition. However, more studies are now focusing on the use of sustainable reagents and processes with minimal carbon footprint.

(iv) **Flexibility:** The organic, fibrillar structure of paper allows it to bend at different angles without losing its integrity. This feature is being exploited towards developing flexible and wearable electronic devices and sensors [8, 14].

(v) **Ease of availability and affordability:** Due to its applications in storage and transfer of information, paper is a ubiquitous material. It is also inexpensive in terms of cost. These features make paper an attractive option for diverse applications as mentioned previously.

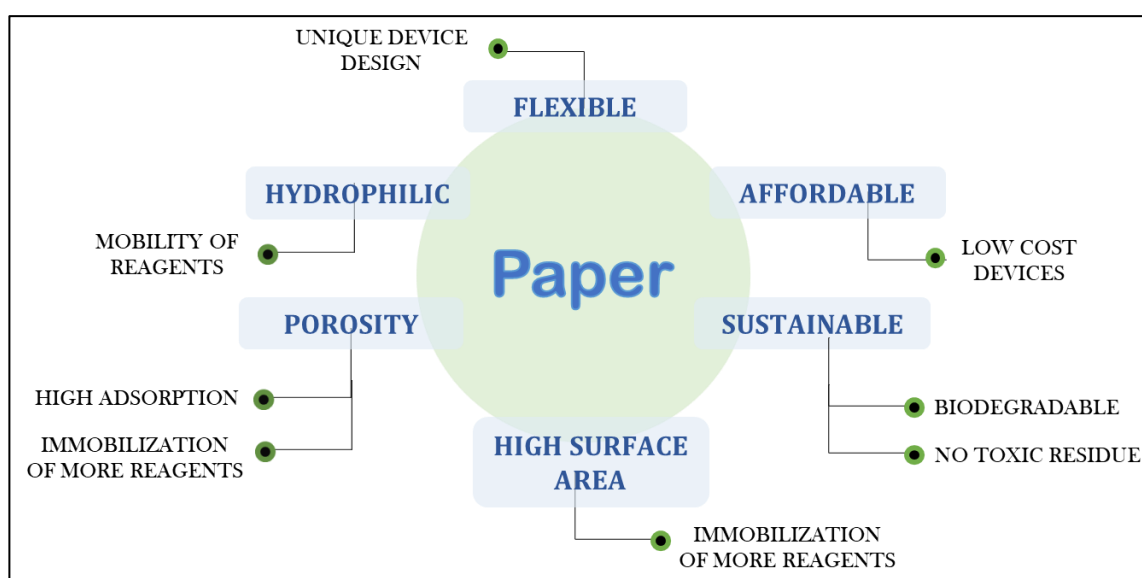


Figure 1.2. Pictorial representation of different characteristic features of paper that make it suitable for wide applications.

These distinctive properties of paper have allowed its utilization towards the development of analytical devices. Owing to advances in materials science and nanotechnology, paper substrates are being used to develop highly sophisticated analytical devices, such as supercapacitors [11], micro-paper analytical devices (μ PADs) [15-17],

biobatteries [18, 19], fully printed electric circuits [20], etc. Paper substrates have evolved from the simpler and conventional colorimetric LFA and dipstick assays to sophisticated and quantitative ‘papertronic’ devices. In place of the conventional colorimetric response, some of these newer devices, particularly papertronics devices, can yield highly specific and quantitative results in a rapid manner. These novel and advanced paper-based devices have been realized by tuning the roughness, porosity, and electrical conductivity of the paper substrates [1, 11, 14, 19]. One of the most prominent paper modifications is imparting conductivity by the deposition of different kinds of nanomaterials in its matrix. Such ‘conducting paper’ have found wide applications in many fields.

1.2 Conducting paper

Conducting (or conductive) paper refers to a type of paper that has been modified by conductive materials (metallic nanoparticles, conducting polymers, carbon nanomaterials, etc.) to exhibit conductivity. Due to the sustainability, low cost, and flexibility of the paper substrate, conducting paper is being explored for a myriad of electronic and electrochemical applications. An entirely new field of ‘papertronics’ has emerged that focuses on the utilization of paper as substrates for flexible electronic devices, such as batteries, capacitors, fuel cells, etc. [19, 21]. In addition, conducting paper has also found wide applications in wearable sensors and other sensing devices in health care monitoring [8, 22].

1.2.1 Nanomaterials-modified conducting paper

Advances in materials sciences and related technologies have enabled the modification of the paper matrix by different types of nanomaterials, such as metallic nanoparticles (Ag, Au, etc.), organic conducting polymers (PEDOT:PSS), carbon nanomaterials (graphene, CNTs, etc.), and their hybrids [23-26]. Modification by inorganic nanoparticles often yields high conductivity and better device performance. However, high costs, difficult processing procedures, and introduction of cracks in the conductive film are some of the disadvantages

faced by inorganic nanomaterial-modified conducting paper [23]. Also, certain nanomaterials such as Ag may not be suitable for certain applications, e. g. electrochemical devices, as Ag tends to oxidise upon repeated cycling potential and presence of buffer environment. Modification by organic nanomaterials, such as PEDOT:PSS, has several advantages like easy processability of the nanomaterial, low cost, high adherence to paper fibres, retention of flexibility, etc. [23, 27]. Different studies have demonstrated the use of organic polymers, such as PEDOT:PSS, polyaniline (PANI), etc., to develop conducting paper-based diagnostic devices [27, 28]. Such flexible sensors have been shown to detect their target analytes, such as cancer biomarkers, cardiac biomarkers, and pathogenic DNA, with excellent sensitivity [29-31]. Though successful, there are certain limitations associated with the use of organic polymers such as complex formulations and limited conductivity of the conducting paper restricting its wider applications.

Carbon nanomaterials (CNMs) are being increasingly utilized towards fabrication of conducting paper. CNMs are a class of nanomaterials that are exclusively made up of carbon atoms within the nano size range (1-100 nm). This class of materials encompasses graphene, single- and multiwalled carbon nanotubes (SWCNTs and MWCNTs, respectively), and buckminsterfullerene (carbon atoms arranged in a spherical shape) among others (**Figure 1.3**).

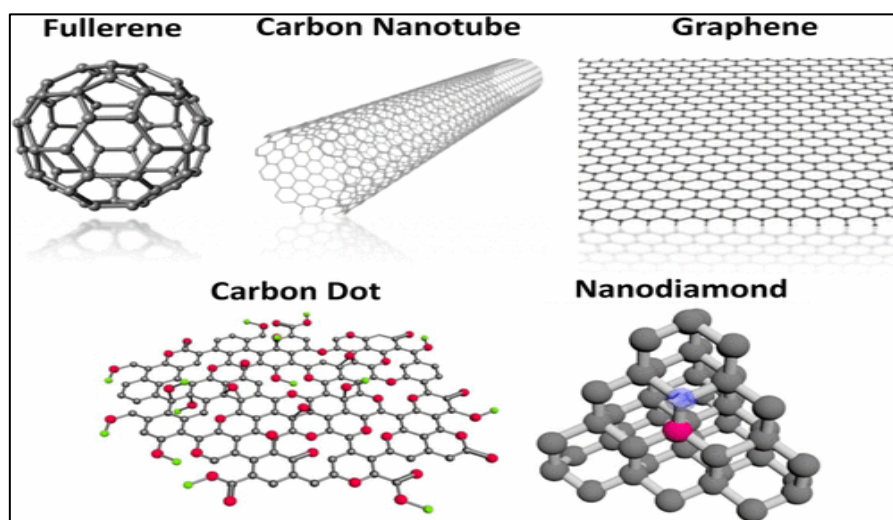


Figure 1.3. Different carbon nanomaterials and their morphologies [32].

CNMs possess interesting physical, chemical, and optical properties owing to their size and morphology (**Table 1.1**). These properties render them useful in numerous biomedical applications [32]. Graphene and reduced graphene oxide (rGO) are 2D CNMs that display excellent electrical conductivity and electrocatalytic effect, and have been widely utilized in developing conducting paper for various applications [24, 33, 34]. Studies have shown that graphene-modified conducting paper can potentially have extensive applications in wearable sensors, biosensors, and other electrochemical devices [24, 25, 35]. Also, its surface area to volume ratio is very high, which makes it useful in immobilization applications and for developing nanocomposites with other nanomaterials (both organic and inorganic) [36]. However, graphene has been shown to agglomerate at fast rates that can have adverse effects on its conductivity [37]. Synthesis of single-sheet graphene and their maintenance has proven time intensive and expensive. Additionally, reducing the number of sheets may increase conductivity, but its mechanical strength is compromised, which is often due to incorporation of defects [38, 39].

Table 1.1. Comparison of some properties of different carbon nanomaterials [40].

<i>Carbon Nanomaterials</i>	<i>Dimensions</i>	<i>Hybridization</i>	<i>Experimental Specific Surface Area ($m^2 g^{-1}$)</i>	<i>Electrical Conductivity ($S cm^{-1}$)</i>	<i>Tenacity</i>	<i>Hardness</i>
Graphite	3	sp ²	~10–20	Anisotropic: $2-3 \times 10^4$	Flexible, non-elastic	High
Graphene	2	sp ²	~1500	~2000	Flexible, elastic	Uppermost (for single layer)
Carbon nanotube	1	mostly sp ²	~1300	Structure-dependent	Flexible, elastic	High
Fullerene	0	mostly sp ²	80–90	10^{-10}	Elastic	High

a) Multiwalled carbon nanotubes (MWCNTs): MWCNTs are rolled up tubes made of carbon, and mostly possess similar properties as graphene (**Figure 1.4**). Internetworked and aligned MWCNTs have been shown to possess exceptional optical and electrical properties. In

addition, they possess exceptionally high mechanical strength over graphene and SWCNTs [41].

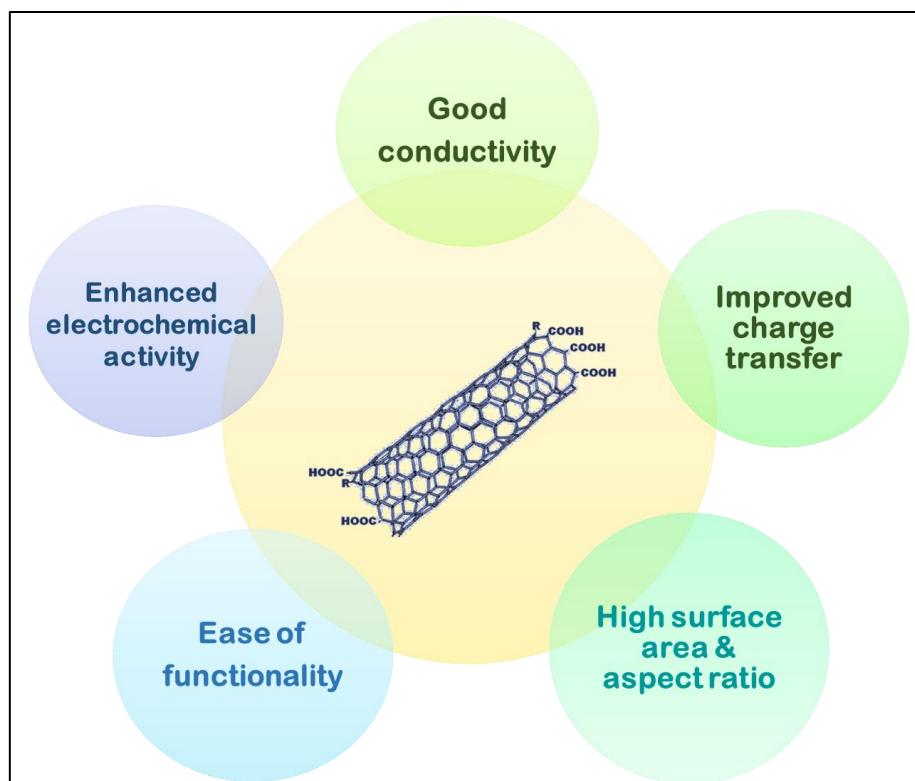


Figure 1.4. Pictorial representation of different properties of MWCNTs.

MWCNTs have been extensively utilized for modification of paper towards various applications. Though they have not been specifically used for the fabrication of conducting paper. However, a recent study has demonstrated the interpenetration of MWCNTs and cellulose nanofibers (CNFs) towards the fabrication of flexible, conductive membranes for capacitive pressure sensing [42]. Other recent studies have demonstrated the utilization of MWCNTs and its composites for fabrication of flexible, affordable, and disposable paper devices for applications including strain sensors, humidity sensing, and monitoring of different physiological parameters such as motion, respiration, and temperature among others [43-46]. MWCNTs have also been coated onto paper substrates to detect cancer biomarkers, such as prostate-specific antigen (PSA), and other physiologically relevant biomarkers like cholesterol [47, 48]. Different coating methods have been employed to coat MWCNTs on paper substrates, which have been discussed in the next section.

1.2.2 Methods of fabrication of conducting paper

Conducting paper substrates have been fabricated using different methods over the years. The most prominently utilized method is the dip coating method, wherein a paper substrate is dipped into a dispersion/colloidal suspension of the desired nanomaterial. The dip velocity and time of dipping may be controlled to enable uniform coating. The primary advantages of this method are use of less reagents, easy instrumentation, and speed of fabrication. However, this method depends on Van der Waals' interactions between the nanomaterial and paper substrates for retention of coating. This method works excellently for nanomaterials that have strong binding properties to paper, e.g., PEDOT:PSS and PANI fibers [49, 50]. MWCNTs also have an intrinsic adherence capability for paper, however, it is difficult to form stable dispersions of MWCNTs in many solvents. This may lead to non-uniform coating and high variance in conductivity values when dip coating is employed. Leaching is another problem that is often faced in dip coating methods.[51]

Other coating methods include sputtering, spray coating, casting coating [52], doctor blade coating, flexographic coating [52], and spin coating [53]. Some of these methods (spray coating, spin coating) do not effectively modulate the porosity or surface roughness of paper substrates, which can be a hindrance in many applications. Additionally, random arrangements of cellulosic fibers within the paper matrix may hamper the accuracy of the resulting paper-based device [54]. *In situ* growth of nanomaterials is another effective method of fabrication of conducting paper. This method has been successfully utilized to modify paper by metallic and other inorganic nanomaterials. However, this method cannot be utilized for coating of MWCNTs on paper, as their synthesis involves very high temperature.

Vacuum filtration is another method utilized for coating of MWCNTs on paper substrates [47, 48]. It is a simple and quick method that utilizes vacuum pumps to pull MWCNT dispersions through a paper substrate. The solvent passes through and MWCNTs are deposited

onto the paper. Though effective, this method has its limitations. Vacuum filtration can only work for paper substrates that have a porous network (e. g. filter paper) and secondly, this method also relies on the intrinsic adhering properties of MWCNTs and paper fibers. This may result in leaching and non-uniform distribution of conductivity on the paper surface.

An effective conducting paper fabrication method is one that would not only impart conductivity to the paper matrix but also enable the modification of surface properties of paper substrates. Additionally, it should enable batch reproducibility and high-volume manufacturing of conducting paper. Most studies on coating of MWCNTs onto paper substrates have relied on formulation of inks: suspensions or pastes stabilized by different additives [43, 45, 55]. Ink formulation enables homogenous dispersion of MWCNTs along with automation of the coating process. This subsequently leads to highly uniform coatings and uniform distribution of conductive networks throughout the paper matrix. Since addition of MWCNTs imparts conductivity to the ink as well, they are referred to as conductive inks.

1.3 Conductive inks

An ink can be defined as a paste, solution, sol, or a gel consisting of a colored dye/pigment that is used for writing/painting patterns/designs onto suitable substrates, such as paper, by using a pen, quill, brush, or other methods. Conductive inks are a special class of inks that consist of an electrically conductive material (e.g., metal nanoparticles) instead of a colored dye or a pigment. Hence, in addition to making a pattern, these inks can impart conductivity to the substrate onto which they are applied. Conductive inks have aroused much interest owing to the advent of flexible, wearable, and printable electronics. They have been utilized in fabricating functional things such as electronic circuits, sensors, and other electrical/electrochemical elements onto paper and other substrates. The rise of conductive inks has further led to advancements in the field of papertronics as well. Paper-based biobatteries and electrochemical cells are being reported with the use of conductive inks formulated

specifically for adhering to paper [56].

In contrast to other methods of paper modification for imparting conductivity, conductive inks can provide uniform thickness, a better control on the conductivity, and enable tuning of the roughness and porosity of the paper substrates, which often pose as bottlenecks in efficient design of paper-based clinical diagnostics [57]. These inks can be coated manually using a paint brush/pen or be printed onto paper using commonly available printing technologies like inkjet, screen, and flexographic printing, etc. The various constituents of conductive inks and the subsequent characteristic features that render them advantageous in the fabrication of paper-based analytical devices are discussed in the next section.

1.3.1 Components of conductive inks

A conductive ink primarily consists of these four constituents: i) a solvent that carries all other constituents of the ink, ii) binder(s) that enables adherence of the ink to the desired substrate, (iii) additives such as rheological modifiers for optimizing the flow properties of the conductive ink according to the application, and emulsifiers to homogenize the different constituents of the ink, and most importantly iv) conductive filler that imparts conductivity to the ink (**Figure 1.5**). In addition to these, there can be other additives as well in the conductive ink that modulate other properties, such as oxidation/degradation rates, thermal evaporation, etc.

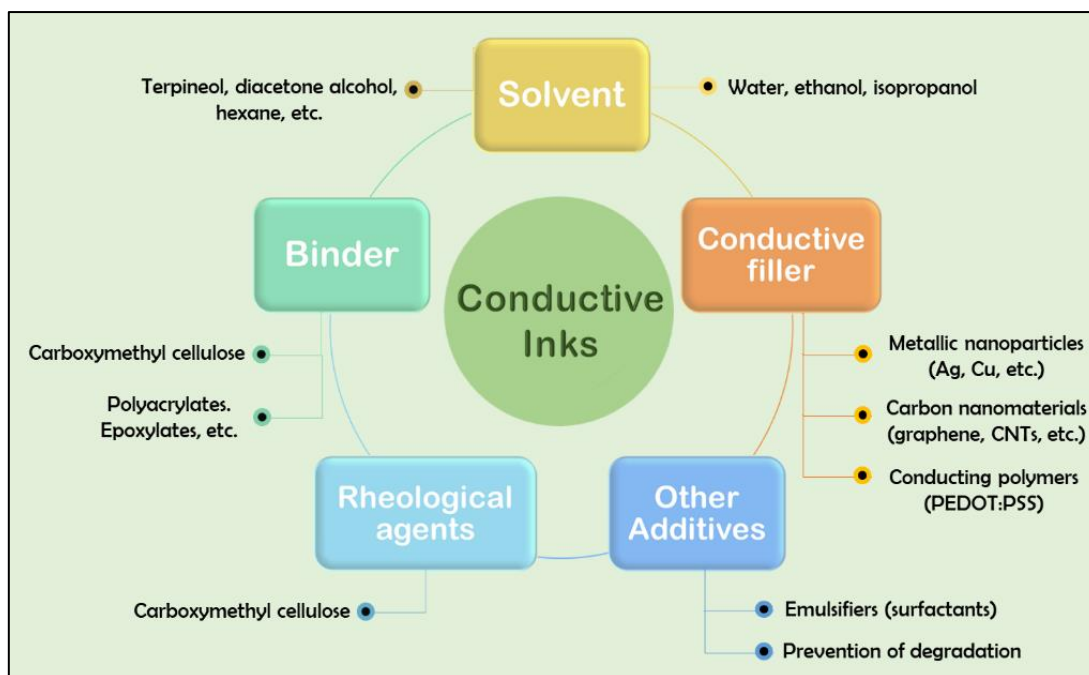


Figure 1.5. Pictorial representation of constituents for the formulation of a conductive ink.

The solvent of a conductive ink is a crucial component, as it acts as a carrier for all the other constituents of the ink. Several studies have focused on water, ethanol, isopropanol, and their mixtures thereof as ink solvents [58]. The primary reason for choosing water could be its high dissolution power. It can dissolve or disperse a range of different reagents and chemical moieties. Secondly, it is non-toxic, works at a neutral pH, and can be evaporated from the ink at a relatively low temperature of 100 °C. At the same time, organic solvents such as ethanol and isopropanol are low boiling in nature, hence can be removed from the ink after coating easily. However, these solvents are limited in the range of polar molecules only. They are not able to dissolve/disperse those molecules that are non-polar in nature. Since, many binders and other additives are hydrophobic and non-polar in nature, dispersing them in solvents such as water and ethanol becomes difficult. Additionally, many applications might not benefit from water-based inks as any introduction of water from the environment might create problems in the device functioning.

The choice of solvent may also depend on the type of application. Diacetone alcohol

(DAA), terpineol (Tp) are other solvents that are widely used in preparation of printable conductive inks. DAA has been found to enhance the conductivity of printed films [59]. Tp is a low surface energy solvent that flows easily and can dissolve many polar and non-polar molecules [60]. Both solvents have been utilized in screen printing applications where the ink should display viscoelastic behavior, i.e., they should possess a high initial viscosity but should flow easily upon pressure application.

Binders are important for a conductive ink as they ensure that the ink binds strongly to the desired substrate. Mostly polymeric binders (acrylates, epoxyates, etc.) are utilized as binders owing to their high adherence to many substrates. In the context of paper substrates, carboxymethylcellulose (CMC) is one of the most prominently used binder. It has a carboxymethyl (-COCH₃) group replacing the hydroxyl groups attached to carbon atom in cellulose. It is less hydrophilic than cellulose, has film-forming capability, and adheres strongly to cellulose fibers present in the paper matrix via hydrogen bonding and Van der Waals' interactions. Moreover, it is available in a wide range of sizes (in terms of molecular weight and chain length) which can prove beneficial in optimizing the ink formulation. Since it is a biopolymer derivative, it is environmentally sustainable and does not leave any toxic residue upon degrading. It is widely used as a processed food additive, packaging material, etc. [61].

In addition, it may serve another important role in ink formulation, i.e., modification of rheology [62]. Rheology, i.e., the flow properties that determine the viscosity and behavior of fluids upon application of external force, is an important consideration for conductive inks. The substances that are added to modify the rheological properties of a conductive ink are referred to as rheological modifiers. The type of application mainly governs the choice of rheology of the conductive ink. For example, a conductive ink prepared for inkjet printing should be of low viscosity and should behave like a Newtonian fluid under normal circumstances. CMC dispersions are thixotropic, i.e., increase in shear rate leads to decrease in their viscosity.

Hence, CMC is often utilized in formulation of conductive inks where shear thinning/thixotropy is required.

1.3.2 Methods of coating conductive inks

There have been several methods for the coating of conductive inks onto different kinds of substrates including paper. Depending upon the application, the inks can also be coated manually onto paper using brushes, pens, etc. Manual coating is dependent on viscosity of the ink; higher viscosity inks can be coated by brushes, while pens are generally employed for low viscosity inks. Printing techniques like aerosol jet printing, screen printing, inkjet printing, etc. provide more reproducibility and enable high-volume manufacturing. They are also faster than other manual methods. Every method has their advantages and disadvantages. For example, inkjet printing is a fast method for printing high resolution patterns on paper, however, the nozzle of an inkjet printer may get clogged over time because of nanomaterial deposition, particularly when CNTs with high aspect ratios are used [57]. Screen printing is one of the oldest and most prominent method of printing. It offers various advantages such as low cost and ease of availability. Also, this method is flexible with respect to the choice of nanomaterials for the conductive ink and can be used for any kind of substrate.

a) Screen printing technology: This is one of the contact printing methods, wherein a screen mesh comes in contact with a substrate and transfers an ink using force through pre-defined cavities in the mesh (**Figure 1.6**). This method offers high resolution and good control on pattern deposition. The thickness of the printing coat can be adjusted by adjusting the pressure applied for it [63]. In this method, a screen mesh (usually made of nylon) is treated by photoactive dyes to produce specific patterns on its surface. A substrate is kept under it and downward force on the ink placed over the screen is applied using a rubber bar known as a squeegee [57, 64]. The force allows the ink to pass through the patterns on the screen to the substrate. After the force is removed, the contact between the screen and substrate

ends yielding high resolution patterns on the substrate.

It is essential that the ink utilized in screen printing should be viscoelastic/thixotropic in nature. Viscoelasticity would allow the ink to thin down upon application of force during screen printing and easily pass on to the substrate. At the same time, removal of force would allow the ink to recover its viscosity and stop accidental bleeding into the substrate.

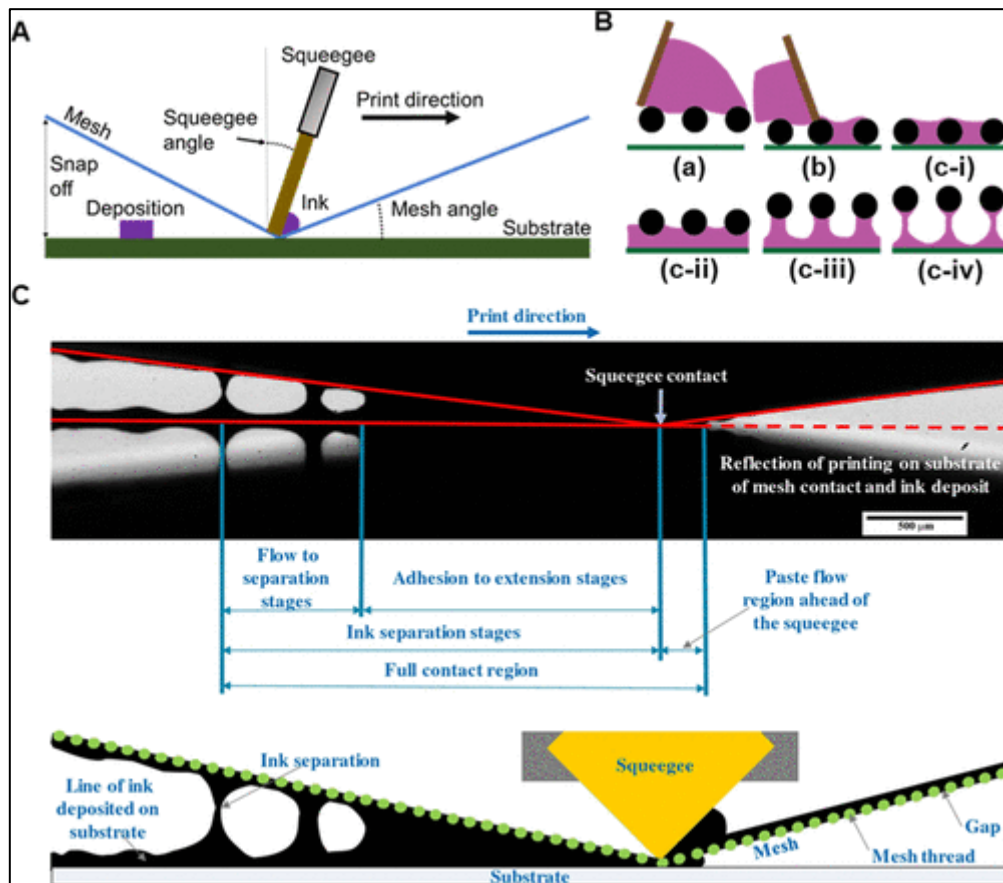


Figure 1.6. Principle and working mechanism of screen-printing method. (A) Diagrammatic representation of screen-printing process, (B) the mechanism of screen printing, wherein (a) fluid on the mesh, (b) force applied by squeegee leading to contact between screen and substrate and filling of cavities (patterns) in the screen by mesh, and (c) separation of the screen from the substrate and removal of ink, and (C) High speed image of the ink transfer by screen printing method and its illustration [57].

Several nanomaterials have been utilized for screen printing ink formulation for printing on paper substrates. Graphene and its composites are the most utilized conductive filler in screen printing inks. High conductivity and resolution have been obtained using graphene-

based screen-printing inks on paper [63, 65, 66]. Similarly, MWCNTs have also been utilized as conductive fillers in several highly conductive screen-printing inks [26, 55, 67]. A primary advantage of addition of CNMs in screen printing inks is that they help in increasing the initial viscosity of the ink and hence, are easily transferred to the substrate with high resolution [68]. Despite the advancements, there is still scope of improvement in screen-printing inks, particularly in relation to the trade-off between the ink composition and the conductivity of the ink.

1.4 Biosensors

Biosensors are defined as devices that integrate a specific biomolecule (or, a bioreceptor), binding specifically to a target analyte, to a transducing element, which then converts the biological signal into another energy form (conductivity/resistivity/voltage/wavelength change, etc.). Since their conception in the 1960s, biosensors have come a long way from the traditional membrane-based enzyme electrodes. In the current times, technological advances have allowed the development of biosensing devices like dermal tattoos, paperfluidics, and thread-based devices that can monitor analyte concentrations in different body fluids including sweat/interstitial fluid, tears and, saliva [36, 69-72]. Different biosensing architectures have emerged that cater to different kinds of applications, e. g., microelectrodes for ion detection, microfluidic biosensors for health care applications, and microbial fuel cells for environmental monitoring [24, 73-76]. The various applications of biosensors are shown in **Figure 1.7**. The reasons for their wide success and applicability are quantitative responses, ease of miniaturization, low power requirements, small volume requirements, and ease of use [73]. They are designed to be used outside of a laboratory, having wide implications in the field of health care and emergency medicine. Further, the utilization of nanomaterials in biosensors has enabled faster response and improved sensitivity and specificity [77, 78]. Many biosensing modalities even allow real time

monitoring of target analytes/parameters. These advantages have made biosensors an attractive alternative to the conventional diagnostic technologies.

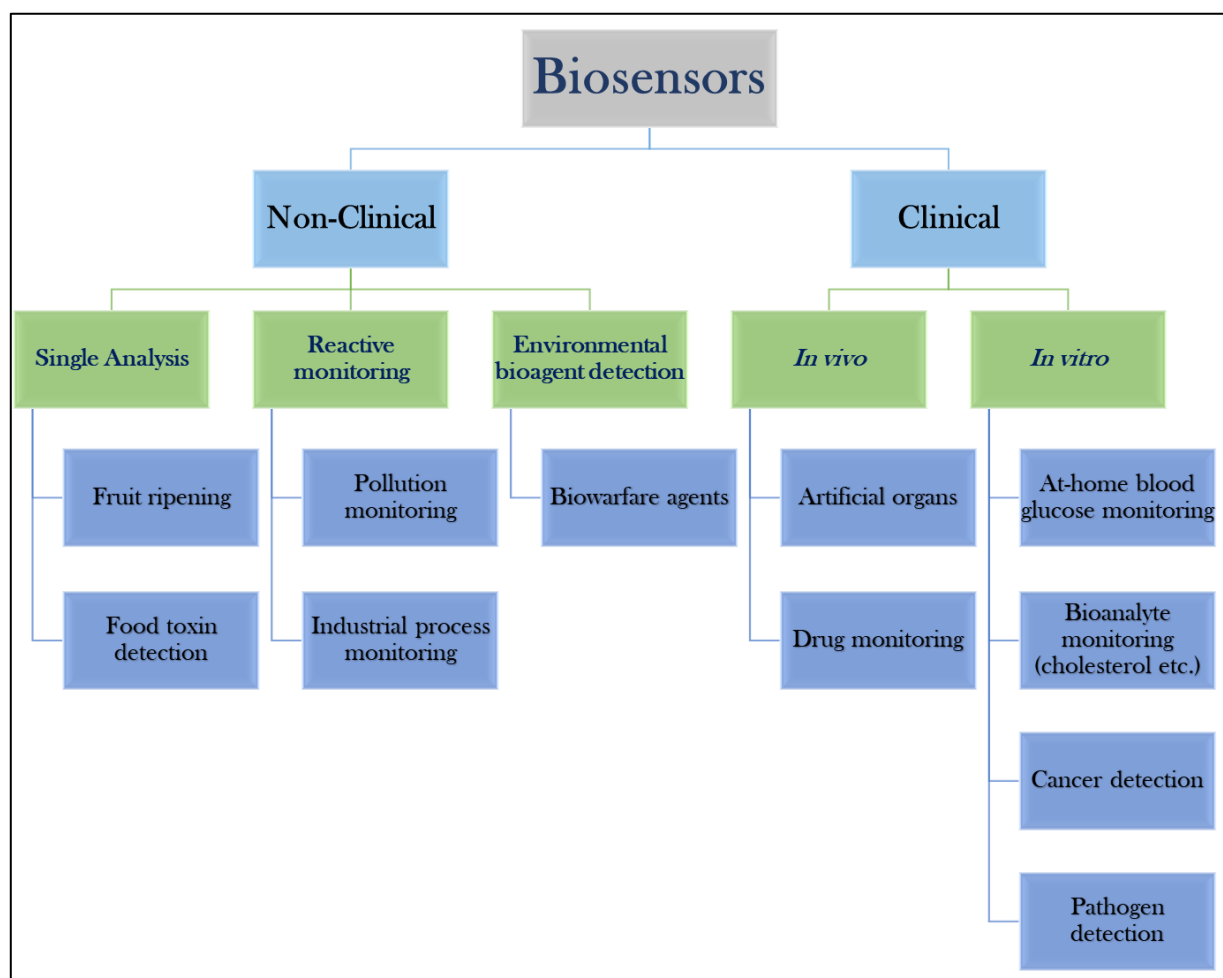


Figure 1.7. Flow chart depicting the various applications of biosensors.

Typically, a biosensor is fabricated by integrating the following elements: i) bioreceptor (antibodies, enzymes, DNA, live cells, etc. depending upon the target), ii) immobilization matrix for immobilization of bioreceptors (nanomaterials, metallic electrodes, polymer films, etc.), and iii) transducer which transforms the biological recognition signal to an observable electrochemical/electrical/optical/piezoelectric signal (**Figure 1.8**). These are described in the following sections.

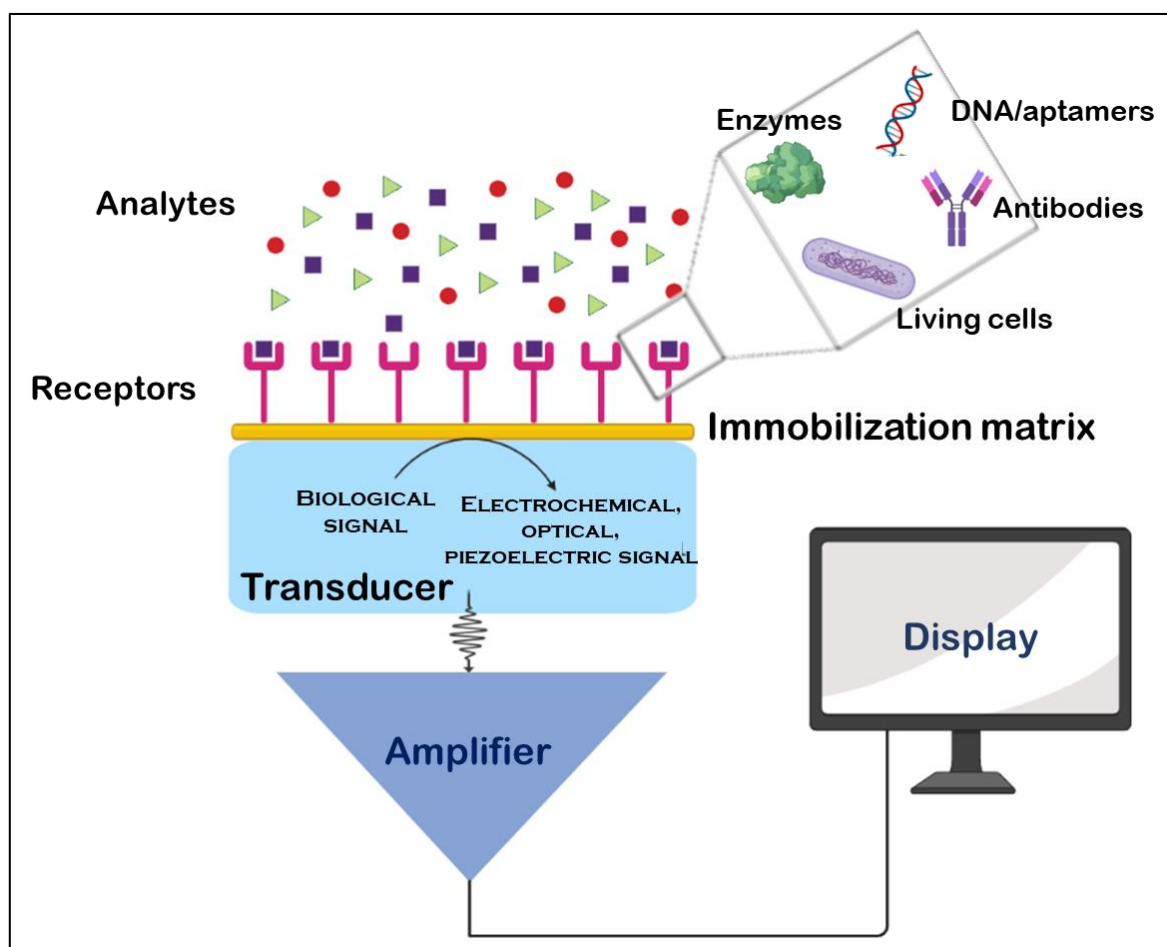


Figure 1.8. Basic components of a biosensor.

1.4.1 Bioreceptors

Bioreceptors refer to biomolecules that possess binding affinity to specific analyte(s). All cellular processes are based upon the principle of ligand-receptor binding, wherein receptors are molecules that bind specifically and with high affinity to a single (or, a family of) biomolecule, referred to as the ligand [79]. This binding/recognition principle is utilized by biosensors. The primary factors that are involved in the choice of a particular bioreceptor include the type of target analyte to be detected, degree of specificity required in the biosensing device, and the application of biosensor. Enzymes and antibodies are the most utilized bioreceptor in biosensing assays. Enzymes bind to specific substrates and process them into products, which is often accompanied by exchange of electrons (current flow). This current

generated can be easily detected by an electrode. Thus, enzymatic biosensors are highly specific and sensitive in nature. The integration of nanomaterials with enzymes has further led to an increase in biosensor performance in terms of sensitivity [80, 81]. However, enzymes are not very thermostable and can degrade readily with slight fluctuations in temperature or ion concentration [80]. Antibodies are immune-mediating molecules with high binding affinity for specific target analytes. Monoclonal antibodies can bind to only one specific analyte, while polyclonal antibodies bind to analogous but different molecules. Contrary to enzymes, antibody-target interaction does not lead to any change in current, hence antibody-based biosensors (immunosensors) can often use labels for signal amplification [82]. Like enzymes, antibodies also suffer from the limitations of low thermostability and degradation with repeated thawing cycles. Antibodies are also very expensive to produce and purify. Whole living cells-based biosensors possess applications in food analysis, pharmacology, heavy metals, environmental monitoring, pesticides, organic contaminants detection, and drug screening [83]. This is because living cells produce stimuli-specific responses and are inexpensive to obtain. However, they are not suitable for every application due to complexities involved in signal analysis.

Nucleic acids (NA) (like DNA, RNA, peptide nucleic acids (PNA), aptamers, DNA nanostructures, etc.) have increasingly become the prominent choice as bioreceptors. Unlike enzymes and antibodies, NAs are highly thermostable and have a long shelf life. They do not lose their binding/recognition ability even after immobilization to a substrate, which is often a requirement in biosensors. NA biosensors have found applications in various fields including infectious agent detection, pollution monitoring, sequence specific information generation, mutation analysis, etc. [84, 85]. All types of NA molecules consist of nitrogenous bases ((adenine (A), thymine (T) or uracil (U), guanine (G), cytosine (C)) linked to sugar molecules (ribose in RNA and deoxyribose in DNA). The sugar molecules are, in turn, linked to phosphate

groups. These three building blocks make up the monomeric unit of NAs known as nucleotides. The nitrogenous bases are highly specific in binding to each other; A always forms two H-bonds with T (or, U in case of RNA) and G always forms three H-bonds with C. This hybridization rule (complementary base pairing) serves as the basic principle of the simplest NA sensors.

In the simplest mechanism of a DNA biosensor, a single stranded DNA (ssDNA) is immobilized onto the biosensing substrate/transducer and allowed to bind to the target DNA strand via complementary base pairing. The ssDNA utilized as the bioreceptor is often referred to as the 'capture' probe. To improve the specificity and sensitivity of biosensors, different hybridization strategies have been developed over the years. The two most prominent DNA hybridization methods utilized in DNA biosensors are as follows:

a) Sandwich hybridization-based DNA biosensors: This is the DNA analog of a sandwich immunoassay, wherein two specific oligonucleotide probes are utilized for capturing the target strand by complementary base pairing (**Figure 1.9**). The capture probe is immobilized onto the biosensing substrate, and the second specific probe, referred to as the 'signal probe' or the 'detector probe,' is kept free and allowed to hybridize to target strand before (or, after) introduction to the biosensing surface. Both the probes have complementary sequences to different regions of the same target DNA strand.

The important factors to consider while designing the probes involved in sandwich hybridization assays are the length of the probes, presence/absence of overhangs, and the distance between the regions identified by the capture and detector probes [86]. It has been shown in polymerase chain reaction (PCR) experiments, that probe length of 18-35 bases is adequate for obtaining specific hybridization to the target sequence. However, the temperature of annealing should also be considered. It has been shown that hybridization at temperature closer to the melting temperatures of the probes yields more specific results [86, 87]. Also, the

probes should not leave any single stranded DNA (ssDNA) overhangs on the target strand after hybridization, as it may lead to a suppressed signal response [88]. The surface roughness of the film onto which the capture probes are immobilized also plays a key role in the resulting device/assay sensitivity.

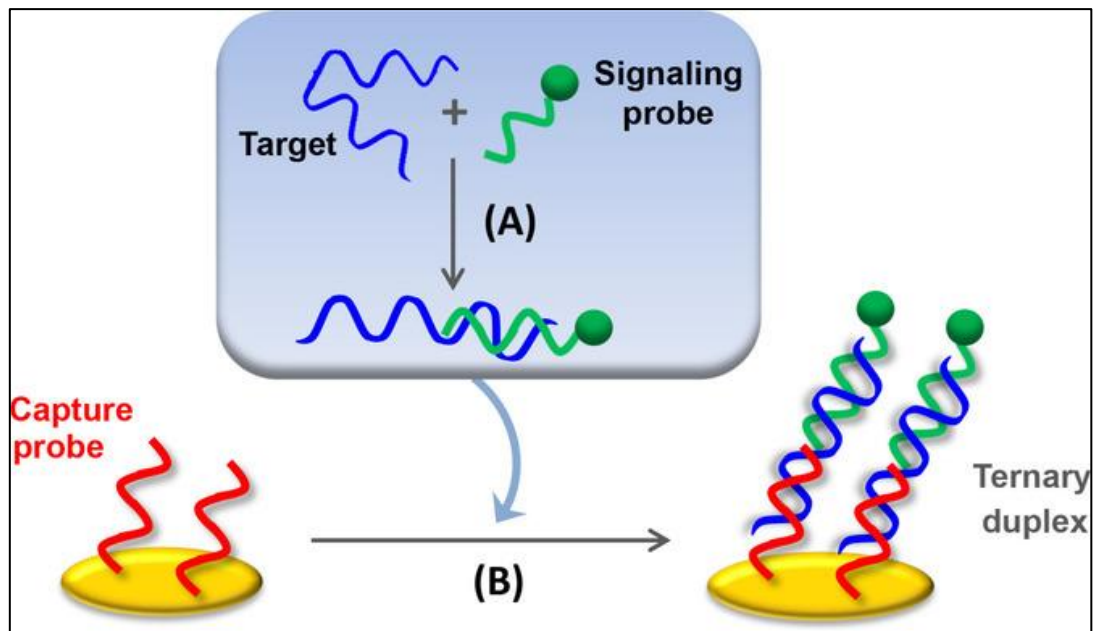


Figure 1.9. Schematic representation of a sandwich DNA hybridization-based biosensor [89].

Several sandwich hybridization-based biosensors have been developed in the past for the detection of DNA and other oligonucleotide biomarkers [90, 91]. Many studies have reported the use of labels such as enzymes, metal nanoparticles, and dyes such as methylene blue (MetB) for signal amplification [90, 91]. While in some cases, the hybridization has been integrated with magnetic beads (MBs) to enhance the selectivity of the assay [92].

b) Supersandwich hybridization-based DNA biosensors: This is a modified sandwich hybridization technique that can achieve signal amplification without using DNA amplification techniques (**Figure 1.10**). In this method, a capture probe is ligated to the 3' end of a detector probe allowing more than one target strands to bind to the detector probe. This is followed by a cascade of hybridization events resulting in the capture of a significantly high

number of detector-target duplex for every capture probe immobilized on biosensing surface. This contrasts with the traditional sandwich hybridization, wherein only one detector-target duplex is captured per molecule of the capture probe. This eventually translates to a very high sensitivity and specificity of the assay.

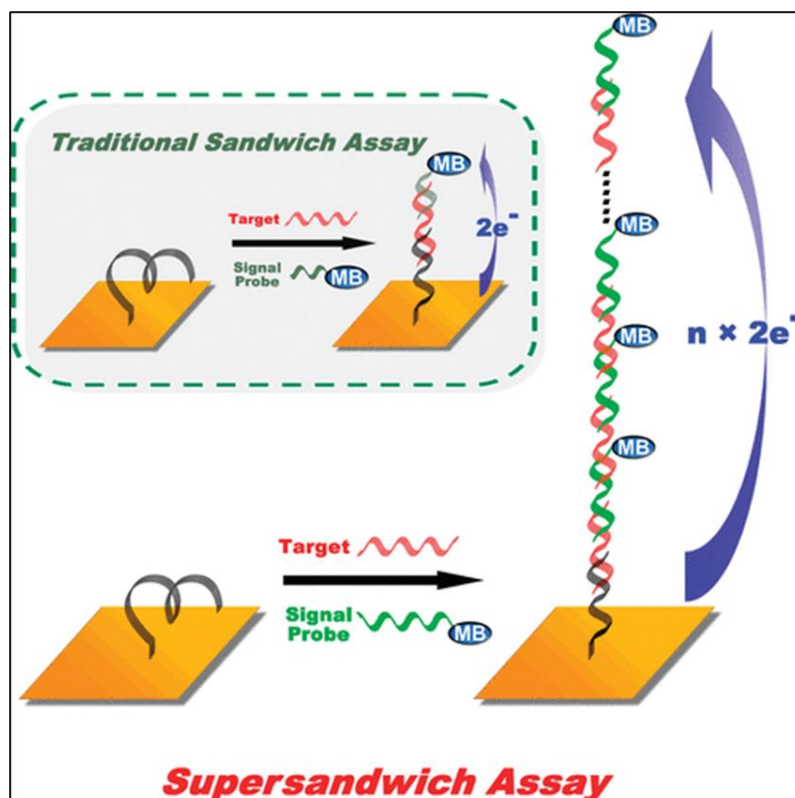


Figure 1.10. Schematic representation of supersandwich DNA assay as compared to traditional hybridization method [93].

One of the first studies to demonstrate this powerful method was by Xia et al. [94], wherein the supersandwich assay was shown to obtain a detection limit of 3 orders of magnitude higher as compared to the traditional method. It does not especially require the use of labels or expensive reagents that are required in amplification methods. This method has been utilized for sensitive detection of DNA methylation status [95], miRNA [96], and pathogenic DNA [94]. In one study, MBs-assisted miRNA extraction was integrated to the supersandwich assay for signal amplification and detection of the miRNA [96]. In this work, we have utilized both the sandwich and the supersandwich method for the detection of

pathogenic DNA. MBs were utilized to enhance the specificity of the assays.

1.4.2 Transducers

Transducers can be roughly classified into the following groups: electrochemical, electronic, optical, thermal, and gravimetric. Electrochemical transducers are the most extensively studied and utilized modality of biosensors. They produce detectable electrochemical signals in the form of voltage (potentiometric), current (amperometric/voltammetric), and impedance (impedimetric) as a result of interactions between the bioreceptor and specific analyte on the transducer surface [78].

a) Electrochemical transducers: Electrochemical transducers have become a cornerstone in the development of biosensors, offering numerous advantages that make them highly attractive for various applications. These transducers play a pivotal role in converting a biological interaction between the bioreceptor and target analyte into an electrical signal, enabling accurate and sensitive detection in biosensing devices [78]. Electrochemical transducers are known to be highly sensitive to minute changes in target concentration, making them invaluable tools in fields like medical diagnostics, environmental monitoring, and food safety [78, 97, 98]. They have been utilized to detect various analytes, including ions, small molecules, proteins, and nucleic acids. Electrochemical biosensors offer the advantage of real-time monitoring. Additionally, the rapid response times allow for continuous measurements, making them suitable for PoC applications and situations where immediate detection is essential, such as glucose monitoring in diabetes management [97, 99]. Electrochemical transducers can be easily integrated into electronic devices using cost-effective methods, enabling sensor networking and addition of other integrative technologies such as Internet of things (IoT) [100, 101]. An electrochemical biosensor comprises a three-electrode system, with the biosensing platform referred to as the working electrode (WE). This WE is connected to a counter electrode (CE) (mostly platinum, Pt) and a reference electrode (RE) (mostly silver-

silver chloride, Ag/AgCl), to complete the circuit and keep potential at the WE constant at any particular instant, respectively. This 3-electrode system is shown in **Figure 1.11(A-C)**.

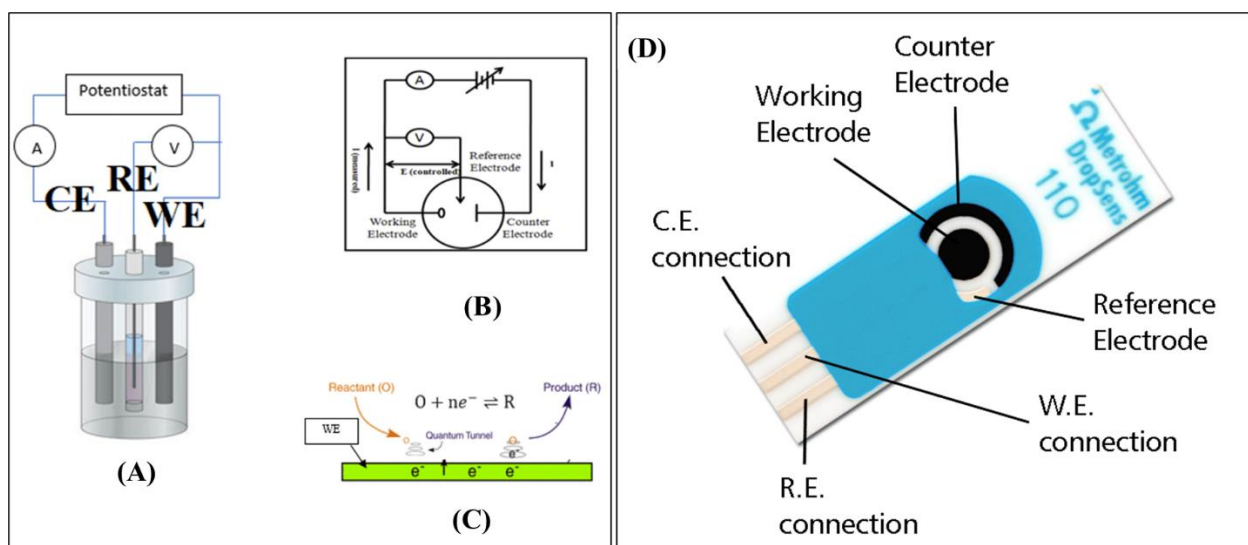


Figure 1.11. (A) Schematic of the 3-electrode assembly showing the WE, RE, and CE connected to a potentiostat, (B) the corresponding circuit diagram, (C) redox reaction at WE surface [102], and (D) Image of a commercial screen-printed electrode (SPE) [103].

The traditional 3-electrode cell has now been transformed into screen-printed electrode (SPE) systems (**Figure 1.11(D)**) [104]. These SPEs have the same configuration as the conventional 3-electrode cell, the only differing factor is that they are entirely printed using inks on different substrates, mostly plastic. SPEs have enabled PoC and wearable technologies. Currently, only the SPEs printed with metal-based inks (Au, Pt, etc.) and carbon inks are available commercially [103]. The WE on these SPEs is often modified by nanomaterials to fabricate a biosensing electrode. This is where conductive ink-modified paper can present an advantage. Paper-based SPEs can be seen as improvised versions of conducting paper-based devices. In general, conducting paper-based electrochemical biosensors have the added advantage that they can be flexible, portable, and lightweight [105]. The integration of conducting paper with electrochemical transducers may lead to lower costs fabrication and operation, and would reduce the sample volume requirements significantly [15, 105].

The fabrication of SPE on paper would go one step further and completely alleviate the

need of external electrodes. The foldability and ‘memory’ of paper to retain shapes has further enabled fabrication of novel origami paper devices and different SPE configurations for electrochemical detection of cancer biomarkers, miRNA, methylation of DNA, ions, among others [15, 106-109]. Using MWCNT-based conductive inks for SPE fabrication would provide a high surface area for bioreceptor immobilization as opposed to the currently available SPEs. In the post-pandemic era, it is imperative that PoC screening and diagnostic devices can be fabricated ‘as per need’ in a fast, reliable, and cost-effective manner. Conducting paper-based electrochemical devices, particularly fully printed SPEs, offer such opportunities. In this work, fabrication of conductive ink-modified paper biosensors has been demonstrated for detection of pathogenic DNA. The conductive inks consisted of carboxyl-functionalized MWCNTs and were optimized for rheology for screen printing applications. Attempts to fabricate fully printed SPEs on paper for the detection of pathogenic DNA have also been made.

1.4.3 Immobilization matrix

Immobilization matrix is the surface onto which bioreceptors are immobilized for binding to the target analyte. It can directly influence the sensitivity of a biosensor because it controls the amount of bioreceptor that can be immobilized onto it. In the current generation of biosensors, the immobilization matrix plays a more active role and acts as the transducing element also. Several nanomaterials have been utilized as both the immobilization matrix and the transducer in electrochemical biosensors. There are different types of immobilization strategies that can be employed in electrochemical biosensors (**Figure 1.12**).




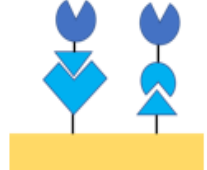

Strategy	Type of binding	Key Features	Illustrations
Adsorption	Weak, Reversible Interaction	- Simple processing -No requirement of external chemical for binding -Minimal Orientation control - Chance of desorption to bulk	
Cross-Linking	Strong, Irreversible Interaction	- Simple processing - Minimal Orientation control -Chance of interference from crosslinking agent	
Covalent-Binding	Strong, Irreversible Interaction	-Binding between the functional groups of substrate and biomolecule -Active site of biomolecule maybe altered due to binding	
Affinity Binding	Strong, Reversible Interaction	-Site and Orientation specific interaction -Requires the formation of external bio-affinity bonds using specific molecules (such as streptavidin-biotin)	
Entrapment	Strong, Irreversible Interaction	-Minimal interaction with biomolecule, thus retention of biomolecular activity -Three-dimensional matrices are incorporated for biomolecular trapping.	

Figure 1.12. Comparison of different types of immobilization techniques [110].

a) Physical immobilization: It refers to the immobilization of bioreceptors such as DNA via Van der Waals' interactions, pi-pi stacking, and other weak interactions. The type of matrix dictates the type of interactions that can occur. For example, MWCNTs have an intrinsic ability to pi-stack with DNA molecules. Hence, they can immobilize DNA efficiently without the use of extra reagents. This method is simple in operation and the resulting biosensing matrix can be regenerated. However, the resultant biofilm can be heterogeneous in nature, i.e., different DNA molecules may be oriented differently on the surface leading to steric hindrance or repulsion. This is a major limitation because of which this method is avoided in biosensor fabrication.

b) Covalent immobilization: This technique involves the formation of covalent linkages between the bioreceptor and immobilization matrix. The matrix should have either of

the -NH_2 , -SH , -OH , -COOH functional groups that can either directly form covalent bonds or can be activated to an unstable intermediate leading to covalent linkage. In fact, the primary advantage of this method is that covalent bonds are extremely difficult to break. They can also help in orientation of the bioreceptor on the matrix. Amide bond formation is the most commonly utilized covalent linking chemistry and EDC-NHS pair is often used as the activator-stabilizer in the same (**Figure 1.13**).

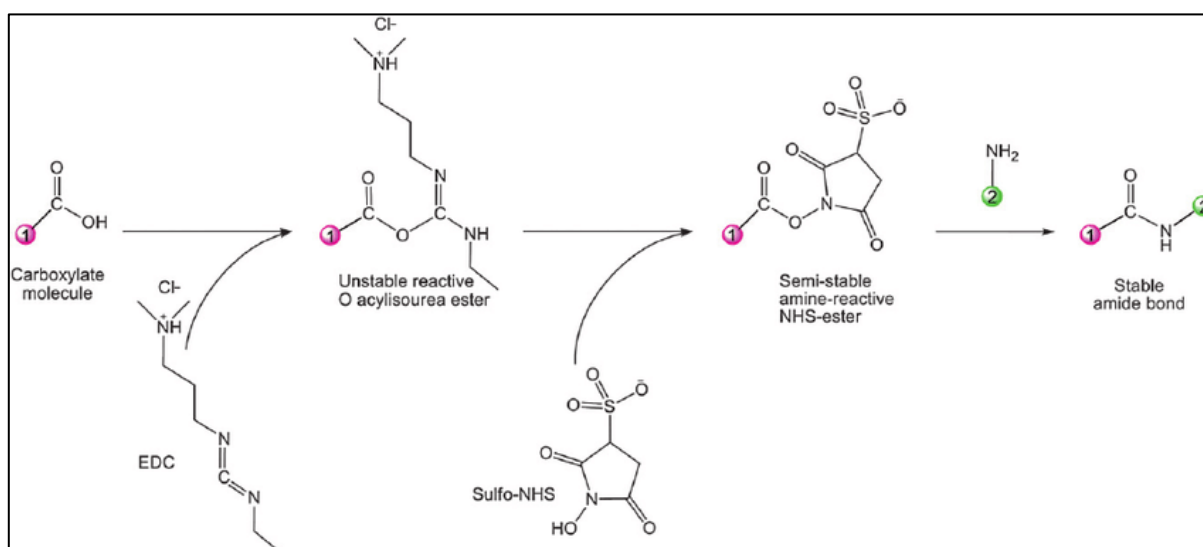


Figure 1.13. Schematic showing the reaction intermediates and final product formed by the EDC-NHS mediated formation of amide bond.

c) Affinity interactions: Affinity-based molecular interactions are non-covalent interactions between certain molecules, such as the biotin-avidin interaction. This method is mostly used when proper orientation of the bioreceptor is required on the immobilization matrix. The biotin-avidin interaction is one of the most specific and strongest non-covalent interactions known in nature. Biotin, also known as vitamin B7, is a small molecule that binds tightly to avidin, a protein found in egg whites. The biotin-avidin interaction is advantageous due to its rapid association rate and remarkable resistance to dissociation even under harsh conditions. Thus, this method has the disadvantage that the biosensing surface cannot be regenerated without the use of harsh treatment. This immobilization method should be utilized when the biosensor is fabricated for single-time use.

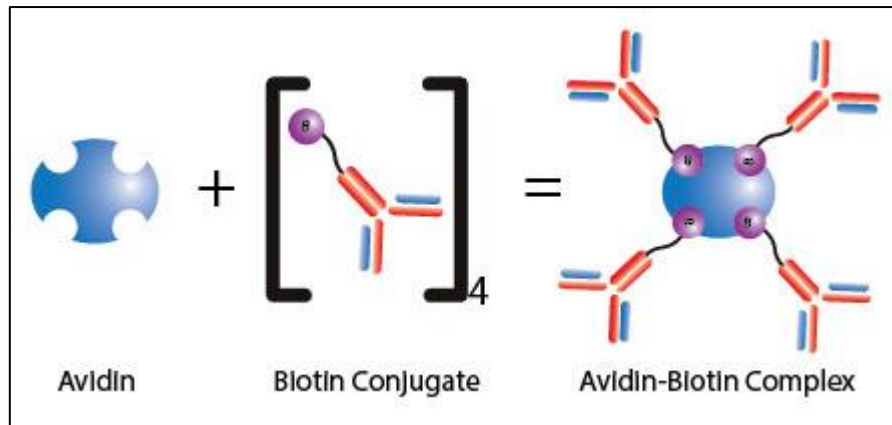


Figure 1.14. Avidin-biotin affinity interactions. Every avidin/streptavidin molecule can bind to four biotin molecules, leading to their role as signal amplification agents in molecular assays [111].

Conducting paper can act as an excellent immobilization matrix, due to high surface area of paper. Depending upon the type of modification for conducting paper fabrication, the immobilization strategy can be chosen. For example, EDC-NHS chemistry can be utilized when conducting paper has been fabricated by rGO or metal oxide modification [24]. The rough surface area of the paper matrix is conducive to the immobilization of a high number of bioreceptors. However, conductive ink coating may lead to smoothening of the paper surface due to masking of fibers. The interaction among the different additives and the conductive filler (e. g. MWCNT) in the ink could be such that it prevents the immobilization of bioreceptors via different methods.

In this work, we have utilized both the covalent method and the affinity-based binding method for immobilization of the bioreceptors (capture probe DNA) onto MBs. The MBs were chosen because the MWCNTs in the conductive ink did not seem to be available for immobilization. MBs also enabled specific sample enrichment. The MBs were integrated to the conductive ink-modified paper electrodes for detection of *Neisseria gonorrhoeae*, which has been discussed in the next section.

1.5 *Neisseria gonorrhoeae*: The biosensor target

Neisseria gonorrhoeae (NG) is a diplococcus, Gram negative bacteria that causes gonorrhea, a sexually transmitted infection (STI) (**Figure 1.15**) [112]. It is an obligate human pathogen, i.e., it specifically infects human cells. It is currently one of three STIs of global concern according to the World Health Organization (WHO) along with Human Immunodeficiency Virus (HIV) and syphilis infection [113]. The WHO has prepared guidelines to reduce the incidence of this curable STI from 82.3 million in per year in 2020 to 8.23 million (90% reduction) till 2030 [114]. Gonorrhea is being touted as serious public health issue around the world due to increasing cases of antimicrobial-resistant (AMR) strains [114]. However, the situation is complicated by inadequate screening measures and lack of reporting of this STI.

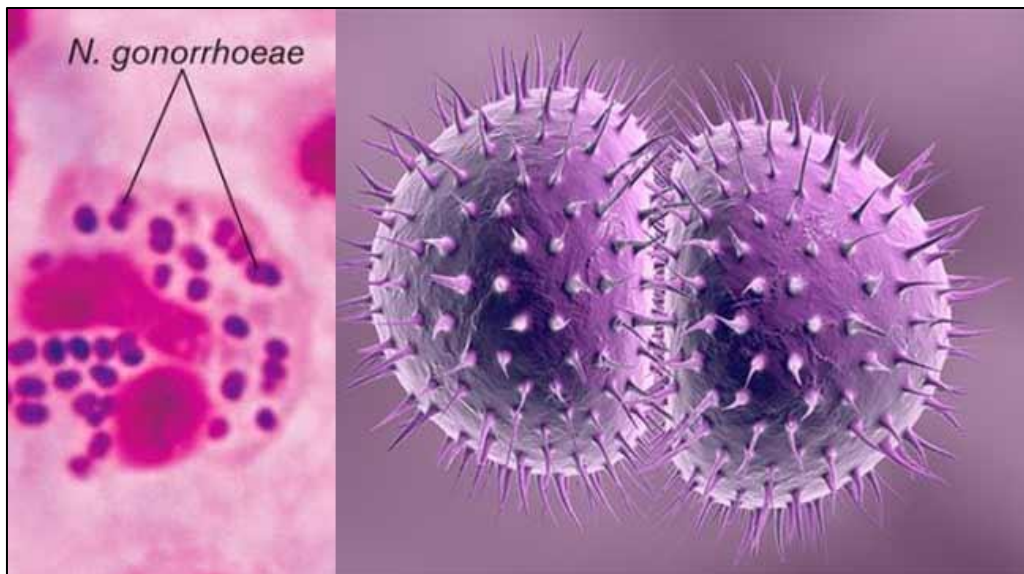


Figure 1.15. *Neisseria gonorrhoeae* (NG) is a Gram negative, diplococcus bacteria that causes gonorrhea. It resides intracellularly in specialized white blood cells, known as polymorphonuclear cells (PMNC) [115].

1.5.1 Gonorrhea: Causes and symptoms

The primary cause of gonorrhea is unprotected sexual intercourse with an infected person, having multiple partners, and unsafe sexual practices. The primary bodily regions to

get affected by gonorrhea are the endothelium of the urogenital area in both women and men. However, the anorectal and pharyngeal endothelium can also be affected by this STI. NG has numerous host adaptations (e.g., adherent polymorphic surface proteins) that enable it to adhere to the mucosal linings and evade the human immune system (**Figure 1.16**) [116].

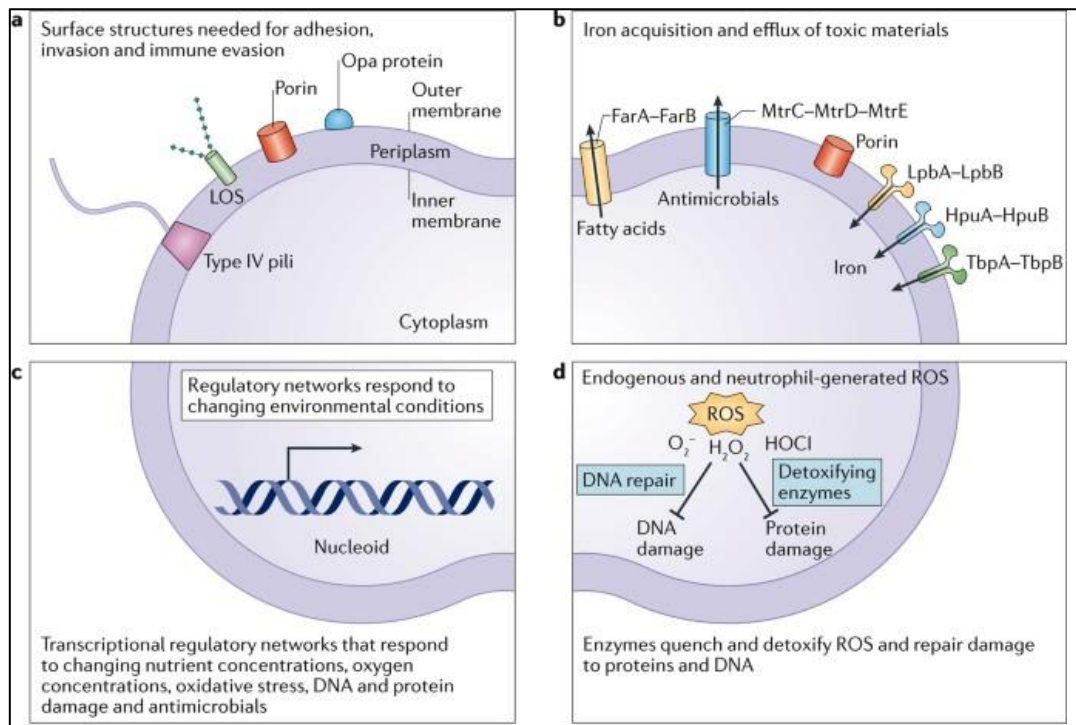


Figure 1.16. Pictorial representation of the different host adaptations of NG and its pathogenesis [116].

Incidence of gonorrhea has been found to be higher in patients with HIV [117]. Commercial sex workers and homosexuals also constitute high-risk population groups for contracting this STI. Conversely, NG infection is associated with a high risk of HIV infection along with other coinfections, such as *Chlamydia trachomatis* (CT) infection [118-120]. Most gonorrhea infections are asymptomatic, i.e., display no symptoms, and to complicate the situation, the symptoms that do appear are often nonspecific and may lead to misdiagnosis in the early stages of infection. This may ultimately lead to a delay in treatment and an increased risk of transmission within a given population. Around 60-80 % of men and >85% women remain asymptomatic [121]. The most typical signs of acute gonococcal urethritis in males

include urethral discharge and dysuria [122]. A US-based study has found that the most frequent causes of acute epididymitis (inflammation of epididymis) in sexually active males (hetero- and homosexuals) between the ages of 14 and 35 are because of NG and CT [123]. Among women, cervicitis with vaginal discharge, bleeding, and dysuria is the most typical symptoms [124]. According to estimates, 10–20 % of infected women may eventually develop pelvic inflammatory disease (PID), which refers to the inflammation of the uterine walls [125]. Almost 15% of infected women may experience fallopian tube blockage and infertility. Pregnant women with this infection may pass it to their newborns as gonococcal conjunctivitis (ophthalmia neonatorum), which may lead to permanent blindness [126].

Lack of routine screening may lead to infections that go untreated, allowing the disease to spread covertly without being found and treated. Regular STI testing and screening is essential for preventing the spread of gonorrhea [127]. Thus, there is a dire need of cost effective PoC devices that enable reliable detection of this infection and lead to effective and timely disease management.

1.5.2 Conventional methods of NG detection

Many methods are available to detect NG or its genetic material in clinical samples. The commonly utilized clinical samples for NG detection are urethral swabs, cervical swabs, and semen. However, urine samples are also frequently test in certain clinical protocols. Pharyngeal and rectal swabs are also collected in suspected cases (particularly, homosexuals). Extragenital (pharyngeal and rectal) infections, that often display no symptoms, completely rely on laboratory investigations for early diagnosis of the disease [128]. Gram staining followed by microscopy is the most common and prominently utilized method for the detection of NG [129]. In this method, samples are inspected under a microscope after staining with specific dyes; the presence of purple-colored, distinctive Gram-negative diplococci indicates NG infection.

Once identified, bacterial culture methods are employed to grow NG in specific culture media for further verification and analysis. This method enables isolation of NG and its serotyping. Once detected, an antibiotic susceptibility test (culturing with different antibiotics) may be performed to determine whether the NG strain is AMR. Evidently, these methods are laborious, depend on the subjective interpretation of the health personnel, and require a lot of time (2-4 days). They are also prone to false-negative findings, particularly in situations with low bacterial loads or when the sample is not collected properly.

Due to their excellent specificity and sensitivity, nucleic acid amplification tests (NAATs) have emerged as the primary tools for identifying NG [130]. These molecular diagnostic tests rely on amplification of specific genes in NG's genetic material using a set of specific primer probes, DNA polymerase, and other reagents. NAATs can be used for non-invasive testing for the identification of asymptomatic infections on a variety of specimen types, including urine, vaginal, rectal, and pharyngeal swabs. NAATs provide quick and precise detection, which makes them extremely useful for gonorrhea diagnosis, especially when prompt treatment and the prevention of further transmission depend on early identification. Polymerase chain reaction (PCR) is the most common NAAT currently in use globally for clinical diagnosis of NG. It has replaced culture techniques as the current gold standard for NG detection. However, PCR also been shown to provide false positives due to cross-hybridization with DNA from other *Neisseria* species [131, 132]. Additionally, it requires many expensive reagents and the current technology is not portable enough to be utilized outside of a laboratory. The requirement of specific temperature conditions and risk of sample contamination also restrict its miniaturization and use outside of a central facility.

1.5.3 Recent advances in NG detection

The efforts to develop electrochemical PoC devices for NG detection has been slow in the past few years. However, there have been attempts at developing optical/visual biosensors

for the same. Recently, loop-mediated isothermal amplification (LAMP) was integrated with Au nanoparticles-enabled lateral flow biosensor (AuNPs-LFB) for multiplex visual detection of NG and CT [133]. The gene targets utilized in the study were *ompA* and *orf1* genes of both NG and CT. The biosensor displayed a detection limit of 50 copies per test with a total analysis time of <45 min. A similar study has reported the integration of AuNPs-LFB with multiple cross displacement amplification (MCDA) for visual detection of NG in clinical samples [134]. While another study has reported a polymer nanoparticle-based biosensor (PNB) integrated to LAMP assay for visual detection of NG within 60 min [135]. More recently, a recombinase polymerase amplification (RPA)-based LFA has been reported for NG *fitA* gene having a detection limit of 10^2 copies μL^{-1} and analysis time of 28 min [136].

A Cas13a-based visual LFA (specific high-sensitivity enzymatic reporter unlocking; SHERLOCK) has been reported for the detection of *porA* pseudogene of NG along with azithromycin resistance. The assay showed 100 % concordance with results obtained from a commercial NG detection system (Roche cobas® 4800) and a detection limit of 10 copies per test [137]. In a different approach, a live cell-Systematic Evolution of Ligands by EXponential enrichment (SELEX) was conducted to select specific aptamers (short oligonucleotides with very high binding affinity to specific targets) for binding to a mixture of different NG strains [138]. One of the aptamers was then integrated to Au NPs towards developing a rapid and specific PoC test. Another study reported on the utility of surface-enhanced Raman scattering (SERS) for the identification of NG and four other STI-causing microorganisms, viz. *Mycoplasma hominis*, *Mycoplasma genitalium*, *Ureaplasma urealyticum*, and *Haemophilus ducreyi* [139]. This method was shown to identify these bacteria in urethral swabs taken from men with 100% and 89% accuracy (from two different multivariate methods) and an analysis time of <15 min.

In a novel approach, a paperfluidic device has been reported for visual lateral flow

detection of NG [69]. This device integrates patient sample lysis with DNA extraction and amplification followed by detection. The analysis could be conducted within a total analysis time of <80 min. The PoC test showed a detection limit of 500 NG cells per device and 100% specificity for analysis of urethral and vaginal swab samples.

It is evident that most of these studies have relied on visual/optical mode of detection. Secondly, isothermal amplification-based techniques have been utilized in most of the studies that require stringent temperature control. Additionally, these techniques, though sensitive, are complex in operation and require expensive reagents. Surprisingly, despite their success, electrochemical biosensors have not been developed in the last 2-4 years for NG detection.

This work entails the development of MWCNT-based conductive inks for the fabrication of conductive paper electrodes, and the design of amplification-free DNA hybridization assays for sensitive and specific detection of NG.

1.6 Objectives of the study

The main aim of this thesis is to fabricate conducting paper sensors for detection of clinically relevant analytes. This aim was further broken down into the following objectives:

1. Synthesis and characterization of the selected nanomaterial(s) and subsequent fabrication of conducting paper electrode.
2. Immobilization of DNA bioreceptors onto the conducting paper for fabrication of the biosensor.
3. Response studies of the fabricated conducting paper biosensor.
4. Real sample analysis.

This work addresses the following questions:

- i. Is it possible to fabricate nanomaterial-modified conducting paper that can further be utilized in electrochemical biosensing? If so, how can batch reproducibility and scalability be ensured?

It was hypothesized that a homogenous carboxylated MWCNT (cMWCNT)-based conductive ink consisting of binders and other additives can be prepared that would adhere to the paper substrate and display appreciable conductivity for electrochemical applications. Further, the rheology of the ink would be modulated to ensure coating via screen printing.

- ii. How can the target analyte be detected with high sensitivity and specificity? Can label-free detection be applied for the same?

The main aim, here, was amplification-free detection of *porA* pseudogene of *N. gonorrhoeae*.

It was hypothesized that the use of specific DNA probes shall ensure specificity. The use of MBs shall also ensure specific capture of the target gene sequence from a milieu of substances.

Methylene blue (MetB) was chosen as a tagging label to enhance sensitivity. A supersandwich assay was designed for label-free detection of target DNA.

This thesis on “Nanomaterials modified conducting paper sensors for biomedical applications” describes recent developments towards the fabrication of MWCNT-modified, conducting paper biosensors for electrochemical detection of *porA* pseudogene of *Neisseria gonorrhoeae*. It comprises of six chapters, with each chapter describing a different aspect of this research work. This chapter entitled “**Introduction and Literature Review**” discussed the background and study rationale of this study, including the definition and types of biosensors with special emphasis on electrochemical and DNA biosensors, use of paper as one of the biosensor components, and use of nanomaterials and further conductive inks in imparting conductivity to paper substrates for biosensing applications. The salient features of *N. gonorrhoeae* and gonorrhea were discussed along with conventional detection strategies for the same. Recent advancements towards development of diagnostic devices for *N. gonorrhoeae* detection were discussed, with emphasis on the current research gap.

Chapter 2 on Materials and Experimental Techniques details the different reagents, buffers, and their compositions utilized in various experiments conducted as part of this study. The different protocols pertaining to the design of specific oligonucleotide probes for biosensing, preparation of conductive inks, fabrication of conductive ink-coated paper electrodes, use of magnetic beads in the DNA hybridization-based assays, and its further integration to conductive paper electrodes for electrochemical analysis have been provided in detail. The basic principles and working of the different characterization techniques utilized for characterization of the conductive inks and the conductive ink-coated paper electrodes have been provided, including X-ray diffraction (XRD), electron microscopy (TEM, (FE)SEM), Raman spectroscopy, atomic force microscopy (AFM), X-ray photon spectroscopy (XPS), rheometry, contact angle studies, electrochemical techniques such as electrochemical impedance spectroscopy (EIS) and cyclic voltammetry (CV). Further, the procedure followed for the screen printing of the conductive ink on paper substrates has been detailed. Details of

the microbial strains utilized in real sample and specificity analyzes have been provided along with the different steps involved in genomic DNA extraction from these microbial strains.

Chapter 3 on Carbon nanomaterial-modified conductive ink for paper-based electrochemical detection of *Neisseria gonorrhoeae* describes the development of MWCNT-based conductive ink and subsequent coating on paper towards electrochemical detection of NG *porA* pseudogene. The ink formulation consisted of carboxylated MWCNTs (cMWCNTs) dispersed in a stable emulsion formed by mixing aqueous CMC gel with Tp and PS80. This cMWCNT ink was used for coating the paper substrates towards fabrication of the cMWCNT@paper electrodes. The lowest mean (\pm standard deviation, SD) value of resistivity of the cMWCNT@paper electrodes was 1.066 (\pm 0.33) Ω .cm after 7 coats (75 μ L ink per coat). Further, an MB-assisted DNA hybridization assay was designed, which comprised specific capture and detector probes (CP and DP, respectively). MBs were utilized in this study to impart specificity to the biosensor, as they allow rapid and precise capturing and separation of the target analyte from a milieu of substances. The MBs were modified by avidin (Av) and used for immobilization of the CP molecules via avidin-biotin affinity interactions. The MetB labeling on DP molecules enabled electrochemical signal amplification. The CP and DP molecules hybridized specifically with a *porA* target DNA sequence (TP) leading to the capture of TP at the MB surface and formation of a ternary sandwich hybridization complex (C-T-D). Thus formed C-T-D/Av/MB samples were drop cast and dried onto the cMWCNT@paper with different TP concentration for electrochemical analysis. The biosensor was found to be within the concentration range of 100 fM–100 nM and sensitivity of 5.09 μ A. ($\log[\text{concentration}]$)⁻¹. Further, the biosensor performance was assessed by detecting genomic gonococcal DNA mixed with DNA from other bacterial strains and proteins such as BSA. Rheological analysis showed that the cMWCNT ink showed shear thinning behavior, which is suitable for screen

printing applications. This is perhaps one of the first few reports on fabrication of paper-based biosensors for electrochemical detection of NG *porA* sequence.

Chapter 4 on Supersandwich DNA assay-integrated paper biosensor for electrochemical detection of *Neisseria gonorrhoeae* details the development of an ultrasensitive and specific conductive paper-based biosensing platform for label-free detection of *porA* pseudogene. For this purpose, composition of the conductive ink was optimized for CMC content via rheological analysis. Viscometric analysis and 3-interval thixotropy test (3iTT) were conducted to determine that 5% CMC in the emulsion base yielded the best viscosity recovery (thixotropy). cMWCNTs were added to this emulsion in CMC:CNT ratio of 1:1, and the resulting ink was labeled C5. Paper substrates were coated with this ink to yield the C5@paper conductive electrodes. The C5@paper electrodes displayed the highest conductivity of 10.1 S cm⁻¹ for 4 coats. After this, an MB-mediated supersandwich DNA hybridization assay was designed, wherein the capture probe (SCP) was 5' aminated for direct immobilization onto carboxylated MBs via EDC-NHS chemistry. The supersandwich detector probes (SDP) has been designed to allow the binding of more than one TP (and SDP) molecules for every SCP molecule, resulting in the formation of 'ladder-like' DNA concatemers. This MB-assisted supersandwich assembly was drop cast (and dried) on C5@paper electrodes for label-free electrochemical detection via EIS. The biosensing assay yielded a linear response within the concentration range, 100 aM-100 nM, with exceptional sensitivity. The performance of this biosensing platform was evaluated by quantifying different concentrations of genomic NG DNA. Specificity studies were conducted by detecting gonococcal genomic DNA with DNA from other bacterial species in high concentration ratio. This study demonstrated the potential of a paper-based device for highly sensitive, label free and efficient STI diagnostics. Rheological studies indicated the potential of screen printability of the C5 conductive ink, which can lead to batch reproduction of fully printed biosensing devices.

Chapter 5 on Screen printing of MWCNT-modified conductive ink towards paper-based biosensor for *Neisseria gonorrhoeae* detection details the results of studies relating to screen printing of the C5 ink onto different paper substrates and their utilization for *N. gonorrhoeae* detection. Screen printing masks were prepared by first designing them in the professional software Corel Draw V and then transferring the designs onto a nylon mesh using a photoactive film. Screen printed electrodes (SPEs) were printed onto paper by utilizing the C5 ink to print the working electrode, and commercial graphite and Ag/AgCl inks to print the counter and reference electrodes, respectively. Rectangular electrodes of size $2 \times 1 \text{ cm}^2$ were also printed for conductivity studies. The conductivity values for office paper and drawing paper were found to be similar at 6 coats. SEM studies revealed that the C5 ink did not seep or leech into the area outside of the printing zone, verifying that the rheological properties were suitable for screen printing. The ink coating was also found to be uniform indicating its homogeneity. As proof of concept, different concentrations of the C-T-D hybridization complexes were drop casted onto the SPEs for electrochemical detection. CV studies revealed that the SPE response is found linear with the log of concentration of C-T-D hybridization complexes. These studies reveal that the ink formulations discussed in this work can potentially be used to fabricate fully printed paper-based PoC biosensors for detection of target analytes.

Chapter 6 on Summary and Future Prospects summarizes the work discussed in this thesis on conductive ink-coated paper biosensors for electrochemical detection of *N. gonorrhoeae*. It further gives an overview of future implications and scope of this research work, such as development of screening kits, wearable devices, and multi-analyte detection systems.

Chapter 2

Materials and Experimental Techniques

2.1 Introduction

This chapter details of the materials, characterization techniques, and other protocols utilized for the formulation of conductive inks, fabrication of conductive paper electrodes, design of biosensing assays, and subsequent biosensing studies. The protocols for buffer preparation, oligonucleotide probe design, and pre-processing involved in the biosensing assays have been discussed. The significance of using MBs and the methods of genomic DNA extraction from different bacteria have also been detailed.

2.2 Chemicals, reagents, and buffers

Carboxylated multi-walled carbon nanotubes (cMWCNT), PS80, and bovine serum albumin (BSA) were purchased from SRL Pvt. Ltd. (India). The oligonucleotide biosensing probes were purchased from IDT (USA). Tp, CMC (high viscosity), and sodium hydroxide (NaOH) pellets were procured from Central Drug House (CDH, India). Carboxylated magnetic beads (MBs; Dynabeads Carboxylic AcidTM MyOneTM) were purchased from Thermo Fisher. Avidin (Av), N-hydroxysuccinimide (NHS), and 1-ethyl-3-(3-dimethylpropyl) carbodiimide (EDC) were procured from Sigma-Aldrich (Merck, Germany). All reagents were used without further purification.

Sodium hydroxide (NaOH, 0.1 M) was utilized for washing MBs before assays. Phosphate buffered saline (PBS; 0.1 M, pH 7) was utilized in the electrochemical studies, wherein ferro-ferricyanide (5 mM) were added as redox probes. Tris-EDTA (TE) buffer (pH 8) was utilized for reconstituting oligonucleotide probes. Tris Borate EDTA (TBE) buffer (0.5×; pH 8) was utilized in gel electrophoresis experiments. PBS (pH 8) was utilized for blocking the unreacted EDC-NHS esters at MB surface after binding of capture oligonucleotide probes. All experiments were conducted in three sets (n = 3). The compositions of the various buffers are given below:

a) PBS (pH 7, 0.1 M)

Monosodium phosphate dihydrate ($\text{NaH}_2\text{PO}_4 \cdot 2\text{H}_2\text{O}$)	0.2 M (39 mL)
Disodium phosphate dihydrate ($\text{Na}_2\text{HPO}_4 \cdot 2\text{H}_2\text{O}$)	0.2 M (61 mL)
Sodium chloride (NaCl)	0.9%
MilliQ water	100 mL
Total volume	200 mL

For electrochemical studies, the PBS was supplemented with:

Potassium hexacyanoferrate(III) ($\text{K}_3[\text{Fe}(\text{CN})_6]$)	5 mM (ferricyanide)
Potassium hexacyanoferrate(II) ($\text{K}_4[\text{Fe}(\text{CN})_6]$)	5 mM (ferrocyanide)

b) PBS (pH 8, 0.1 M)

Monobasic sodium phosphate ($\text{NaH}_2\text{PO}_4 \cdot 2\text{H}_2\text{O}$)	0.2 M
Dibasic sodium phosphate ($\text{Na}_2\text{HPO}_4 \cdot 2\text{H}_2\text{O}$)	0.2 M
Sodium chloride (NaCl)	0.9%
MilliQ water	100 mL
Total volume	200 mL

2.3 Design and selection of oligonucleotide probes

The DNA probes for the studies were selected and designed using available software, viz. NCBI-PrimerBLAST, NCBI Nucleotide BLAST, and Clustal Omega. IDT Oligoanalyzer was utilized for determining cross-hybrids and secondary structures, if any. Firstly, a library consisting of twenty different sets of primers specific to gonococcal *porA* pseudogene was prepared using NCBI-PrimerBLAST. NCBI Nucleotide BLAST was used to align these primers with different gonococcal strains and other non-gonococcal genomic DNA sequences to select the primers with the maximum specificity to NG. The genomes of the following bacterial species were used in alignment: *N. sicca*, *N. mucosa*, *N. lactamica*, *N. meningitidis*,

Enterococcus faecalis, *Ureaplasma urealyticum*, *Chlamydia trachomatis*, *Mycoplasma genitalium*, *Staphylococcus aureus*, *Escherichia coli*, *Klebsiella pneumoniae*, and *Lactobacillus fermentum*. The forward primer having 100% alignment with gonococcal DNA, and negligible alignment score with non-gonococcal DNA was designated as the capture probe. An adjacent sequence specific for NG was chosen as the detector probe. A non-complementary (NC) sequence was designed depending upon the target, capture, and detector probe sequences.

For the supersandwich assay, the capture sequence was ligated to the 3' end of the detector probe to yield the supersandwich detector probe. This would allow more than one target strands to bind to the detector probe and lead to the formation of 'supersandwich DNA structures.' The sequences of all the probes utilized in this work and other details are provided in **Chapters 3** and **4**. The probes were procured in lyophilized form with modifications on capture and detector probes to enable immobilization or signal amplification. These probes were reconstituted in TE buffer (100 μ M stock concentration) and stored at -20 °C as stock solutions. These stocks were further aliquoted and serially diluted for biosensing studies. Fresh dilutions were prepared before every analysis. The details of immobilization of the capture probes have been discussed in **Section 2.6**. The detailed protocols for the electrochemical biosensing assays are provided in **Section 2.6** and **Chapters 3-5**.

2.4 Formulation of conductive inks

The conductive inks were formulated towards the fabrication of conductive paper electrodes. The composition of a conductive ink is dependent upon the type of application. For example, conductive inks prepared for inkjet/laserjet printing are often thinner than those prepared for screen printing or painting.

In essence, the rheology of the conductive ink plays an important role in its effectiveness towards a particular application. Screen printable/paintable conductive inks also need to be

thixotropic, i.e., their viscosity should not only decrease linearly with force applied (measured as shear rate) but should also regain its original value once the force is removed. Thixotropy allows the ink to form high resolution pattern without any spilling or seeping in the substrate matrix. This property becomes even more significant in case of paper substrates, as their fibers can take up ink through capillary action and lead to distorted, low-resolution patterns. The details of conductive ink formulations have been discussed in **Section 1.3 (Chapter 1)**.

In this study, screen-printable conductive inks have been formulated using Tp and water as the solvents, CMC as the binder and rheological modifier, and PS80 as an emulsifier. Two conductive inks, cMWCNT (1% w/v cMWCNT) and C5 (5% w/v cMWCNT), were prepared for fabrication of paper electrodes. The details of the formulations are provided in the respective chapters (**Chapters 3 and 4**).

2.5. Screen printing of conductive inks

Screen printing is an affordable and prominent method to print conductive inks onto various substrates with good resolution. The basic principles and apparatus of the screen-printing technique have been discussed previously in **Section 1.3 of Chapter 1**. The rheology of the conductive ink formulations used in this thesis work were optimized for screen printing applications. Particularly, the C5 ink was screen printed onto different kinds of paper substrates. For screen printing, patterns were designed using CorelDraw V professional software (**Figure 2.1(A)**). The dimensions of the 3-electrode assembly pattern are given in **Figure 2.1(B)**. Further, a negative mask of the patterns was obtained on a nylon mesh supported by a wooden frame. Both the nylon mesh and the frame were procured commercially, and the mask was also prepared via industrial sources. The mask frame was fixed using a holder and paper was placed under the mask. A rubber squeegee was utilized to push the ink through the nylon mesh and transfer of pattern to the paper substrate. Three different kinds of paper were printed-regular

office paper and ivory paper. The paper substrates were dried at 120 °C for 5 min after every coat. A total of 6 coats were printed to achieve desirable conductivity values.

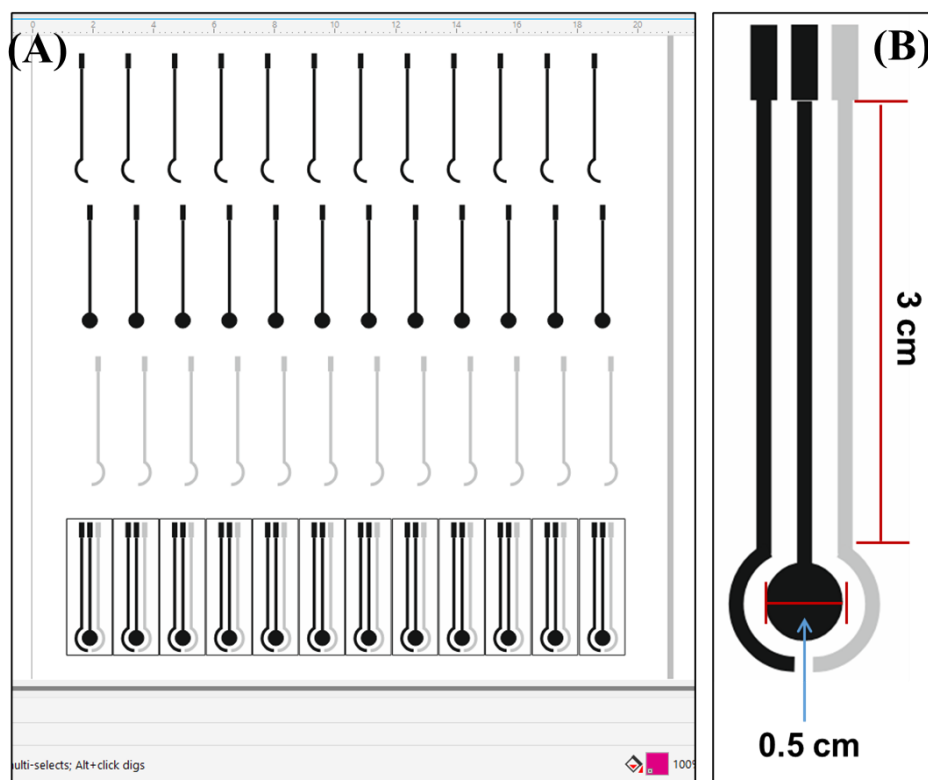


Figure 2.1. (A) Photograph of the Corel Draw sheet showing the patterns of the SPE designed for screen printing, and (B) A magnified view of the SPE showing the dimensions and length of the working electrode.

The 3-electrode assembly was printed onto paper to fabricate an SPE, wherein the C5 ink was used to print the WE, the CE was printed using commercial graphite ink, and the RE was printed by commercial Ag/AgCl ink. Rectangular patterns of size $2 \times 1 \text{ cm}^2$ were also printed for conductivity studies. These patterns were cut into smaller strips of $1 \times 1 \text{ cm}^2$ size for conductivity measurements. The results of screen printing of the C5 ink have been provided in **Chapter 5**.

2.6 Characterization Techniques

Many techniques were utilized for characterization of the conductive inks and the resulting paper-based conductive electrodes. The cMWCNTs utilized in the study for

conductive ink preparation were characterized for chemical composition and size (diameter) via X-ray diffraction (XRD) and transmission electron microscopy (TEM), respectively. The conductive inks were characterized for flow properties via rheometry. The surface morphology of the conductive ink-coated paper electrodes was studied via techniques, such as scanning electron microscopy (SEM), field emission SEM (FESEM), and atomic force microscopy (AFM). The wettability of the paper electrodes was compared to bare paper by contact angle studies. X-Ray photoelectron spectroscopy (XPS) and Raman spectroscopic analyses were conducted to study the elemental and structural composition, and verify the presence of cMWCNT in the dried ink. The electrochemical analyses were conducted via EIS and CV.

2.6.1. X-ray diffraction

The X-ray diffraction (XRD) technique is a non-destructive technique utilized for studying the chemical composition, crystals phases, and determination of crystal structure [140]. This method can effectively deduce the crystallographic form and size (grain size) of crystalline materials, and can also determine whether a material (in powder form) is of polycrystalline nature. The wavelength of X-rays is in range with the interplanar distance (d) within a crystalline sample. Hence, upon incidence, they can either completely pass through or ‘deflected’ by the atoms arranged in a specific order within the crystal lattice. At certain angles, the X-rays interfere in a constructive manner leading to significant increase in the intensity of X-ray diffraction. This leads to the formation of distinctive intensity patterns for every unique crystalline compound. The constructive interference follows the Bragg’s law given by:

$$n\lambda = 2d_{hkl}\sin \theta \quad (\text{Eq. 2.1})$$

where, ‘ λ ,’ ‘ θ ’ and ‘ d ’ are the wavelength of electromagnetic radiation, diffraction angle, and lattice spacing in a crystalline sample, respectively (**Figure 2.2**).

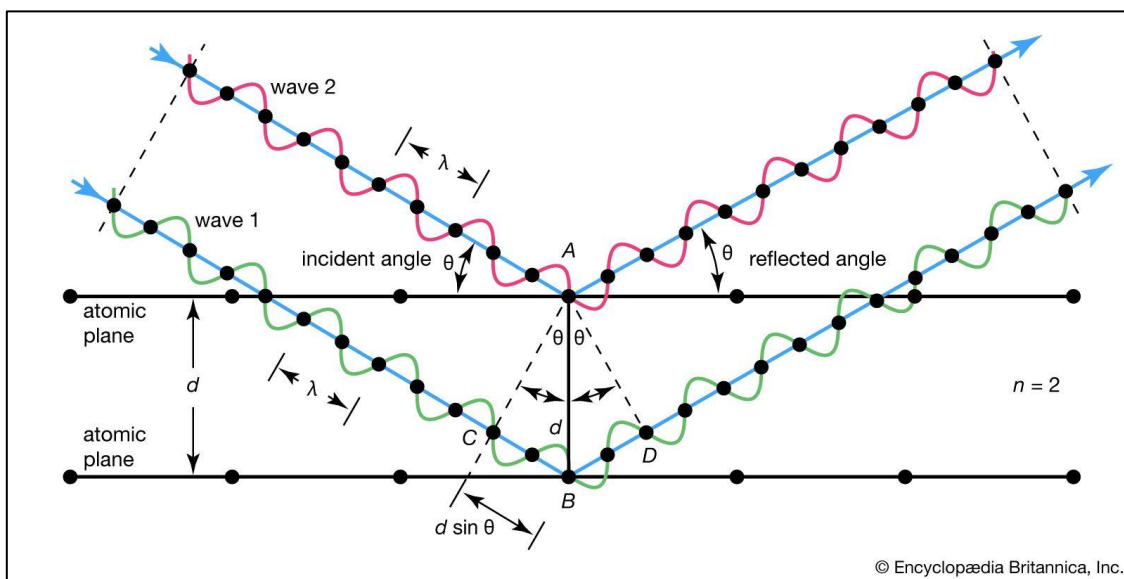


Figure 2.2. Diagram explaining Bragg's diffraction (principle of XRD) [141].

An XRD spectrum is recorded by an X-ray diffractometer that is composed of the following main components: i) the X-ray tube, ii) sample holder, and iii) X-ray detector. The filament in the X-ray tube produces electrons upon heating (thermionic emission), which are further accelerated by application of voltage towards the sample placed on the sample holder. The X-ray interference is recorded by the X-ray detector, which also converts the interference pattern into count rate given as the output.

A **Bruker D-8 Advance** instrument was utilized to record the XRD spectrum of cMWCNTs (**Figure 2.3(A)**), having Cu K α radiation, voltage, and current of X-ray tube of 1.54 Å, 40 kV, and 40 mA, respectively. An XRD spectrum of a quaternary nanocomposite- yttria-doped zirconia-reduced graphene oxide (rGO) (nYZR) is depicted in **Figure 2.3(B)**, wherein the standard peaks of both yttria-doped zirconia (planes labeled) and rGO (denoted 'R') are separately visible as reported in the literature. The XRD results of cMWCNTs have been discussed in **Chapter 3**.

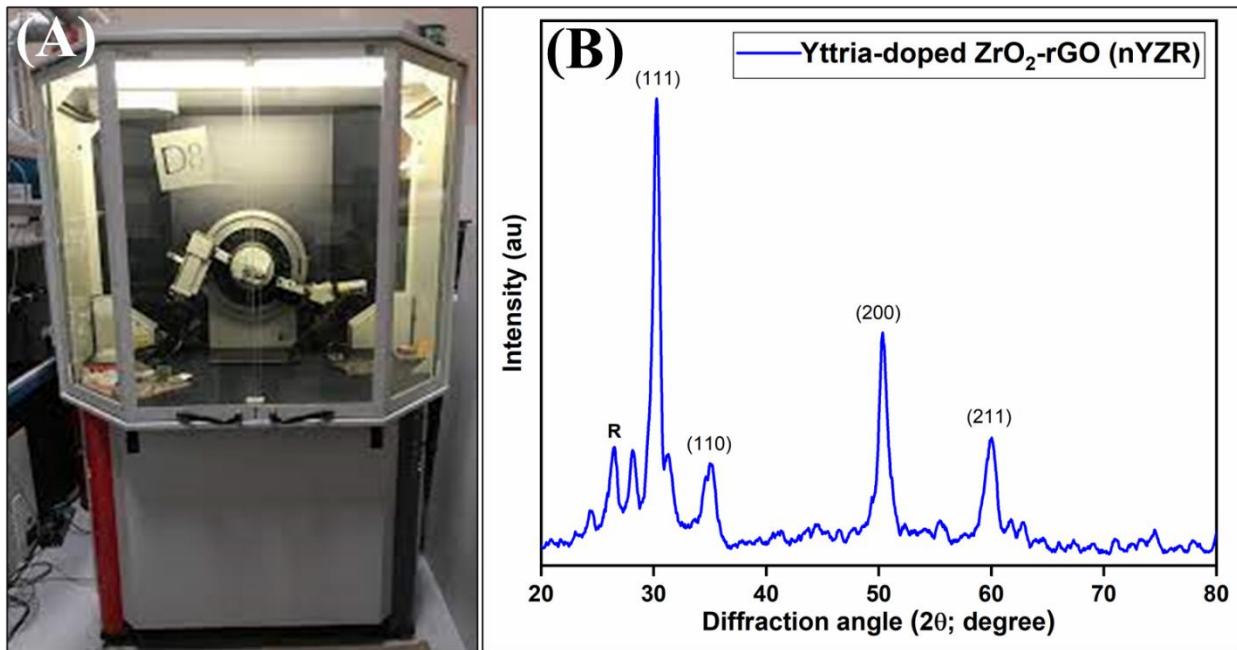


Figure 2.3. (A) X-ray diffractometer (Bruker D-8 Advance model), and (B) XRD spectrum of nYZR with peaks corresponding to the lattice planes of tetragonal yttria-doped zirconia (JCPDS 48-0224) [73].

Precautions:

- i. The thickness of the film under investigation should be sufficient to prevent contact of the X-rays with the substrates.
- ii. The powder should be ground well before analysis.
- iii. The sample quantity should be adequate to prevent noise in the recordings.
- iv. Shielding of the instrument should be effective to prevent accidental exposure to X-rays.

2.6.2. Transmission electron microscopy

Transmission electron microscopy (TEM) is a technique that utilizes high energy electrons to visualize the morphology of desired materials and provide precise information about their crystal structure and composition. Electrons have a much smaller wavelength than visible light, hence the magnification provided by TEM is several orders of magnitude higher

than regular microscopy. The magnification provided by TEM can reach up to 1000 k \times with a limit of resolution of as low as 1 nm (or less) [142, 143]. **Figure 2.4(A)** depicts a schematic diagram of the main components of a TEM instrument [143]. An electron gun generates an electron beam that is focused by electromagnetic lenses and metallic apertures in the TEM column. Since electrons can scatter and lose their energy upon interaction with air, the TEM instrument operates in high vacuum conditions. The electron beam is incident onto the sample placed on a specialized sample holder referred to as a TEM grid. A TEM grid most commonly consists of a circular Cu grid coated with a carbon film. Powder samples are dissolved in 30% ethanol or a suitable slow-evaporating solvent and placed onto a TEM grid for drying and analysis. Suitable sample thickness for TEM analysis should not exceed 100 nm [142]. The transmitted electrons from the sample are refocused and projected onto the detector screen after magnification to obtain a visual image. Crystal lattice fringes can also be visualized using parallel detectors in TEM. This thesis work entails the characterization of cMWCNTs via a JEOL JEM 3200 FS model TEM instrument at an accelerating voltage of 200 kV (**Figure 2.4(B)**). The results of these studies are discussed in **Chapter 3**.

Precautions:

- i. The solvent should be slow evaporating to prevent fast drying of the sample, which may lead to change in sample microstructure in some instances.
- ii. The sample should be dispersed homogeneously in the solvent before preparation of the TEM grid.
- iii. The sample thickness should be less than 100 nm ideally to allow proper electron transmission.

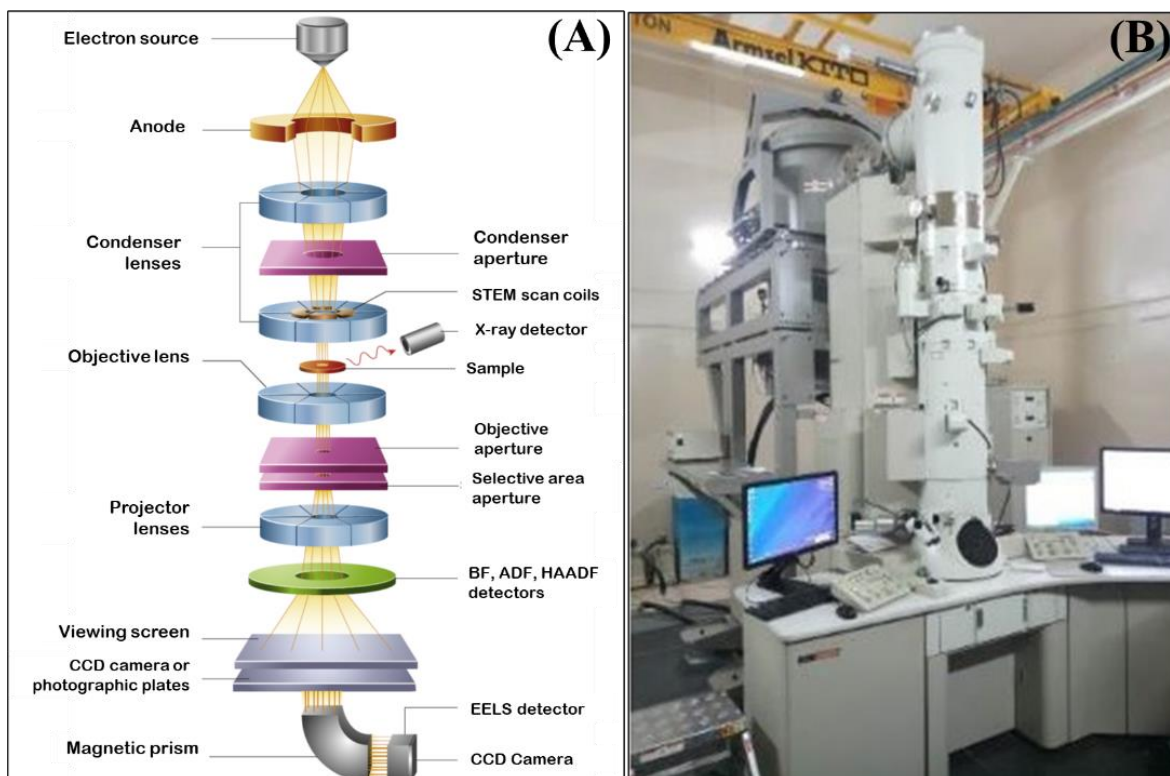


Figure 2.4. (A) A simplified schematic displaying the various components of a TEM instrument [143], and (B) A photograph of the JEOL JEM 3200 FS model electron microscope.

2.6.3 Scanning electron microscopy

This technique is a counterpart of TEM that is mostly utilized to visualize a desired material's surface morphology. It also uses high energy electron beams for visualization, hence displays better resolution than optical microscope but not as high as TEM. Contrary to TEM, multiple electron beams are focused on the sample (taped to a sample holder via carbon tape) as spots, ranging in size from 1-5 nm [144]. **Figure 2.5(A)** depicts a schematic representation of a SEM instrument. The electron source is generally composed of tungsten or lanthanum hexaboride. The electron beams are focused and directed to the sample through a set of apertures and condenser lenses. When the electron beams hit the surface of the sample, they can either be reflected, deflected at an angle, or/and back scattered. Different detectors collect

these electrons to form a final image after amplification. Non-conductive samples are often sputtered by Au before analysis to enhance secondary electron emission and hence, improve the resolution of imaging.

In this thesis, SEM studies were undertaken via a Zeiss EVO 18 model instrument (**Figure 2.5(B)**) to study the changes in surface morphology of paper after ink coating and subsequent modifications by MBs. The results of these studies are discussed in detail in **Chapters 3-5**. **Figure 2.5(C)** shows the SEM image of a paper substrate modified with CuO nanoparticles. These nanoparticles were grown *in situ* onto paper (Whatman filter paper) via hydrothermal method and were found to have a flower-like morphology upon further magnification.

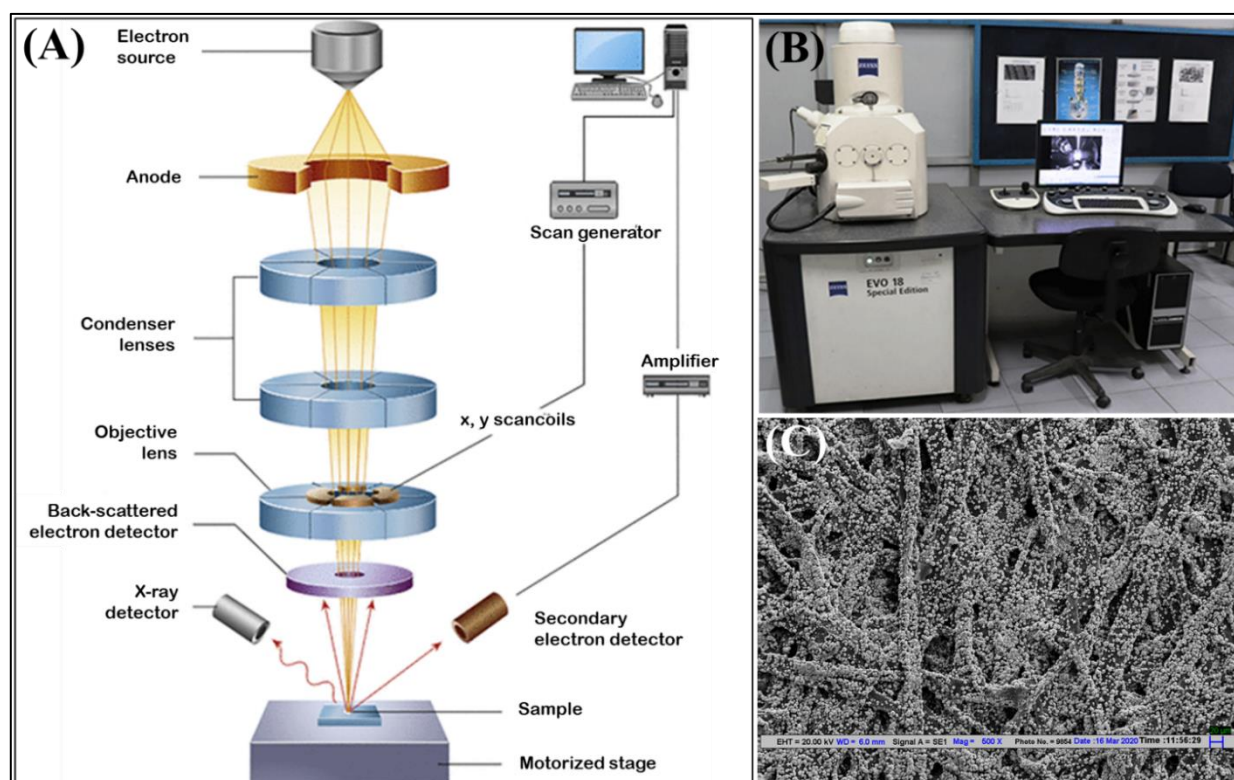


Figure 2.5. (A) Simplified schematic of a SEM instrument [143], (B) A photograph of the Zeiss EVO 18 model SEM instrument, and (C) SEM image of CuO nanoparticles grown onto paper.

Precautions:

- i. Non-conductive samples must be coated by a thin film (~5 nm) of a conductive metal like Au for proper analysis and imaging.
- ii. The samples should be dried to remove any surface adsorbed water molecules to improve resolution.
- iii. The sample size should not be more than $\sim 0.5 \times 0.5 \text{ cm}^2$.

2.6.4 Field emission scanning electron microscopy

Field emission scanning electron microscopy (FESEM) works on the same principles as SEM. However, a major difference between the two techniques is the method of electron generation. FESEM utilizes a field emission gun (FEG) that utilizes a potential gradient to generate electrons as opposed to thermionic emission in SEM. This enables FESEM to produce high resolution images of a desired material's surface topology at very low voltages. FESEM offers better resolution than SEM and hence, can be utilized to produce noise-free images of beam-sensitive materials such as paper.

In the present work, a JEOL JSM-7800F Prime electron microscope (**Figure 2.6(A)**) was utilized to study the surface of conductive ink-coated paper electrodes at an accelerating voltage of 10 kV. An FESEM image of one of the diagonal edges of the conductive ink-coated paper is shown in **Figure 2.6(B)**. The different layers of ink coating are almost visible in the image, which have engulfed and completely masked the cellulose fibers in paper. The detailed results of these studies are provided in **Chapter 4**.

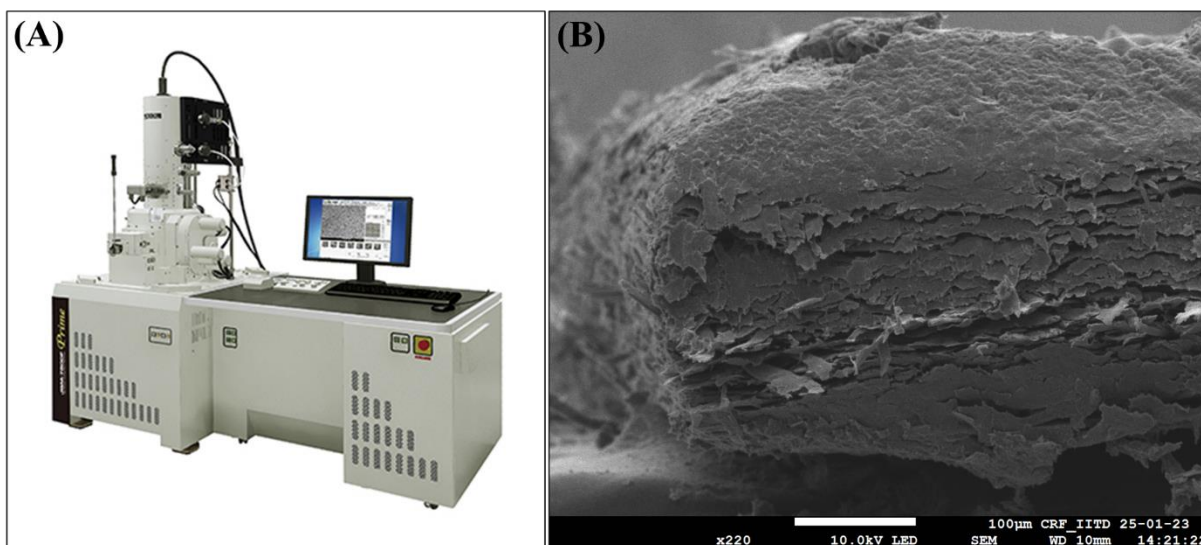


Figure 2.6. (A) Photograph of the JEOL JSM-7800F Prime model electron microscope, and (B) FESEM image of a diagonal edge of the conductive ink-coated paper showing the different layers of ink coated sequentially onto the paper substrate.

Precautions:

- i. Though sample charging is prevented because of low voltage, non-conductive samples should still be coated by a thin film (~5 nm) of a conductive metal like Au for good resolution.
- ii. The samples should be dried to remove any surface adsorbed water molecules to improve resolution.

2.6.5. Atomic force microscopy

Atomic force microscopy (AFM) is a powerful technique to image the surface topography of desired samples with sub-nm resolution [145]. It is also referred to as scanning force microscopy (SFM). The high resolution of this technique allows it to determine the surface roughness of a specific sample. Unlike electron microscopy, AFM can be used to analyze non-conducting samples without any modification. Additionally, it can operate in air and even fluid environments, enabling the imaging of biomacromolecules and their interactions

in the native environment [145, 146]. AFM works by scanning a sharp, tiny tip mounted on a flexible microcantilever onto the sample surface (**Figure 2.7(A)**). As the probe tip scans the surface, the cantilever is deflected depending upon the surface topology of the sample. This deflection translates to the positional change in laser beam reflection from the cantilever as monitored by a photodiode array detector. This enables the acquisition of a high-resolution 3D image of the sample surface.

AFM can operate under different imaging modes, viz. (i) the contact or static mode, (ii) intermittent contact (tapping) mode, and (iii) the non-contact mode. The contact mode was the first imaging mode to be developed [145]. As the name implies, the probe remains in contact with the sample throughout the analysis duration, wherein either the cantilever force or height (z-position) are kept constant and deflection is monitored with or without a feedback mechanism, respectively. This method is ideally suited for flat, hard surfaces. However, the image resolution may suffer due to damage to probe/sample or ‘slip-stick’ movement of the probe on the surface. In the intermittent (tapping) contact mode, the AFM probe oscillates at its resonant frequency, leading to contact/non-contact with the sample surface. The non-contact mode operates in a similar fashion, with the exception that the probe oscillates at a much lower frequency and is kept out of contact with the sample surface via a feedback mechanism. The change in oscillation frequency with change in interactions of the probe with the sample surface is recorded and an image is generated.

In this thesis, the surface roughness of the ink-coated paper electrode was compared to that of bare paper using AFM analysis. The analysis was carried out on an Asylum Research MFP3D-BIO-AFM instrument (**Figure 2.7(B)**). The results of the analysis have been discussed in **Chapter 4**.

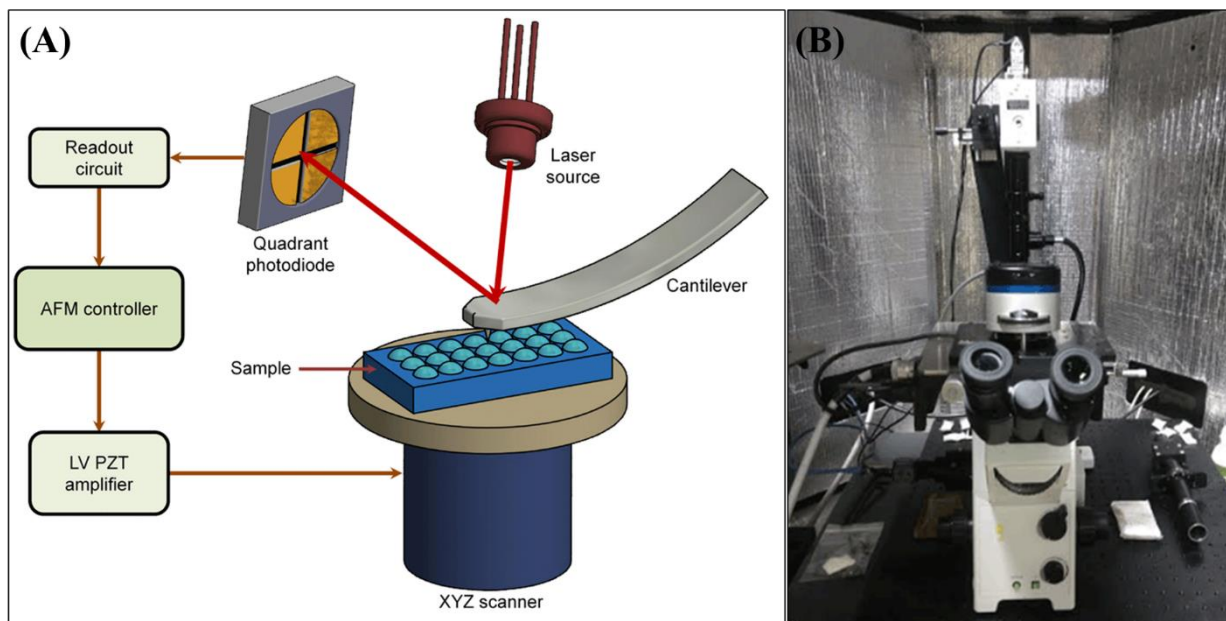


Figure 2.7. (A) Schematic representing the basic AFM instrumentation and working principle [147], and (B) A photograph of the Asylum Research MFP3D-BIO-AFM instrument used in this study.

Precautions:

- i. The samples should be stored in clean, dry conditions until analysis to reduce errors in surface roughness and height calculations.
- ii. The AFM probe should be cleaned before analysis to prevent contaminant-related errors.
- iii. The instrument should be mounted on a stable surface with no vibrations.

2.6.6. Raman spectroscopy

Raman spectroscopy is a physicochemical technique that elucidates the vibrational spectrum of desired material(s), which is also referred to as the ‘structural fingerprint.’ It is based on the principle of Raman effect, which describes the inelastic scattering of photons upon interaction with a specific material. The interaction of a monochromatic laser with molecules can result in change in the vibrational states of the electrons and eventually scattering of the laser light (**Figure 2.8(A)**). This scattering can be of two types: elastic (or Rayleigh scattering), which is the most observed, or inelastic (Stokes and anti-Stokes Raman scattering), which is

rarer but results in the change in wavelength of the scattered photons [148]. When the photons gain energy after interaction, it is said to be Stokes scattering and when they lose energy after interaction, it is said to be anti-Stokes scattering. Molecules having polar bonds are said to be Raman-active as their polarizability may change during the vibrations [148].

Near-infrared (NIR) sources are commonly used to prevent background fluorescence. Raman spectroscopy records the change in the frequency of the incident and scattered light photons, which is often recorded in wavenumbers ($\bar{\nu}$). Based upon the vibrational energy of molecules in a specific material, a spectrum is obtained generally within the range of 100-3000 cm^{-1} . A Raman spectrum is unique for a particular material, hence named as the structural signature. Raman spectroscopy can be utilized to differentiate between different carbon nanomaterials, despite having the same chemical composition. Raman spectroscopy was employed in this work to analyze dried ink and verify the presence of MWCNTs in the ink. The study was conducted on a Renishaw Invia II spectrometer using a 514 nm laser (**Figure 2.8(B)**). The results are discussed in **Chapter 3**.

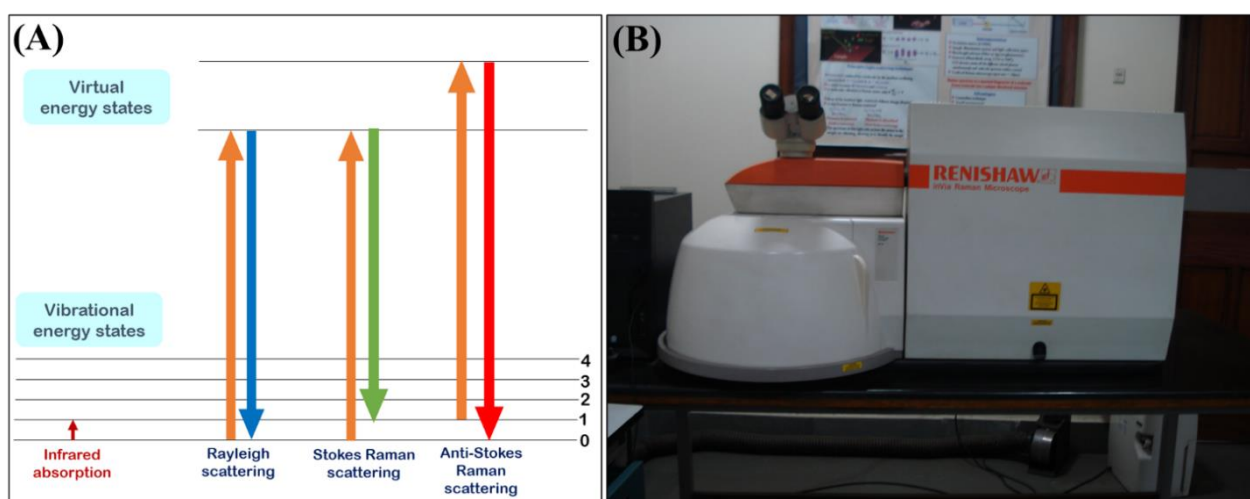


Figure 2.8. (A) Stokes and anti-Stokes Raman scattering as shown in an energy level diagram, and (B) A photograph of the Renishaw Invia II Raman spectrometer.

Precautions:

- i. The sample should be stored in a clean, dry environment before analysis to avoid contamination.
- ii. The laser spot size should be such that burning of the sample is prevented.

2.6.7 Contact angle studies

Contact angle refers to the angle at which a solid surface comes in contact with a liquid/vapor material. It is a quantitative measure of the wettability of a surface. Contact angle studies are important to understand the adhesive properties of a solid surface with aqueous or oily fluids [149]. In addition to determining the hydrophilicity/hydrophobicity of a surface, it helps in determining the surface energy, surface tension, and interfacial tension between two phases/materials. The Young equation is used to define the balance between the solid, liquid, and gas phases, given by:

$$\gamma_{SG} = \gamma_{SL} + \gamma_{LG} \cos\theta_c \quad (\text{Eq. 2.2})$$

where, γ_{LG} , γ_{SL} , and γ_{SG} , refer to the liquid/gas, the solid/liquid, and the solid/gas surface tensions, respectively, and θ_c is the contact angle (**Figure 2.9(A)**).

The main parameters that affect contact angle are surface microenvironment, roughness, and the type of material. A contact angle goniometer is an instrument that determines the contact angle of desired surfaces. One prominent methodology utilizes the sessile drop method to determine the contact angle. A liquid drop (mostly water) is placed on the surface of interest and its image is captured by the goniometer (**Figure 2.9(B)**). The image is then analyzed to determine the contact angle of the surface. A contact angle of $<90^\circ$ indicates good wettability and hydrophilicity of the surface under investigation, while $>90^\circ$ indicates hydrophobicity or low wettability. In this work, contact angle measurements were conducted using a DataPhysics OCA15EC instrument (**Figure 2.9(C)**) to determine the changes in wettability after

modification of paper by conductive ink. The results of this study have been discussed in detail in **Chapter 3**.

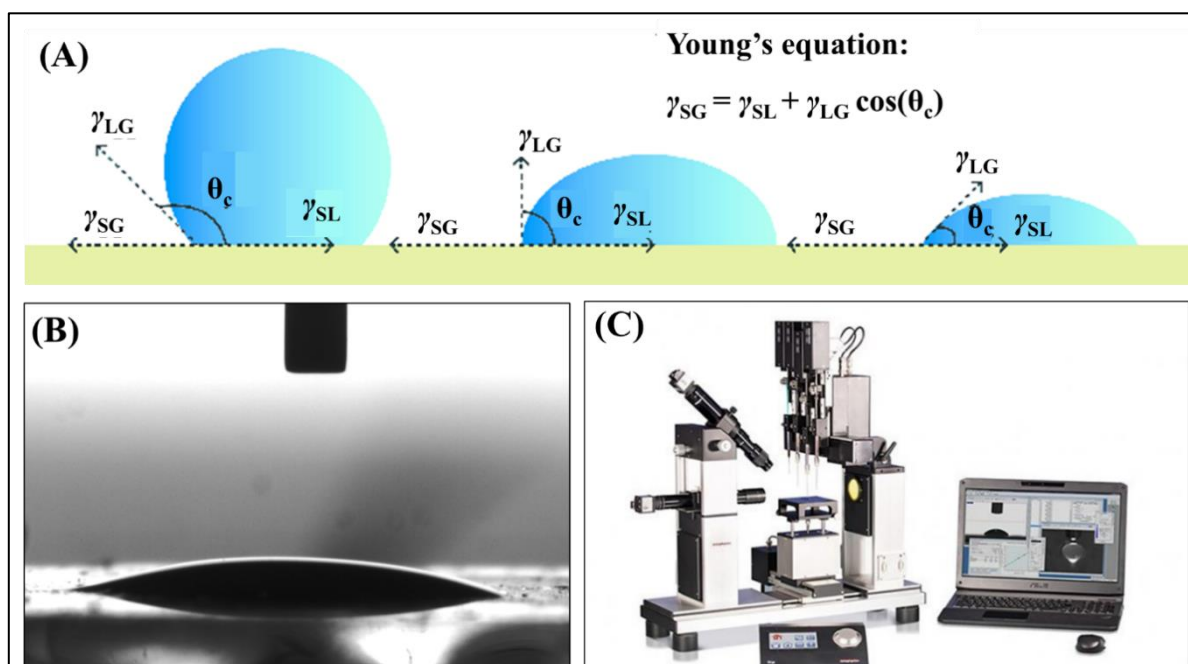


Figure 2.9. (A) Diagram illustrating the Young's equation and calculation of contact angle [150], (B) Image of a water droplet on an ITO electrode as taken by a contact angle goniometer. The shape of the droplet indicates that the electrode is hydrophilic in nature, and (C) Photograph of the Data Physics OCA15EC model contact angle measurement system.

Precautions:

- i. The liquid droplet should be stable on the sample before measurements.
- ii. The instrument should be kept in a humid-free, stable chamber having no vibrations.
- iii. The sample under investigation should be devoid of any contaminants/adsorbed water molecules to prevent errors in measurement.

2.6.8 X-Ray photoelectron spectroscopy

Based on the principle of photoelectric effect, X-ray photoelectron spectroscopy (XPS) is a powerful technological aid to deduce the elemental composition, chemical formula, binding energy, and electronic states of any given material [151]. Photoelectric effect is the phenomenon in which X-rays having specific energy (<1 keV), when incident on the surface of

a material, lead to ejection of photoelectrons from the surface atoms. The energy values of these photoelectrons are unique to the type of element present in the material and are measured by an electron energy analyzer. The resulting spectrum reveals peaks at certain binding energies which can be utilized to determine the electronic states of the atoms in the material under investigation. The binding energy is given by:

$$E_{\text{binding}} = E_{\text{photon}} - (E_{\text{kinetic}} + \phi) \quad (\text{Eq. 2.3})$$

where, ϕ refers to the work function whose value depends on the material type and the spectrophotometer. Additionally, the intensities of the peaks are used to estimate the concentration of a particular element in the given sample.

In this work, XPS experiments were conducted to study the elemental composition of the dried ink and to determine whether any microstructural changes were induced in the cMWCNTs during ink formulation. The studies were conducted on an AXIS Supra (Kratos Analytical Ltd.) instrument (**Figure 2.10**) with a dual Al $K\alpha$ /Mg $K\alpha$ achromatic X-ray source. The results of XPS studies have been discussed in **Chapter 3**.

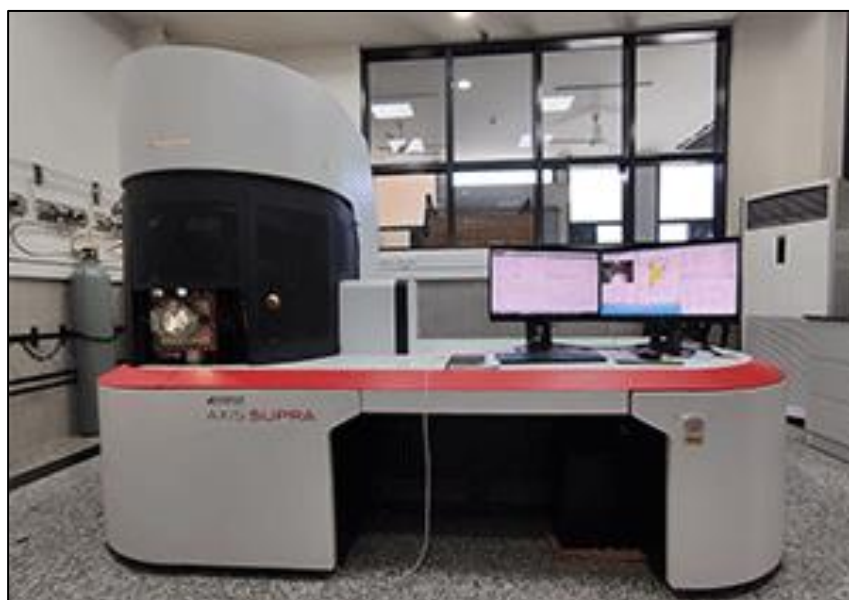


Figure 2.10. Photograph of the AXIS Supra model XPS instrument.

Precautions:

- i. The sample should be dry and stable in ultrahigh vacuum conditions.
- ii. The instrument should be kept in a humid-free, stable chamber having no vibrations.
- iii. Powder samples should be analyzed in pellet form.

2.6.9 Rheometry

Rheology is the science of the deformation and flow properties of fluids, while rheometry refers to the experimental techniques utilized for determining the rheological properties of fluids, including viscosity, shear stress, strain, and their correlation with each other. Based on the rheological properties, fluids can be said to be either Newtonian or non-Newtonian. Newtonian fluids have constant viscosity irrespective of the force applied. Water and honey are common examples of Newtonian fluids. While non-Newtonian fluids exhibit interesting behavior when force is applied to them. Some non-Newtonian fluids tend to get more viscous with increase in the force (or, shear rate) applied. These fluids are referred to as rheopectic in nature, e. g. cornstarch solution. Other non-Newtonian fluids deform upon application of force and their viscosity decreases with increase in shear rate. These are referred to as shear thinning/thixotropic fluids. Viscoelastic fluids tend to regain their viscosity after the removal of force after a certain time. Thus, rheological properties are directly related to the internal structure of fluids and intramolecular forces. Viscosity is also affected by temperature; higher temperatures lead to decrease in viscosity of the same fluid. Rheological analysis is important in determining the flow behavior of fluids, viscosity measurements, and understanding the internal microstructure and homogeneity of the fluid composition.

This work involves the rheological analysis of the conductive ink formulations, particularly their flow behavior. The change in viscosity with shear rate has been studied along with their viscoelastic behavior. The analyzes were conducted on an Anton Paar rheometer

with a parallel plate geometry (40 mm plate diameter) at 25 °C (**Figure 2.11**). The results are discussed in detail in **Chapters 3** and **4**. The following techniques were utilized in analysis:

a) Viscometry: It is conducted to determine whether a fluid is Newtonian or non-Newtonian in nature. The shear rate is increased in a specific range keeping the stress constant, and the change in the viscosity is measured.

b) 3-interval thixotropy test (3iTT): It is a rheological technique utilized to study thixotropic behavior of fluids and simulate the processes of printing, painting, etc. The viscosity is measured in three intervals: in the interval I, the viscosity is monitored for a fixed period at low shear rate, interval II involves an abrupt and significant increase in shear rate (simulation of printing) and monitoring of viscosity changes. The shear rate is restored in Interval III to the same value as that in Interval I and the recovery of viscosity is measured with time. This analysis reveals important information about the fluid under investigation and hints at its performance in real-life, e. g. issues like dripping or leakage issues during printing process, formation of uniform patterns, etc. are linked to the speed and percentage recovery in viscosity of the fluids. This test can also be utilized to optimize the rheology of fluids.

Precautions:

- i. The measurements should be made at constant temperature to avoid fluctuations.
- ii. The plate should not be touched during measurements.
- iii. The volume of the samples should be constant through different measurements and should be chosen wisely depending upon the plate size to avoid under/overflowing.



Figure 2.11. Photograph of the Anton Paar MCR 302 rheometer used in the study.

2.6.10 Conductivity measurement studies

Electrical conductivity refers to the measure of the ease of conduction of current (or, electrons) through a material. It is the inverse of resistivity, which refers to the resistance to the flow of current within a material having a unit length and a unit cross-section area. Mathematically, the resistivity (ρ) is given by:

$$\rho = RA/l \quad (\text{Eq. 2.4})$$

where, R is the resistance, A is the cross-section area, and l is the length of the material. Conductivity (σ), being the reverse of resistivity, is given by:

$$\sigma = 1/\rho \quad (\text{Eq. 2.5})$$

The units of conductivity are Siemens per meter ($S\ m^{-1}$), but is often given by $S\ cm^{-1}$ or $mho\ cm^{-1}$. The values of resistivity range from 10^{-8} to $10^{16}\ \Omega.cm$, classifying materials into

conductors (low resistivity), semiconductors (medium to high range resistivity), and insulators (high resistivity) [152]. A four-probe (4P) conductivity meter is used for ultrasensitive measurements of resistivity (and hence, conductivity) of desired materials [152]. In this method, four equidistant probes are arranged linearly (in-line) onto a sample (generally a film/solid) (**Figure 2.12(A)**). The two outer probes inject current (I) through the sample and the inner two probes measure the voltage drop (V) caused because of it. The slope of the curve of V vs. I yields the R value in accordance to Ohm's law (**Figure 2.12(B)**). The resistivity measurements by a 4P method are affected by the geometry and dimensions of the sample [152]. For semi-infinite bulks and infinite 2D sheets, the resistivity (ρ_o) is given by the following equation:

$$\rho_o = 2\pi S (R) \quad (\text{Eq. 2.6})$$

where, S is the distance between the probes (in cm). However, for samples where thickness (t) of the sample in consideration is negligible compared to the probe distance ($t \ll S$), an error factor (G') is introduced which is given by,

$$G' = \frac{2S}{t} \ln 2 \quad (\text{Eq. 2.7})$$

and the resistivity of the sample (ρ) is given by,

$$\rho = \rho_o/G' \quad (\text{Eq. 2.8})$$

In this work, a 4P in-line conductivity meter (SES Instruments Pvt. Ltd., India) was used to determine the conductivity of the conductive ink-coated paper electrodes (**Figure 2.11(C)**). The probe distance (S) was 0.2 cm and sample size taken was $1 \times 1 \text{ cm}^2$. All measurements were conducted at 25 °C (maintained by a temperature controller). The above equations (**Eq. 2.5-2.8**) were utilized for determining the conductivity values. The results of these studies are detailed in **Chapters 3-5**.

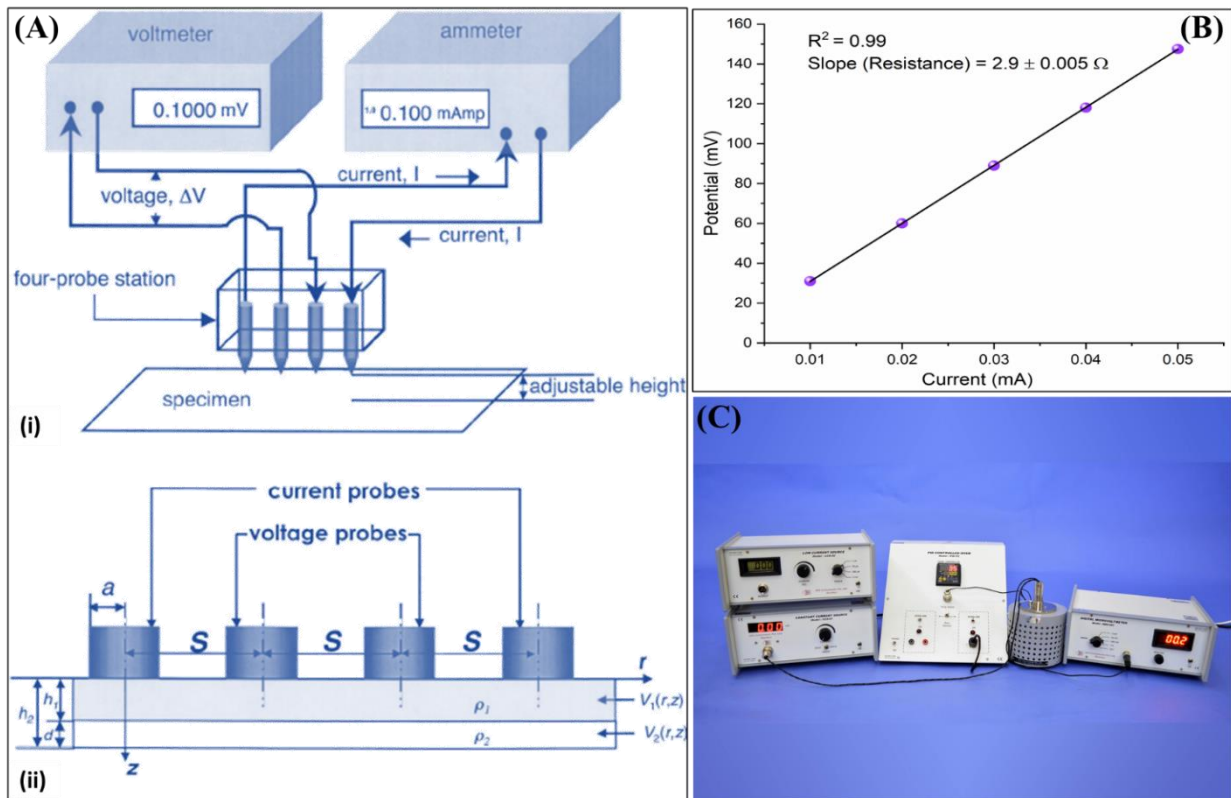


Figure 2.12. (A) (i) Schematic diagram of the 4-probe (4P) conductivity meter, and (ii) the magnified view of the four probes showing the interprobe distance, S [153], (B) A V vs. I curve of the cMWCNT@paper electrode used for calculating resistance, R , of the electrode, and (C) A photograph of the conductivity meter (SES Instruments Pvt. Ltd.) used in the study.

Precautions:

- i. The probes should not be placed on the edge of the sample as it may vary the recorded values.
- ii. The outer probes should be equidistant from both edges of the sample.
- iii. The probe tips should be cleaned before use to avoid measurement errors due to contamination.
- iv. The probe tips should be gently placed over the sample to prevent sample damage and should be in contact with the sample throughout measurements.

2.6.11 Agarose gel electrophoresis

Agarose gel electrophoresis is a powerful molecular biology technique to resolve DNA and RNA molecules (and other oligonucleotides) according to their molecular size. It is also used in visualization and rough estimation of the size of amplification products obtained after PCR and other NAATs. In this method, DNA/RNA samples are loaded onto agarose gel and immersed in a running buffer (mostly Tris acetate EDTA, TAE or TBE buffer). An electric field is applied to the gel and the samples are allowed to migrate through the pores in the gel for a fixed period. The DNA molecules migrate to different distances depending upon their molecular size: the larger molecules migrate the slowest and the smaller molecules migrate to farther distances. The shape of the DNA can also affect the migration distance: single stranded DNA (ssDNA) migrates faster than linear double stranded DNA (dsDNA), which in turn, migrates faster than coiled DNA. A DNA ladder, consisting of DNA molecules of specific different molecular sizes, is run along with the samples to estimate the molecular size of the samples. However, prior information is required about the shape of the DNA molecules under investigation. A colored dye is used to track the migration of DNA samples in the gel to avoid running into the buffer. Ethidium bromide (EtBr), added in the gel at the time of its preparation, is used to visualize the separated DNA samples in the gel under UV irradiation. EtBr stacks with the nucleotide bases and fluoresces orange upon irradiation with UV light. A typical gel electrophoresis unit consists of a power supply for voltage application and a buffer tank (for gel immersion during run) along with electrode connections at two ends (**Figure 2.13(A)**). The direction of movement and resolution of DNA molecules based on size is shown in **Figure 2.13(B)**.

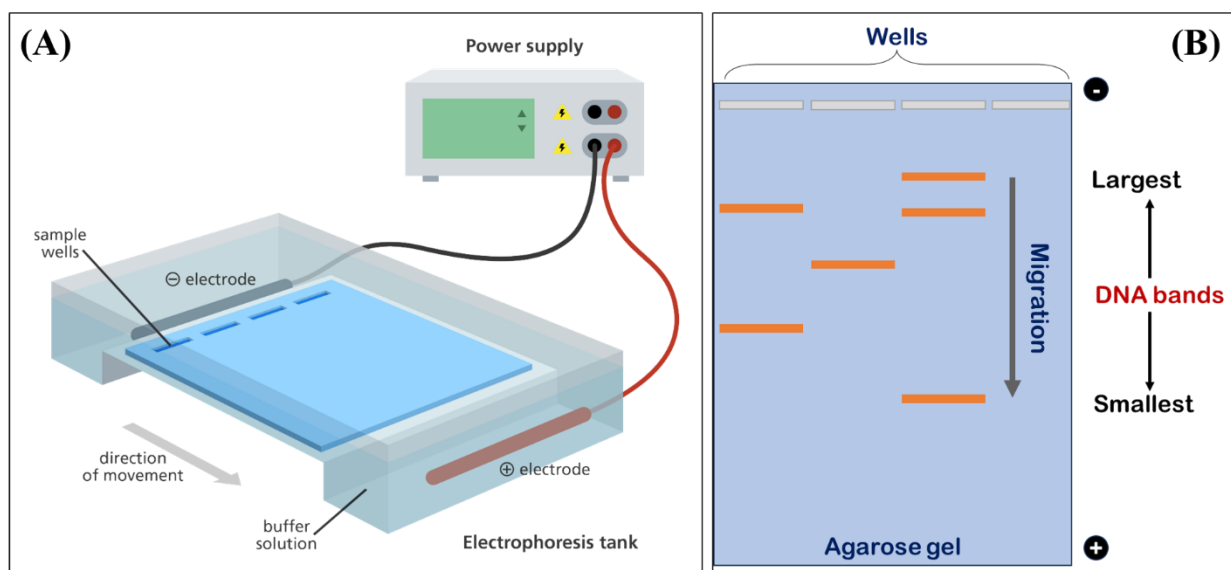


Figure 2.13. Schematic diagram depicting (A) a typical gel electrophoresis unit [154], and (B) direction of movement of DNA molecules in the gel and their separation based on molecular size.

In this thesis work, gel electrophoresis experiments were conducted to determine the formation of supersandwich DNA structures, and the optimum temperature for the same. Briefly, 10 μL of equimolar concentrations (10 μM) each of capture (CP), target (TP), and supersandwich detector probes (SDP) were mixed in different tubes and incubated at 25 $^{\circ}\text{C}$ and 55 $^{\circ}\text{C}$ for 5, 10, and 15 min. A set of negative controls was also prepared (mixture of CP and SDP without TP) to determine that no cross-hybridization occurred between the CP and SDP. Three percent agarose gel was prepared in 0.5 \times TBE buffer and EtBr (0.5 $\mu\text{g}/\text{mL}$ gel) was mixed into it before casting into a plate. A gel comb was placed in the gel to prepare wells for sample loading. After setting, the gel was kept in the gel electrophoresis unit (BioRad) and immersed in buffer. Five microliters of each sample were mixed with 1 μL Coomassie blue dye (6 \times) and loaded onto different wells in the gel. A voltage of 90 V was applied to the gel for 20 min for migration of DNA samples within the gel. The gel was subsequently removed from the buffer tank and kept under UV irradiation for DNA visualization. The results of these experiments are discussed in **Chapter 4**.

Precautions:

- i. Buffer should be freshly prepared before electrophoresis.
- ii. The voltage value should not exceed 100 V to avoid overheating of gel.
- iii. The gel should be completely set before electrophoresis and should be immersed in buffer to prevent drying and clogging of pores.
- iv. Gel comb should be properly inserted in the gel to enable uniform size of all wells.

2.6.12 Electrochemical techniques

Electrochemical (or, electroanalytical) techniques utilize the principles of electrochemistry to study various physicochemical phenomenon, such as corrosion, interfacial chemistry, redox activity, etc. They can also be utilized to monitor changes (other than corrosion), such as immobilization of biomolecules, on the WE surface by measuring the change in current/potential with other parameters such as time, current, voltage, etc. at the WE surface. These techniques form the basis of all electrochemical biosensors, wherein they are applied for quantification of a specific analyte on a particular WE. In this work, electrochemical impedance spectroscopy (EIS) and cyclic voltammetry (CV) were performed to assess the performance and other characteristics (storage stability, reproducibility, etc.) of the conductive paper electrodes in a buffer system and measure the response of the electrodes to different concentrations of the TP and genomic DNA. The studies were conducted on an Autolab (PGSTAT 302N model, Metrohm, Netherlands) Potentiostat/Galvanostat (**Figure 2.14**), with Ag/AgCl as the RE and platinum (Pt) as the CE.



Figure 2.14. Photograph of an PGSTAT 302N Autolab (Metrohm, Netherlands) potentiostat/galvanostat [155].

(a) Cyclic voltammetry (CV)

CV is a potential sweep-based electroanalytical technique that measures the current change as a function of potential change [156]. The potential is swept in a cyclic manner with time, i.e., its value is first increased to a pre-set value and then cycled back to the initial value. The current is recorded between the WE and CE, while RE is utilized to keep the potential of WE always stable. The resulting I vs. V curve is referred to as a cyclic voltammogram. These voltammograms can yield important information such as identification of redox species, determination of redox potential of a chemical species, effects of physical phenomenon such as corrosion and biofouling, etc. [157].

In general, two types of processes can occur at the interface of WE and buffer in which it is immersed, i) Faradaic, and ii) non-Faradaic processes. The Faradaic process refers to the charge transfer at the WE-buffer interface that follows the Faradays's law. Faradaic process or

Faradaic current emerges when a redox reaction (exchange of electrons) takes place at the WE interface, i.e.,



where, O and R represent the oxidized and reduced forms of a chemical species, respectively, with n being the number of electrons exchanged. The Randles-Sevcik equation shows that the peak currents are not only correlated to the scan rate and concentration of the redox species, but also to the effective surface area of the electrode. Further, the difference between the two peak potentials (ΔE_p), is inversely proportional to the number of electrons exchanged per cycle (n), i.e.

$$\Delta E_p = E_{\text{panodic}} - E_{\text{pcathodic}} = 59/n \text{ mV} \quad (\text{Eq. 2.10})$$

So, for $n = 1$, the difference equates to 59 mV. However, in real systems this value may vary (generally > 59 mV) depending upon the features of the WE. In this thesis work, CV studies were undertaken to study the electrochemical stability of the fabricated conductive paper electrodes, biosensing performance, and interference analysis among other studies. Ferro-ferricyanide ($\text{Fe}(\text{CN})_6^{3-/4-}$) (5 mM in 0.1 M PBS buffer, pH 7) was used as the redox mediator ($n=1$) for analyzing the electrochemical behavior of the fabricated electrodes. Scan rate of 50 mV s^{-1} was applied for all electrochemical studies unless otherwise specified. All measurements were recorded in triplicates.

Precautions:

- i. The potential window for CV should be chosen as per the WE.
- ii. The distance between the WE and RE should remain constant to avoid measurements errors.
- iii. The electrode area immersed in the buffer should remain constant for all studies.

(b) Electrochemical impedance spectroscopy (EIS)

EIS is one of the more complex electrochemical techniques, efficient in evaluating the microstructure of an electrode and studying various interfacial characteristics of an electrochemical system. An electrochemical system can be considered as an electrical circuit, wherein the different components can be considered analogous to the elements of an electric circuit [158]. For example, the adsorbed ionic layer on the WE can behave as a resistance. However, there is an electric double layer of ions at the WE surface in real situations which is dynamic in nature and hence, may act as a capacitor (C_{dl}) in ideal systems (**Figure 2.15**). The different elements can be contributed by mass transfer processes, diffusion, and other physicochemical phenomena occurring at the WE surface [159]. For current to flow through the system, the resistance imposed by the WE/buffer interface and the buffer solution itself need to be overcome. Additionally, the charge transfer resistance (R_{ct}) should also be overcome for charge transfer to occur at WE surface. Mass transfer, which enables the movement of redox agents at the electrode surface from the bulk solution, adds another component of resistance referred to as Warburg impedance (W). Thus, the impedance (Z) caused by these multiple components at the WE surface, is what is determined by EIS. In this technique, an AC signal (sinusoidal potential) is applied to the WE leading to a phase shift. The impedance equation is given by:

$$Z = Z_0 (\cos\phi + i\sin\phi) \quad (\text{Eq. 2.11})$$

where, Z is the impedance vector, Z_0 is its magnitude, and ϕ is the phase shift between voltage and current.

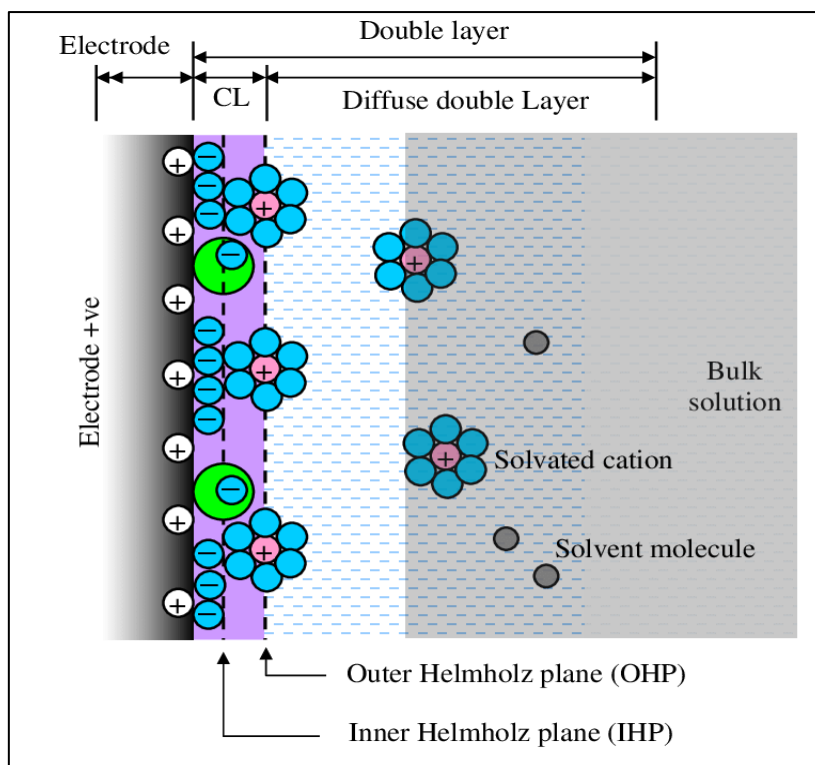


Figure 2.15. Diagram depicting an electric double layer formed at the working electrode in an electrochemical system [160].

Figure 2.16(A(i)) depicts a complex plane plot (known as ‘Nyquist plot’) of Z_{im} (imaginary value of Z caused due to capacitive current) vs. Z_{real} (caused by resistance elements in the system). A Nyquist plot is a perfect semicircular curve for circuits consisting of only R and C . The corresponding circuit explaining the plot is given in **Figure 2.16(A(ii))**. However, at low frequencies mass transfer/diffusion (W) dominates the electrochemical system that is given by a straight line at 45° (**Figure 2.16(B)**). The corresponding electrical circuit that is used to fit this curve plot is referred to as the Randles’ circuit. The diameter of the semicircle represents the R_{ct} value, while the horizontal shift from the origin is given as solution resistance (R_s). Higher the conductivity of the WE, smaller is the semicircle.

In real life systems, the C_{dl} does not act as a perfect capacitor and can also show resistance. Also, non-homogenous distribution of electroactive sites on the WE can also lead to pseudocapacitive behavior. In these cases, the W (or, C_{dl}) are often replaced by an element

known as the constant phase element (CPE, or Q).

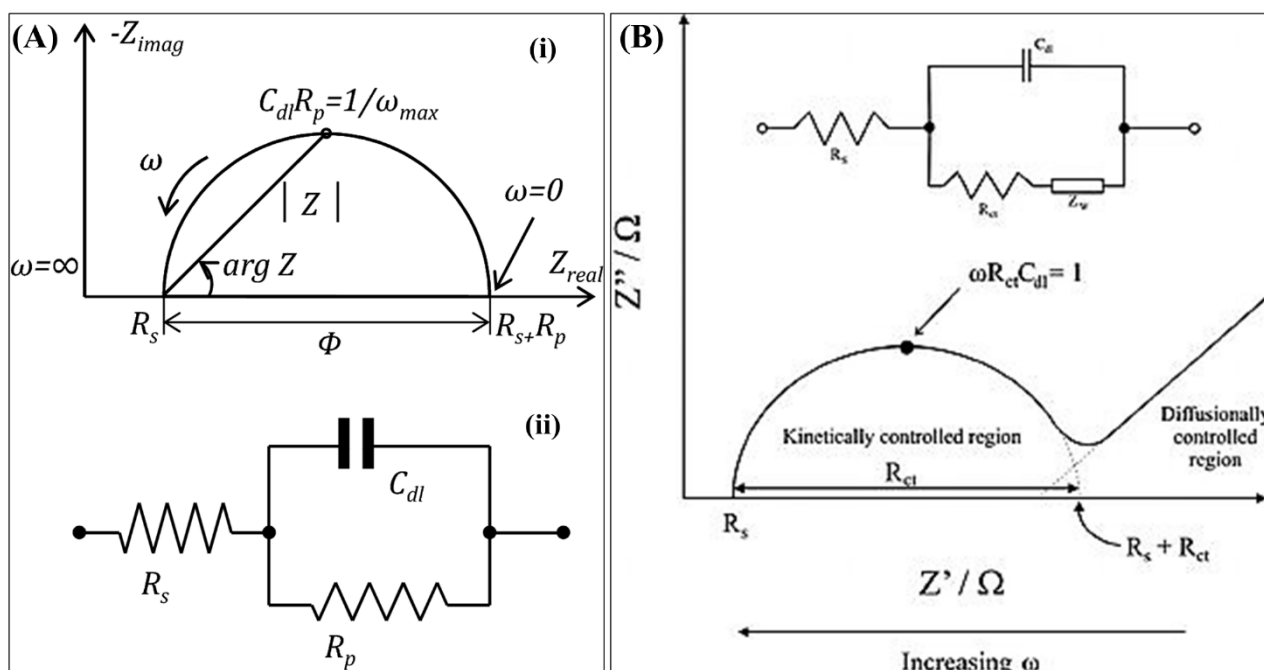


Figure 2.16. (A) (i) Representation of a Nyquist plot between $-Z_{imag}$ (capacitive Z) and Z_{real} (resistive Z) showing values of different parameters, including Z, R_s , R_{ct} , etc., and (ii) The corresponding electrical circuit explaining the different elements that contributed to the plot. (B) A Nyquist plot depicting the influence of Warburg impedance, W, and the corresponding equivalent circuit (known as the Randles' circuit) [161].

EIS has wide applications in understanding the WE microstructure, mass transfer processes, and has been widely used in bioanalysis and biosensing [158, 161]. A primary advantage of using EIS as transducing modality in biosensors is that EIS is a label free and non-destructive technique to quantify various electrode parameters. Other than the R_{ct} , heterogeneous electron transfer rate constant (K_0) of a specific electrode material can also be determined using the following equation:

$$K_0 = RT/n^2F^2A R_{ct}C \quad (\text{Eq. 2.13})$$

where R is the gas constant, T is absolute temperature (in K), F is the Faraday's constant, A is the electrode area ($= 1 \text{ cm}^2$), R_{ct} is the charge transfer resistance obtained from the Nyquist plot, C is the bulk concentration of redox probe (in M) and n is the number of electrons transferred

per redox molecule. The K_0 determines the rate at which an electron gets transferred from the redox molecule to the WE/buffer interface. Thus, this value can determine whether a particular electrode material is electrocatalytic or not.

In this study, EIS was employed for characterization of the ink-coated paper electrodes and their performance in label free biosensing studies based on supersandwich hybridization assay. All EIS studies were conducted in PBS (pH 7; with 5 mM ferro-ferricyanide). The open circuit potential (amplitude) was 0.1 V for all studies and the EIS response was measured in the frequency range of 0.1-10⁵ Hz. The results of these studies have been discussed in **Chapter 4**.

Precautions:

- i. The contact of the WE with the potentiostat should not be rusted.
- ii. The electrode area in buffer contact should be constant during all measurements
- iii. The buffer should not be stirred during the measurements.

2.7. Magnetic bead-assisted DNA hybridization assays

2.7.1 Significance of magnetic beads in assays

Magnetic beads (MBs) have found a significant role in clinical diagnostics, particularly molecular assays. MBs are mostly composed of superparamagnetic iron oxide (Fe₂O₃), which can range in size from a few μm to a few nm (nanoparticles). These magnetizable particles can be surface-modified to introduce various functional groups such as -NH₂, -COOH, -epoxy, -avidin, etc. These modifications enable MBs to selectively capture biomolecules, including nucleic acids, proteins, and even living cells. Thus, they have been efficiently used in molecular assays in sample enrichment, i.e., specific capture of biomolecules from a mixture of different substances [162]. Apart from molecular diagnostics, MBs have been utilized in various applications, including DNA extraction and amplification, DNA sequencing, immunoassays, cell sorting, protein purification, etc. [163]. More recently, MB-based assays are being

integrated with biosensing platforms for faster and quantitative analysis [164-166].

MBs enable rapid and highly specific capture of target analyte (owing to the availability of target-specific biomolecules on MB surface), which is one of the advantages of using them in molecular diagnostics. MB-based assays enable easy handling, can also be automated, and are compatible with a diverse array of sample types and volumes [163]. The use of MBs can also reduce cross-contamination and non-specific binding of molecules as they can be washed several times while retaining the molecules of interest bound on their surface.

In this thesis work, commercially procured carboxylated MBs (~1 μm in size) were utilized for immobilization of capture probes (CP and SCP) and subsequent capture of TP and formation of the CP-TP-DP hybridization complexes. We further integrated modified MBs with the ink-coated paper electrodes for biosensing studies and real sample analysis.

2.7.2 Immobilization of capture probes onto MBs

Immobilization of bioreceptor is one of the most important parts of biosensor design as it directly affects the sensitivity and specificity of the biosensor. The principles of different types of immobilization methods have been discussed in **Section 1.4.3 (Chapter 1)**. In this study, the capture probes for the traditional sandwich (CP) and supersandwich (SCP) were immobilized onto the MBs via indirect avidin (Av)-biotin affinity method and the direct EDC-NHS chemistry-based method, respectively.

Prior to immobilization, 10 mg MBs were first washed with 0.1 M NaOH for 10 min (3 \times) followed by washing with MilliQ water (3 \times) with slow tilt rotation to remove excess NaOH. The detailed protocols are as follows:

a) Avidin-biotin affinity-based immobilization: For this methodology to work, the CPs used in the study were biotinylated at the 5' end and Av was immobilized onto MBs via EDC-NHS chemistry (the amine groups of Av would form covalent bonds with carboxyl

groups on the MBs). For Av immobilization, freshly prepared solutions of EDC ($50 \mu\text{g mL}^{-1}$) and NHS ($150 \mu\text{g mL}^{-1}$) were added to the washed MBs ($100 \mu\text{L}$ final volume). The MBs were then incubated at room temperature for 30 min on slow tilt rotation. The thus activated beads were then washed again with MilliQ water (1 mL ; $3\times$) to remove any unreacted and excess EDC/NHS and their derivatives. Av was then added to the beads ($100 \mu\text{g}$ avidin per mg of beads) and the volume was made up to $100 \mu\text{l}$ by sterile MilliQ water. This mixture was allowed to incubate at room temperature for 2 h to yield MBs covalently linked with avidin via amide bond formation. The resulting Av/MBs were washed with 0.1% BSA and PBS (pH 8) to block any non-specific sites on the MBs, and redispersed in MilliQ water to a final MB concentration of 10 mg mL^{-1} . The thus formed Av/MBs complexes were stored at $4 \text{ }^\circ\text{C}$ and used within a day of storage.

After this, the CP (5'-biotin, 1800 pmol/mg beads) molecules were added to the Av/MBs and allowed to incubate at room temperature for 10 min with slow tilt rotation. The thus modified Av/MBs were washed with MilliQ water ($3\times$) and redispersed in MilliQ water for further studies. The C/Av/MBs were not stored for more than 24 h after preparation. The results of related electrochemical studies have been provided in **Chapter 3**.

b) EDC-NHS chemistry-mediated immobilization: For this method, the SCP molecules were modified with an NH_2 -C6-spacer molecule at the 5' end. Six thymine residues (T) were also attached after the amine-functionalized spacer to increase the spacer length. The avidin-biotin method was replaced with this direct method to: i) reduce total pre-analysis time, and ii) reduce the net cost of the analysis. This also ensured the removal of an extra protein layer from the MBs (avidin), which might have led to varied results in EIS (variations in the amount of the avidin molecules immobilized on MBs might interfere with the electrochemical signal and lead to erroneous results.)

In this method, freshly prepared EDC (50 mg mL^{-1}) and NHS (150 mg mL^{-1}) were added

to washed MBs (final volume 100 μL), which were then incubated with tilt rotation mixing at room temperature for 45 min. Thereafter, thus modified MBs were washed with DI water ($5\times$) to remove extra EDC/NHS and were incubated with SCP (2000 pmol/mg MBs) with mixing at room temperature for 1 h. The SCP-modified MBs (SCP/MB) were washed with DI water ($5\times$) to remove non-specifically bound and unbound SCP. This was followed by blocking with 0.1% BSA and PBS (pH 8). The thus prepared SCP/MB were stored in MilliQ water with a final concentration of 10 mg mL^{-1} at $4\text{ }^\circ\text{C}$ and were used within 24 h of preparation. The results of corresponding electrochemical studies are discussed in **Chapter 4**.

2.7.3 Electrochemical MB-assisted hybridization assay

After immobilization of the capture probes onto MBs, the hybridization assays (traditional and supersandwich) were performed to capture different concentrations of TP (*porA* pseudogene sequence) via complementary base pairing followed by sandwich (or, supersandwich) formation by the addition of DP (or, SDP). To avoid confusion, the detailed protocols for the hybridization complex formation and further biosensing analyzes are provided in the respective chapters (**Chapters 3 -5**).

The different parameters that were determined to evaluate the performance of the fabricated paper-based biosensing platforms are as follows:

- (i) **Linearity or linear range:** The dynamic range within which the biosensor response can be fit into a linear equation, $y = mx + c$, is referred to as the linear range. The linear range was determined by plotting the signal response vs. concentration of the TP and fitting the resulting data points in a linear equation. An R^2 value of 0.9 and above is considered a linear response.
- (ii) **Sensitivity:** The sensitivity (change in the signal response per unit concentration) was determined by the slope (m) of the calibration curve of the biosensor.

- (iii) **Limit of detection:** The following equation was utilized to calculate the limit of detection (LOD, or detection limit):

$$\text{Detection limit} = 3\sigma/m \quad (\text{Eq. 2.14})$$

where, m is the sensitivity of the biosensor and σ is the standard deviation in the biosensor response to blank (negative control).

- (iv) **Specificity:** The specificity was assessed by recording the biosensor response to the genomic NG DNA and then comparing it to the response obtained after mixing with DNA from other bacterial species (**Section 2.8**).
- (v) **Response time and stability:** The amount of time taken by the biosensing platform to reach a stable signal response to a specific TP concentration was determined via electrochemical analysis (CV and EIS). Stability is defined as the ability of the biosensor to produce a stable response to a specific TP concentration for a fixed duration.
- (vi) **Reproducibility:** All experiments were conducted in triplicates and three recordings were made for every concentration every time. The results were shown as mean of 3×3 (= 9) measurements.

2.8. Real sample analysis and specificity studies

The performance of the electrochemical biosensing platform towards genomic DNA detection was evaluated as an indication to its clinical applicability. For this purpose, NG genomic DNA was first extracted using one of two methods: commercial QIAGEN DNA extraction method and the boiling method. In the commercial method, the DNA was extracted from cultured NG cells (WHO M strain) using a set of standardized buffers, including the resuspension buffer, lysis buffer, proteinase K and RNase H, and finally chilled ethanol/isopropanol. The DNA was filtered through filters (obtained in the commercial kits) using buffers to improve purity.

The boiling method of DNA extraction is a crude yet simple and faster method for DNA

isolation. It is also cost effective; hence it is commonly preferred over the commercial kit methods in clinical labs. Firstly, a few bacterial colonies were diluted with sterile MilliQ water (1 mL) and cell lysis was induced by incubating the bacterial suspension at 90 °C for 1 h. The thus lysed cells were centrifuged at 1200 rpm for 5 min to precipitate out the cell debris. Thus obtained supernatant consisted of DNA and was stored at -20 °C till further use. DNA extracted using boiling method has lower purity than DNA extracted from commercial kits. It is because the boiling method does not completely remove RNA and other contaminants such as proteins from the lysed cells.

The DNA molecules extracted both by commercial and boiling methods were diluted to different concentrations using MilliQ water and stored at -20 °C until further analysis. Different concentrations of the extracted NG genomic DNA were subjected to ultrasonication for 10 min for shearing into smaller by bath ultrasonication. The sheared DNA molecules were then denatured at 95 °C for 5 min. Thereafter, the protocols mentioned in **Section 2.7** were followed to determine the concentration of genomic DNA. The results were compared to those obtained by using similar concentrations of TP.

Clinical samples consist of DNA from other microorganisms and human cells, which can potentially add background noise to the detection signal. Proteins/RNA are also sometimes present as contaminants. Hence, non-gonococcal DNA from different bacterial species was utilized for interferent studies. In brief, DNA from different bacteria was extracted by the boiling method and mixed with gonococcal DNA (50:1 concentration ratio). The effect of the DNA interferents on the electrochemical signal was then observed using the protocols mentioned in the above paragraphs and **Section 2.7**. The bacterial species included in the study are: *Neisseria meningitidis* (NM), *Neisseria sicca* (NS), *Neisseria mucosa* (NMu), *Escherichia coli* (EC), *Lactobacillus fermentum* (LF), *Chlamydia trachomatis* (Ch), *Staphylococcus aureus* (SA), *Enterococcus faecalis* (EF), *Klebsiella pneumoniae* (KP), *Ureaplasma urealyticum* (U),

and a cocktail of all these bacterial DNA (M). BSA was used as an interferent protein. The results of these studies have been discussed in **Chapters 3 and 4**.

The following chapter deals with the fabrication of conductive paper by coating of a cMWCNT-based conductive ink, and its further utilization for traditional DNA hybridization-based electrochemical detection of *porA* pseudogene sequence of NG.

Chapter 3
Carbon Nanomaterial-Modified Conductive
Ink for Paper-Based Electrochemical
Detection of Neisseria gonorrhoeae

3.1. Introduction

Paper-based electrochemical devices have been developed toward the detection of analytes such as cancer biomarkers, proteins, and DNA [24, 30, 31, 167, 168]. Development of paper-based diagnostics does not require a clean room facility, which subsequently leads to reduces costs of production and ease of use.

Electrochemical paper biosensors are cost effective, sensitive, and yield quantitative results within a short period (few seconds to few minutes) [15]. Many methods utilized for modifying the paper matrix with conductive nanomaterials, such as *in situ* polymerization/growth, dip coating, etc. are not scalable and may yield unreliable results in terms of distribution of conductive networks [24]. Capillary flow is also one of the hindrances for electrochemical paper devices as the buffer can seep through the paper matrix leading to high background noise. Non-specific adsorption can also occur owing to the rough surface of paper matrices resulting in poor sensitivity. Additionally, the pores cannot be completely blocked as it may prevent the interaction of target analyte and redox probes with the electrode surface.

Conductive inks have been projected as an attractive method for the development of paper electrochemical biosensors [169, 170]. The ink properties, such as rheology, wettability, conductivity, etc. are modified easily to suit the desired application. Ink coating also modulates the porosity of the paper substrate [171]. Various printing techniques can be utilized to coat these conductive inks, including screen printing, inkjet printing, etc., which enables batch reproducibility and high-volume production [58, 172, 173].

CNMs such as MWCNTs are being increasingly used for conductive ink development. They possess excellent thermal and chemical stability, and can operate in different buffer conditions with a large potential window [58]. They are also cost-effective and have been

utilized for fabrication of printed biosensors, strain sensors, and pseudocapacitors [43, 58, 173]. Though conductive inks have wide applications in flexible and printed electronics [169-171], literature on conductive ink-coated, electrochemical paper biosensors for clinical diagnostics remains scarce [170, 172].

N. gonorrhoeae (NG) infection causes gonorrhea, a curable STI with nonspecific symptoms. Increased risk of HIV infection, infertility, epididymitis, neonatal ophthalmia, etc. are some of the serious health problems associated with gonorrhea [120]. This infection is highly under-reported and under-diagnosed in both developed and developing nations. Thus, there is need of a reliable and affordable screening device for gonorrhea detection.

This chapter contains results of studies conducted towards the fabrication of an MWCNT ink-coated paper biosensor for the electrochemical detection of *porA* pseudogene sequence of NG.

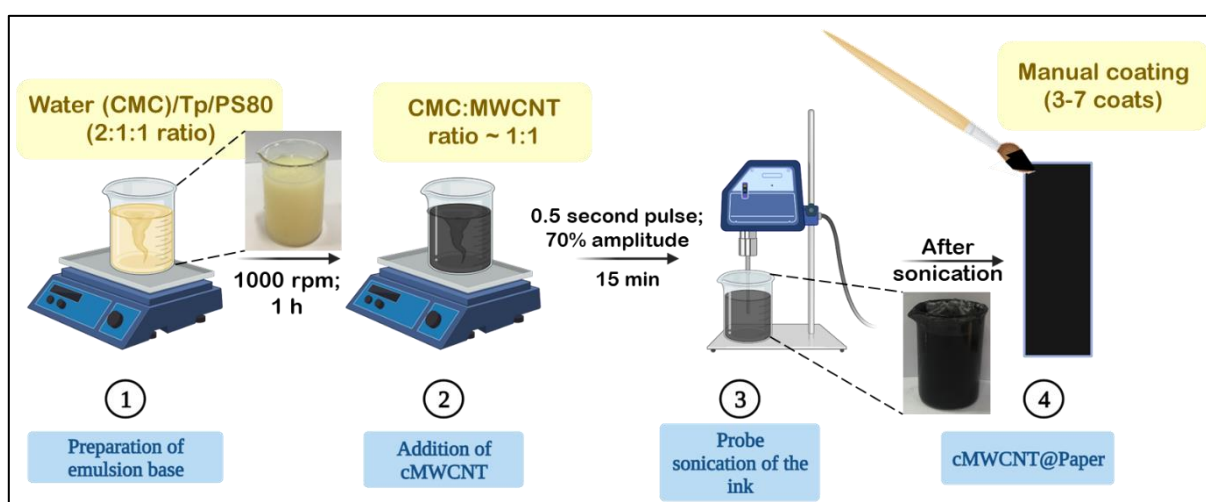
3.2 Experimental details

3.2.1 Conductive ink formulation

The desired ink formulation was accomplished by first dispersing CMC (1.5% w/v) in MilliQ water followed by mixing with Tp and PS80 (optimized ratio 2:1:1 (water: Tp: PS80)) (**Scheme 3.1**). The resulting emulsion was stirred at ~500 rpm for 2 h followed by addition of cMWCNTs (1 % w/v). This conductive emulsion was kept on magnetic stirring at ~1000 rpm for 1 h. Probe ultrasonication was used to homogenize the resulting conductive ink in an ice bath (0.5 s pulse; 70 % amplitude for 15 min). Overheating of the samples was prevented by pausing the ultrasonication after every 5 minutes. The thus obtained homogenous conductive ink was stored at 4 – 10 °C to prevent evaporation of the solvent.

3.2.2 Fabrication of MWCNT ink-coated paper electrodes

The MWCNT ink (75 μL per coat) was coated onto paper substrates ($2 \times 2 \text{ cm}^2$ in size) uniformly using a paint brush (Faber Castell No. 4) (**Scheme 3.1**). These MWCNT ink-coated paper electrodes were incubated within the temperature range of 80–130 $^\circ\text{C}$ for a period of 5–15 min. This was done to optimize the annealing temperature and time, and determine their effect on the conductivity. The number of coats (n) were also optimized to obtain desirable conductivity without compromising the adhesion of ink on paper. For conductivity studies, smaller strips ($1 \times 1 \text{ cm}^2$) of cMWCNT@paper electrodes were cut. After optimization, cMWCNT@paper electrodes of size $2 \times 1 \text{ cm}^2$ were fabricated for electrochemical studies. The electrodes were stored in dry conditions at room temperature till further use.



Scheme 3.1. Steps involved in the development of the conductive ink and the cMWCNT@paper electrodes.

3.2.3 Electrochemical magnetic DNA hybridization assay

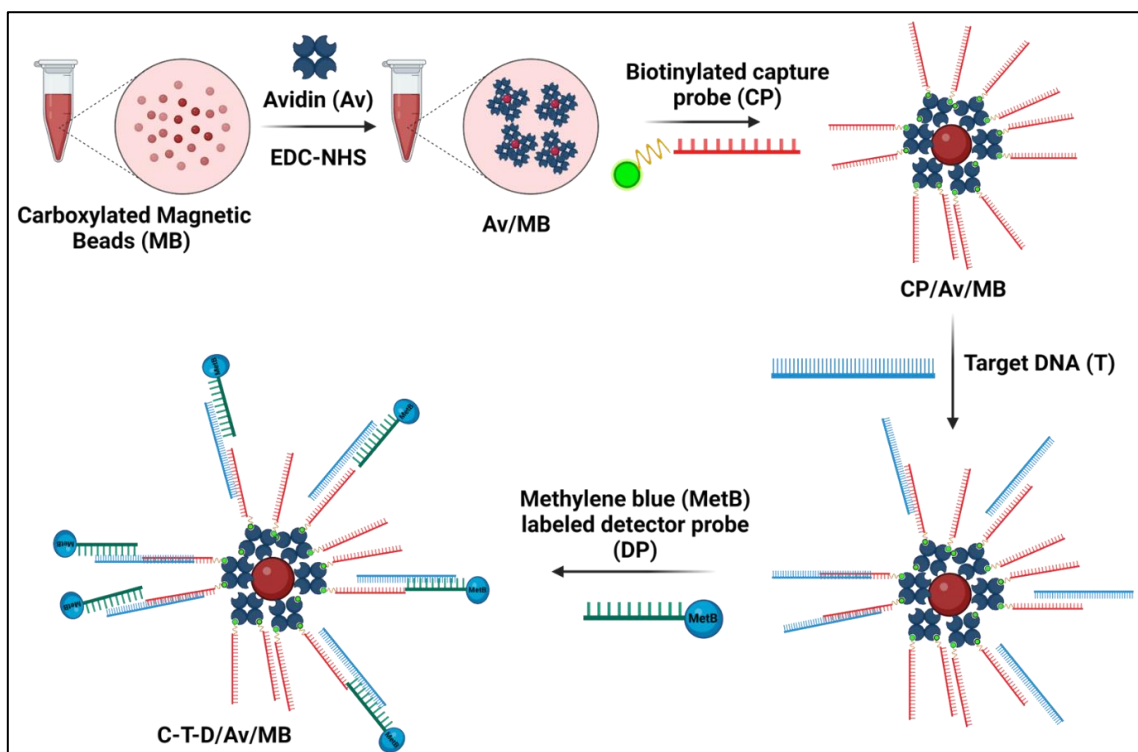
A set of DNA probes was selected and designed to specifically capture the target *porA* pseudogene sequence (labeled as TP for target probe) at two adjacent sites (**Table 3.1**). Biotin was utilized for labeling the capture probe (CP) at the 5' end and methylene blue was tagged at the 3' end of the detector probe (DP) for signal amplification. Specific capture and detection

of gonococcal DNA was conducted by developing an MB-assisted assay. The MBs were used primarily to separate TP from a mixture of other substances. While labeling of MetB on the DP would ensure signal amplification during the electrochemical detection.

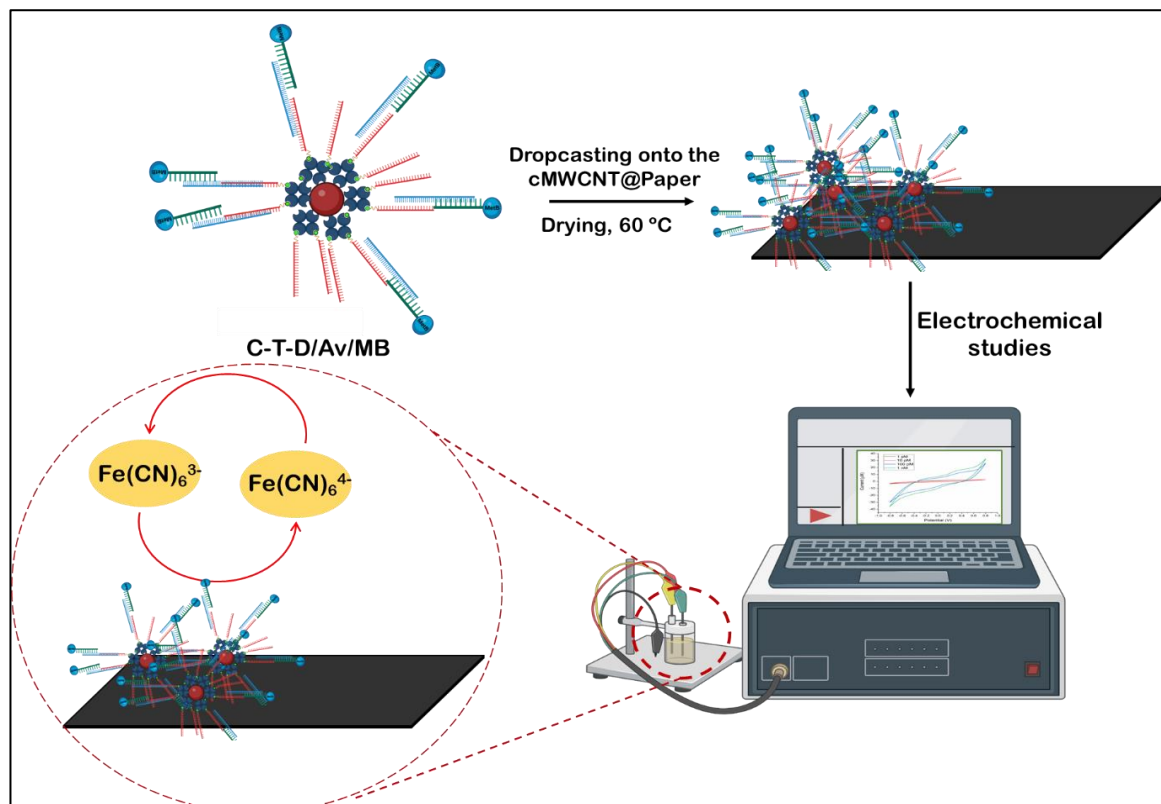
Table 3.1. DNA sequences of the biosensor oligonucleotide probes.

<i>Probe name</i>	<i>Probe ID</i>	<i>Sequence</i>	<i>Melting temperature (T_m; °C)</i>
<i>Capture Probe</i>	(CP)	5'Biotin-CCT GCT ACT TTC ACG CTG GA 3'	62
<i>Detector Probe</i>	(DP)	5'AAG TAA TCA GAT GAA ACC AGT TC-Met Blue 3'	62
<i>Target strand</i>	(T)	5'GAA CTG GTT TCA TCT GAT TAC TTT CCA GCG TGA AAG TAG CAG G 3'	65
<i>Non-complementary probe</i>	(NC)	5'TTG ATT GAG CGT CAT AGA TCG GAC GGC ACT AGT CAG TAC TCG A 3'	63

For the immobilization of CP on the MBs, avidin-biotin interactions were utilized. The detailed protocol for immobilization of CP on MB (CP/Av/MB) is given in **Section 2.7.2**. After the immobilization, CP/Av/MB probes were washed with Milli Q water and TP solutions (100 fM-100 nM) were mixed with the probes. This was followed by incubation at 60 °C for 15 min with tilt rotation. Subsequently, DP was added to the C-T/Av/MB assembly and incubated at 60 °C for 15 min with tilt rotation. This would ensure formation of a sandwich hybridization complex at the MB surface (C-T-D/Av/MB; **Scheme 3.2**). The probes were washed with MilliQ water (3-5 ×) after every modification to ensure removal of unbound probes. The resulting C-T-D/Av/MB probe complexes were dispersed in MilliQ water (30 µL). The MB-assisted sandwich structure was drop cast onto the cMWCNT@paper electrodes (1 × 1 cm²) and dried at 60 °C for 15 min. The electrochemical response of the modified cMWCNT@paper electrodes was analyzed by CV (**Scheme 3.3**).



Scheme 3.2. Schematic diagram depicting the various steps involved in the MB-assisted sandwich DNA hybridization assay.



Scheme 3.3. Schematic diagram depicting the integration of the MB-assisted DNA hybridization complex with the cMWCNT@paper electrodes for electrochemical analysis.

3.3 Results and discussion

3.3.1 XRD and TEM analysis

The XRD spectrum of the cMWCNTs used in this study shows a sharp peak centered at 26.2° , which corresponds to the (002) plane of carbon nanotubes (**Figure 3.1(A)**). Smaller peaks at about 43.4° and 54.2° were also observed, which correspond to (100) and (004) planes, respectively. The TEM image (**Figure 3.1(B)**) reveals that the average diameter of the nanotubes used in the study is 117.12 nm. **Figure 3.1(C)** shows a single nanotube having length exceeding in microns, indicating the high aspect ratio of the cMWCNTs.

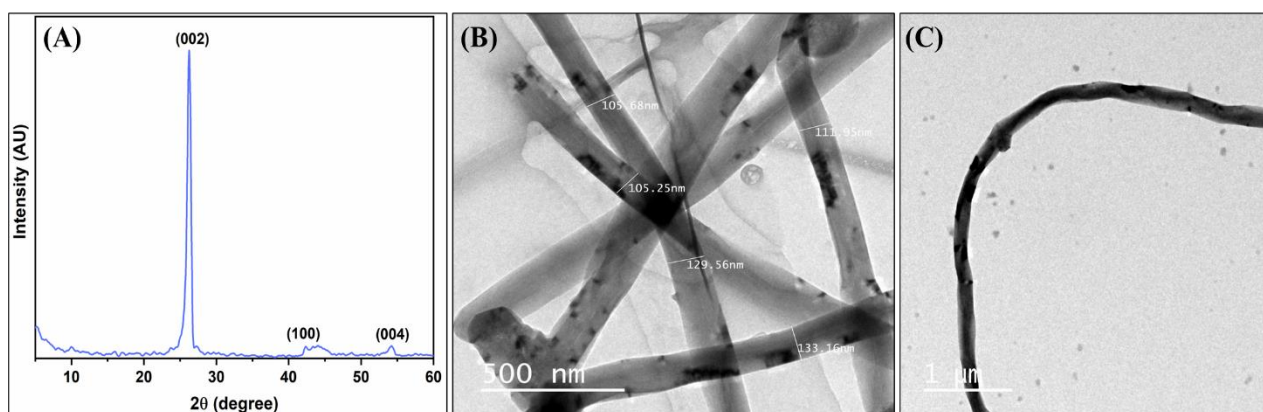


Figure 3.1. (A) XRD spectrum, and (B, C) TEM images of the cMWCNTs used in the formulation of conductive ink.

3.3.2 SEM and contact angle studies

SEM analysis was conducted to visualize the surface of the cMWCNT@paper electrode(s) before and after modification with MBs (**Figures 1(A-F)**). The rough surface of paper consisting of cellulose fibers is clearly visible in **Figures 3.2(A)** and **(B)**. An additive/modifying agent was also observed (**Figure 3.2 (B)**) that may probably have been added to whiten or change the porosity of the paper. While the MWCNT ink coating seems to be uniformly spread on the paper matrix, which indirectly hints at the homogeneity of the conductive ink (**Figure 3.2(C)**). The photograph of a cMWCNT@paper electrode is shown in

the inset of **Figure 3.2(C)**. Upon magnification, the MWCNTs were visible in the ink matrix (**Figure 3.2(D)**). Further, **Figure 3.2(E)** shows the SEM image of the Av/MB/cMWCNT@paper electrode, which appears smoother in comparison to cMWCNT@paper electrode. Further, the Av/MBs seem to have completely covered the ink surface (5 mg beads were adsorbed on $1 \times 1 \text{ cm}^2$ of cMWCNT@paper electrode). Further magnification reveals spherical Av/MBs distributed evenly on the cMWCNT@paper electrode surface without aggregation in a specific region (**Figure 3.2(F)**).

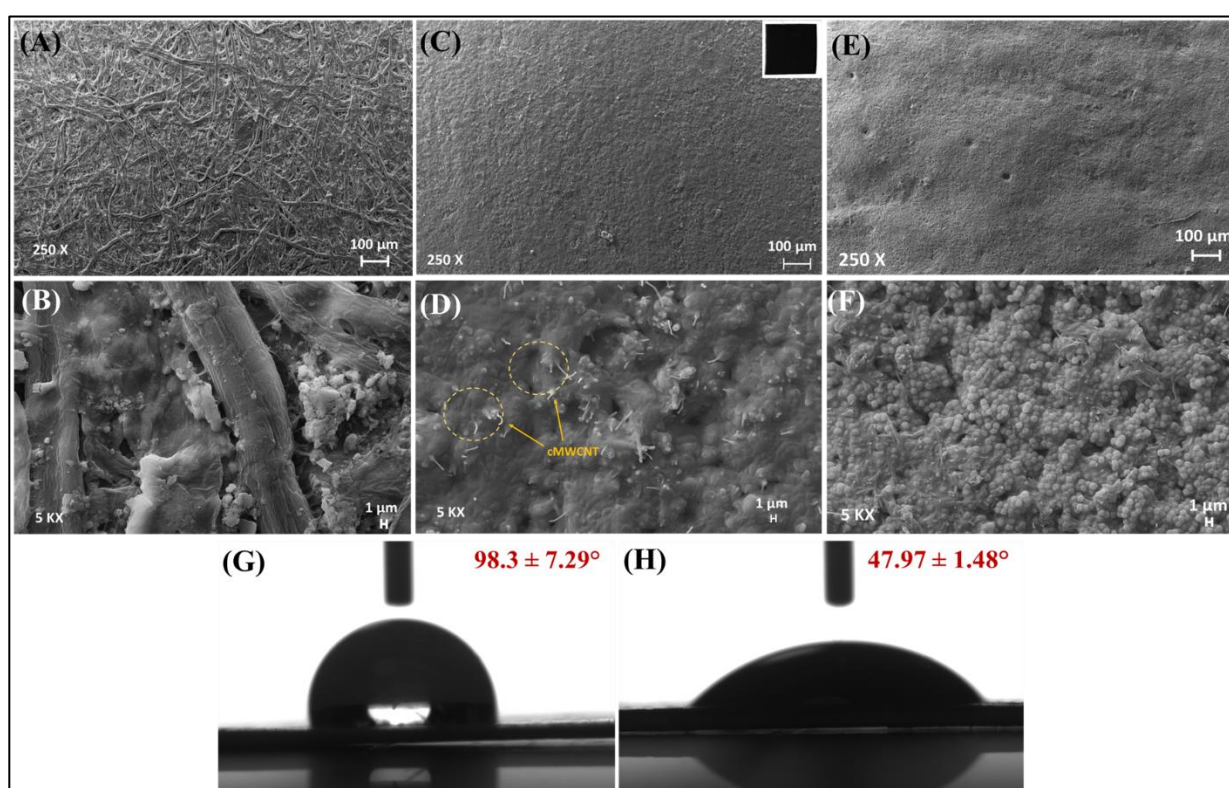


Figure 3.2. SEM images of (A, B) bare paper, (C, D) cMWCNT ink-coated paper (cMWCNT@paper) (inset of (C) shows the photograph of the cMWCNT@paper electrode ($2 \times 2 \text{ cm}^2$)), and (E, F) Av/MB/cMWCNT@paper electrode. Contact angle measurements for (G) bare paper, and (H) cMWCNT@paper electrode.

The wettability of bare paper and cMWCNT@paper electrodes was assessed by contact angle measurements (**Figures 3.2(G)** and **(H)**). The contact angle of bare paper was found to be $98.3 \pm 7.29^\circ$ (mean \pm error) (**Figure 3.2(G)**). Evidently, the contact angle decreased to 47.97

$\pm 1.48^\circ$ after coating of paper by the conductive ink (3 coats, 75 μL for one coat) (**Figure 3.2(H)**). The high value of contact angle of the bare paper may have been due to the presence of modifiers in the paper, which was also indicated by SEM analysis. The hydrophilic nature of CMC present in the ink may contribute to the decrease in the contact angle after ink coating. Further, other residual ink constituents (Tp and PS80) may also perhaps contribute to the observed lower contact angle of the ink due to low surface tension [174].

3.3.3 Conductivity studies

Conductivity studies were conducted to optimize the annealing temperature, annealing time, and the number of ink coatings (n) by determining the conductivity of the cMWCNT@paper electrodes. (**Figure 3.3(A)**). The resistivities of the cMWCNT@paper electrodes were calculated after annealing at 80-130 $^\circ\text{C}$ for 5-15 min ($n = 3$) (**Figure 3.3(A)**). An increase in annealing temperature and time led to decrease in the resistivity of the cMWCNT@paper electrodes. The minimum value of conductivity was observed at 120 $^\circ\text{C}$ for 10 min. Subsequently the annealing time was fixed at 10 min, and the resistivity was calculated for the same temperature range. No significant change in the resistivity was observed at temperatures over 120 $^\circ\text{C}$ (**Figure 3.3(B)**). Hence, the optimum annealing temperature and time were chosen as 120 $^\circ\text{C}$ for 10 min, respectively. The evaporation and degradation of Tp and possibly, PS80, at temperatures $> 100^\circ\text{C}$ may have led to the reduction in resistivity with temperature and time. The mean (\pm SD) resistivity of the cMWCNT@paper at $n = 7$ decreased from 9.89 (± 1.2) $\Omega\cdot\text{cm}$ at $n = 1$ to 1.066 (± 0.31) $\Omega\cdot\text{cm}$ (**Figure 3.3(C)**). The corresponding highest value of conductivity was found to be 0.938 S cm^{-1} ($n = 7$). The equations utilized in the calculations for determining the conductivity of the cMWCNT@paper electrodes are given in **Section 2.6.10 (Eqs. 2.5-2.8)**.

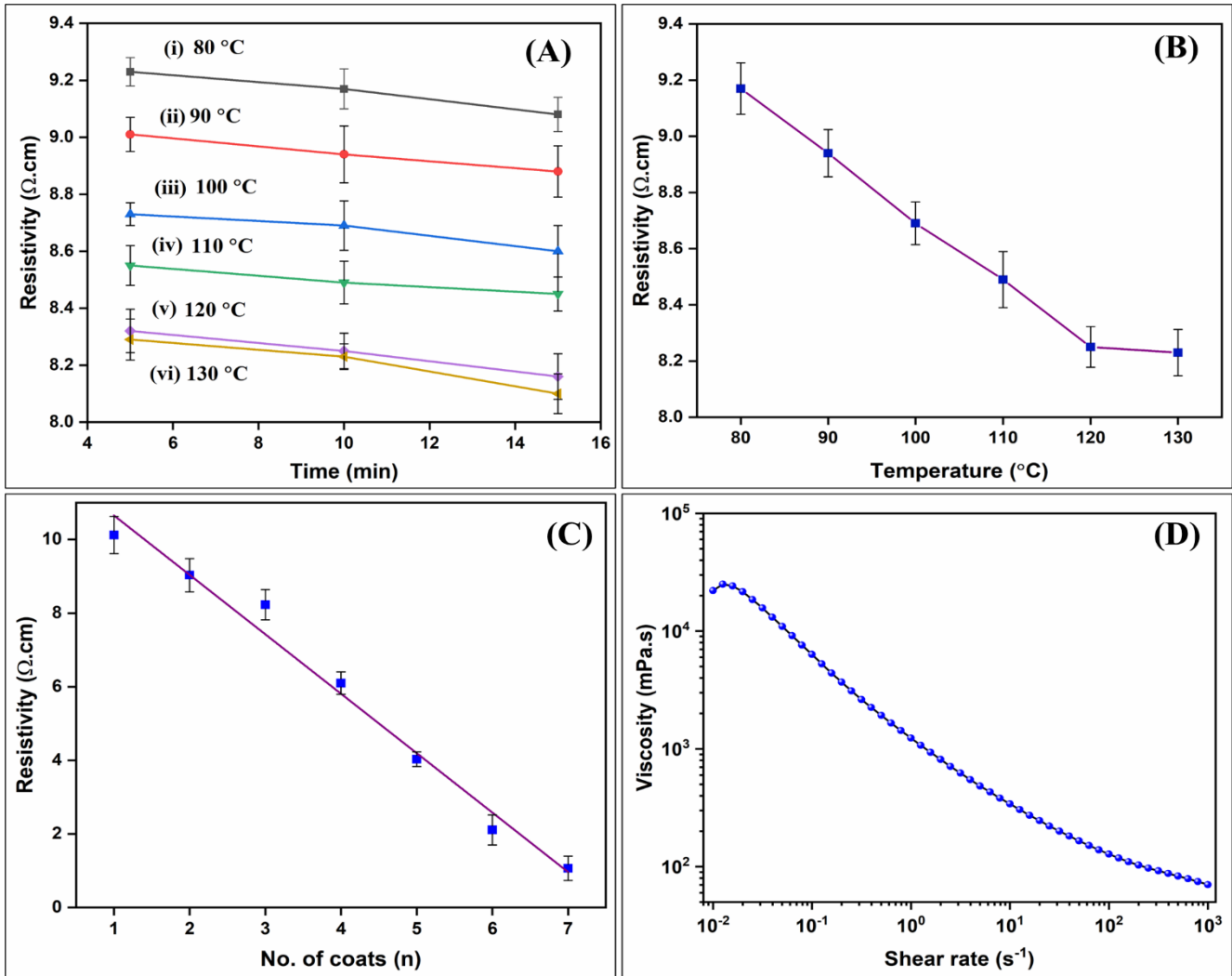


Figure 3.3. (A) Resistivity of the cMWCNT@paper electrodes vs. annealing time at different annealing temperatures, (B) Change in resistivity of the cMWCNT@paper electrodes with temperature after annealing for 10 min., (C) Resistivity of the cMWCNT@paper electrodes vs. number of coats of the conductive ink, and (D) Viscosity of the cMWCNT ink vs. shear rate displaying thixotropic behavior.

Further, the increase in the amount of cMWCNT loading after every coat may account for the decrease in resistivity. cMWCNTs are known to form highly inter-networked matrix leading to high conductivity. **Table 3.2** provides a comparison of some recently reported MWCNT-based screen-printing inks with the present work.

Table 3.2. A comparative analysis of some recently reported MWCNT-based inks.

<i>S. No.</i>	<i>Nanomaterial</i>	<i>Binder</i>	<i>Resistivity</i>	<i>Applications</i>	<i>Reference</i>
1.	MWCNT	--	--	All-in-one fabric-based supercapacitors	[175]
2.	MWCNT/PEDOT:PSS	PEDOT:PSS	$51.31 \pm 0.25 \Omega \text{ sq}^{-1}$	Flexible heating	[26]
3.	Graphene/MWCNT/Carbon black	Water-based acrylic resins	$4 \Omega \text{ sq}^{-1}$	Electrothermal films	[67]
4.	dihydroxyphenyl-functionalized multi-walled carbon nanotubes (MWNT-f-OH)/carbon black/graphite	waterborne acrylic resins	up to $29 \Omega \text{ sq}^{-1}$	Electrochemiluminescent devices	[22]
5.	Functionalized MWCNT	Hydroxyethyl cellulose	--	Humidity sensing	[176]
6.	MWCNT	PVP	$0.5\text{--}13 \Omega \text{ sq}^{-1}$	Patch antennas	[55]
7.	Carboxyl-functionalized MWCNT	Carboxymethyl cellulose	$1.066 \pm 0.31 \Omega \text{ sq}^{-1}$	DNA Biosensor	Present work

Another important factor in determining the application of paper-based biosensors is scalability in the fabrication process. The use of an established printing technology for coating of the prepared cMWCNT conductive ink can ensure scalability and batch reproduction of the paper electrodes with minimal errors. The flow behavior of an ink dictates its printability. Hence, rheological analysis was conducted to analyze the flow properties of the prepared cMWCNT ink. As shown in **Figure 3.3(D)**, the cMWCNT ink displayed a shear thinning or thixotropic behavior, i.e., its viscosity decreased linearly with increase in shear rate. This kind of rheological behavior is considered ideal for screen printing. The initial apparent viscosity of the cMWCNT ink was found to be 22 Pa.s. The presence of CMC may account for the high initial viscosity; however, the carbon nanomaterials are also known to increase the viscosity of inks. Thus, while both CMC and cMWCNT can together contribute to the high initial viscosity, the shear thinning behavior of the ink is, perhaps, mostly due to CMC, which is a well-known rheology modifier and a thixotropic agent. These results indicate the suitability of the

formulated ink for screen printing suggesting that the formulated ink can be used for the batch production of low cost SPEs.

3.3.4 Raman and XPS analyses

In order to verify the presence of cMWCNT in the formulated conductive ink, Raman spectroscopic and XPS analyses were undertaken. The ink was first dried overnight at 120 °C followed by incubation at 350 °C for 2 h. This ensured the degradation of CMC and any other residual ink constituent. Raman and XPS studies were conducted on the thus obtained dried ink powder. **Figure 3.4(A)** shows the presence of the G and D band in the Raman spectrum of the dried ink, which are the characteristic Raman feature of graphitic carbon-containing materials. The G band, observed at 1582.53 cm⁻¹, occurs due to the tangential vibrations of the C atoms. The presence of a single, sharp graphitic peak at ~1582 cm⁻¹ suggests the multiwalled nature of the carbon nanotubes (and the large diameter). Other bands, D and G', were observed at 1353.69 cm⁻¹ and 2705.54 cm⁻¹, respectively. These manifest due to the double resonance Raman processes, wherein the D band is indicative of the disorder induced by structural defects, amorphous carbon, etc. While the G' band is dispersive in nature, i.e., its frequency depends upon the excitation wavelength of the laser. The G and G' bands together act as the Raman signature indicating the presence of graphitic sp² carbon. Further, the degree of defects in the material can be estimated by the I_D/I_G ratio. These defects may either be induced by some physicochemical interaction or already present (structural defect) in the MWCNT structure. The I_D/I_G ratio for the dried ink was found to be 0.66, which indicates the presence of less defects in the MWCNT structure.

The surface elemental composition of the dried ink was determined by XPS analysis. The major peaks in the survey scan spectra can be attributed to C1s (284.5 eV) and O1s (530.5 eV), which verifies the presence of cMWCNTs in the dried ink (**Figure 3.4(B)**). Deconvolution

reveals the presence of five characteristic peaks for the C1s (**Figure 3.4(C)**). The C1s main peak located at 284.5eV (C=C) corresponds to the sp^2 hybridization. Further, sp^3 hybridized C-C bonds are also indicated as given by the peak at 285.1eV. The epoxy/hydroxy (-C-O), carbonyl groups (C=O) and carboxyl groups (O-C=O) of the cMWCNT are indicated by the remaining peaks observed at 286.3 eV, 287.2 eV and 289.6 eV, respectively. In case of O1s, the deconvoluted peaks at 530.5eV and 531.3 eV can be attributed to the C=O and C-O bonds, respectively (**Figure 3.4(D)**). The O atoms in carboxyl groups and water adsorbed at the surface are indicated by the peaks at 533.5 eV and 534.5 eV, respectively [177-180]. These results clearly reveal the presence of the cMWCNTs in the intact form in the as-prepared dried ink.

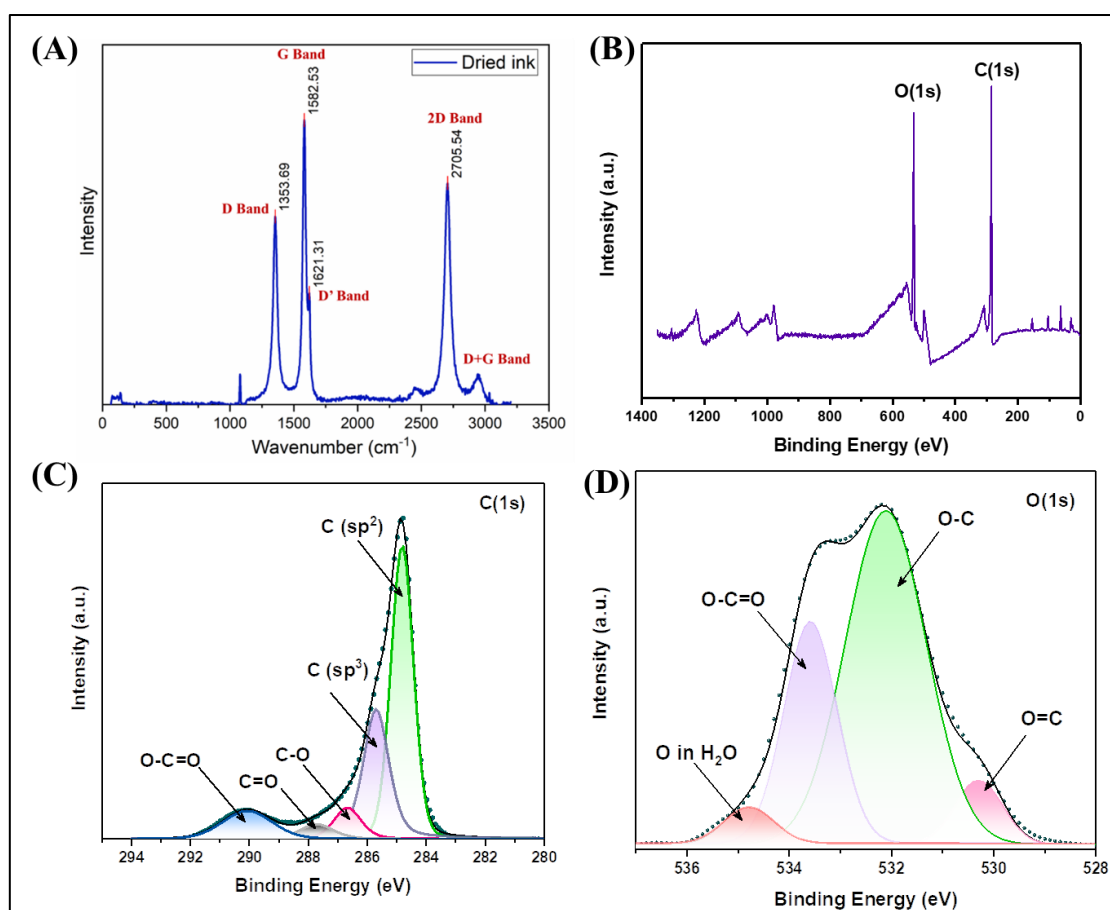


Figure 3.4. (A) Raman spectrum, (B) XPS survey scan, (C) deconvoluted peaks of C1s, and (D) deconvoluted peaks of O1s.

3.3.5 Electrochemical characterization studies

An essential parameter that affects biosensing performance is the continuous use stability. It is essential for a biosensing electrode to yield stable response when immersed in a buffer for long durations. The biosensor's electrochemical response should be stable upon continual cycling in buffer. It should not vary over time given all other conditions are the same. The continuous use stability of the cMWCNT@paper electrodes was evaluated by CV studies. As shown in **Figure 3.5(A)**, the cMWCNT@paper electrode yielded stable CV response even after 20th cycle, without any background noise. It may be noted that this study was conducted after 20 minutes of immersion in the buffer, as it took time to stabilize within the buffer. The presence of CMC, which is swelling nature, in the ink matrix may be partially accounted for the time taken to stabilize. The eventual (and continued) stability of the electrode response indicates that the electrochemical response of the electrode was not hindered by the hydrophilic nature of CMC. The cMWCNT@paper electrodes were also assessed for their storage stability. CV responses of the cMWCNT@paper electrodes were recorded for 7-90 days followed by determination of the peak current density (J) (**Figure 3.5(B)**). The current density (J) is given by,

$$J = I/A \quad (\text{Eq. 3.4})$$

where, I is the current and A is the surface area. The geometric surface area of the electrodes used in the electrochemical analysis was 1 cm², hence the J and I values were same. No significant change was found in the value of current density of the cMWCNT@paper electrodes until 30 days (99.7% of response on 7 days). Subsequently, the current density reduced to 97.78% and 94.8% of initial response at 60 and 90 days, respectively. This indicates that the cMWCNT@paper electrodes can be stored and used for up to 60 days in dry conditions at room temperature, eliminating the requirement of special storage conditions.

Batch reproducibility of the cMWCNT@paper electrodes was also determined, as it is an important consideration for the device reproducibility. CV responses of 10 electrodes chosen randomly from different batches were recorded (**Figure 3.5(C)**). The peak J value of the cMWCNT@paper electrodes was found to be $27.03 \pm 0.38 \mu\text{A cm}^{-2}$ (mean \pm SD). This indicates that the ink coatings on the electrodes were uniform in nature and yielded stable and similar electrochemical response for the same number of ink coats. This further points toward the homogenous nature of the cMWCNT ink.

The electrochemical response of the cMWCNT@paper electrodes after adsorption of MBs, Av/MBs, and CP/Av/MBs was recorded. The electrochemical peak response of the MB/cMWCNT@paper was found to be slightly less than that of the cMWCNT@paper electrode (**Figure 3.5(D)**). The MBs were commercially acquired and, according to the manufacturer, composed of superparamagnetic iron oxide coated with highly crosslinked polystyrene and a hydrophilic layer of glycidyl ether. This layer of polymer, while conserving the superparamagnetic behavior, is perhaps responsible for the relatively lower electrochemical response of the MB/cMWCNT@paper electrode. Additionally, these beads are carboxylated which renders a negative charge on them, which may subsequently lead to repulsion of the negatively charged ferro-ferricyanide from the electrode surface. The electrochemical responses of the Av/MB/cMWCNT@paper and CP/Av/MB/cMWCNT@paper electrodes reduced significantly thereafter. This can be attributed to the insulating nature of Av and DNA molecules. The bulky nature of Av can potentially block the electron transfer at the electrode surface. Additionally, this study indirectly confirmed the modification of MBs with avidin and subsequent immobilization of CP onto the Av/MBs via biotin-avidin interactions.

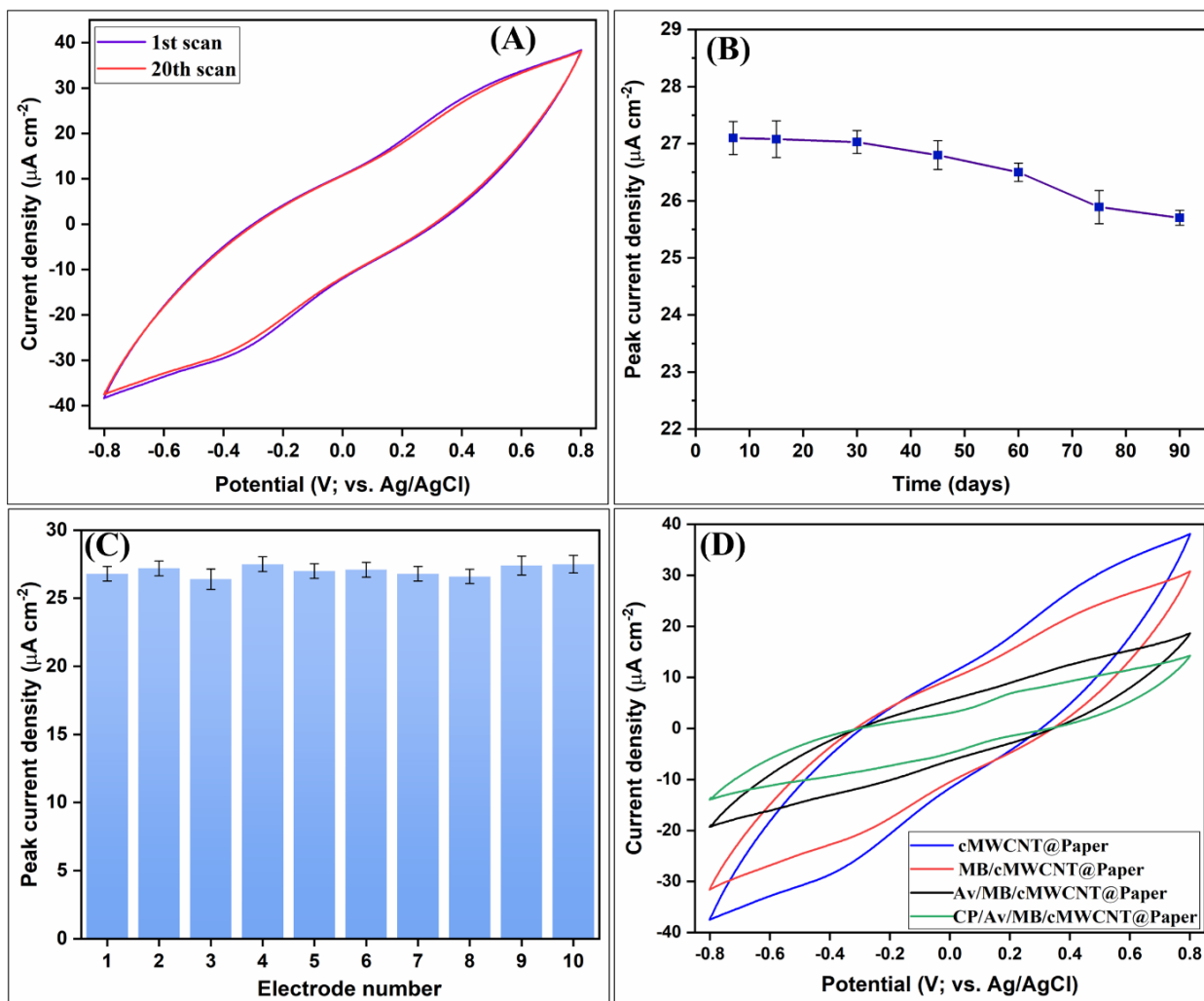


Figure 3.5. (A) Continuous use stability as depicted by CV scans of change in current density with potential for the cMWCNT@paper electrodes, (B) storage stability as indicated by change in peak current density of the cMWCNT@paper electrodes over a period of 7-90 days, (C) Batch reproducibility as indicated by variability in the peak current density values of different cMWCNT@paper electrodes, and (D) CV scans showing the change in the current density of the cMWCNT@paper electrodes before and after deposition of MBs and other biomolecules.

3.3.6 Electrochemical response studies

Specific detection of gonococcal *porA* pseudogene was attained by designing an MB-assisted sandwich DNA hybridization assay and integrating it with cMWCNT@paper electrodes for electrochemical analysis. Prior to response studies, the amount of MBs required to yield a significant response on the cMWCNT@paper electrodes was optimized (**Figure**

3.6(A)). The optimal amount of MBs was found to be 0.5 mg as there was a significant change in the current response. Hence, all further response studies were conducted with 0.5 mg MBs. The minimum time required for CV response saturation after drop casting of the C-T-D/Av/MB assembly was also determined (response time) (**Figure 3.6(B)**). The response of the C-T-D/Av/MB/cMWCNT@paper electrode(s) was found to saturate after 20 min as determined by detecting 1 pM TP. Thus, 20 min was chosen as the response time and all the recordings were made 20 min after introduction of the modified electrodes in the buffer. The change in current density of the cMWCNT@paper with change in the TP concentration (100 fM–100 nM) is shown in **Figure 3.6(C)**. The net change in current density (ΔJ) for different TP concentrations was calculated as:

$$\Delta J = J_c - J_0 \quad (\text{Eq. 3.5})$$

where, J_0 is the peak current density of the blank CP/Av/MB/cMWCNT@paper electrode and J_c is the peak current density for a particular concentration of target DNA. A calibration plot was obtained which showed that the ΔJ values increased linearly with log of TP concentration (**Figure 3.6(D)**). The corresponding linear equation is as follows:

$$\Delta J = 5.09 \times \log[\text{concentration}] + 12.59, R^2 = 0.98 \quad (\text{Eq. 3.6})$$

The participation of the tagged MetB molecules in electron transfer at the electrode surface may perhaps have contributed to the observed trend in the current density with TP concentration. Notably, the redox peaks are more visible at higher TP concentrations (**Figure 3.6(C)**). The sensitivity and detection limit of the biosensing assay were found to be $5.09 \mu\text{A} \cdot (\log[\text{concentration}])^{-1}$ and 0.13 pM, respectively.

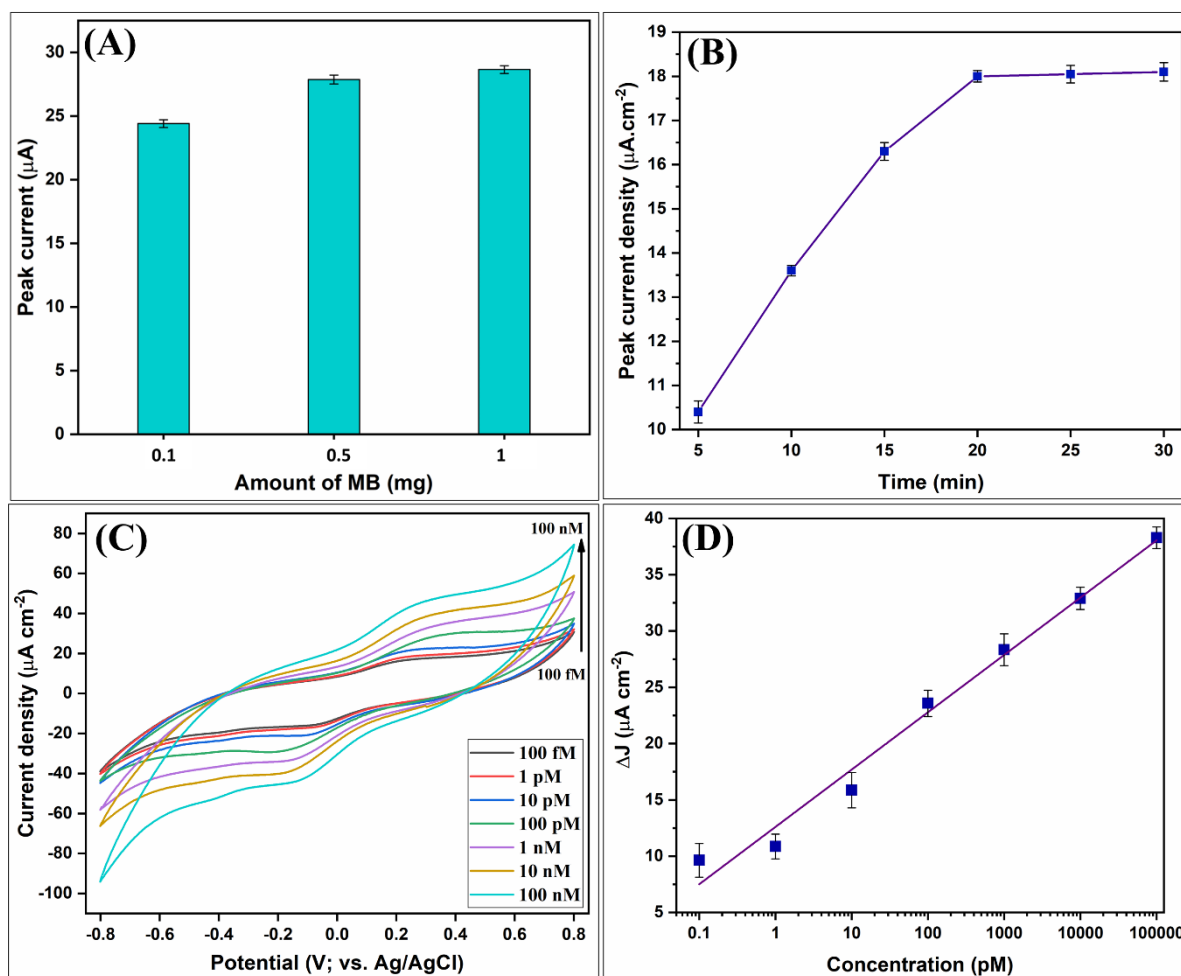


Figure 3.6. (A) Peak current density of the C-T-D/Av/MB/cMWCNT@paper electrodes (100 pM T concentration) with respect to different amounts of MB, (B) The peak current density of the C-T-D/Av/MB/cMWCNT@paper electrode for 1 pM target concentration (*porA* TP) with time, (C) Change in current density with increasing concentration of the C-T-D hybridization complex at the cMWCNT@paper electrode surface, and (D) the calibration graph showing net change in peak current density (ΔJ) vs. the log of TP concentration.

3.3.7 Real sample analysis and specificity studies

The response of the biosensing electrode towards different concentrations of genomic DNA isolated from NG was recorded to evaluate the applicability of the electrochemical biosensing assay in practical situations. The detailed protocol followed for preparation of the genomic DNA for biosensing analysis is given in **Section 2.6**. The response of the biosensing electrode to the genomic DNA was recorded compared to the same concentration of synthetic

TP used in the response studies (**Figure 3.7(A)**). It was found that the responses to the genomic DNA and synthetic TP strand were similar with 98-99% recovery rates.

The effect of DNA/protein interferents on the biosensing response was also evaluated by determining the response of the biosensing electrode to genomic DNA mixed with nonspecific DNA molecules (**Figure 3.7(B)**). The results indicated that there was no significant change in the peak response of the biosensing electrode in the presence of DNA from the following species: *Neisseria meningitidis* (NM), *Ureaplasma urealyticum* (U), *Streptococcus aureus* (SA), *Enterococcus faecalis* (EF), *Chlamydia trachomatis* (Ch), and a mixture of all these bacterial DNA (M). Furthermore, BSA was used as the protein interferent. The interferant DNA and proteins (BSA) did not lead to a significant variation in the peak response of the C-T-D/Av/MB/cMWCNT@paper biosensing electrodes. This indicates that the oligonucleotide probes used in the study are specific in nature. This also highlights the significance of MB-mediated sample enrichment.

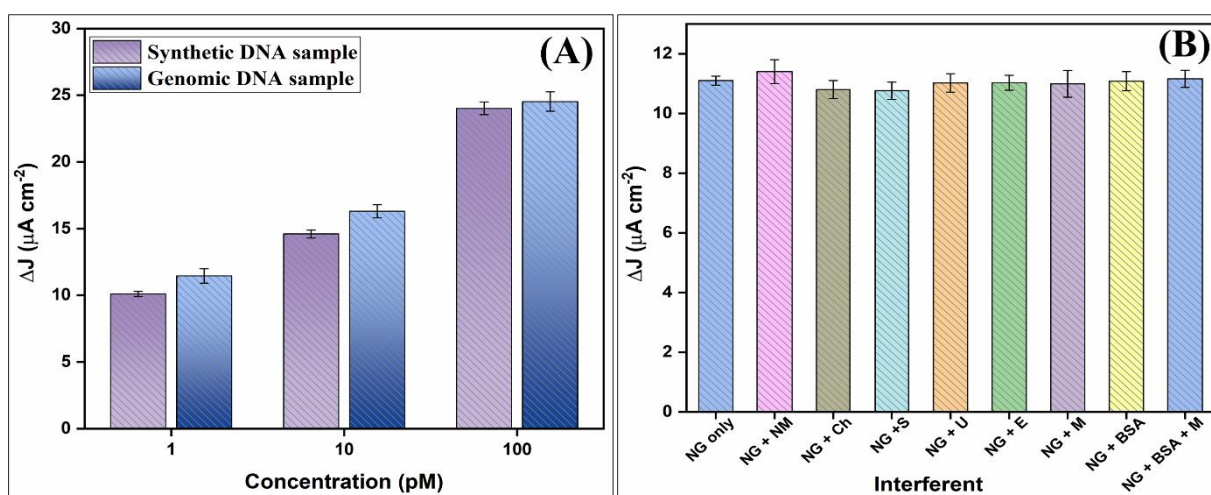


Figure 3.7. (A) Comparison of biosensing signal obtained for different of TP concentration with extracted gonococcal genomic DNA, and (B) the net current density change shown by the C5@paper electrodes when exposed to mixture of gonococcal DNA and non-gonococcal DNA.

Table 3.3 provides the details of some recent studies on development of paper-based printed electrochemical biosensors for the detection of pathogenic DNA.

Table 3.3. Some recent studies on paper-based electrochemical biosensors for detection of pathogenic DNA.

S. No.	Ink formulation/ Nanomaterial	Target pathogen	Linear range	Sensitivity (LOD)	Reference
1.	Graphene nanosheets	-- (dsDNA)	0.2-5 pg mL ⁻¹	0.00656 mA pg ⁻¹ cm ⁻²	[25]
2.	Graphene oxide-modified carbon ink screen printed on paper	<i>Orientia tsutsugamushi</i> (single stranded DNA)	0.05 × 10 ² pg μL ⁻¹ to 6.3 × 10 ² pg μL ⁻¹	1228.4 μA cm ⁻² ng ⁻¹ (20 pg μL ⁻¹)	[33]
3.	Carbon graphene ink (commercial)	Hepatitis B virus	50 pM-100 nM	-- (1.45 pM)	[106]
4.	Ni-Au/CNT/PVA (vacuum filtration and drop casting)	HIV DNA	10 nM–1 μM	-- (0.13 nM)	[14]
5.	Ag nanoprisms electrodeposited on graphene quantum dots (GQDs)	<i>Leishmania infantum</i>	1 zM - 1 nM	1 zM (LOQ*)	[181]
6.	cMWCNT	<i>Neisseria gonorrhoeae</i>	100 fM-100 nM	5.09 μA (log[concentration]) ⁻¹ (0.13 pM)	Present work

3.4 Conclusion

This study demonstrated the formulation of an MWCNT-based conductive ink and its subsequent utilization towards fabrication of a paper-based electrochemical biosensor. The conductive ink was coated onto paper to yield cMWCNT@paper electrodes with maximum conductivity of 0.98 S.cm⁻¹. These paper-based electrodes were integrated to an MB-assisted, sandwich DNA hybridization assay for the electrochemical detection of NG *porA* pseudogene. The cMWCNT@paper electrodes were shown to possess excellent continuous use stability, storage stability, and batch reproducibility. The electrochemical DNA biosensing assay proved highly specific and sensitive to the *porA* pseudogene sequence in a wide linear range spanning 3 orders of magnitude (100 fM-100 nM). Genomic gonococcal DNA was detected using the paper-based biosensor with excellent recovery. MBs enabled sample enrichment, which imparted selectivity to the biosensing assay. The presence of gonococcal genomic DNA was

detected even in the presence of non-gonococcal DNA present in 50 times higher concentrations. Further, the formulated ink displayed thixotropy, pointing toward its screen printability.

This study has demonstrated the development of efficient paper-based electrodes using a homogenous, cMWCNT-based conductive ink, which can be further utilized in electrochemical biosensing. It should be noted that although the fabricated paper-based biosensor detected gonococcal DNA efficiently, its detection limit could further be improved. Additionally, the conductivity and rheology of the ink could be further improved to improve the sensing characteristics and enable batch reproduction of conductive paper electrodes. The details of these improvements have been discussed in the upcoming chapter.

These results have been published as “Carbon nanotubes modified conductive ink for application to paper-based electrochemical biosensors for pathogenic DNA detection” in the New Journal of Chemistry, 2023 May; 47(23): 10930-10941 [182].

Chapter 4

Supersandwich DNA Assay-Integrated Paper Biosensor for Electrochemical Detection of Neisseria gonorrhoeae

4.1. Introduction

Conductive ink-modified biosensing electrodes have been fabricated for detection of analytes, such as hormones, metal ions, DNA, etc. [58, 105]. The high aspect ratio and surface area of MWCNTs coupled with conductivity render them suitable for different applications. MWCNTs also have intrinsic adhesion ability to various substrates like paper and plastics, rendering them useful for wearable and flexible electronics applications. They possess exceptional mechanical strength and thermostability, enabling their utilization in different electrochemical applications. Hence, they can serve as effective conductive fillers in conductive inks. Many studies have focused on the utilization of MWCNT-based composites for conductive ink formulation [14, 26, 55]. However, many conductive inks currently suffer from limitations such as long-term stability issues, requirement of substrate pre-treatment, flexibility issues, etc. Additionally, the conductivity is often hampered because of the use of excessive binders/additives in the ink to enhance adhesion/homogeneity of the ink [55]. Thus, there is still a great void in literature addressing these issues regarding conductive inks.

Various pathogens, such as *Vibrio cholerae* [183], *Haemophilus influenzae* [183], SARS-CoV-2 [184, 185], Zika virus [186, 187], etc., have been detected using paper-based DNA biosensors in the recent years. The design of different kinds of DNA-based sensing modalities has been enabled by highly specific DNA base pairing [134, 135, 184]. A few attempts have been made in the recent past for the detection of gonococcal DNA. Most studies on gonococcal diagnostics have employed amplification methods integrated to visual mode of detection [134, 135] (please see **Section 1.5.3**). Electrochemical detection of PCR amplicons of NG has also been reported previously [188]. Visual detection and amplification-based approaches suffer from limitations, such as is often semi-quantitative nature, stringent temperature control, and requirement of expensive reagents. Supersandwich DNA hybridization is a promising alternative technique to amplification-based biosensors. This

method offers several advantages, such as no requirement of labels, high sensitivity, and ability to be integrated to different biosensing transducers [94, 96, 189]. This method further enables enzyme-free signal amplification and does not require any stringent temperature controls [95, 96, 189]. Various applications of the supersandwich hybridization-based biosensors include pathogen detection [190], and miRNA detection [96], among others. We hypothesize that supersandwich-based assays can be utilized effectively for sensitive and specific detection of NG.

This chapter details the results pertaining to the optimization of the conductive ink formulation (mentioned in last chapter) towards the fabrication of conductive paper-based electrodes. The formulation of the conductive ink has been modified to i) improve the conductivity of the resulting paper electrodes, and ii) optimize the rheology of the ink for further printing applications. The paper electrodes fabricated via modification by the optimized ink were further integrated to an MB-assisted supersandwich DNA assay for ultrasensitive, label-free detection of NG *porA* pseudogene sequence.

4.2. Experimental details

4.2.1. Design of oligonucleotide probes

The detailed protocol for the design of the oligonucleotide probes for the supersandwich assay has been provided in **Section 2.3**. Table 4.1 summarizes the details of the DNA probes utilized in the study. The formation of supersandwich DNA ‘ladder-like’ concatemers was confirmed by gel electrophoresis studies.

Table 4.1. Details of DNA oligonucleotide probes used in this work.

S. No.	Probe codename	Probe type	Sequence (5'—3')	Melting temperature (°C)
1.	SCP	Capture probe	5' NH ₂ -TTT TTT CCT GCT ACT TTC ACG CTG GA 3' (26 bases) (5' amino C6 modification)	59
2.	SDP	Supersandwich detector probe	5'AAG TAA TCA GAT GAA ACC AGT TCC CTG CTA CTT TCA CGC TGG A 3' (43 bases)	50.8
3.	TP	Target strand	5'GAA CTG GTT TCA TCT GAT TAC TTT CCA GCG TGA AAG TAG CAG G 3' (43 bases)	66.2
4.	NC	Non-complementary probe	5'TTG ATT GAG CGT CAT AGA TCG GAC GGC ACT AGT CAG TAC TCG A 3' (43 bases)	67

4.2.2 Formulation of the conductive ink

The amount of binder in the conductive ink was optimized before its formulation. For this, CMC (1, 2.5 and 5% *w/v*) was dispersed in DI water followed by mixing with Tp (2:1 ratio). PS80 was added to stabilize and emulsify this CMC in water/Tp system. Vigorous stirring (1000 rpm, 2h) was employed to mix the resulting emulsions, which were designated as CMC₁, CMC_{2.5} and CMC₅ for 1%, 2.5% and 5% *w/v* CMC, respectively. Rheological studies were undertaken to choose CMC₅ as the base for the conductive ink. cMWCNTs were dispersed in CMC₅ in 1:1 ratio at 1000 rpm (overnight stirring). The thus formulated conductive emulsion was kept in an ice bath and ultrasonicated using a Ti probe. The sonication was conducted at 70% amplitude with 1 s pulse for 20 min, with intermittent breaks of 5 min. The thus formed conductive ink was named as C5 and stored at 4 °C – 10 °C until further use.

4.2.3 Rheological analyses

Viscometric analyses of the emulsion bases were conducted within the shear rate range of 0.1-100 s⁻¹. Further, the viscosity recovery after stress removal was assessed via a 3-interval

thixotropy test (3iTT). The test simulates different coating processes, including screen printing, wherein the printing process leads to a significant and sudden change in applied stress. Pre-shearing was performed at 0.1 s^{-1} for 20 s before the 3iTT. After this, the applied shear rate was changed in three intervals – I interval at 0.1 s^{-1} for 30 s (stabilization of viscosity), II interval at 200 s^{-1} for 15 s (simulating screen printing process), and III interval at 0.1 s^{-1} for 120 s (recovery of viscosity).

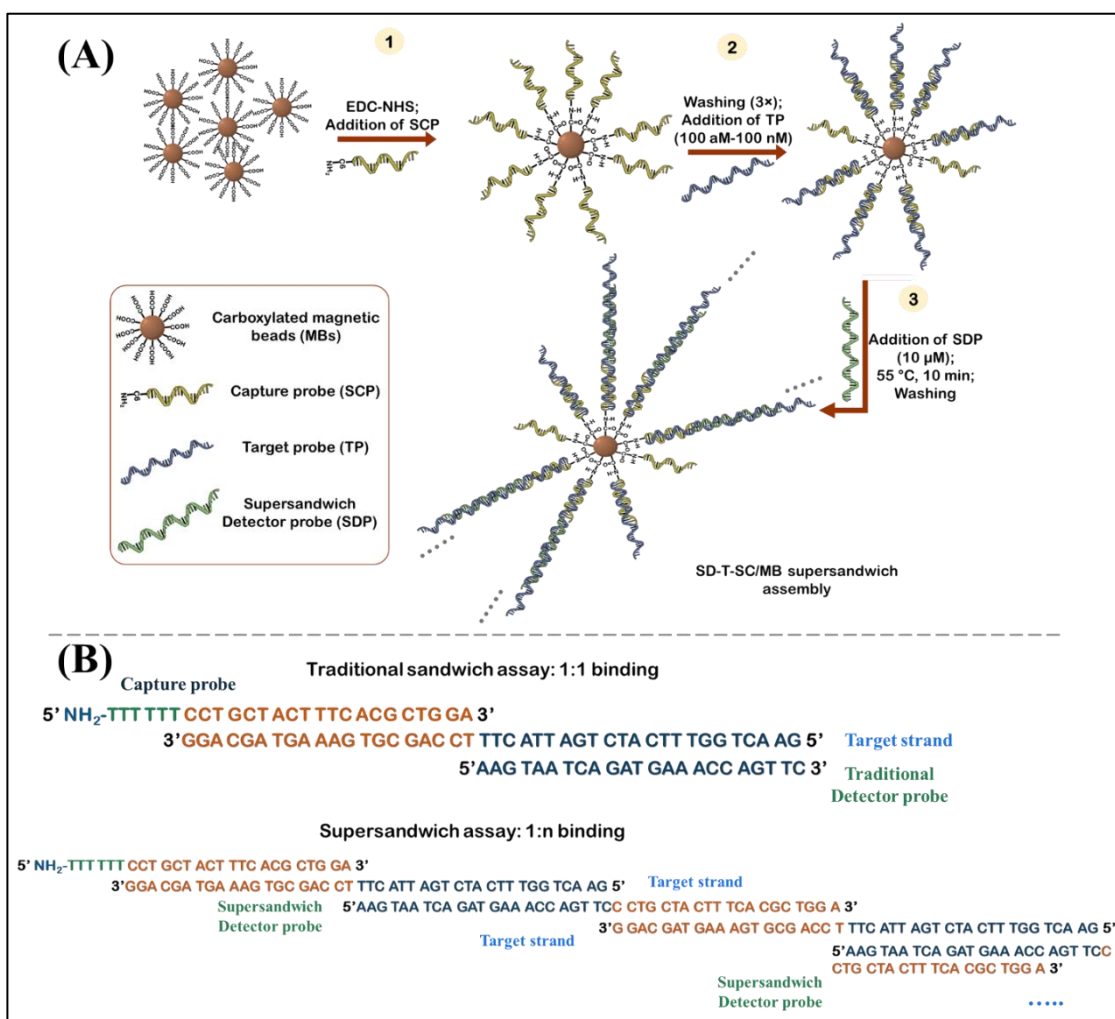
4.2.4 Fabrication of C5@paper electrodes

The C5 ink was coated onto drawing paper (200-300 gsm, $6 \times 6 \text{ cm}^2$) using a paint brush (Faber-Castell No. 4). The methodology is the same as followed in the previous chapter (Chapter 3).

4.2.5 Electrochemical magnetic bead-assisted DNA supersandwich assay

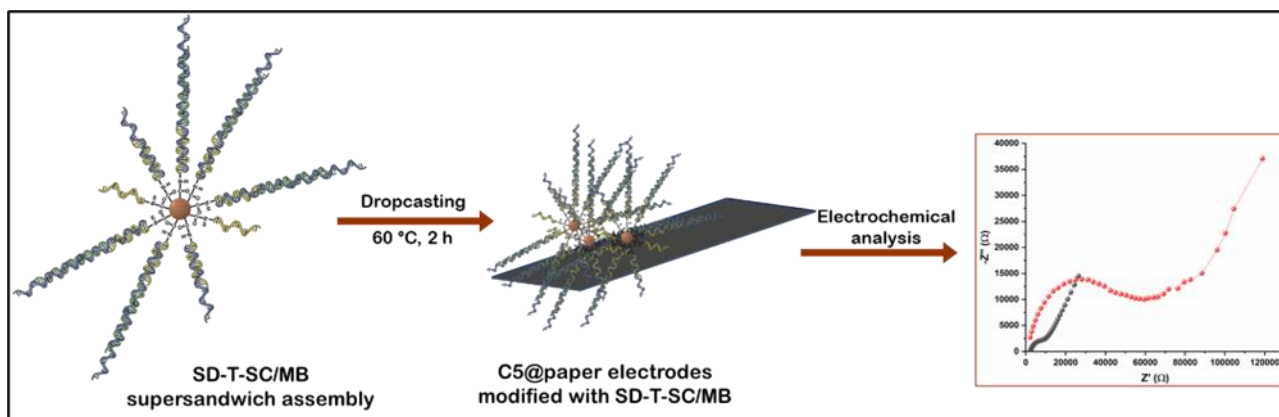
a) SCP immobilization: The detailed methodology for SCP immobilization has been given in Section 2.7.2 (Chapter 2).

b) Supersandwich assay: SCP/MBs (5 mg) were washed and redispersed in DI water (500 μL ; final concentration of 10 mg mL^{-1}). Fifty microliters of TP (100 aM-100 nM, or 5 zmol – 5 pmol) was mixed with SCP/MBs (1 mg bead per reaction). Thereafter, SDP (10 μM , 50 μL) was added to T-SC/MB and kept at $55 \text{ }^\circ\text{C}$ for 10 min with tilt rotation. Washing was performed with DI water after every step (3 \times) to remove unbound probes. The SD-T-SC/MB assembly was redispersed in PBS buffer (pH 7, 30 μL) for electrochemical studies (Scheme 4.1(A)). The principle of supersandwich DNA binding has been provided in Scheme 4.1(B). Briefly, the SDP is designed such that after binding with the TP, there is still a 20-mer DNA sequence left open for binding to an adjacent target site. This leads to the formation of a ‘DNA ladder’-like structure and is referred to as a 1:n binding [94].



Scheme 4.1. Schematic diagram depicting (A) the steps in the formation of MB-assisted supersandwich hybridization assembly for *N. gonorrhoeae* detection, and (B) comparison between sandwich and supersandwich DNA hybridization.

c) Electrochemical analysis: The C5@paper electrodes were modified by drop casting the SD-T-SC/MB assembly (30 μL, in PBS) (Scheme 4.2). These electrodes were slow dried at 60 °C for 2 h. Thereafter, impedance measurements (0.1-10⁵ Hz at 0.01 V) for every electrode were taken. The correlation between the charge transfer resistance (R_{ct}) of the modified C5@paper electrodes with different concentrations of TP was plotted as a calibration curve.



Scheme 4.2. Integration of the MB-assisted DNA supersandwich assembly with the C5@paper electrodes for electrochemical detection of *N. gonorrhoeae* via EIS.

4.3. Results and discussion

4.3.1. Rheological optimization of the conductive ink

The rheology of the ink formulation was optimized by changing the CMC concentration, which acts both as a rheology modifier and a binder. This study aimed at preparation of a homogenous, thixotropic ink, i.e., the ink displays shear thinning behavior upon stress application followed by viscosity recovery once the stress is removed. Thixotropy allows smooth application of the ink on paper and other substrates [191]. Thixotropy is a characteristic feature in most screen-printing inks and commercial paints [191]. CMC is a known and prominently used rheological modifier and thixotropic agent [192].

The influence of CMC concentration on the flow properties of the ink was determined by examining the viscosity of three different solvent bases—CMC₁, CMC_{2.5} and CMC₅, corresponding to 1%, 2.5% and 5% w/v CMC, respectively. **Figure 4.1(A)** shows the curve of viscosity vs. shear rate (0.1-100 s⁻¹) on a log scale. There was a linear correlation between the viscosity and the shear rate for all three emulsion bases, indicating towards shear thinning behavior. The initial apparent viscosities for CMC₁, CMC_{2.5} and CMC₅ at 0.1 s⁻¹ were found to be 3.48 Pa.s, 14.42 Pa.s, and 18.9 Pa.s, respectively. The increase in the apparent viscosity of

the emulsion bases with increase in CMC content indicates that it is potentially the main contributor to the viscosity of the final ink. The 3-interval thixotropy test (3iTT) was conducted to analyze the thixotropic behavior of the emulsion bases. As shown in **Figure 4.1(B)**, the highest apparent viscosity was displayed by CMC₅ (18.4 Pa.s) at 0.1 s⁻¹ (30 s), while CMC₁ exhibited the lowest apparent viscosity (3.48 Pa.s) at the same shear rate and time. In accordance with the shear thinning behavior, there was a significant drop in the viscosity values of the emulsion bases at shear rate of 200 s⁻¹, wherein they decreased to 0.68 Pa.s and 0.76 Pa.s at 45 s (200 s⁻¹) for CMC₁ and CMC_{2.5}, respectively. While the viscosity of CMC₅ decreased to ~5.8 % of its initial apparent viscosity at 30 s (1.08 Pa.s at 45 s), which is slightly better than CMC_{2.5}. These results indicate that the flow of CMC₁ would be the highest during screen printing, while CMC₅ would flow slowly through the screen mesh. The apparent viscosities of the three emulsion bases recovered to different degrees after shear rate recovery from 200 s⁻¹ to 0.1 s⁻¹. The % recovery in viscosity of CMC₁, CMC_{2.5} and CMC₅ was found to be 62.5%, 59.3% and 98.4%, respectively, after 75 s. **Table 4.2** summarizes the change in apparent viscosities of the three emulsion bases as a function of shear rate. Seepage and dripping of inks are two major factors that determine the efficiency of the screen-printing process. These two factors in turn are indicated by viscosity recovery. The higher is the recovery, the lower are the risks involved with seeping and dripping of ink—thus leading to high resolution printing. Additionally, very low viscosity of ink may allow creation of air bubble and very high viscosity may lead to non-uniformly printed patterns [191]. Keeping these factors in consideration, CMC₅ was chosen as the emulsion base for the conductive ink as it displayed appreciable decrease in viscosity at high shear rate and the highest recovery upon removal of stress.

Table 4.2. Apparent viscosities of the different emulsion bases at different shear rates as determined by 3iTT.

Name of emulsion	CMC content (% w/v)	Apparent viscosity (Pa. s)			% recovery in apparent viscosity
		0.1 s ⁻¹ (time, t = 30 s)	200 s ⁻¹ (t = 45 s)	0.1 s ⁻¹ (t = 75 s)	
CMC ₁	1	3.48	0.68	2.17	62.5
CMC _{2.5}	2.5	14.42	0.76	8.55	59.3
CMC ₅	5	18.4	1.08	18.1	98.4

cMWCNT were uniformly dispersed into the CMC₅ emulsion base to yield the conductive ink, named as C5. The effect of addition of cMWCNT on the rheological behavior of the ink was analyzed (**Figures 4.1(C) & (D)**). The addition of cMWCNT led to a significant increase in the initial apparent viscosity of the conductive C5 ink as compared to the base CMC₅ emulsion (**Figure 4.1(C)**). However, the thixotropy was retained by the C5 ink. Interestingly, as shown in **Figure 4.1(D)**, a decrease of ~100 times was displayed by the C5 ink; the initial viscosity value of 329.8 Pa. s (0.1 s⁻¹) decreased to 3.79 Pa.s (200 s⁻¹). Moreover, the viscosity recovery was found to be 90% after stress removal (as recorded at t = 75 s). These results suggested that despite the rise in initial apparent viscosity of the C5 ink, the addition of cMWCNT did not interfere with the thixotropy of the conductive ink. This further confirmed that the C5 ink could be potentially used for high-resolution screen printing. Other studies have also led to similar results wherein addition of conductive fillers such as MWCNT, silver, and graphene led to an increase in the initial viscosity of the ink while not interfering with thixotropic properties of the binder and other additives [26, 65, 191]. It has been reported that carbon nanomaterials enhance the mechanical strength of the ink, which may contribute to better viscosity recovery [65]. Further the retention of colloidal stability of the C5 ink at high shear rates can be explained by the stabilization and interplay of weak intermolecular (*van der Waals*) and steric interactions among cMWCNTs, CMC, and other dispersants (PS80) in the

ink [26]. As a result, the screen-printing of this ink may lead to high resolution patterns.

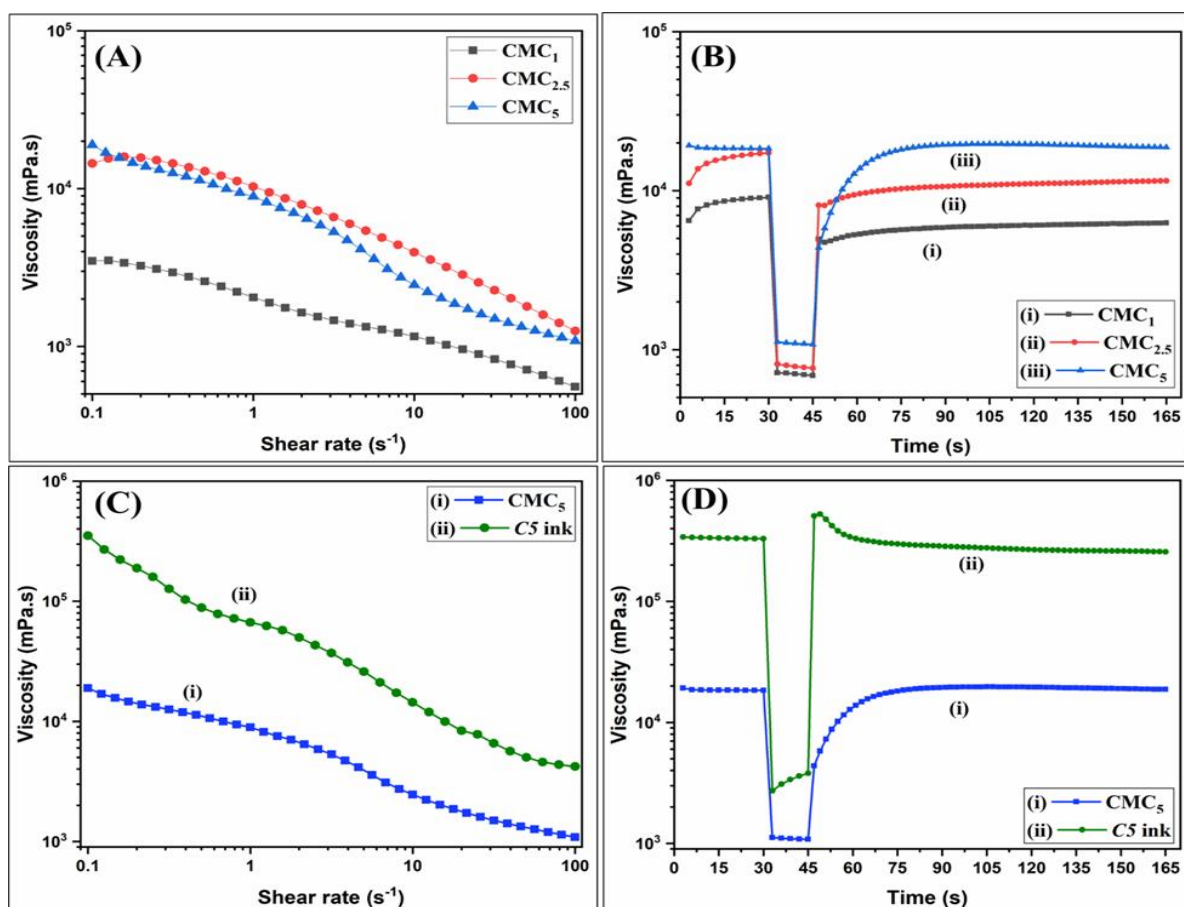


Figure 4.1. (A) Viscometric analysis: change in viscosity of the CMC₁, CMC_{2.5} and CMC₅ base emulsions with shear rate in the range 0.1-100 s⁻¹, (B) Results of the 3iTT for the CMC₁, CMC_{2.5} and CMC₅ base emulsions (change in viscosity with abrupt change in the shear rate), (C) Change in viscosity of the CMC₅ base emulsion and the C5 ink with shear rate (0.1-100 s⁻¹), and (D) A comparison of the results of the 3iTT for CMC₅ base emulsion and the C5 ink.

4.3.2. Morphological analysis of the C5@paper electrodes

a) **SEM/FESEM analysis:** SEM and FESEM were conducted to study the surface morphology of the fabricated C5@paper electrodes (**Figure 4.2(A-F)**). As shown in **Figures 4.2(A) & (B)**, the cellulose fibers of bare paper are clearly visible. After coating with the C5 ink (**Figures 4.2(C) & (D)**), these fibers seem to be completely covered by the ink. There is uniformity to the ink coating, which appears granular in texture. Further, the CMC (and possibly PS80) seem to have enveloped cMWCNTs, though they can be seen protruding out of the ink

matrix (**Figure 4.2(D)**). Upon further magnification, different ink coats can be seen on a tilted lateral side of the C5@paper electrode with cMWCNT dispersed over the entire surface (FESEM, 20kx; **Figure 4.2(E)**). **Figure 4.2(F)** shows a magnified image of a CNT embedded onto the C5@paper matrix, having an apparent diameter of 67.6 nm.

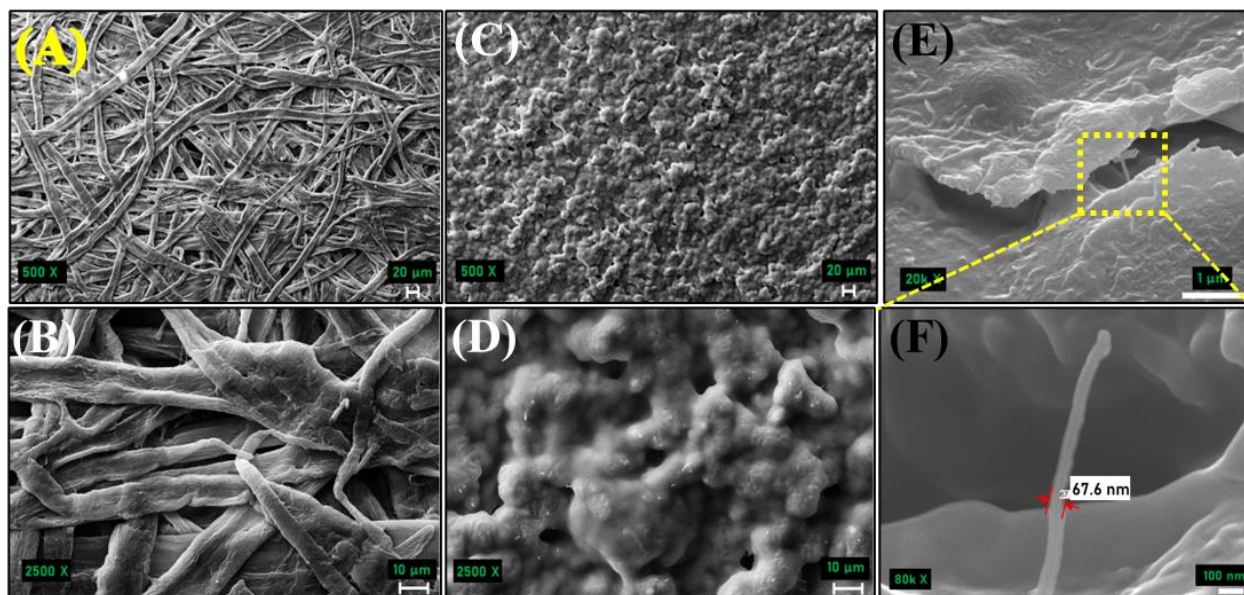


Figure 4.2. SEM images of (A, B) bare paper, and (C, D) C5@paper electrodes at different magnifications. (E) FESEM image of the C5@paper electrode, and (F) High magnification FESEM image showing cMWCNT in the ink matrix.

b) AFM analysis: The surface roughness C5@paper electrodes was compared to bare paper by AFM studies (**Figure 4.3**). The RMS surface roughness of bare paper (**Figure 4.3(A)**) and the C5@paper electrode (**Figure 4.3(B)**) were found to be 168.2 nm and 41.6 nm, respectively. This masking of the cellulose fibers by the ink may account for this reduction in the surface roughness after ink coating. These results can be explained from an observation that the constituents of ink coating may have led to lower friction force as compared to bare paper, further indicating that the coating is smooth despite grainy appearance [193].

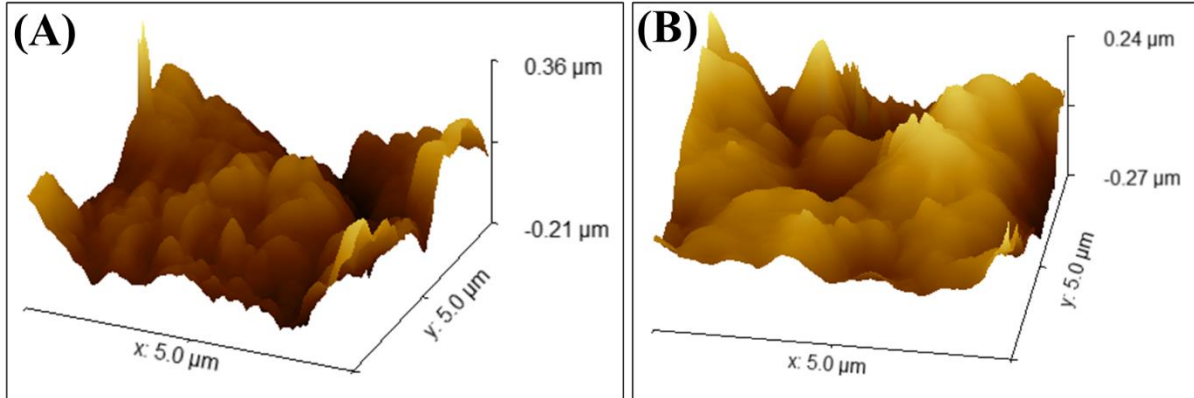


Figure 4.3. AFM images of the (A) bare paper, and (B) C5@paper electrode. The RMS roughness decreased upon ink coating from 168.2 nm for bare paper to 41.6 nm for C5@paper electrode.

4.3.3 Conductivity studies

The 4-probe conductivity method was utilized to determine the conductivity of the C5@paper electrodes. **Section 2.6.10 (Eqs. 2.5-2.8)** provides the calculations involved in the measurement of conductivity. Annealing of the C5@paper electrodes was performed at 120 °C for 10 min after every coat. As is evident from **Figure 4.4(A)**, increasing the number of ink coats led to an obvious increase in the conductivity of the C5@paper electrodes, with a maximum value observed at 4 coats. The observed increase in conductivity may be contributed to the increase in the cMWCNT content after each coat. Interestingly, the conductivity gradually seemed to saturate for 5-8 coats. This may be due to a fine interplay between the insulating nature of CMC and the conductive nature of cMWCNTs, both of which were present in the same concentration in the ink. The competing and contrasting nature of the binder and the CNTs may have led to saturation in the conductivity after 4 coats. Similar results were reported by a recent study, wherein the conductivity of a graphene-based ink continued to increase with number of (printing) coats until saturation [63].

The C5@paper electrode displayed a maximum conductivity of $10.1 \pm 0.24 \text{ S. cm}^{-1}$ ($0.1 \pm 0.026 \text{ } \Omega \cdot \text{cm}$) ($n = 4$ coats). Recently, a conductivity value of 14.99 S. cm^{-1} was reported for a

MWCNT/PEDOT:PSS screen printing ink after 5 printing passes [26]. Of note is the fact that the study utilized PEDOT:PSS, which is a conductive polymer, as a binder. This led to a significant enhancement in the conductivity of the MWCNT ink as reported. Resistivity in the range of $0.5\text{-}13 \Omega \text{ sq}^{-1}$ of has also been reported for an MWCNT ink using PVP as a binder [55]. Ten weight percent MWCNT was utilized as the conductive filler in this study. The importance of the binder used in the ink preparation is highlighted by results of these studies. A conductive binder (like PEDOT:PSS) may lead to a significant increase in the conductivity values by many orders of magnitude, while an insulating polymer may lead to a reduction in the same despite the concentration of the conductive filler. Keeping this in consideration, it can be inferred that the high conductivity of the C5 ink, despite the use of a low amount of MWCNT (5% *w/v*) and a binder (CMC) that is non-conductive, may be contributed to the effective ink preparation method. Further, the effect of bending at different angles ($45\text{-}180^\circ$) on the conductivity of the C5@paper electrodes was also studied (**Figure 4.4(B)**). The conductivity of the C5@paper electrodes did not change significantly until 135° bending. Thereafter, a significant decrease in the conductivity was observed at the bending angle of 180° . The uniform dispersion of cMWCNTs in the ink matrix and homogeneity of the ink may be accounted for the retention of conductivity till 135° [194]. However, bending at higher angles ($\geq 180^\circ$) may lead to cracks in the surface of the paper, eventually cracking the ink coating itself. This may have contributed to the drop in conductivity at higher bending angles.

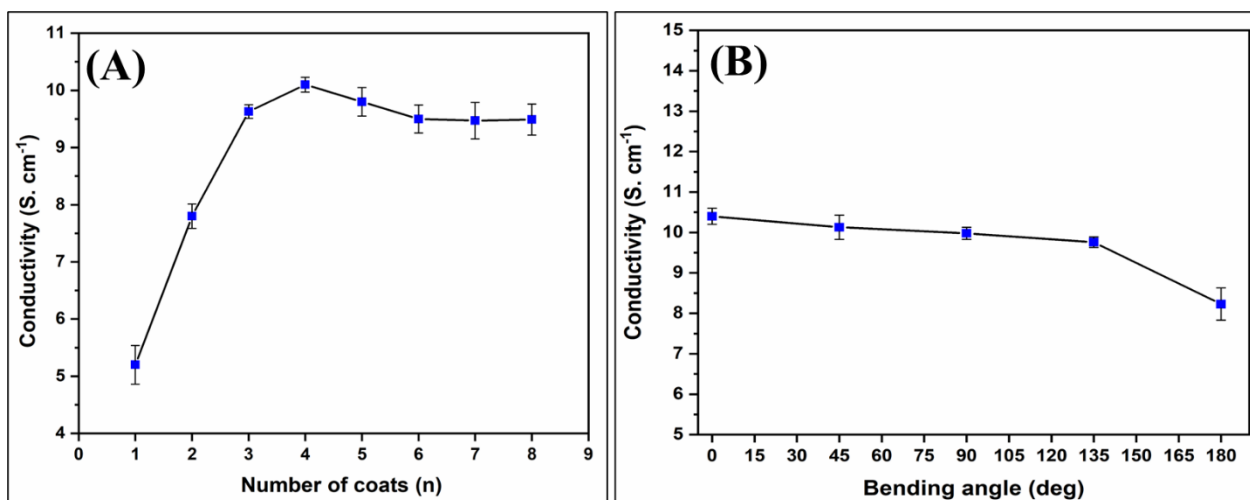


Figure 4.4. Conductivity of the C5@paper electrode vs. (A) number of coats, and (B) bending angle.

4.3.4. Electrochemical stability and reproducibility studies

CV and EIS studies were undertaken to evaluate the electrochemical performance of the fabricated C5@paper electrodes. The continuous use stability of the electrodes in buffer (aqueous) conditions was determined by running multiple CV cycles. No significant change in the CV response of the electrode was observed even after 50 cycles (**Figure 4.5(A)**), which suggests towards their stability in buffer conditions. However, the pseudocapacitive nature of the C5@paper electrodes may have led to a higher charging current relative to the faradaic current. The high values of charging current may also be contributed to the swelling of CMC in aqueous conditions. Thus, further electrochemical studies were conducted via EIS. The charge transfer resistance (R_{ct}) of 10 randomly selected electrodes was calculated via EIS studies to assess the batch reproducibility of the C5@paper electrodes (**Figure 4.5(B)**). To determine the R_{ct} values, Nyquist plots were fitted with an equivalent circuit given by ($R_s(Q_1[R_{ct}Q_2])$), wherein R_s is the solution resistance, R_{ct} is the charge transfer resistance, and Q_1 and Q_2 are the CPE associated is the constant phase element (CPE) associated with diffusion at the electrode surface and the (pseudo)capacitance of the double layer formed at the electrode surface, respectively (**Figure 4.5(C)**). The presence of Q_1 and Q_2 in the equivalent circuit

suggests that the double layer capacitance of the electrode surface may be behaving in a non-ideal manner. This also points towards the non-homogeneity of the active site distribution over the electrode surface [37]. Further, the mean (\pm SD) R_{ct} of C5@paper electrodes was found to be $940.29 \pm 0.72 \Omega$ (**Figure 4.5(B)**), with no significant variations among R_{ct} values of different electrodes. The homogeneity of the C5 ink and its uniform coating on paper may account for the reproducibility in EIS results. The storage stability of the electrodes was determined by calculating the R_{ct} of the C5@paper electrodes during 1-30 days (**Figure 4.5(D)**). No significant change was found ($\sim 0.5\%$) in the R_{ct} during this duration, wherein the initial R_{ct} value of 940Ω decreased to 935.2Ω at Day 30. This indicates that the C5 electrodes can be stored for at least 30 days in dry conditions at room temperature.

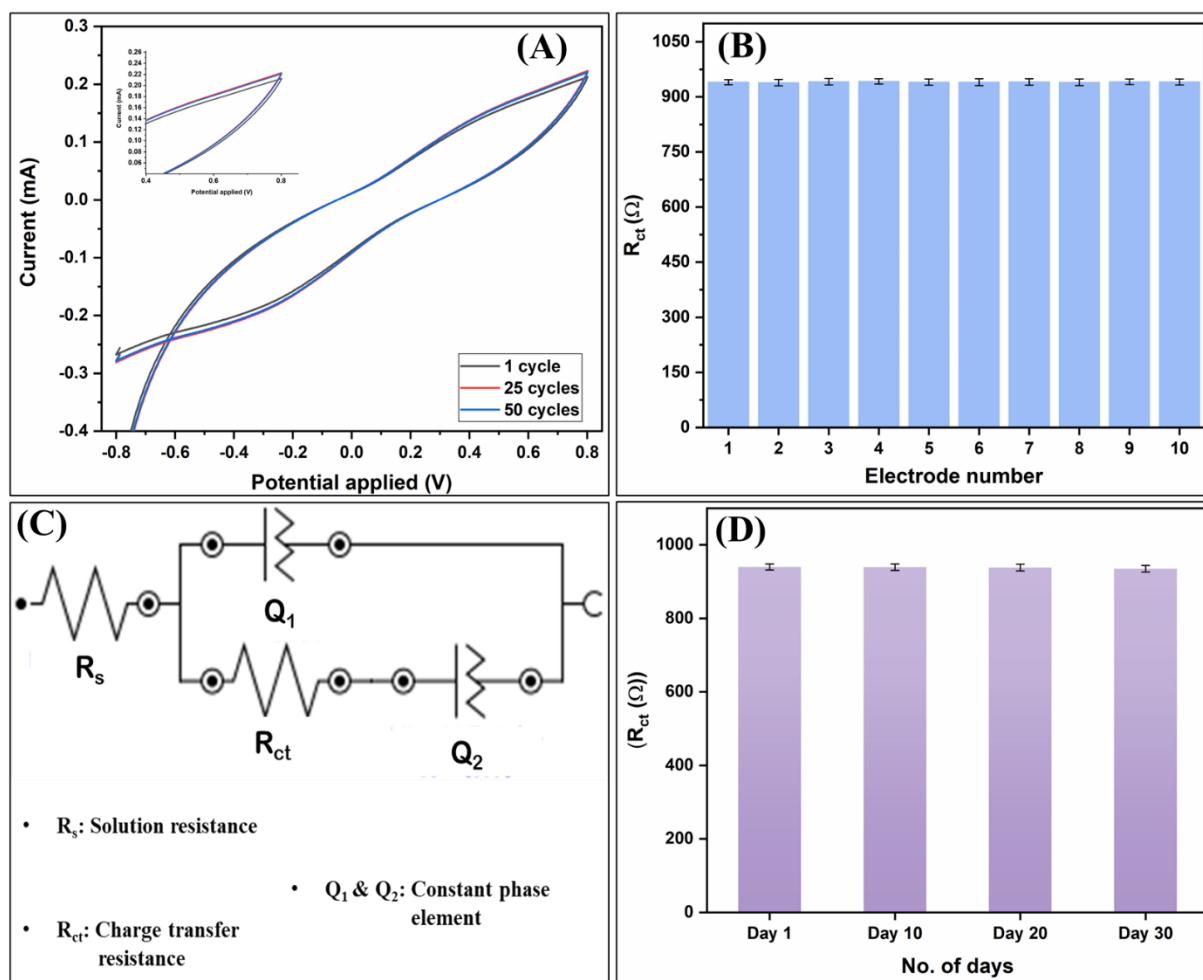


Figure 4.5. (A) CV curves of the C5@paper electrode at 1st, 25th, and 50th cycle displaying the

continuous use stability. Inset shows a magnified view of the CV curves, **(B)** R_{ct} values of randomly selected C5@paper electrodes from different batches, **(C)** Equivalent circuit model fitted into the Nyquist plots, and **(D)** R_{ct} of the C5@paper electrodes measured at every 10 days of storage in dark, dry conditions at room temperature.

4.3.5 Electrochemical response studies

EIS studies were conducted to monitor the effect of modifications (SCP/MB drop casting) on C5@paper electrodes (**Figure 4.6(A)**). The R_{ct} of the C5@paper electrode ($940 \pm 4.2 \Omega$) increased significantly after modification with SCP/MB ($3.28 \pm 0.06 \text{ k}\Omega$) and BSA/SCP/MB ($4.11 \pm 0.09 \text{ k}\Omega$). This increase can be contributed to the insulating nature of the immobilized DNA and BSA molecules. **Figure 4.5(C)** shows the equivalent circuit fitted into the EIS curves.

Further, the formation of supersandwich DNA ‘ladder-like’ assembly between the SCP, TP, and SDP probes was confirmed via gel electrophoresis studies (**Figure 4.6(B)**). The study was conducted at two different temperatures-25 °C and 55 °C-to ascertain if the formation of the supersandwich structure is temperature dependent. It was found that DNA bands of size range ~100 bp and higher were formed at both the temperatures after 5 min of incubation. This eliminates the need of any temperature-specific incubation, which is often the case in amplification-based assays. Even so, 55 °C for 10 min was selected as the optimized reaction condition for the electrochemical DNA hybridization studies. The higher temperature would ensure blocking of any non-specific interactions that are more favorable at low temperature. Additionally, the mobility of SCP molecules may be restrained due to its immobilization onto MBs during the assay, and DNA hybridization may be restricted due to steric hindrance. Thus, the optimum incubation time was chosen as 10 min to account for losses due to these factors.

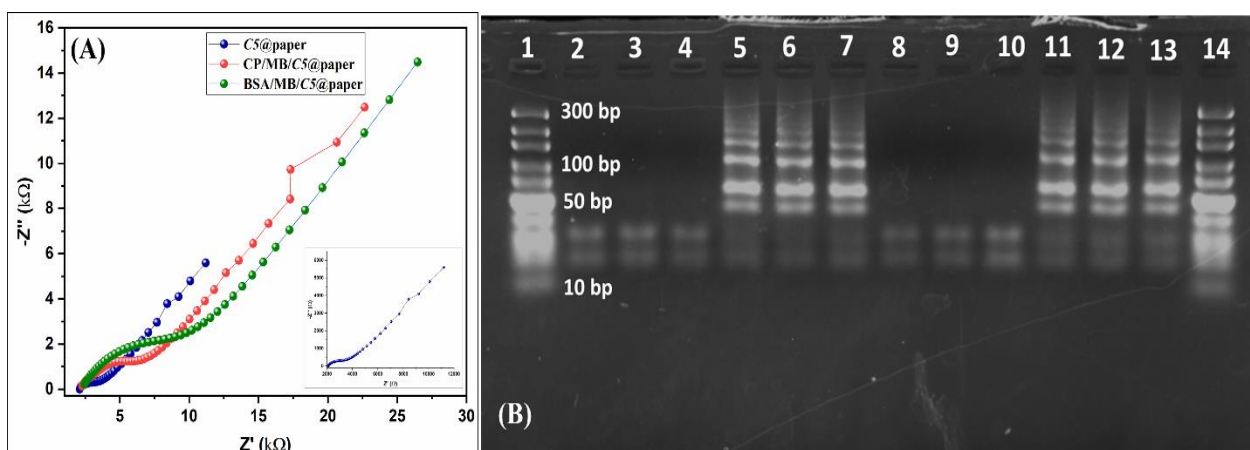


Figure 4.6. (A) Nyquist plots of the C5@paper, SCP/MB/C5@paper, and the BSA/SCP/MB/C5@paper electrodes. Inset shows the magnified view of the Nyquist plot of the C5@paper electrode, and (B) Gel electrophoresis results showing the formation of DNA supersandwich structures at different temperature and time. Lane 1, 14: DNA ladder (10-300 bp), Lanes 2-4: SCP and SDP without TP (negative control) incubated at 25 °C for 5, 10 and 15 min respectively, Lanes 5-7: Supersandwich structures formed by hybridization of SCP, TP and SDP at 25 °C for 5, 10 and 15 min, respectively, Lanes 8-10: SCP and SDP without TP incubated at 55 °C for 5, 10 and 15 min respectively, and Lanes 11-13: Supersandwich structures formed by hybridization of SCP, TP and SDP at 55 °C for 5, 10 and 15 min, respectively.

Further, **Figure 4.7(A)** shows the EIS response of the C5@paper electrodes to the TP in the concentration range of 100 aM-100 nM. Evidently, the impedance increased upon increase in TP concentration. The change in the R_{ct} (ΔR_{ct}) was calculated by the following equation:

$$\Delta R_{ct} = R_m - R_0 \quad (\text{Eq. 4.1})$$

where, R_m is the measured R_{ct} for every concentration and R_0 is the R_{ct} of the blank BSA/SCP/MB/C5@paper electrode. The correlation between the ΔR_{ct} values and concentration of the *porA* TP was found to be linear in nature as shown in **Figure 4.7(B)**. The corresponding linear equation is given by,

$$\Delta R_{ct} = 26.21 \times \log[\text{concentration}] + 111.99, R^2 = 0.98 \quad (\text{Eq. 4.2})$$

The linear range of the assay was found to be 100 aM – 100nM (10^9 orders of magnitude) with an exceptional sensitivity of $26.21 \text{ k}\Omega (\log[\text{concentration}])^{-1}$ and detection limit of 45 aM. The formation of large supersandwich DNA concatemers may account for the enhanced sensitivity of the biosensing assays.

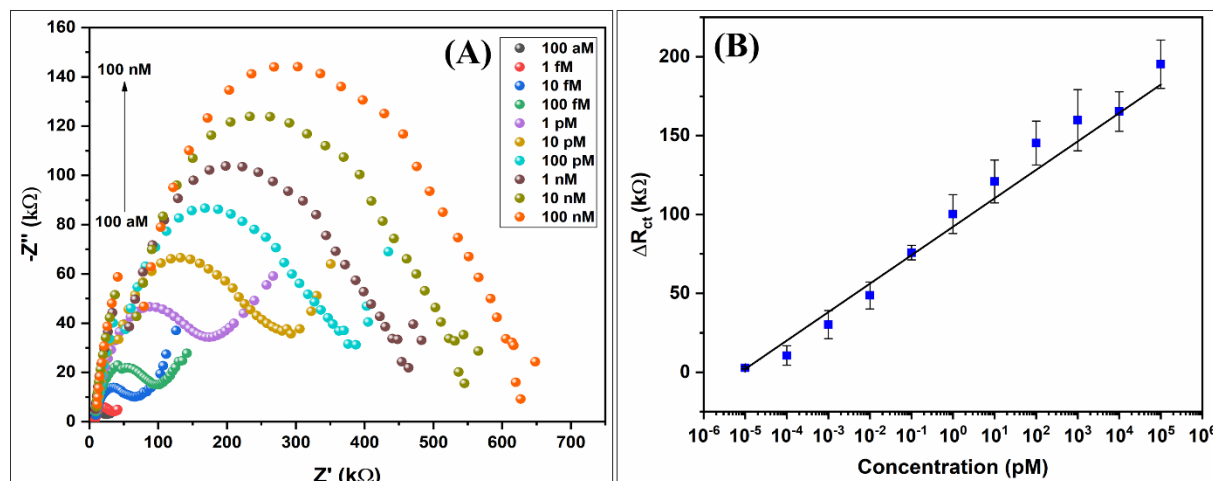


Figure 4.7. (A) Nyquist plots of the C5@paper electrodes for different concentrations of the TP, and (B) Corresponding calibration curve showing linear correlation between ΔR_{ct} and log of TP concentration.

The C5@paper electrode-based biosensing assay described here seems to be possessing an improved detection limit over other recent works on the development of paper-based, electrochemical biosensors for pathogenic DNA detection. As per gel electrophoresis studies, the longest and the shortest supersandwich DNA duplex lengths were considered to be 150 bp and 69 bp, respectively (**Figure 4.6(B)**). Accordingly, the detection limit (45 aM) was found to be equivalent to $10\text{-}22 \text{ copies } \mu\text{L}^{-1}$. Recent studies on colorimetric detection of NG reported detection limit of 20 copies/test and 50 copies/test based on MCDA and LAMP, respectively [134, 135]. Another study reported a detection limit of $10 \text{ copies } \mu\text{L}^{-1}$ for a Cas13a-based specific assay (SHERLOCK) developed for detection of *porA* and azithromycin resistance gene of NG [137]. It is worth mentioning here that this assay was only tested against purified dsDNA. These results demonstrate that the proposed biosensing assay is noteworthy in relation to

recently reported works, in terms of its simple yet efficient detection strategy, use of limited reagents and sample volume, and label-free detection in an electrochemical system.

Table 4.3. Summary of recent reports on paper-based DNA biosensors for detection of pathogens.

S. No.	Ink formulation/ Nanomaterial	Type of DNA assay	Target pathogen	Linear range	Sensitivity (LOD)	Reference
1.	Tungsten disulphide quantum dots	Traditional hybridization	Specific meningitis	1 nM – 100 μ M	(1 nM)	[195]
2.	Oxidized graphitic carbon nitride	Traditional hybridization	Norovirus	10^{-7} - 10^2 μ M	--(100 fM)	[196]
3.	Carbon graphene ink (commercial)	Traditional hybridization (pyrrolidinyl peptide nucleic acid-mediated)	Hepatitis B virus	50 pM- 100 nM	-- (1.45 pM)	[106]
4.	Ni–Au composite/CNT/PVA	Traditional hybridization	HIV DNA	10 nM – 1 μ M	(0.13 nM)	[14]
5.	Ag nanoprisms electrodeposited on graphene quantum dots (GQDs)	Traditional hybridization	<i>Leishmania infantum</i>	1 zM - 1 nM	1 zM (LOQ*)	[181]
6.	Graphene nanosheets	Direct analysis	-- (dsDNA)	0.2-5 pg mL^{-1}	0.00656 $\text{mA pg}^{-1} \text{cm}^{-2}$	[25]
7.	cMWCNT	Supersandwich hybridization	<i>Neisseria gonorrhoeae</i>	100 aM- 100 nM (5 zmol-5 pmol)	26.21 kΩ pM^{-1} (17.1 fM)	This work

Currently, the gold standard for NG detection in clinical samples is PCR. These results were further compared to commercial PCR assays in terms of detection limit. GeneProof® has commercialized an NG dual target PCR kit whose detection limit is claimed to be 0.109 copies μL^{-1} [197]. While a different study has reported the detection limit of this assay to be 1.5 copies μL^{-1} [198]. A detection limit of $10\text{E-}7$ dilution has been reported for another assay for *porA* detection [199], while another reported a detection limit of 10^2 - 10^3 copies mL^{-1} (0.1-1 copy μL^{-1}) [93]. It should be noted here that the length of DNA concatemers obtained in this

supersandwich biosensor was unknown and hence the detection limit (10^{-22} copies μL^{-1}) is an approximate value. While, the copy number is more accurately determined in PCR assays as the length of amplicons is known. Another factor involved is the immobilization of capture probe: PCR assays allow the amplification to proceed in aqueous conditions without any surface capture of molecules. While in this biosensor, the SCP was immobilized onto MBs. This may affect the binding of SCP-TP-SDP binding. Thus, these factors need to be considered while comparing the performance parameters of biosensors and PCR, particularly detection limit.

4.3.5. Real sample analysis and specificity studies

The response of the biosensor towards genomic DNA extracted from NG (mixed and WHO M strains) was assessed and compared to the response to synthetic TP in the same concentration range (100 aM-1 pM). The change in the ΔR_{ct} values of the biosensing electrode for equal concentrations of the synthetic TP and genomic DNA was not significant (**Figure 4.8(A)**). This suggests that the biosensing assay can be utilized in practical, clinical situations.

Further, the genomic DNA of NG was mixed with other bacterial DNA, viz. *Neisseria mucosa* (NMu), *Neisseria meningitidis* (NM), *Neisseria sicca* (NS), *Klebsiella pneumoniae* (KP), *Enterococcus faecalis* (EF), *Escherichia coli* (EC), *Staphylococcus aureus* (SA), and *Lactobacillus fermentum* (LF), and was used for assessing the biosensor response. Since the boiling method was utilized to extract DNA, all samples would have perhaps been contaminated by proteins and RNA. The detailed protocol for this study has been provided in **Section 2.6** of **Chapter 2**. The value of ΔR_{ct} of the C5@paper biosensing electrode did not change significantly in the presence of other bacterial DNA (**Figure 4.8(B)**). These studies highlight the importance of using MBs that were used for sample enrichment. The high specificity of the designed oligonucleotide probes may also contribute to the high specificity to NG DNA observed here.

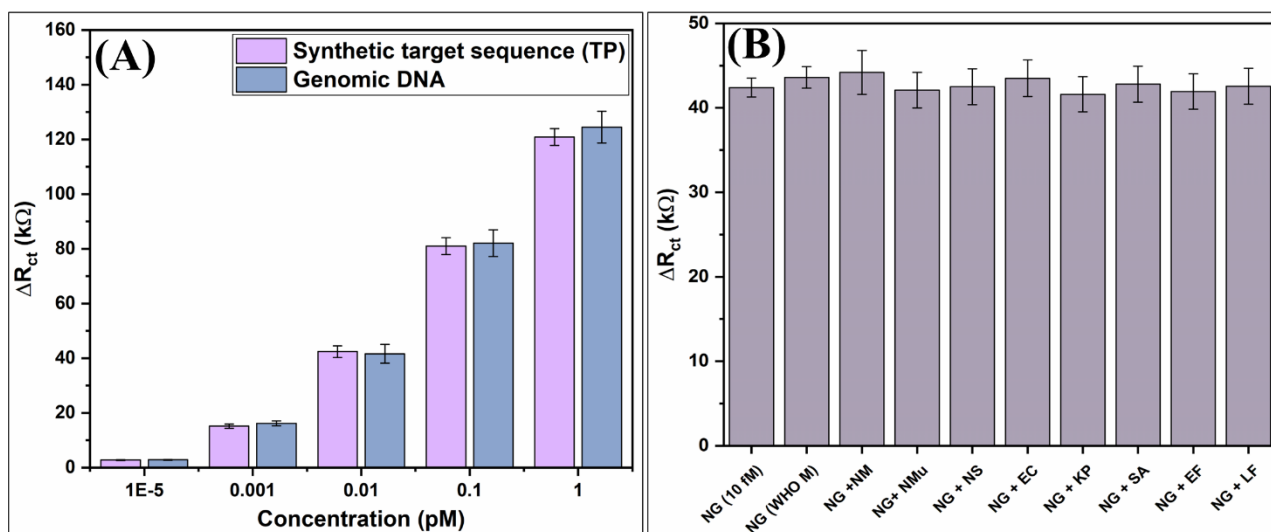


Figure 4.8. (A) Bar graph showing the ΔR_{ct} values of the C5@paper electrodes in response to synthetic TP and genomic DNA from NG (100 aM – 1 pM), and (B) the ΔR_{ct} values in response to NG DNA mixed with other bacterial DNA.

4.4. Conclusion

In this work, the composition of a conductive ink (C5) was optimized and was subsequently utilized to fabricate conducting paper electrodes (C5@paper) for detection of *N. gonorrhoeae* in a label-free and ultrasensitive manner. The flow properties of the C5 ink were optimized to make it suitable for screen printing. The maximum conductivity value at 4 coats of the C5@paper electrodes was found to be 10.1 S. cm⁻¹. A supersandwich DNA hybridization assay was designed mediated by magnetic beads. The DNA assay was integrated with the C5@paper electrodes and the resulting biosensor was found to be sensitive within the linear range of 100 aM-100 nM and detection limit of 45 aM. The specificity of the biosensing assay for gonococcal DNA was verified by detecting genomic NG DNA from a mixture of non-gonococcal DNA. The utility of paper-based biosensors for DNA detection is highlighted in this work along with the potential of conductive inks in biosensor fabrication. An attempt to shed light on gonorrhoea and STIs in general as a diagnostic challenge has also been made.

The conductive ink was optimized for both conductivity and rheology in this work. Hence, it is imperative to optimize the screen-printing process for the conductive ink, and determine the utility of the fabricated screen-printed electrodes (SPEs) for biosensing applications. These studies have been discussed in the upcoming chapter (**Chapter 5**).

These results have been published as “Conductive ink-coated paper-based supersandwich DNA biosensor for ultrasensitive detection of Neisseria gonorrhoeae” in Biosensors, 2023 April; 13(4):486 [200].

Chapter 5
Screen Printing of MWCNT-Modified
Conductive Ink Towards Paper-Based Biosensor
for Neisseria gonorrhoeae Detection

5.1 Introduction

Conductive inks are increasingly being employed in the fabrication of printed biosensors. Especially in the current times, it is imperative that on-demand, cost-effective, field-deployable biosensing devices should be developed that can produce fast and reliable results in order to deal with population-wide screening or any medical emergency situations. The development of efficient conductive inks can help in realizing the fabrication of such ‘on-demand’ and all-printed biosensors. Different methods can be employed to coat conductive inks onto desired substrates, such as inkjet printing, aerosol printing, spray coating, screen printing, etc. Out of these, screen printing is the most prominent method employed in the fabrication of biosensors. It offers flexibility in the choice of the substrate, good pattern resolution, and control over pattern deposition [57]. However, viscosity of the ink is a crucial factor to impart screen-printability; the ink should be thixotropic in nature for efficient screen printing. At the same time, the conductivity cannot be compromised largely by the addition of extra additives. Thus, there needs to be a delicate balance and trade-off between the conductivity and viscosity of a screen printable conductive ink.

Conductive inks can be screen printed to yield the entire three-electrode electrochemical system onto the desired substrates such as paper [201, 202]. These printed assemblies are referred to as screen-printed electrodes (SPEs). They eliminate the need of external electrodes in an electrochemical system. Due to their portability and cost effectiveness, they can be deployed at the PoC for mass screening and early detection of many asymptomatic infections and diseases, such as COVID-19, STIs, infectious diseases, etc. [203-205]. Commercially available SPEs are fabricated by the screen printing of inks having conductive (micro/nano)materials such as metals (Ag, Au, Pt, etc.), or carbon black/graphite onto plastic substrates [103]. These SPEs are employed in biosensing applications by modifying the WE by nanomaterials to enhance its surface area/electrochemical activity. Screen printing of

conductive inks to yield SPEs can potentially alleviate this step entirely as the nanomaterials would be directly printed onto the substrates. This would eventually lead to immobilization of more bioreceptors on the WE surface without any prior modifications.

Currently, the SPEs are printed on plastic substrates. With increasing focus on sustainability and ‘green’ alternatives, however, there has been a shift from the traditional plastic substrates to the more sustainable and biodegradable paper [1, 20, 174]. Recent studies have demonstrated the development of paper-based SPEs for various applications [25, 108, 206]. The screen printing of paper with conductive inks poses a special challenge: the hydrophilicity and porosity of paper may lead to the seeping of the inks into the matrix (lateral flow) and lead to poor resolution patterns [12]. Secondly, the more porous the paper, the lesser conductivity it would exhibit after screen printing [12]. Thus, the choice of the type of paper may also dictate the device performance. These factors should be considered while formulating a conductive ink for paper-based devices.

The most prominent role of screen-printed paper biosensors is in the field of clinical diagnostics [30, 76, 207]. Screen-printed paper biosensors can be deployed in mass screening of infectious diseases such as STIs, and can have a significant impact on disease burden. Screen-printed paper devices have been developed for PoC detection of several biomarkers such as glucose, enzymes, cancer markers, etc. [201, 207-209]. Gonorrhoea is such a disease that requires population-wide surveillance and PoC testing devices for timely detection and proper medical intervention.

This chapter contains results of the studies relating to the screen printing of an MWCNT-based conductive ink (C5) and subsequent fabrication of fully printed paper-based SPE. As proof of concept, the paper-based SPEs were utilized to detect NG *porA* DNA sequence using the traditional sandwich hybridization principle.

5.2 Experimental details

5.2.1 Conductive ink formulation

The C5 conductive ink that was formulated in **Chapter 4** and optimized for rheology was utilized in this study for screen printing. Briefly, the conductive ink was prepared by dispersing 5% *w/v* CMC (in water) in a mixture of Tp and PS80 (1:1) by magnetic stirring at 1000 rpm for 2 h. Subsequently, cMWCNTs (5% *w/v*) were dispersed in this emulsion with vigorous stirring conducted overnight at 1000 rpm to yield the C5 conductive ink. The detailed protocol is provided in Section 4.2.2 of **Chapter 4**.

5.2.2 Screen printing of the C5 conductive ink onto paper

The protocol of the screen-printing process has been detailed in **Section 2.5 of Chapter 2**.

5.2.3 Conductivity studies

For conductivity studies, several coats of the C5 ink were made to print rectangular patterns ($2 \times 1 \text{ cm}^2$) onto paper substrates (office paper and ivory paper). The printed patterns were dried after every coat at 120 °C for 5 min. Thereafter, these printed patterns were cut into half to yield two printed strips of $1 \times 1 \text{ cm}^2$ in size for conductivity measurements. The strips were stored in dry conditions until analysis.

5.2.4 Electrochemical studies

Electrochemical stability of the SPEs was analyzed by recording their CV response in repeated cycles. For biosensing studies, equimolar concentrations of the capture probe, CP, target, TP, and the detector probe, DP (10 μL each) were mixed and drop casted on the working electrode of the SPE followed by drying at 60 °C for 15 min. This was repeated for different concentrations of TP. Thereafter, 30 μL of PBS (pH 7 with ferri/ferrocyanide) buffer was drop cast onto the working electrode for CV studies.

5.3 Results and discussion

5.3.1 Screen printing studies

Screen printing works by forcing an ink through a mask onto the substrate using a squeegee. The mask allows the ink to pass through the pattern to be printed only allowing high resolution printing (**Figure 5.1(A)**). The principle and working of screen printing are discussed in detail in **Section 1.3.2**. The C5 ink was screen printed onto two kinds of paper: regular office paper having a grammage of ~80-100 gsm and ivory paper with grammage of 250 gsm. **Figure 5.1(B)** shows the image of the mask screen utilized in printing SPE and other patterns onto the paper substrates.

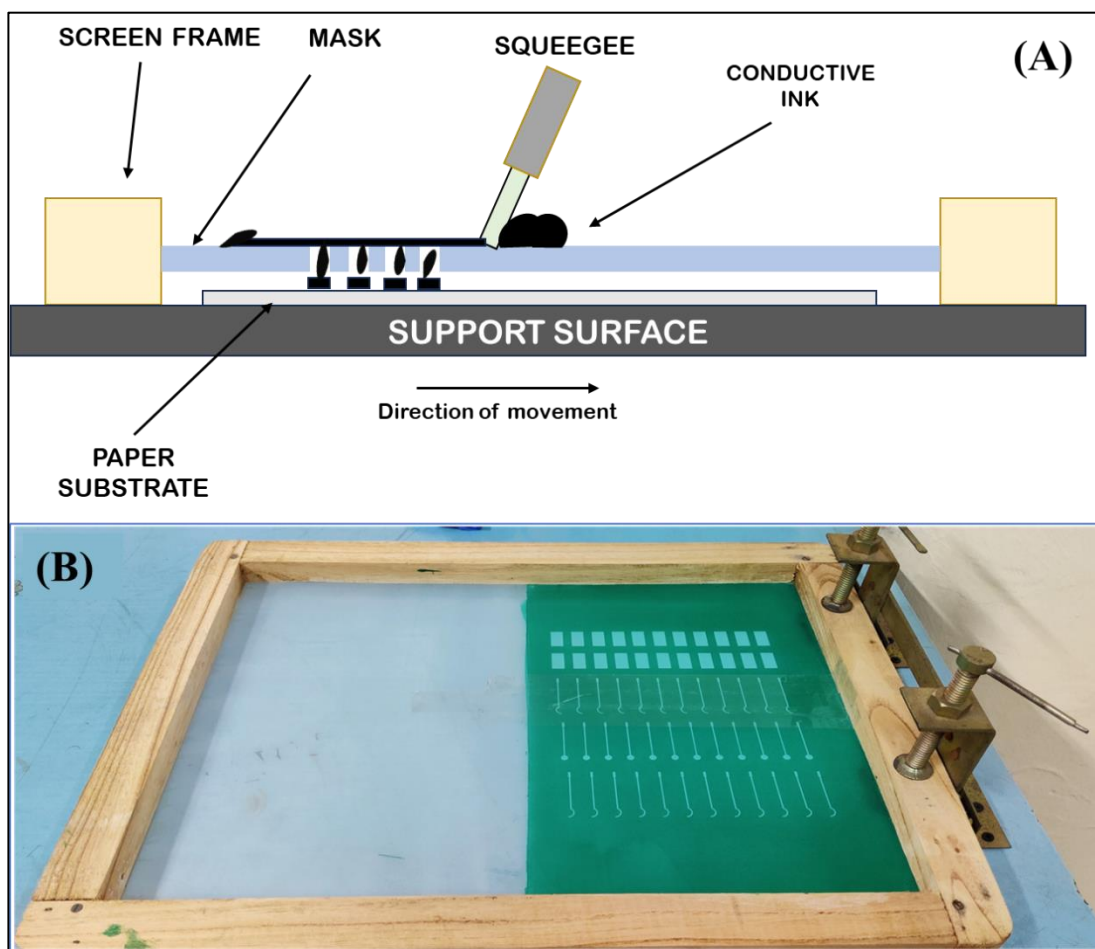


Figure 5.1. (A) Schematic showing the process of screen printing, and (B) A photograph of the screen-printing mask utilized in the study.

The photographic images of the resulting patterns (after 6 coats) on ivory paper are shown in **Figure 5.2(A & B)** (the images are not to scale). Upon visual inspection, both the rectangular patterns (**Figure 5.1(A)**, size $2 \times 1 \text{ cm}^2$) and SPEs (**Figure 5.1(B)**) appear uniform with sharp images. The dimensions of the SPE are provided in **Figure 2.1**. Both the width of each electrode path (vertical lines) and the interelectrode distance in the SPE is 0.2 mm (200 μm). The printing of clear, continuous lines verifies that the C5 ink is suitable for screen printing. Further, it indicates that the resolution of the screen printing is at least 200 μm . This is comparable to some recent studies on the development of screen printable conductive inks. A CNT/carbon black(CB) ink has been screen printed to yield patterns with line width of 50-500 μm [206]. In another study, graphene/CB composite inks have yielded line widths of 100-140 μm [65]. This study also demonstrated that there is a strong correlation between the viscosity of the printing ink and the resolution of printing. Inks with good viscosity recovery after removal of force often perform better in screen printing applications.

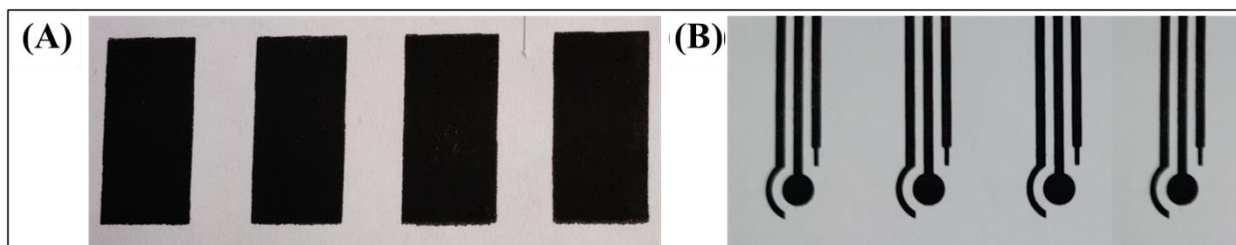


Figure 5.2. Photographic images of (A) rectangular pattern, and (B) SPE printed onto ivory paper by the C5 ink (without Ag/AgCl) (the images are not to scale).

5.3.2 SEM studies

Figure 5.3(A) shows the screen-printed ivory paper with both the printed and the nonprinted regions. The boundary between the printed and nonprinted region is very clear, uniform, and appears like a straight line, indicating the resolution and preciseness of the screen-printing process. Further, the printing coat appeared uniform and covered the cellulose fibers entirely in the printed region (**Figure 5.3(B)**), pointing towards the homogeneity and the

superior viscoelastic properties of the C5 ink (please see **Chapter 4** for details).

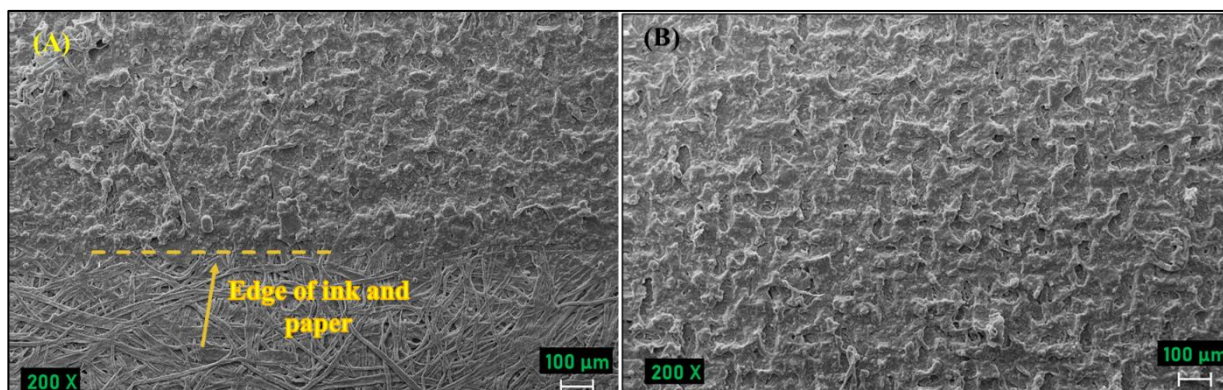


Figure 5.3 SEM images of (A) the screen-printed paper showing the printed and nonprinted regions, and (B) the surface morphology of the printed patterns.

5.3.3 Conductivity studies

The resistivity of the printed patterns was found to reduce with increase in the number of coats, as has also been observed in earlier chapters. The calculations utilized for the conductivity calculations were the same as given in **Section 2.6.10 (Eqs. 2.5-2.8)**. This decrease in resistivity may be attributed to the increase in the MWCNT content after every printing pass. The maximum conductivity of the printed ivory and office paper, as found by the 4-probe method, were found to be 3.37 S. cm^{-1} and 3.48 S. cm^{-1} , respectively. The similar values of conductivity for these different types of paper indicated that the C5 ink is capable of printing paper substrates having different grammage values. Similar trend has been observed in other studies, wherein the resistivity of the printed patterns decreased upon increasing the thickness of the printing coats [63, 65]. Another study showed that patterns printed by graphene/CNT/CB composite yielded a sheet resistance of $4 \Omega \text{ sq}^{-1}$ [67]. However, it must be noted that CNT composites may possess higher conductivity values than pristine MWCNT owing to the synergistic effect of other conductive nanomaterials.

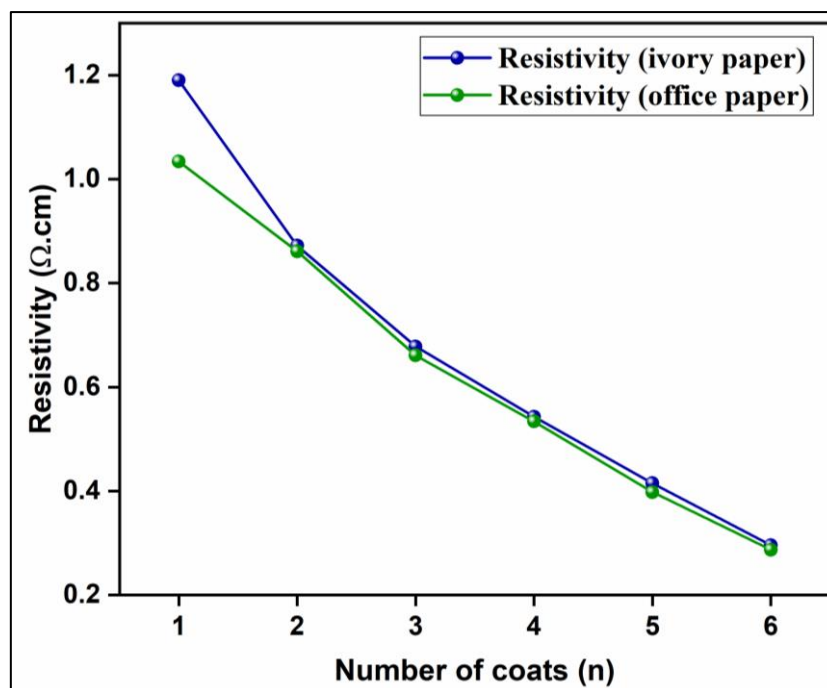


Figure 5.4. Resistivity of ivory and office paper with number of coats.

5.3.4 Electrochemical characterization

Electrochemical studies were performed to determine the stability of the SPEs in buffer conditions. As shown in **Figure 5.5(A)**, the CV curves are continuous and devoid of noise until 20th CV cycle. A comparison of the 1st and 20th CV cycle of the same SPE revealed a slight reduction in the redox peak current value. This might be because of adsorption of ions on the ink surface and further seeping into the ink matrix, which might repel other like-charged ions to migrate to the electrode surface. Considering that one CV cycle takes around 2 min to complete, the SPE showed stable response till 40 min. This is significant considering that the binder in the C5 ink, CMC, is highly hydrophilic in nature.

The SPE also yielded a noise-free and continuous semicircular Nyquist plot followed by a straight line, indicating that diffusion-mediated processes are also occurring at the electrode surface (**Figure 5.5(B)**). The corresponding equivalent circuit is shown in the inset of **Figure 5.5(B)**. The R_{ct} of the SPE was found to be 5.6 k Ω , which is much higher than the

values obtained for manually coated C5@paper electrodes (**Chapter 4**). This might be because the thickness of the ink obtained after screen printing is less than that obtained by manual coating of paper. Also, there is the presence of CPE in place of both C_{dl} and W , indicating that not only the double layer is partially resistive in nature but the diffusion of ions to the electrode surface might be leading to their adsorption at the electrode surface [73].

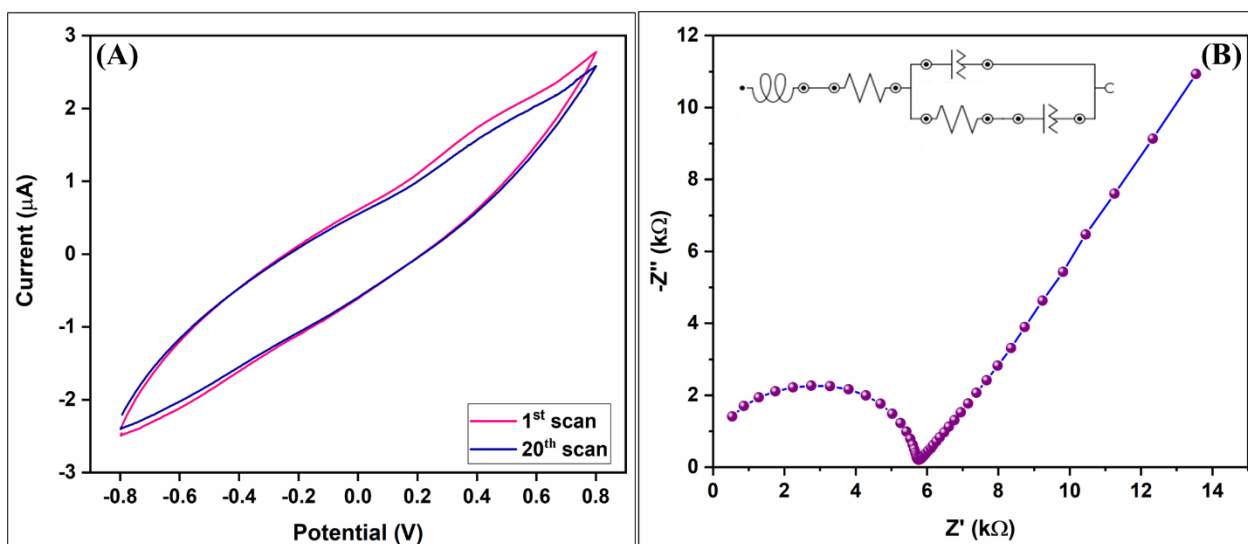


Figure 5.5. (A) CV response of the SPEs at 1st and 20th CV cycle indicating the continuous use stability, and (B) Nyquist plot of the SPE with the equivalent model circuit in the inset.

5.3.5 Electrochemical response studies

As proof of concept, the SPEs were utilized to detect different concentrations of the NG *porA* pseudogene sequence (TP). The traditional sandwich hybridization method was utilized for forming a ternary duplex among the capture (CP), TP, and the detector probe (DP). The sequences of these probes are provided in **Table 3.1** of **Chapter 3**. The DP is labeled with MetB at 3'end, hence CV studies were conducted to measure change in the signal. As the concentration of the CP-TP-DP ternary complex increased on the WE of the SPE surface, the current signal increased significantly (**Figure 5.6(A)**). This was attributed to the synergistic electron exchange mediated by the MetB on the DP surface and the ferro-ferricyanide present in the buffer. Evidently, the redox peaks were not very visible at low concentrations of TP (**Figure 5.6(B)**). However, with 10-fold increase in concentration at the WE surface, the redox

peaks became visible and prominent, which can only be due to the increase in the MetB concentration (since, the concentration of ferro-ferricyanide in the buffer is fixed).

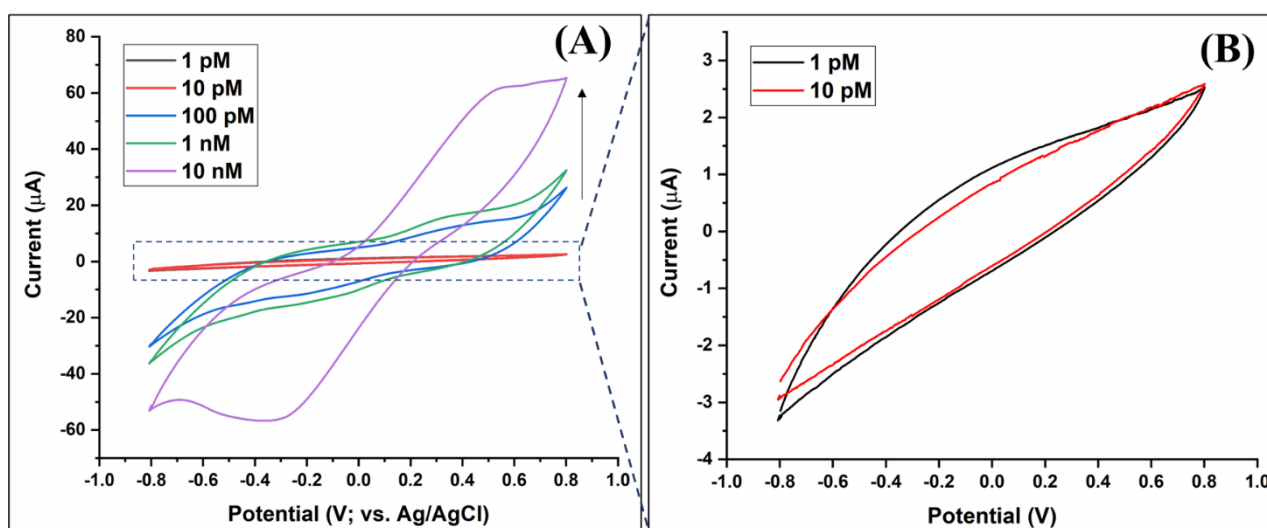


Figure 5.6. (A) CV response of the SPE with change in concentration of CP-TP-DP complex in the range of 1 pM-10 nM, and (B) Magnified view of the CV curves obtained for 1 and 10 pM CP-TP-DP complexes.

The response was also found to be linear within the concentration range of 1 pM- 10 nM given by the equation:

$$\text{Peak current, } I_p = 13.596 \times (\log[\text{concentration}]) + 1.848, R^2 = 0.95 \text{ (Eq. 5.1)}$$

The corresponding linear calibration curve is given in **Figure 5.7**. The sensitivity of the SPE biosensor was found to be $13.59 \pm 1.69 \mu\text{A} \cdot (\log[\text{concentration}])^{-1}$ with a detection limit of 0.92 pM. Generally, the concentration of the detector probe (DP) should be taken in excess of the target DNA to ensure hybridization [88]. Since, in this assay, there was a chance of unbound DP to adsorb on the WE surface leading to nonspecific signal, the concentration of DP was kept equal to the concentration of TP. This reduced signal generation from the non-bound DP to a large extent. The value of sensitivity is higher than that obtained in MB-mediated sandwich assay (**Chapter 3**). This is possibly due to the elimination of MBs from the assay; DNA hybridization takes place differently in aqueous and surface-immobilized conditions [88]. The probe density on the MB surface can directly affect the target capture, and subsequently the

device sensitivity, which is not the case when hybridization occurs in aqueous conditions.

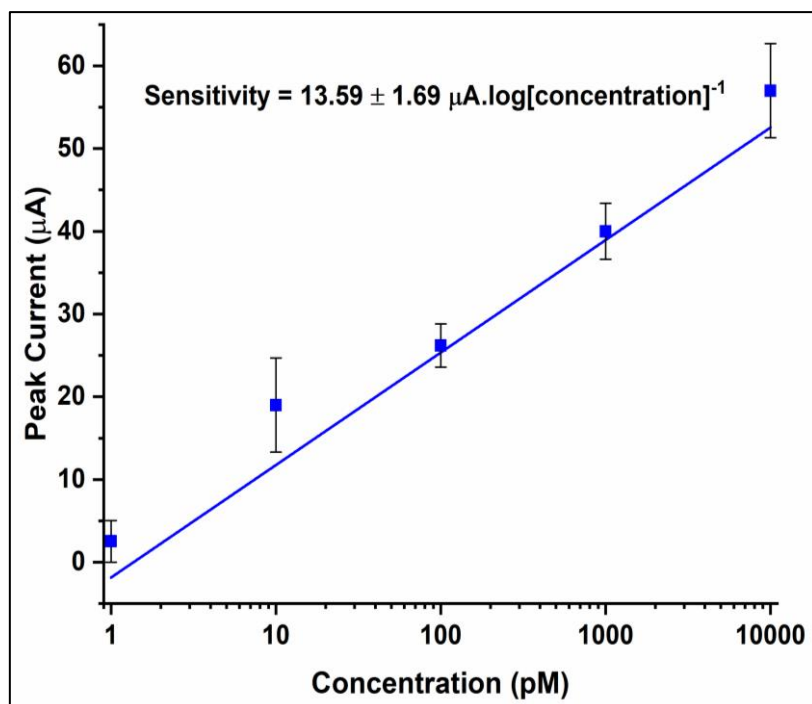


Figure 5.7. Linear calibration curve between peak current obtained by the SPE biosensor and concentration of CP-TP-DP complex.

This study demonstrates the potential utility of the paper-based SPE in detection of gonorrhea and PoC diagnostics in general.

5.4 Conclusion

This chapter has described the results of studies conducted to demonstrate the screen printability of the C5 ink and the utilization of the printed electrodes for biosensing applications. Masks were made on a nylon mesh screen using patterns designed on a professional software. The C5 ink was thereafter printed on regular office paper (grammage ~ 100 gsm) and ivory paper (grammage ~250 gsm). SEM analysis revealed the uniformity of the printed ink coats and absence of seeping into nonprinted zone of paper. The conductivity values of both the printed conducting paper were found to be similar at 6 printing coats, indicating that the ink successfully managed to coat two different kinds of paper with different porosities.

Electrochemical studies found that the SPEs were stable in buffer conditions until 20 CV cycles and displayed a stable EIS response indicating the stability of the printed layer on the electrode surface. As proof of concept, the SPEs were shown to detect NG porA pseudogene sequence within the linear range of 1 pM – 10 nM with a sensitivity of $13.59 \pm 1.69 \mu\text{A} \cdot (\log[\text{concentration}])^{-1}$.

This study demonstrates the fabrication of an all-printed paper-based biosensing device with the potential of application at the PoC. It highlights the role of conductive inks towards PoC device fabrication and opens new possibilities for gonococcal diagnostics.

*These results entitled “Screen printed MWCNT-modified conductive ink towards paper-based biosensor for *Neisseria gonorrhoeae* detection” have been prepared for submission in *Microchimica Acta*.*

Chapter 6
Summary and Future Prospects

6.1 Summary

The primary objective of this thesis was to develop fabricate conductive paper electrodes for detection of analytes of clinical significance. *Neisseria gonorrhoeae porA* pseudogene was chosen as the target analyte after literature review. The development of these biosensors was organized through a defined set of objective steps including fabrication and characterization of nanomaterial-modified conducting paper, selection, and immobilization of specific DNA probes for biosensing applications, electrochemical characterization, and response studies (detection of target analyte), and real sample analysis via detection of NG genomic DNA. All results have been discussed in detail in the preceding **Chapters 1-5**.

Chapter 1 discussed the background and study rationale of this work. It discussed the current role of characteristic features of paper, nanomaterials-modified conducting paper, and provided an overview of the different methods and uses of conductive paper fabrication. Additionally, literature review on conductive ink formulations, properties of MWCNTs and their use as conductive fillers in inks was provided. The basic components and type of biosensors were discussed with special emphasis on DNA biosensors. Two types of detection principles of DNA biosensors: sandwich hybridization and supersandwich hybridization, were highlighted through literature evidence. Gonorrhea, the STI caused by NG, was discussed with focus on its causes, symptoms, and conventional methods of detection. Recent advances in gonorrhea detection were summarized along with the current gap in research on the same.

Chapter 2 provided details of the different experimental techniques that were utilized to characterize the morphology, structure, elemental composition, and other physicochemical properties of conductive ink formulations and ink-coated paper electrodes. Basic principles and working of techniques such as XRD, TEM, SEM, FESEM, AFM, XPS, Raman spectroscopy, etc. were summarized. The details of CV and EIS utilized for electrochemical characterization and evaluation of biosensing parameters were discussed. The details of the different protocols

and experimental studies for optimizing conductive ink formulations for conductivity and rheology, fabrication of conducting paper electrodes, immobilization of capture probe onto magnetic beads and subsequent capture of the target DNA for biosensing analysis, and genomic DNA extraction for real sample analysis were provided.

Chapter 3 described the results of the studies relating to the fabrication of MWCNT-modified conducting paper biosensor for electrochemical detection of NG. A cMWCNT (1% w/v)-based ink was prepared and coated onto paper for fabrication of conducting paper. The optimum annealing temperature and time for the cMWCNT@paper electrodes were found to be 120 °C and 10 min., respectively. The least resistivity of these electrodes was found to be 1.066 Ω.cm (mean value). The conductive ink was further found to be shear thinning in nature, indicating its suitability for screen printing. SEM studies revealed that the cMWCNT ink covered the cellulose fibers completely upon coating in a uniform manner. Avidin-modified magnetic beads (Av/MBs) were also further shown to be adsorbed uniformly onto the cMWCNT@paper electrodes. While contact angle studies showed that the wettability increased after ink coating, i.e., the contact angle of the cMWCNT@paper electrodes was found to be significantly lower than that of bare paper. Further, these electrodes were shown to be batch reproducible as determined by CV studies with good storage stability and continuous use stability (stability checked in buffer till 25 cycles). The Av/MBs were further utilized for immobilization of CP and further specific capturing of different concentrations of TP on the MB surface. MetB-labeled DP molecules were used to sandwich hybridize and form the C-T-D/Av/MB complexes. These complexes were drop casted onto the conductive cMWCNT@paper electrodes for biosensing studies. The electrochemical biosensing assay displayed linear trend in the concentration range of 100 fM-100 nM, with detection limit of 0.13 pM and sensitivity of $5.09 \mu\text{A} \cdot [\log(\text{concentration})]^{-1}$. Further, the performance of the biosensing assay was evaluated by determining the concentration of genomic NG DNA.

Interferent analysis revealed that the biosensor was highly specific to NG DNA. This chapter led to conception of further studies wherein the conductive ink formulation and the principle of detection of NG DNA were modified in order to enhance conductivity and rheological properties of the conductive ink and sensitivity of the biosensor, respectively.

Chapter 4 details of the studies relating to the optimization of the conductive ink (C5) formulation for rheology and conductivity, and its utilization in the fabrication of conductive C5@paper electrodes for biosensing applications. The emulsion base of the C5 ink was chosen from a set of three bases via viscometry and 3iTT studies; the base with 5% *w/v* CMC, having the highest initial apparent viscosity, shear thinning behavior, and fastest (and most) viscosity recovery, was chosen for further studies. The ratio of the MWCNT:CMC was kept 1:1, i.e. 5% *w/v* cMWCNTs were utilized as the conductive filler. The maximum conductivity value of the C5@paper electrodes was $10.1 \pm 0.24 \text{ S}\cdot\text{cm}^{-1}$ for 4 coats of the C5 ink (75 μL for each coat). Further, a supersandwich DNA hybridization assay was developed assisted by MBs. The detector probe, SDP, was designed such that it led to the binding of more than one TP-SDP hybridization complexes for every molecule of capture probe, SCP. Gel electrophoresis studies confirmed that in addition to the 43 base pairs (bp) long SCP-TP-SDP duplex, there were duplex of more than 100 bp long without any cross-hybridization (or, nonspecific binding). The MB-assisted supersandwich assay was performed in the same manner as discussed in Chapter 3, except that the TP and SDP were added simultaneously to the SCP/MBs. EIS studies revealed that the biosensor response was linear within the TP concentration range of 100 aM-100 nM with a detection limit of 45 aM. The biosensor was further shown to be highly specific and was used to detect different concentrations of genomic gonococcal DNA.

Chapter 5 discusses results of studies conducted screen printing of the conductive ink C5, which was optimized for rheology in **Chapter 4**. SPEs were printed onto office paper and ivory paper, wherein C5 ink was utilized to print the WE, and commercial graphite and

Ag/AgCl inks were utilized to print CE and RE, respectively. Conductivity studies revealed the maximum conductivity of patterns printed on ivory and office paper to be 3.37 S. cm⁻¹ and 3.48 S.cm⁻¹ (after 6 coats), indicating that the ink coated both types of paper in a similar manner. Further, the presence of a clear boundary between the printed layer and nonprinted paper fibers was observed in SEM studies. Evidently, the printed ink did not show any leeching/seeping into the nonprinted zone. SEM studies also revealed the homogenous nature of the printed C5 ink on the paper substrates. The SPEs were further shown to be stable in buffer conditions using CV studies, however the CV responses of different SPEs varied slightly more than the manually coated paper electrodes reported in previous chapters. As proof of concept, different concentrations of CP-TP-DP hybrid duplex were detected by the SPEs. The biosensing response was found to be linear within the concentration range of 1 pM – 10 nM and sensitivity of 13.59 ± 1.69 μA. (log[concentration])⁻¹. This study demonstrated the screen printability of the C5 ink and subsequent utilization of the SPEs towards biosensing applications.

The sensing parameters of conductive ink-modified paper biosensors demonstrated in this thesis are summarized in **Table 6.1**.

Table 6.1. Biosensing parameters of the cMWCNT@paper, C5@paper, and C5-based SPE biosensing platforms for detection of NG *porA* sequence.

Fabricated Electrodes	Detection principle	Detection limit	Linear detection range	Sensitivity
cMWCNT@paper	Traditional sandwich hybridization	0.13 pM	100 fM – 100 nM	5.09 μA. (log[concentration]) ⁻¹
C5@paper	Supersandwich hybridization	45 aM	100 aM – 100 nM	22 kΩ. (log[concentration]) ⁻¹
SPEs	Traditional sandwich hybridization	0.22 pM	1 pM – 10 nM	13.59 ± 1.69 μA. (log[concentration]) ⁻¹

It was observed that the sensitivity of the SPE for detection of NG was like that of cMWCNT@paper biosensing platform. However, its linear range was not as wide. This could have possibly been because of more variance in the base CV signal of the SPEs. However, the

C5@paper electrode employing supersandwich DNA hybridization principle of detection, demonstrated the widest linear range and lowest detection limit of all. This could only be explained by the amplification effect of the supersandwich DNA.

6.2 Future prospects

The work presented in this thesis is an effort to fabricate and utilize conductive ink-coated paper biosensors for clinical diagnostics, particularly *Neisseria gonorrhoeae* detection. The prospects of this work in the coming future are immense, and other studies may build upon this thesis work to develop advanced biosensing and PoC technologies. The conductivity of the conducting paper can further be improved by replacing cMWCNT with MWCNT hybrid nanocomposites as conductive fillers or using conductive additives. A recent study has demonstrated that addition of PEDOT:PSS to MWCNTs enhanced both conductivity and adherence to paper substrates significantly [26]. Further, the conductive ink formulation can be further optimized to adhere to other substrates in addition to paper. This can potentially expand the range of substrates that can be utilized in device fabrication. For example, replacing CMC with ethyl cellulose can yield adherence to not only paper, but to plastic substrates as well. However, since ethyl cellulose is not thixotropic, another additive may need to be added to optimize rheology. Another potential development towards enhancing conductivity could be the utilization of additives that can be easily removed from the printed ink after printing. Polyimines have been utilized in a recent study to form stable dispersion of MWCNTs, wherein they were depolymerized by heat/acid leading to enhanced conductivity of the resulting films on plastic substrates [210]. Further, the MB-mediated assays can be automated and integrated to SPEs for specific and rapid analysis [166]. Isothermal amplification methods, such as RCA or RPA, can be integrated to the conductive ink-modified paper electrodes to avoid the use of MBs in the biosensing assay.

This work also paves the way towards development of PoC diagnostic devices that are

sensitive and reliable. Some of the potential technologies where this work can potentially expand to are as follows:

- i. **Biosensing swabs:** Thread-based devices are being developed for the detection and analysis of various physiological markers [211, 212]. On similar lines, cotton swabs can be designed to not only collect samples, but also analyze them for the presence of inflammation markers that correlate to an infection. The samples can then further be analyzed for the presence of NG or other STI-causing microorganisms.
- ii. **At-home screening tests:** Efforts should be made to develop at-home paper/SPE-based screening tests for gonorrhea. In fact, the demand for at-home sample self-collection and self-screening for STIs has increased in the post-COVID-19 era [213]. Gonorrhea is often underreported due to lack of awareness/access to STI clinics, absence of symptoms, or stigma associated with STIs. Development of such kits may promote better personal health care management and convince affected individuals to visit clinics for timely diagnosis.
- iii. **Papertronics:** Papertronics can be envisioned as an extension of printed electronics. An integrated paper-based device can be devised, wherein the battery, the biosensing substrate, and related electronics are entirely fabricated onto paper substrates [21]. Such devices can significantly lower the cost of diagnostic tests and enable rapid screening and analysis for STIs and other infections.
- iv. **On-paper PCR:** Recently, NAATs have been integrated to cotton fiber-based electrodes for sensitive detection of bacterial DNA [212]. Similarly, PCR or other isothermal amplification techniques, such as RCA or RPA, can be potentially integrated to paper-based electrochemical devices. In fact, many studies have demonstrated the promise of paper-based platforms for nucleic acid extraction, amplification, and detection [214]. An

integrated paper-based device that can extract, amplify, and then detect gonococcal DNA can potentially help in timely diagnosis and intervention for this infection.

- v. Multi-microbe screening devices: Studies have shown that NG infection can be accompanied by other pathogenic infections, such as *Chlamydia trachomatis* or/and *Trichomonas vaginalis* (coinfections) [118, 119]. Thus, conducting paper-based devices can be envisioned wherein these coinfections can be detected simultaneously, similar to how cancer biomarkers are being analyzed by multiplex biosensors [30]. Such devices can play a significant role in reducing the burden of gonorrhoea and its coinfections.

References

7. References

- [1] D. Tobjörk, R. Österbacka, Paper electronics, *Advanced Materials*, 23(17) (2011) 1935-1961.
- [2] A. Jain, R. Jain, S. Jain, Paper Chromatography of Carbohydrates, Basic Techniques in Biochemistry, Microbiology and Molecular Biology: Principles and Techniques, Springer, Humana, New York, NY, 2020, pp. 263-264.
- [3] V. Shirshahi, G. Liu, Enhancing the analytical performance of paper lateral flow assays: From chemistry to engineering, *TrAC Trends in Analytical Chemistry*, 136 (2021) 116200.
- [4] V.-T. Nguyen, S. Song, S. Park, C. Joo, Recent advances in high-sensitivity detection methods for paper-based lateral-flow assay, *Biosensors and Bioelectronics*, 152 (2020) 112015.
- [5] S. Belsare, G. Côté, Development of a colorimetric paper fluidic dipstick assay for measurement of glycated albumin to monitor gestational diabetes at the point-of-care, *Talanta*, 223 (2021) 121728.
- [6] J. Liu, D. Mazumdar, Y. Lu, A simple and sensitive “dipstick” test in serum based on lateral flow separation of aptamer-linked nanostructures, *Angewandte Chemie International Edition*, 45(47) (2006) 7955-7959.
- [7] A. Russo, B.Y. Ahn, J.J. Adams, E.B. Duoss, J.T. Bernhard, J.A. Lewis, Pen-on-paper flexible electronics, *Advanced Materials*, 23(30) (2011) 3426-3430.
- [8] L. Gao, C. Zhu, L. Li, C. Zhang, J. Liu, H.-D. Yu, W. Huang, All paper-based flexible and wearable piezoresistive pressure sensor, *ACS Applied Materials & Interfaces*, 11(28) (2019) 25034-25042.
- [9] X. Dai, Z. Guo, The gorgeous transformation of paper: from cellulose paper to inorganic paper to 2D paper materials with multifunctional properties, *Journal of Materials Chemistry A*, 10(1) (2022) 122-156.
- [10] Y.-L. Chen, X. Zhang, T.-T. You, F. Xu, Deep eutectic solvents (DESs) for cellulose dissolution: A mini-review, *Cellulose*, 26 (2019) 205-213.
- [11] B. Yan, J. Zheng, L. Feng, W. Chen, W. Yang, Y. Dong, S. Jiang, Q. Zhang, S. He, All-cellulose-based high-rate performance solid-state supercapacitor enabled by nitrogen doping and porosity tuning, *Diamond and Related Materials*, 128 (2022) 109238.
- [12] T. Liang, X. Zou, R.K. Pal, J. Xie, M.K. Assasie-Gyimah, J. Liu, W. Guo, C. Chen, M. Tenorio, D. Sullivan, Tunable electrical properties of embossed, cellulose-based paper for skin-like sensing, *ACS Applied Materials and Interfaces*, 12(46) (2020) 51960-51968.
- [13] M. Irimia-Vladu, “Green” electronics: Biodegradable and biocompatible materials and devices for sustainable future, *Chemical Society Reviews*, 43(2) (2014) 588-610.
- [14] Q. Lu, T. Su, Z. Shang, D. Jin, Y. Shu, Q. Xu, X. Hu, Flexible paper-based Ni-MOF composite/AuNPs/CNTs film electrode for HIV DNA detection, *Biosensors and Bioelectronics*, 184 (2021) 113229.

- [15] E. Solhi, M. Hasanzadeh, P. Babaie, Electrochemical paper-based analytical devices (ePADs) toward biosensing: Recent advances and challenges in bioanalysis, *Analytical Methods*, 12(11) (2020) 1398-1414.
- [16] M. Costa, B. Veigas, J. Jacob, D. Santos, J. Gomes, P. Baptista, R. Martins, J. Inácio, E. Fortunato, A low cost, safe, disposable, rapid and self-sustainable paper-based platform for diagnostic testing: lab-on-paper, *Nanotechnology*, 25(9) (2014) 094006.
- [17] E. Noviana, T. Ozer, C.S. Carrell, J.S. Link, C. McMahon, I. Jang, C.S. Henry, Microfluidic paper-based analytical devices: from design to applications, *Chemical Reviews*, 121(19) (2021) 11835-11885.
- [18] M. Landers, S. Choi, Small-scale, storable paper biobatteries activated via human bodily fluids, *Nano Energy*, 97 (2022) 107227.
- [19] Y. Gao, S. Choi, Stepping toward Self-Powered papertronics: Integrating biobatteries into a single sheet of paper, *Advanced Materials Technologies*, 2(1) (2017) 1600194.
- [20] A. Sudheshwar, N. Malinverno, R. Hischier, B. Nowack, C. Som, The need for design-for-recycling of paper-based printed electronics—A prospective comparison with printed circuit boards, *Resources, Conservation and Recycling*, 189 (2023) 106757.
- [21] M. Landers, Integrated Components and Biobatteries for Disposable Papertronic Devices, State University of New York at Binghamton, 2022.
- [22] Y. Liao, R. Zhang, H. Wang, S. Ye, Y. Zhou, T. Ma, J. Zhu, L.D. Pfefferle, J. Qian, Highly conductive carbon-based aqueous inks toward electroluminescent devices, printed capacitive sensors and flexible wearable electronics, *RSC Advances*, 9(27) (2019) 15184-15189.
- [23] S. Kumar, Nanomaterials modified paper based biosensors for cancer detection, Delhi Technological University, New Delhi, 2016, p. 247.
- [24] S. Kumar, S. Kumar, S. Srivastava, B.K. Yadav, S.H. Lee, J.G. Sharma, D.C. Doval, B.D. Malhotra, Reduced graphene oxide modified smart conducting paper for cancer biosensor, *Biosensors and Bioelectronics*, 73 (2015) 114-122.
- [25] J. Mohanraj, D. Durgalakshmi, R.A. Rakkesh, S. Balakumar, S. Rajendran, H. Karimi-Maleh, Facile synthesis of paper based graphene electrodes for point of care devices: A double stranded DNA (dsDNA) biosensor, *Journal of Colloid and Interface Science*, 566 (2020) 463-472.
- [26] A.S. Pillai, A. Chandran, S.K. Peethambharan, MWCNT ink with PEDOT:PSS as a multifunctional additive for energy efficient flexible heating applications, *Applied Materials Today*, 23 (2021) 100987.
- [27] S. Kumar, P. Rai, J.G. Sharma, A. Sharma, B.D. Malhotra, PEDOT:PSS/PVA-nanofibers-decorated conducting paper for cancer diagnostics, *Advanced Materials Technologies*, 1(4) (2016) 1600056.
- [28] G. Paul, S. Verma, O. Jalil, D. Thakur, C.M. Pandey, D. Kumar, PEDOT:PSS-grafted graphene oxide-titanium dioxide nanohybrid-based conducting paper for glucose detection, *Polymers for Advanced Technologies*, 32(4) (2021) 1774-1782.

- [29] S. Kumar, C.M. Pandey, A. Hatamie, A. Simchi, M. Willander, B.D. Malhotra, Nanomaterial-modified conducting paper: Fabrication, properties, and emerging biomedical applications, *Global Challenges*, 3(12) (2019) 1900041.
- [30] K. Ratajczak, M. Stobiecka, High-performance modified cellulose paper-based biosensors for medical diagnostics and early cancer screening: A concise review, *Carbohydrate Polymers*, 229 (2020) 115463.
- [31] Q.H. Nguyen, M.I. Kim, Nanomaterial-mediated paper-based biosensors for colorimetric pathogen detection, *Trends in Analytical Chemistry*, 132 (2020) 116038.
- [32] G. Hong, S. Diao, A.L. Antaris, H. Dai, Carbon nanomaterials for biological imaging and nanomedicinal therapy, *Chemical Reviews*, 115(19) (2015) 10816-10906.
- [33] D. Kala, T.K. Sharma, S. Gupta, V. Verma, A. Thakur, A. Kaushal, A.V. Trukhanov, S.V. Trukhanov, Graphene oxide nanoparticles modified paper electrode as a biosensing platform for detection of the htrA gene of *O. tsutsugamushi*, *Sensors*, 21(13) (2021) 4366.
- [34] M. Cao, D.B. Xiong, L. Yang, S. Li, Y. Xie, Q. Guo, Z. Li, H. Adams, J. Gu, T. Fan, Ultrahigh electrical conductivity of graphene embedded in metals, *Advanced Functional Materials*, 29(17) (2019) 1806792.
- [35] S. Burrs, M. Bhargava, R. Sidhu, J. Kiernan-Lewis, C. Gomes, J. Claussen, E. McLamore, A paper based graphene-nanocauliflower hybrid composite for point of care biosensing, *Biosensors and Bioelectronics*, 85 (2016) 479-487.
- [36] S. Kumar, N. Gupta, B.D. Malhotra, Ultrasensitive biosensing platform based on yttria doped zirconia-reduced graphene oxide nanocomposite for detection of salivary oral cancer biomarker, *Bioelectrochemistry*, 140 (2021) 107799.
- [37] H. Du, J. Zhang, C. Fang, G.J. Weng, Modeling the evolution of graphene agglomeration and the electrical and mechanical properties of graphene/polypropylene nanocomposites, *Journal of Applied Polymer Science*, 140(2) (2023) e53292.
- [38] M. Li, H. Zhou, Y. Zhang, Y. Liao, H. Zhou, The effect of defects on the interfacial mechanical properties of graphene/epoxy composites, *RSC Advances*, 7(73) (2017) 46101-46108.
- [39] J.W. Suk, R.D. Piner, J. An, R.S. Ruoff, Mechanical properties of monolayer graphene oxide, *ACS Nano*, 4(11) (2010) 6557-6564.
- [40] R. Raccichini, A. Varzi, S. Passerini, B. Scrosati, The role of graphene for electrochemical energy storage, *Nature Materials*, 14(3) (2015) 271-279.
- [41] J.S. Bulmer, A. Kaniyoor, J.A. Elliott, A meta-analysis of conductive and strong carbon nanotube materials, *Advanced Materials*, 33(36) (2021) 2008432.
- [42] H. Zhang, X. Sun, M.A. Hubbe, L. Pal, Highly conductive carbon nanotubes and flexible cellulose nanofibers composite membranes with semi-interpenetrating networks structure, *Carbohydrate Polymers*, 222 (2019) 115013.

- [43] K. Thiyagarajan, G. Rajini, D. Maji, Fully printed MWCNT strain sensor over paper substrate for human motion monitoring, *Flexible and Printed Electronics*, 7(4) (2022) 045003.
- [44] K. Thiyagarajan, G. Rajini, D. Maji, Cost-effective, disposable, flexible, and printable MWCNT-based wearable sensor for human body temperature monitoring, *IEEE Sensors Journal*, 22(17) (2021) 16756-16763.
- [45] K. Thiyagarajan, G. Rajini, D. Maji, Flexible, highly sensitive paper-based screen printed MWCNT/PDMS composite breath sensor for human respiration monitoring, *IEEE Sensors Journal*, 21(13) (2020) 13985-13995.
- [46] X. Qi, P. Matteini, B. Hwang, S. Lim, Roll stamped Ni/MWCNT composites for highly reliable cellulose paper-based strain sensor, *Cellulose*, 30(3) (2023) 1543-1552.
- [47] S. Veeralingam, S. Badhulika, Enzyme immobilized multi-walled carbon nanotubes on paper-based biosensor fabricated via mask-less hydrophilic and hydrophobic microchannels for cholesterol detection, *Journal of Industrial and Engineering Chemistry*, 113 (2022) 401-410.
- [48] S. Ji, M. Lee, D. Kim, Detection of early stage prostate cancer by using a simple carbon nanotube@paper biosensor, *Biosensors and Bioelectronics*, 102 (2018) 345-350.
- [49] F. Tritscher, A. Mularczyk, A. Forner-Cuenca, V. Hacker, M. Bodner, Surfactant doped polyaniline coatings for functionalized gas diffusion layers in low temperature fuel cells, *Materials Advances*, 4(12) (2023) 2573-2585.
- [50] L. Deng, Y. Zhang, S. Wei, H. Lv, G. Chen, Highly foldable and flexible films of PEDOT:PSS/Xuan paper composites for thermoelectric applications, *Journal of Materials Chemistry A*, 9(13) (2021) 8317-8324.
- [51] J.E. Atkinson, Fate of Conductive Ink Pigments During Recycling and Landfill Deposition of Paper-Based Printed Electronics, Western Michigan University, United States -- Michigan, 2017, p. 93.
- [52] C. Nash, Y. Spiesschaert, G. Amarandei, Z. Stoeva, R.I. Tomov, D. Tonchev, I. van Driessche, B.A. Glowacki, A comparative study on the conductive properties of coated and printed silver layers on a paper substrate, *Journal of Electronic Materials*, 44(1) (2015) 497-510.
- [53] S. Khan, L. Lorenzelli, R.S. Dahiya, Technologies for printing sensors and electronics over large flexible substrates: A review, *IEEE Sensors Journal*, 15(6) (2014) 3164-3185.
- [54] K. Mahato, B. Purohit, A. Kumar, P. Chandra, Chapter Six - Paper-based biosensors for clinical and biomedical applications: Emerging engineering concepts and challenges, in: A. Merkoçi (Ed.), *Comprehensive Analytical Chemistry*, Elsevier2020, pp. 163-188.
- [55] H. Menon, R. Aiswarya, K.P. Surendran, Screen printable MWCNT inks for printed electronics, *RSC Advances*, 7(70) (2017) 44076-44081.
- [56] S. Tuurala, T. Kallio, M. Smolander, M. Bergelin, Increasing performance and stability of mass-manufacturable biobatteries by ink modification, *Sensing and Bio-Sensing Research*, 4 (2015) 61-69.
- [57] N. Zavanelli, W.-H. Yeo, Advances in screen printing of conductive nanomaterials for stretchable electronics, *ACS Omega*, 6(14) (2021) 9344-9351.

- [58] J.R. Camargo, L.O. Orzari, D.A.G. Araujo, P.R. de Oliveira, C. Kalinke, D.P. Rocha, A.L. dos Santos, R.M. Takeuchi, R.A.A. Munoz, J.A. Bonacin, Development of conductive inks for electrochemical sensors and biosensors, *Microchemical Journal*, 164 (2021) 105998.
- [59] Y.Z.N. Htwe, M. Mariatti, Printed graphene and hybrid conductive inks for flexible, stretchable, and wearable electronics: Progress, opportunities, and challenges, *Journal of Science: Advanced Materials and Devices*, 7(2) (2022) 100435.
- [60] M.R. Ahmed, W. Mirihanage, P. Potluri, A. Fernando, Highly stable graphene inks based on organic binary solvents, *Particle & Particle Systems Characterization*, 40(2) (2023) 2200153.
- [61] J.V. Karabinos, M. Hindert, Carboxymethylcellulose, in: M.L. Wolfrom (Ed.), *Advances in Carbohydrate Chemistry*, Academic Press 1954, pp. 285-302.
- [62] K. Dimic-Misic, P.A.C. Gane, J. Paltakari, Micro- and nanofibrillated cellulose as a rheology modifier additive in CMC-containing pigment-coating formulations, *Industrial & Engineering Chemistry Research*, 52(45) (2013) 16066-16083.
- [63] P. He, J. Cao, H. Ding, C. Liu, J. Neilson, Z. Li, I.A. Kinloch, B. Derby, Screen-printing of a highly conductive graphene ink for flexible printed electronics, *ACS Applied Materials Interfaces*, 11(35) (2019) 32225-32234.
- [64] N. Kapur, S.J. Abbott, E.D. Dolden, P.H. Gaskell, Predicting the behavior of screen printing, *IEEE Transactions on Components, Packaging & Manufacturing technology*, 3(3) (2013) 508-515.
- [65] L. Liu, Z. Shen, X. Zhang, H. Ma, Highly conductive graphene/carbon black screen printing inks for flexible electronics, *Journal of Colloid and Interface Science*, 582 (2021) 12-21.
- [66] K. Arapov, E. Rubingh, R. Abbel, J. Laven, G. de With, H. Friedrich, Conductive screen printing inks by gelation of graphene dispersions, *Advanced Functional Materials*, 26(4) (2016) 586-593.
- [67] Y. Liao, Y. Tian, X. Ma, M. Zhao, J. Qian, X. Wang, Screen-printed high-performance flexible electrothermal films based on three-dimensional intercalation graphene nanosheets/MWCNT/carbon black composite, *ACS Applied Materials and Interfaces*, 12(42) (2020) 48077-48083.
- [68] D. Janczak, G. Wróblewski, M. Słoma, M. Jakubowska, The influence of graphene screen printing paste's composition on its viscosity, *Photonics Applications in Astronomy, Communications, Industry, and High-Energy Physics Experiments 2015*, SPIE, 2015, pp. 1193-1199.
- [69] A.L. Horst, J.M. Rosenbohm, N. Kolluri, J. Hardick, C.A. Gaydos, M. Cabodi, C.M. Klapperich, J.C. Linnes, A paperfluidic platform to detect *Neisseria gonorrhoeae* in clinical samples, *Biomedical Microdevices*, 20 (2018) 1-7.
- [70] D. Paul, P. Naik, S. Roy, Developing a point-of-care molecular test to detect SARS-CoV-2, *Transactions of the Indian National Academy of Engineering*, 5 (2020) 229-232.
- [71] R. He, H. Liu, T. Fang, Y. Niu, H. Zhang, F. Han, B. Gao, F. Li, F. Xu, A colorimetric dermal tattoo biosensor fabricated by microneedle patch for multiplexed detection of health-related biomarkers, *Advanced Science*, 8(24) (2021) 2103030.

- [72] L. Chen, A. Ghiasvand, B. Paull, Applications of thread-based microfluidics: Approaches and options for detection, *TrAC Trends in Analytical Chemistry*, (2023) 117001.
- [73] S. Kumar, N. Gupta, B.D. Malhotra, Ultrasensitive biosensing platform based on yttria doped zirconia-reduced graphene oxide nanocomposite for detection of salivary oral cancer biomarker, *Bioelectrochemistry*, 140 (2021) 107799.
- [74] R. Daly, T. Narayan, H. Shao, A. O’Riordan, P. Lovera, Platinum-based interdigitated micro-electrode arrays for reagent-free detection of copper, *Sensors*, 21(10) (2021) 3544.
- [75] B. Patella, T. Narayan, B. O’Sullivan, R. Daly, C. Zanca, P. Lovera, R. Inguanta, A. O’Riordan, Simultaneous detection of copper and mercury in water samples using in-situ pH control with electrochemical stripping techniques, *Electrochimica Acta*, 439 (2023) 141668.
- [76] J.F. Loo, A.H. Ho, A.P. Turner, W.C. Mak, Integrated printed microfluidic biosensors, *Trends in Biotechnology*, 37(10) (2019) 1104-1120.
- [77] J. Wang, Carbon-nanotube based electrochemical biosensors: A review, *Electroanalysis: An International Journal Devoted to Fundamental and Practical Aspects of Electroanalysis*, 17(1) (2005) 7-14.
- [78] B.D. Malhotra, M.A. Ali, Nanomaterials in biosensors: Fundamentals and applications, *Nanomaterials for biosensors: Fundamentals and applications*, Elsevier Inc.2018, pp. 1-74.
- [79] P. Bongrand, Ligand-receptor interactions, *Reports on Progress in Physics*, 62(6) (1999) 921.
- [80] M.H. Hassan, C. Vyas, B. Grieve, P. Bartolo, Recent advances in enzymatic and non-enzymatic electrochemical glucose sensing, *Sensors*, 21(14) (2021) 4672.
- [81] L. Farzin, M. Shamsipur, L. Samandari, S. Sheibani, Advances in the design of nanomaterial-based electrochemical affinity and enzymatic biosensors for metabolic biomarkers: A review, *Microchimica Acta*, 185 (2018) 1-25.
- [82] S.A. Lim, M.U. Ahmed, Electrochemical immunosensors and their recent nanomaterial-based signal amplification strategies: A review, *RSC Advances*, 6(30) (2016) 24995-25014.
- [83] N. Gupta, V. Renugopalakrishnan, D. Liepmann, R. Paulmurugan, B.D. Malhotra, Cell-based biosensors: Recent trends, challenges and future perspectives, *Biosensors and Bioelectronics*, 141 (2019) 111435.
- [84] Y. Du, S. Dong, Nucleic acid biosensors: Recent advances and perspectives, *Analytical Chemistry*, 89(1) (2017) 189-215.
- [85] A. Hashem, M.M. Hossain, M. Al Mamun, K. Simarani, M.R. Johan, Nanomaterials based electrochemical nucleic acid biosensors for environmental monitoring: A review, *Applied Surface Science Advances*, 4 (2021) 100064.
- [86] C. Dieffenbach, T. Lowe, G. Dveksler, General concepts for PCR primer design, *PCR methods appl*, 3(3) (1993) S30-S37.
- [87] D.L. Hyndman, M. Mitsuhashi, PCR primer design, *PCR Protocols*, (2003) 81-88.

- [88] R. Miranda-Castro, N.d.l. Santos-Álvarez, M.J. Lobo-Castañón, Understanding the factors affecting the analytical performance of sandwich-hybridization genosensors on gold electrodes, *Electroanalysis*, 30(7) (2018) 1229-1240.
- [89] R. Miranda-Castro, N.d.l. Santos-Álvarez, M.J. Lobo-Castañón, Understanding the factors affecting the analytical performance of sandwich-hybridization genosensors on gold electrodes, *Electroanalysis*, 30(7) (2018) 1229-1240.
- [90] J. Mandli, H. Mohammadi, A. Amine, Electrochemical DNA sandwich biosensor based on enzyme amplified microRNA-21 detection and gold nanoparticles, *Bioelectrochemistry*, 116 (2017) 17-23.
- [91] J.Y. Lim, S.S. Lee, Sensitive detection of microRNA using QCM biosensors: Sandwich hybridization and signal amplification by TiO₂ nanoparticles, *Analytical Methods*, 12(42) (2020) 5103-5109.
- [92] Z. Wang, Y. Fan, J. Chen, Y. Guo, W. Wu, Y. He, L. Xu, F. Fu, A microfluidic chip-based fluorescent biosensor for the sensitive and specific detection of label-free single-base mismatch via magnetic beads-based “sandwich” hybridization strategy, *Electrophoresis*, 34(15) (2013) 2177-2184.
- [93] L. Zhao, A. Liu, R. Li, S. Zhao, Multiplex TaqMan real-time PCR platform for detection of *Neisseria gonorrhoeae* with decreased susceptibility to ceftriaxone, *Diagnostic Microbiology and Infectious Disease*, 93(4) (2019) 299-304.
- [94] F. Xia, R.J. White, X. Zuo, A. Patterson, Y. Xiao, D. Kang, X. Gong, K.W. Plaxco, A.J. Heeger, An electrochemical supersandwich assay for sensitive and selective DNA detection in complex matrices, *Journal of the American Chemical Society*, 132(41) (2010) 14346-14348.
- [95] Q. Feng, M. Wang, L. Qin, P. Wang, Dual-signal readout of DNA methylation status based on the assembly of a supersandwich electrochemical biosensor without enzymatic reaction, *ACS Sensors*, 4(10) (2019) 2615-2622.
- [96] L. Wang, T. Shan, L. Pu, J. Zhang, R. Hu, Y. Yang, J. Yang, Y. Zhao, Glucometer-based electrochemical biosensor for determination of microRNA (let-7a) using magnetic-assisted extraction and supersandwich signal amplification, *Microchimica Acta*, 189(12) (2022) 444.
- [97] A. Yang, F. Yan, Flexible electrochemical biosensors for health monitoring, *ACS Applied Electronic Materials*, 3(1) (2020) 53-67.
- [98] A. Singh, A. Sharma, A. Ahmed, A.K. Sundramoorthy, H. Furukawa, S. Arya, A. Khosla, Recent advances in electrochemical biosensors: Applications, challenges, and future scope, *Biosensors*, 11(9) (2021) 336.
- [99] M.J. Russo, M. Han, P.E. Desroches, C.S. Manasa, J. Dennaoui, A.F. Quigley, R.M. Kapsa, S.E. Moulton, R.M. Guijt, G.W. Greene, Antifouling strategies for electrochemical biosensing: Mechanisms and performance toward point of care based diagnostic applications, *ACS Sensors*, 6(4) (2021) 1482-1507.

- [100] M.A. Sadique, S. Yadav, P. Ranjan, M.A. Khan, A. Kumar, R. Khan, Rapid detection of SARS-CoV-2 using graphene-based IoT integrated advanced electrochemical biosensor, *Materials Letters*, 305 (2021) 130824.
- [101] M. Mayer, A.J. Bäumner, A megatrend challenging analytical chemistry: Biosensor and chemosensor concepts ready for the internet of things, *Chemical Reviews*, 119(13) (2019) 7996-8027.
- [102] M.H. Fahmy Taha, H. Ashraf, W. Caesarendra, A brief description of cyclic voltammetry transducer-based non-enzymatic glucose biosensor using synthesized graphene electrodes, *Applied System Innovation*, 3(3) (2020) 32.
- [103] Screen-printed electrodes, 2023. https://www.dropsens.com/en/screen_printed_electrodes_pag.html. (Accessed July 15 2023).
- [104] P. Yáñez-Sedeño, S. Campuzano, J.M. Pingarrón, Screen-printed electrodes: Promising paper and wearable transducers for (bio) sensing, *Biosensors*, 10(7) (2020) 76.
- [105] I.A. de Araujo Andreotti, L.O. Orzari, J.R. Camargo, R.C. Faria, L.H. Marcolino-Junior, M.F. Bergamini, A. Gatti, B.C. Janegitz, Disposable and flexible electrochemical sensor made by recyclable material and low cost conductive ink, *Journal of Electroanalytical Chemistry*, 840 (2019) 109-116.
- [106] C. Srisomwat, P. Teengam, N. Chuaypen, P. Tangkijvanich, T. Vilaivan, O. Chailapakul, Pop-up paper electrochemical device for label-free hepatitis B virus DNA detection, *Sensors and Actuators B: Chemical*, 316 (2020) 128077.
- [107] V. Caratelli, A. Ciampaglia, J. Guiducci, G. Sancesario, D. Moscone, F. Arduini, Precision medicine in Alzheimer's disease: An origami paper-based electrochemical device for cholinesterase inhibitors, *Biosensors and Bioelectronics*, 165 (2020) 112411.
- [108] S. Boonkaew, S. Chaiyo, S. Jampasa, S. Rengpipat, W. Siangproh, O. Chailapakul, An origami paper-based electrochemical immunoassay for the C-reactive protein using a screen-printed carbon electrode modified with graphene and gold nanoparticles, *Microchimica Acta*, 186 (2019) 1-10.
- [109] Y. Liu, K. Cui, Q. Kong, L. Zhang, S. Ge, J. Yu, A self-powered origami paper analytical device with a pop-up structure for dual-mode electrochemical sensing of ATP assisted by glucose oxidase-triggered reaction, *Biosensors and Bioelectronics*, 148 (2020) 111839.
- [110] M. Asal, Ö. Özen, M. Şahinler, H.T. Baysal, İ. Polatoğlu, An overview of biomolecules, immobilization methods and support materials of biosensors, *Sensor Review*, 39(3) (2018) 377-386.
- [111] I. Leinco Technologies, Streptavidin & Ultravidin™ Conjugates, 2023. <https://www.leinco.com/streptavidin-reagents/>. (Accessed July 14 2023).
- [112] M. Unemo, W.M. Shafer, Antimicrobial resistance in *Neisseria gonorrhoeae* in the 21st century: past, evolution, and future, *Clinical Microbiology Reviews*, 27(3) (2014) 587-613.
- [113] Global health sector strategy on sexually transmitted infections 2016-2021: toward ending STIs, World Health Organization, 2016.
- [114] Global health sector strategies on, respectively, HIV, viral hepatitis and sexually transmitted infections for the period 2022-2030, World Health Organization, Geneva, Switzerland, 2022.

- [115] S. Aryal, Habitat and Morphology of *Neisseria gonorrhoeae*, 2022. (Accessed July 12 2023).
- [116] S.J. Quillin, H.S. Seifert, *Neisseria gonorrhoeae* host adaptation and pathogenesis, *Nature Reviews Microbiology*, 16(4) (2018) 226-240.
- [117] K.-Y. Lin, H.-Y. Sun, T.-F. Lee, Y.-C. Chuang, U.-I. Wu, W.-C. Liu, S.-Y. Chang, Y.-J. Chen, C.-C. Hung, S.-C. Chang, High prevalence of sexually transmitted coinfections among at-risk people living with HIV, *Journal of the Formosan Medical Association*, 120(10) (2021) 1876-1883.
- [118] X. Su, W. Le, X. Zhu, S. Li, B. Wang, G. Madico, Z. Yang, C.E. Chaisson, R.E. McLaughlin, S. Gandra, *Neisseria gonorrhoeae* infection in women increases with rising gonococcal burdens in partners: *Chlamydia* coinfection in women increases gonococcal burden, *The Journal of Infectious Diseases*, 226(12) (2022) 2192-2203.
- [119] R. Guy, J. Ward, H. Wand, A. Rumbold, L. Garton, B. Hengel, B. Silver, D. Taylor-Thomson, J. Knox, S. McGregor, Coinfection with *Chlamydia trachomatis*, *Neisseria gonorrhoeae* and *Trichomonas vaginalis*: A cross-sectional analysis of positivity and risk factors in remote Australian Aboriginal communities, *Sexually Transmitted Infections*, 91(3) (2015) 201-206.
- [120] J. Whelan, J. Eeuwijk, E. Bunge, E. Beck, Systematic literature review and quantitative analysis of health problems associated with sexually transmitted *Neisseria gonorrhoeae* infection, *Infectious Diseases and Therapy*, 10(4) (2021) 1887-1905.
- [121] J.C. Dombrowski, Chlamydia and gonorrhea, *Annals of Internal Medicine*, 174(10) (2021) ITC145-ITC160.
- [122] J. Sherrard, D. Barlow, Gonorrhoea in men: Clinical and diagnostic aspects, *Sexually Transmitted Infections*, 72(6) (1996) 422-426.
- [123] S.N. Taylor, Epididymitis, *Clinical Infectious Diseases*, 61(suppl_8) (2015) S770-S773.
- [124] C.K. Walker, R.L. Sweet, Gonorrhea infection in women: prevalence, effects, screening, and management, *International Journal of Women's Health*, (2011) 197-206.
- [125] R. Detels, A.M. Green, J.D. Klausner, D. Katzenstein, C. Gaydos, H.H. Handsfield, W. Pequegnat, K. Mayer, T.D. Hartwell, T.C. Quinn, The incidence and correlates of symptomatic and asymptomatic *Chlamydia trachomatis* and *Neisseria gonorrhoeae* infections in selected populations in five countries, *Sexually Transmitted Diseases*, 38(6) (2011) 503.
- [126] S.J. Curry, A.H. Krist, D.K. Owens, M.J. Barry, A.B. Caughey, K.W. Davidson, C.A. Doubeni, J.W. Epling, A.R. Kemper, M. Kubik, Ocular prophylaxis for gonococcal ophthalmia neonatorum: US Preventive Services Task Force reaffirmation recommendation statement, *Jama*, 321(4) (2019) 394-398.
- [127] C.A. Gaydos, J.H. Melendez, Point-by-point progress: Gonorrhea point of care tests, *Expert review of molecular diagnostics*, 20(8) (2020) 803-813.
- [128] C.K. Kent, J.K. Chaw, W. Wong, S. Liska, S. Gibson, G. Hubbard, J.D. Klausner, Prevalence of rectal, urethral, and pharyngeal Chlamydia and gonorrhea detected in 2 clinical settings among men

- who have sex with men: San Francisco, California, 2003, *Clinical Infectious Diseases*, 41(1) (2005) 67-74.
- [129] M. Unemo, H.S. Seifert, E.W. Hook III, S. Hawkes, F. Ndowa, J.-A.R. Dillon, Gonorrhoea, *Nature Reviews Disease Primers*, 5(1) (2019) 79.
- [130] J.R. Papp, J. Schachter, C.A. Gaydos, B. Van Der Pol, Recommendations for the laboratory-based detection of *Chlamydia trachomatis* and *Neisseria gonorrhoeae*—2014, Morbidity mortality weekly report. Recommendations reports, Centers for Disease Control, USA, 2014, p. 1.
- [131] A. Upton, C. Bromhead, D.M. Whiley, *Neisseria gonorrhoeae* false-positive result obtained from a pharyngeal swab by using the Roche Cobas 4800 CT/NG assay in New Zealand in 2012, *Journal of Clinical Microbiology*, 51(5) (2013) 1609-1610.
- [132] T.M. Pryce, V.J. Hiew, E.J. Haygarth, D.M. Whiley, Second-and third-generation commercial *Neisseria gonorrhoeae* screening assays and the ongoing issues of false-positive results and confirmatory testing, *European Journal of Clinical Microbiology & Infectious Diseases*, 40 (2021) 67-75.
- [133] X. Chen, Q. Zhou, W. Yuan, Y. Shi, S. Dong, X. Luo, Visual and rapid identification of *Chlamydia trachomatis* and *Neisseria gonorrhoeae* using multiplex loop-mediated isothermal amplification and a gold nanoparticle-based lateral flow biosensor, *Frontiers in Cellular and Infection Microbiology*, 13 (2023) 200.
- [134] X. Chen, L. Huang, Q. Zhou, Y. Tan, X. Tan, S. Dong, A nanoparticle-based biosensor combined with multiple cross displacement amplification for the rapid and visual diagnosis of *Neisseria gonorrhoeae* in clinical application, *Frontiers in Microbiology*, 12 (2021) 747140.
- [135] X. Chen, Q. Zhou, X. Wu, S. Wang, R. Liu, S. Dong, W. Yuan, Visual and rapid diagnosis of *Neisseria gonorrhoeae* using loop-mediated isothermal amplification combined with a polymer nanoparticle-based biosensor in clinical application, *Frontiers in Molecular Biosciences*, 8 (2021) 702134.
- [136] J. Yang, M. Fan, X. Chen, Y. Chen, M. Huang, X. Wang, Q. Lu, M. Zou, H. Song, X. Min, Leak-proof probe for accurate detection of *Neisseria gonorrhoeae* by recombinase polymerase amplification-mediated lateral flow strip, *Analytica Chimica Acta*, 1258 (2023) 341176.
- [137] H. Luo, W. Chen, Z. Mai, J. Yang, X. Lin, L. Zeng, Y. Pan, Q. Xie, Q. Xu, X. Li, Development and application of Cas13a-based diagnostic assay for *Neisseria gonorrhoeae* detection and azithromycin resistance identification, *Journal of Antimicrobial Chemotherapy*, 77(3) (2022) 656-664.
- [138] S. Malhotra, S. Gupta, S. Sood, Selection of DNA aptamers against *Neisseria gonorrhoeae* causing sexually transmitted infection (STI), *Molecular Biotechnology*, (2023) 1-9.
- [139] S.M. Berus, M. Adamczyk-Popławska, B. Młynarczyk-Bonikowska, E. Witkowska, T. Szyborski, J. Waluk, A. Kamińska, SERS-based sensor for the detection of sexually transmitted pathogens in the male swab specimens: A new approach for clinical diagnosis, *Biosensors and Bioelectronics*, 189 (2021) 113358.

- [140] D. Su, Advanced electron microscopy characterization of nanomaterials for catalysis, *Green Energy & Environment*, 2(2) (2017) 70-83.
- [141] X-ray diffraction, 2023. <https://www.britannica.com/science/X-ray-diffraction>. (Accessed 7 July 2023).
- [142] C. Tang, Z. Yang, Transmission electron microscopy (TEM), Membrane characterization, Elsevier 2017, pp. 145-159.
- [143] B.J. Inkson, Scanning electron microscopy (SEM) and transmission electron microscopy (TEM) for materials characterization, Materials characterization using nondestructive evaluation (NDE) methods, Elsevier 2016, pp. 17-43.
- [144] G. Hübschen, I. Altpeter, R. Tschuncky, H.-G. Herrmann, Materials characterization using nondestructive evaluation (NDE) methods, Woodhead Publishing 2016.
- [145] D. Johnson, N. Hilal, W.R. Bowen, Basic principles of atomic force microscopy, Atomic force microscopy in process engineering: An introduction to AFM for improved processes and products, Elsevier 2009, pp. 1-30.
- [146] A. Alessandrini, P. Facci, AFM: A versatile tool in biophysics, *Measurement Science and Technology*, 16(6) (2005) R65.
- [147] B.O. Alunda, Y.J. Lee, Cantilever-based sensors for high speed atomic force microscopy, *Sensors*, 20(17) (2020) 4784.
- [148] R.S. Das, Y. Agrawal, Raman spectroscopy: Recent advancements, techniques and applications, *Vibrational Spectroscopy*, 57(2) (2011) 163-176.
- [149] D.Y. Kwok, A.W. Neumann, Contact angle measurement and contact angle interpretation, *Advances in colloid and interface science*, 81(3) (1999) 167-249.
- [150] J. Yang, Y. Yang, Z. He, B. Chen, J. Liu, A personal desktop liquid-metal printer as a pervasive electronics manufacturing tool for society in the near future, *Engineering*, 1(4) (2015) 506-512.
- [151] D. Meroni, L. Lo Presti, G. Di Liberto, M. Ceotto, R.G. Acres, K.C. Prince, R. Bellani, G. Soliveri, S. Ardizzone, A close look at the structure of the TiO₂-APTES interface in hybrid nanomaterials and its degradation pathway: An experimental and theoretical study, *The Journal of Physical Chemistry C*, 121(1) (2017) 430-440.
- [152] I. Miccoli, F. Edler, H. Pfnür, C. Tegenkamp, The 100th anniversary of the four-point probe technique: The role of probe geometries in isotropic and anisotropic systems, *Journal of Physics: Condensed Matter*, 27(22) (2015) 223201.
- [153] C.-W. Wang, K. Cook, A. Sastry, Conduction in multiphase particulate/fibrous networks: Simulations and experiments on Li-ion anodes, *Journal of the Electrochemical Society*, 150(3) (2003) A385.
- [154] yourgenome, What is gel electrophoresis?, 2023. (Accessed 10 July 2023).
- [155] M. Autolab, Autolab PGSTAT302N-High Performance, 2018.

- [156] A.J. Bard, R.W. Murray, Electrochemistry, *Proceedings of the National Academy of Sciences*, 109(29) (2012) 11484-11486.
- [157] B.D. Malhotra, A. Chaudhary, Biosensors for clinical diagnostics industry, *Sensors and Actuators B: Chemical*, 91(1-3) (2003) 117-127.
- [158] H.S. Magar, R.Y. Hassan, A. Mulchandani, Electrochemical impedance spectroscopy (EIS): Principles, construction, and biosensing applications, *Sensors*, 21(19) (2021) 6578.
- [159] A. Lasia, Electrochemical impedance spectroscopy and its applications, *Modern aspects of electrochemistry*, Springer 2002, pp. 143-248.
- [160] M. Mithu, G. Fantoni, J. Ciampi, Effect of electrolyte temperature on Faradaic effect in electrochemical microdrilling, *International Journal of Precision Technology*, 7(1) (2017) 17-31.
- [161] E.P. Randviir, C.E. Banks, Electrochemical impedance spectroscopy: An overview of bioanalytical applications, *Analytical Methods*, 5(5) (2013) 1098-1115.
- [162] L.F. Huergo, K.A. Selim, M.S. Conzentino, E.C. Gerhardt, A.R. Santos, B. Wagner, J.T. Alford, N. Deobald, F.O. Pedrosa, E.M. de Souza, Magnetic bead-based immunoassay allows rapid, inexpensive, and quantitative detection of human SARS-CoV-2 antibodies, *ACS Sensors*, 6(3) (2021) 703-708.
- [163] L. Dai, F. Xu, L. Wu, L. Peng, G. Fu, Magnetic bead-based nucleic acid extraction apparatus and use method, in: U.S.P.a.T. Office (Ed.) Google Patents, Sansure Biotech Inc., 2021.
- [164] X. Yu, H.-S. Xia, Z.-D. Sun, Y. Lin, K. Wang, J. Yu, H. Tang, D.-W. Pang, Z.-L. Zhang, On-chip dual detection of cancer biomarkers directly in serum based on self-assembled magnetic bead patterns and quantum dots, *Biosensors and Bioelectronics*, 41 (2013) 129-136.
- [165] Y. Xianyu, Q. Wang, Y. Chen, Magnetic particles-enabled biosensors for point-of-care testing, *Trends in Analytical Chemistry*, 106 (2018) 213-224.
- [166] J. Min, M. Nothing, B. Coble, H. Zheng, J. Park, H. Im, G.F. Weber, C.M. Castro, F.K. Swirski, R. Weissleder, Integrated biosensor for rapid and point-of-care sepsis diagnosis, *ACS Nano*, 12(4) (2018) 3378-3384.
- [167] T. Pinheiro, A.C. Marques, P. Carvalho, R. Martins, E. Fortunato, Paper microfluidics and tailored gold nanoparticles for nonenzymatic, colorimetric multiplex biomarker detection, *ACS Applied Materials and Interfaces*, 13(3) (2021) 3576-3590.
- [168] S. Khaliliazar, A. Toldrà, G. Chondrogianis, M.M. Hamed, Electroanalytical paper-based nucleic acid amplification biosensors with integrated thread electrodes, *Analytical Chemistry*, 93(42) (2021) 14187-14195.
- [169] B. Yao, J. Zhang, T. Kou, Y. Song, T. Liu, Y. Li, Paper-based electrodes for flexible energy storage devices, *Advanced Science*, 4(7) (2017) 1700107.
- [170] C. Zhao, J. Wang, Z.-q. Zhang, Z. Sun, Z. Maimaitimin, Silver-based conductive ink on paper electrodes based on micro-pen writing for electroanalytical applications, *ChemElectroChem*, 9(21) (2022) e202200948.

- [171] T.S. Tran, N.K. Dutta, N.R. Choudhury, Graphene inks for printed flexible electronics: Graphene dispersions, ink formulations, printing techniques and applications, *Advances in colloid and interface science*, 261 (2018) 41-61.
- [172] W.T. Fonseca, K.R. Castro, T.R. de Oliveira, R.C. Faria, Disposable and flexible electrochemical paper-based analytical devices using low-cost conductive ink, *Electroanalysis*, 33(6) (2021) 1520-1527.
- [173] M. Mass, L.S. Veiga, O. Garate, G. Longinotti, A. Moya, E. Ramón, R. Villa, G. Ybarra, G. Gabriel, Fully inkjet-printed biosensors fabricated with a highly stable ink based on carbon nanotubes and enzyme-functionalized nanoparticles, *Nanomaterials*, 11(7) (2021) 1645.
- [174] R.P. Tortorich, H. Shamkhalichenar, J.-W. Choi, Inkjet-printed and paper-based electrochemical sensors, *Applied Sciences*, 8(2) (2018) 288.
- [175] L. Jiang, H. Hong, J. Hu, X. Yan, Fabrication and seamless integration of insensitive-bending fully printed all-in-one fabric-based supercapacitors based on cost-effective MWCNT electrodes, *ACS Applied Materials and Interfaces*, 14(10) (2022) 12214-12222.
- [176] V.S. Turkani, D. Maddipatla, B.B. Narakathu, T.S. Saeed, S.O. Obare, B.J. Bazuin, M.Z. Atashbar, A highly sensitive printed humidity sensor based on a functionalized MWCNT/HEC composite for flexible electronics application, *Nanoscale Advances*, 1(6) (2019) 2311-2322.
- [177] F.G. Pacheco, A.A. Cotta, H.F. Gorgulho, A.P. Santos, W.A. Macedo, C.A. Furtado, Comparative temporal analysis of multiwalled carbon nanotube oxidation reactions: Evaluating chemical modifications on true nanotube surface, *Applied Surface Science*, 357 (2015) 1015-1023.
- [178] S. Augustine, P. Kumar, B.D. Malhotra, Amine-functionalized MoO₃@ RGO nanohybrid-based biosensor for breast cancer detection, *ACS Applied BioMaterials*, 2(12) (2019) 5366-5378.
- [179] V. Duc Chinh, G. Speranza, C. Migliaresi, N. Van Chuc, V. Minh Tan, N.-T. Phuong, Synthesis of gold nanoparticles decorated with multiwalled carbon nanotubes (Au-MWCNTs) via cysteaminium chloride functionalization, *Scientific Reports*, 9(1) (2019) 1-9.
- [180] G. Stando, S. Han, B. Kumanek, D. Łukowiec, D. Janas, Tuning wettability and electrical conductivity of single-walled carbon nanotubes by the modified Hummers method, *Scientific Reports*, 12(1) (2022) 1-13.
- [181] F. Farshchi, A. Saadati, M. Hasanzadeh, Optimized DNA-based biosensor for monitoring *Leishmania infantum* in human plasma samples using biomacromolecular interaction: A novel platform for infectious disease diagnosis, *Analytical Methods*, 12(39) (2020) 4759-4768.
- [182] N. Gupta, D. Kumar, A. Das, S. Sood, B.D. Malhotra, Carbon nanotubes modified conductive ink for application to paper-based electrochemical biosensors for pathogenic DNA detection, *New Journal of Chemistry*, 47(23) (2023) 10930-10941.
- [183] A. Saadati, M. Ehsani, M. Hasanzadeh, F. Seidi, N. Shadjou, An innovative flexible and portable DNA based biodevice towards sensitive identification of *Haemophilus influenzae* bacterial genome: A new platform for the rapid and low cost recognition of pathogenic bacteria using point of care (POC) analysis, *Microchemical Journal*, 169 (2021) 106610.

- [184] Y. Yang, J. Liu, X. Zhou, A CRISPR-based and post-amplification coupled SARS-CoV-2 detection with a portable evanescent wave biosensor, *Biosensors and Bioelectronics*, 190 (2021) 113418.
- [185] C. Hwang, N. Park, E.S. Kim, M. Kim, S.D. Kim, S. Park, N.Y. Kim, J.H. Kim, Ultra-fast and recyclable DNA biosensor for point-of-care detection of SARS-CoV-2 (COVID-19), *Biosensors and Bioelectronics*, 185 (2021) 113177.
- [186] E. Khristunova, E. Dorozhko, E. Korotkova, B. Kratochvil, V. Vyskocil, J. Barek, Label-free electrochemical biosensors for the determination of Flaviviruses: Dengue, Zika, and Japanese Encephalitis, *Sensors*, 20(16) (2020) 4600.
- [187] A. Bishoyi, M.A. Alam, M.R. Hasan, M. Khanuja, R. Pilloton, J. Narang, Cyclic voltammetric-paper-based genosensor for detection of the target DNA of Zika virus, *Micromachines*, 13(12) (2022) 2037.
- [188] R. Verma, S. Sood, R. Singh, G. Sumana, M. Bala, V.K. Sharma, J.C. Samantaray, R.M. Pandey, B.D. Malhotra, Coupling electrochemical response of a DNA biosensor with PCR for *Neisseria gonorrhoeae* detection, *Diagnostic Microbiology and Infectious Disease* 78(1) (2014) 16-23.
- [189] J. Wang, A. Shi, X. Fang, X. Han, Y. Zhang, Ultrasensitive electrochemical supersandwich DNA biosensor using a glassy carbon electrode modified with gold particle-decorated sheets of graphene oxide, *Microchimica Acta*, 181 (2014) 935-940.
- [190] J. Li, J. Jiang, Y. Su, Y. Liang, C. Zhang, A novel cloth-based supersandwich electrochemical aptasensor for direct, sensitive detection of pathogens, *Analytica Chimica Acta*, 1188 (2021) 339176.
- [191] H. Hong, H. Jiyong, K.-S. Moon, X. Yan, C.-p. Wong, Rheological properties and screen printability of UV curable conductive ink for flexible and washable E-textiles, *Journal of Materials Science & Technology*, 67 (2021) 145-155.
- [192] M. Edali, M.N. Esmail, G.H. Vatistas, Rheological properties of high concentrations of carboxymethyl cellulose solutions, *Journal of Applied Polymer Science*, 79(10) (2001) 1787-1801.
- [193] Y. Zheng, Z. He, Y. Gao, J. Liu, Direct desktop printed-circuits-on-paper flexible electronics, *Scientific Reports*, 3(1) (2013) 1786.
- [194] H.Y. Pekturk, M. Elitas, M. Goktas, B. Demir, S. Birhanu, Evaluation of the effect of MWCNT amount and dispersion on bending fatigue properties of non-crimp CFRP composites, *Engineering Science & Technology, an International Journal*, 34 (2022) 101081.
- [195] R. Gupta, M.O. Valappil, A. Sakthivel, A. Mathur, C.S. Pundir, K. Murugavel, J. Narang, S. Alwarappan, Tungsten disulfide quantum dots based disposable paper based lab on genochip for specific meningitis DNA detection, *Journal of the Electrochemical Society*, 167(10) (2020) 107501.
- [196] A. Rana, M. Killa, N. Yadav, A. Mishra, A. Mathur, A. Kumar, M. Khanuja, J. Narang, R. Pilloton, Graphitic carbon nitride as an amplification platform on an electrochemical paper-based device for the detection of norovirus-specific DNA, *Sensors*, 20(7) (2020) 2070.
- [197] GeneProof(R), GeneProof *Neisseria gonorrhoeae* PCR Kit, 2022. (Accessed 10/04/2023 2023).

- [198] D. Golparian, B. Hellmark, M. Unemo, Analytical specificity and sensitivity of the novel dual-target GeneProof *Neisseria gonorrhoeae* PCR kit for detection of *N. gonorrhoeae*, *Apmis*, 123(11) (2015) 955-958.
- [199] N. Goire, M. Ohnishi, A.E. Limnios, M.M. Lahra, S.B. Lambert, G.R. Nimmo, M.D. Nissen, T.P. Sloots, D.M. Whiley, Enhanced gonococcal antimicrobial surveillance in the era of ceftriaxone resistance: A real-time PCR assay for direct detection of the *Neisseria gonorrhoeae* H041 strain, *Journal of Antimicrobial Chemotherapy*, 67(4) (2012) 902-905.
- [200] N. Gupta, D. Kumar, A. Das, S. Sood, B.D. Malhotra, Conductive ink-coated paper-based supersandwich DNA biosensor for ultrasensitive detection of *Neisseria gonorrhoeae*, *Biosensors*, 13(4) (2023) 486.
- [201] J.R. Camargo, T.A. Silva, G.A. Rivas, B.C. Janegitz, Novel eco-friendly water-based conductive ink for the preparation of disposable screen-printed electrodes for sensing and biosensing applications, *Electrochimica Acta*, 409 (2022) 139968.
- [202] A.E. Oliveira, A.C. Pereira, M.A. de Resende, Fabrication of low-cost screen-printed electrode in paper using conductive inks of graphite and silver/silver chloride, *Electroanalysis*, 35(2) (2023) e202200093.
- [203] L. Fabiani, M. Saroglia, G. Galatà, R. De Santis, S. Fillo, V. Luca, G. Faggioni, N. D'Amore, E. Regalbuto, P. Salvatori, Magnetic beads combined with carbon black-based screen-printed electrodes for COVID-19: A reliable and miniaturized electrochemical immunosensor for SARS-CoV-2 detection in saliva, *Biosensors and Bioelectronics*, 171 (2021) 112686.
- [204] N.-B. Mincu, V. Lazar, D. Stan, C.M. Mihailescu, R. Iosub, A.L. Mateescu, Screen-printed electrodes (SPE) for *in vitro* diagnostic purpose, *Diagnostics*, 10(8) (2020) 517.
- [205] M. Sher, A. Faheem, W. Asghar, S. Cinti, Nano-engineered screen-printed electrodes: A dynamic tool for detection of viruses, *TrAC Trends in Analytical Chemistry*, 143 (2021) 116374.
- [206] M. Go, X. Qi, P. Matteini, B. Hwang, S. Lim, High resolution screen-printing of carbon black/carbon nanotube composite for stretchable and wearable strain sensor with controllable sensitivity, *Sensors and Actuators A: Physical*, 332 (2021) 113098.
- [207] F. Arduini, L. Micheli, D. Moscone, G. Palleschi, S. Piermarini, F. Ricci, G. Volpe, Electrochemical biosensors based on nanomodified screen-printed electrodes: Recent applications in clinical analysis, *TrAC Trends in Analytical Chemistry*, 79 (2016) 114-126.
- [208] P. Lamas-Ardisana, G. Martínez-Paredes, L. Añorga, H. Grande, Glucose biosensor based on disposable electrochemical paper-based transducers fully fabricated by screen-printing, *Biosensors and Bioelectronics*, 109 (2018) 8-12.
- [209] N. Sahraei, M. Mazloum-Ardakani, J. Mohiti, A. Moradi, A. Khoshroo, E. Emadi, F. Vajhadin, Flexible paper-based immunosensor for the detection of specific cancer-derived exosomes, *Journal of the Electrochemical Society*, 169(12) (2022) 127514.

- [210] B. Martin, J.P. Claverie, Depolymerizable polyimines triggered by heat or acid as binders for conductive inks, *ACS Applied Polymer Materials*, 4(7) (2022) 4912-4918.
- [211] H. Chen, Y. Liu, S. Feng, Y. Cao, T. Wu, Z. Liu, Cotton thread-based multi-channel photothermal biosensor for simultaneous detection of multiple microRNAs, *Biosensors and Bioelectronics*, 200 (2022) 113913.
- [212] S. Khaliliazar, I. Öberg Månsson, A. Piper, L. Ouyang, P. Réu, M.M. Hamed, Woven electroanalytical biosensor for nucleic acid amplification tests, *Advanced Healthcare Materials*, 10(11) (2021) 2100034.
- [213] E.N. Kersh, M. Shukla, B.H. Raphael, M. Habel, I. Park, At-home specimen self-collection and self-testing for sexually transmitted infection screening demand accelerated by the COVID-19 pandemic: A review of laboratory implementation issues, *Journal of Clinical Microbiology*, 59(11) (2021) 10.1128/jcm.02646-20.
- [214] J.R. Choi, K.W. Yong, R. Tang, Y. Gong, T. Wen, F. Li, B. Pingguan-Murphy, D. Bai, F. Xu, Advances and challenges of fully integrated paper-based point-of-care nucleic acid testing, *TrAC Trends in Analytical Chemistry*, 93 (2017) 37-50.

Publications from Thesis

1. **Gupta N**, Kumar D, Das A, Sood S, Malhotra BD. Carbon nanotubes modified conductive ink for application to paper-based electrochemical biosensor for pathogenic DNA detection. *New Journal of Chemistry*. 2023; 47:10930.
2. **Gupta N**, Kumar D, Das A, Sood S, Malhotra BD. Conductive ink-coated paper-based supersandwich DNA biosensor for ultrasensitive detection of *Neisseria gonorrhoeae*. *Biosensors*. 2023; 13(4):486.
3. **Gupta N**, Kumar D, Das A, Sood S, Malhotra BD. Screen printed MWCNT-modified conductive ink towards paper-based biosensor for *Neisseria gonorrhoeae* detection. To be submitted to *Microchimica Acta*.

Other Publications

1. Kaur S, **Gupta N**, Malhotra BD. Recent developments in wearable & non-wearable point-of-care biosensors for cortisol detection. *Expert Review of Molecular Diagnostics*. 2023 Mar 4; 23(3):217-30.
2. **Gupta N***, Todi K*, Narayan T, Malhotra BD. Graphitic carbon nitride-based nanoplatfoms for biosensors: design strategies and applications. *Materials Today Chemistry*. 2022 Jun 1; 24:100770. (*Equal authors)
3. Kumar S*, **Gupta N***, Malhotra BD. Ultrasensitive biosensing platform based on yttria doped zirconia-reduced graphene oxide nanocomposite for detection of salivary oral cancer biomarker. *Bioelectrochemistry*. 2021 Aug 1; 140:107799. (*Equal authors)
4. **Gupta N**, Augustine S, Narayan T, O’Riordan A, Das A, Kumar D, Luong JH, Malhotra BD. Point-of-care PCR assays for COVID-19 detection. *Biosensors*. 2021 May 1; 11(5):141.
5. **Gupta N**, Renugopalakrishnan V, Liepmann D, Paulmurugan R, Malhotra BD. Cell-based biosensors: Recent trends, challenges and future perspectives. *Biosensors and Bioelectronics*. 2019 Sep 15; 141:111435.

Conferences and Presentations

1. **Gupta N**, Kumar D, Das A, Sood S, Malhotra BD. Carbon nanotubes modified conductive ink for application to paper-based electrochemical biosensor for detection of

- Neisseria gonorrhoeae*. In the International Biobanking Symposium (IBS) 2023 Annual Conference & Exhibition 2023 Feb 23-24, Institute of Liver and Biliary Sciences (ILBS), New Delhi.
2. **Gupta N**, Kumar D, Das A, Malhotra BD. Conductive ink coated flexible paper biosensor for magnetic bead-assisted electrochemical detection of pathogenic bacteria. In the Conference on Recent Advances in Nano Medical Sciences (RANMS-2022) 2022 June 22-23. Institute of Nano Medical Sciences (INMS), University of Delhi, New Delhi.
 3. **Gupta N**, Das A, Kumar D, Malhotra BD. Carbon nanomaterial-based conductive ink for flexible paper-based biosensors. In the International Conference on Innovations in Biotechnology and Life Sciences (ICIBLS 2020) 2020 Dec 18-20, Delhi Technological University, New Delhi.
 4. **Gupta N**, Das A, Kumar D, Malhotra BD. Carbon nanomaterial based conductive ink for papertronic applications: An optimization study. In the IEEE-5th International Conference on Emerging Electronics (IEEE-ICEE) 2020 Nov 26-28, Indian Institute of Delhi (IIT) Delhi.
 5. **Gupta N**, Kumar S, Malhotra BD. Yttria-stabilized zirconia-based nanocomposite for ultrasensitive detection of oral cancer biomarker. In the Indo-Japan Workshop on Biomolecular Electronics and Organic Nanotechnology for Environment Preservation-2018 (IJWBME-2018) 2018 Dec 6-9, CSIR-National Physical Laboratory (CSIR-NPL), New Delhi.
 6. **Gupta N**, Kumar S, Malhotra BD. Yttria-stabilized zirconia nanocomposite with reduced graphene oxide for highly sensitive detection of oral cancer biomarker. In the NANO2018, the XIV International Conference on Nanostructured Materials (ICNM) 2018 June 24-29, City University of Hong Kong, Kowloon Tong, Hong Kong SAR.

Workshops

1. Hands-On Workshop on Analytical Instrumentation. International Student Chapter-American Chemical Society, 2022 July 14-15, CSIR-Central Scientific Instruments Organization (CSIR-CSIO), Chandigarh, Punjab.

PAPER



Cite this: *New J. Chem.*, 2023, 47, 10930

Carbon nanotubes modified conductive ink for application to paper-based electrochemical biosensors for pathogenic DNA detection†

Niharika Gupta,^a D. Kumar,^b Asmita Das,^a Seema Sood^c and Bansil D. Malhotra^{*a}

We report the results of studies relating to the development of a conductive ink-coated, paper-based electrochemical DNA hybridization assay for the detection of the *porA* pseudogene of *Neisseria gonorrhoeae* (gonococcal DNA), the causative agent of gonorrhoea. Briefly, a conductive and highly homogenous ink was prepared by dispersing carboxylated MWCNTs (cMWCNTs) in a stable emulsion consisting of terpineol as solvent, carboxymethyl cellulose (CMC) as binder and polysorbate 80 (PS80) as the stabilizing agent. This cMWCNT-based ink was coated onto paper substrates to obtain cMWCNT@paper electrodes with a mean (\pm standard deviation, SD) resistivity of 1.066 (\pm 0.33) Ω cm. Furthermore, a magnetic bead (MB)-mediated hybridization assay comprising a specific 5'-biotinylated capture DNA probe (C) and 3'-methylene blue (MetB)-tagged detector DNA probe (D) was designed. These probes hybridized specifically with a *porA* target DNA sequence (T) forming a sandwich hybridization complex (C-T-D) at the MB surface. Thus formed C-T-D/Av/MB samples with different T concentrations were drop cast and adsorbed onto the cMWCNT@paper for electrochemical detection. The linear detection range and sensitivity of the electrochemical biosensing assay were found to be 100 fM–100 nM and 5.09 μ A (log[concentration])⁻¹, respectively. The biosensing assay was further shown to detect the target genomic gonococcal DNA in a mixture consisting of different DNA and protein interferents indicating its clinical viability. The results of rheological studies reveal that this thixotropic cMWCNT ink can be utilized for screen printing. These studies demonstrate the utilization of a conductive ink formulation for the fabrication of paper-based electrochemical sensing electrodes having high potential for cost-effective batch production and application in point-of-care (PoC) clinical diagnostics.

Received 3rd April 2023,
Accepted 9th May 2023

DOI: 10.1039/d3nj01557b

rsc.li/njc

1. Introduction

The field of paper diagnostics has recently aroused much interest. Paper-based devices for medical diagnostics have evolved from the traditional dipstick and lateral flow assays into straightforward wearable and microfluidic platforms for simultaneous detection of multiple analytes.^{1–3} These devices can be used for the detection of various analytes ranging from cancer biomarkers to DNA amplification products and bulky proteins.^{1,4–7} Features such as high surface-to-volume ratio, capillary flow, high adsorption capacity, biocompatibility, and ease of disposability have led to the

application of paper as an efficient and cost-effective substrate for clinical diagnostics. Optical transduction *via* nanoparticles and other agents such as dyes is one of the most prominent choices for application to biosensing, (intracellular) parameter monitoring, cellular imaging, *etc.*^{8–13} And likewise, most commercial paper-based diagnostic devices employ visual detection of the target analyte *via* colour change/formation. However, with increasing emphasis on the development of cost-effective and sensitive point-of-care (PoC) devices, there is increased interest in the development of electrochemical paper-based diagnostics.

Electrochemical paper biosensors are quantitative in nature, which, coupled with high sensitivity, may prove highly advantageous toward developing a low-cost diagnostic device.¹⁴ However, the poor conductivity of paper is currently one of the major bottlenecks for paper-based electrochemical devices.⁷ This may perhaps be addressed by using conductive nanomaterials onto a desired paper matrix *via* dip coating, *in situ* growth/polymerization, and direct drop casting.⁷ While these

^a Department of Biotechnology, Delhi Technological University, Delhi 110042, India

^b Department of Applied Chemistry, Delhi Technological University, Delhi 110042, India

^c Department of Microbiology, All India Institute of Medical Sciences (AIIMS), New Delhi 110016, India. E-mail: bansi.malhotra@gmail.com

† Electronic supplementary information (ESI) available. See DOI: <https://doi.org/10.1039/d3nj01557b>

methods have succeeded in terms of conductive paper fabrication, many of these methods are not scalable. Also, the coating of nanomaterials can be non-uniform and uncontrollable due to the nature of the synthesis and fabrication method. For example, *in situ* growth of nanomaterials, though efficient, is difficult to control. This may eventually lead to batch-to-batch variations and subsequently, low sensitivity. Additionally, the same properties that render a paper substrate advantageous for biosensing appear to hinder the electrochemical applications of paper-based biosensors. For example, the high degree of capillary flow allows the buffer to easily flow through the paper matrix leading to lower signal-to-noise ratio. And the paper substrate may be prone to high non-specific adsorption resulting in poor sensitivity. At the same time, complete blocking of the pores in the paper matrix may render it unsuitable for interaction with the buffer that contains the target analyte and redox probes required for electrochemical analysis. Leaching of nanomaterials is another issue that is presently hindering the development of paper-based electrochemical biosensors.

In this context, conductive inks have been projected to be a promising option toward the fabrication of paper-based electrochemical biosensors. Conductive inks comprise conductive nanomaterials and binders that impart enhanced conductivity and strong adherence to the target substrate (in this case, paper), respectively.^{15,16} The wettability of these inks can be modified using additives and, in turn, their coating may allow tuning of the capillary flow at the paper surface.¹⁷ Different printing techniques are available that can be used to coat these inks on paper substrates, such as inkjet printing, screen printing, flexographic printing, *etc.*^{18–20} Conductive, printable inks have found prominent applications in the field of flexible and printed electronics.^{15–17} However, there are only a few reports on conductive ink-coated paper electrodes for electrochemical detection of different analytes.^{16,19} Traditionally, silver nanoparticles (Ag NPs) are used as conductive fillers in screen printable inks for printable electronics applications. However, Ag NPs are not suitable for electroanalytical applications as they get easily oxidized on repeated electrochemical cycles. Thus, carbon nanomaterials such as graphene, carbon nanotubes (CNTs), *etc.* have aroused increased interest for the development of conductive, screen-printing inks. Carbon nanomaterials have been found to have electroanalytical applications due to their high surface-to-volume ratio, chemical inertness, high conductivity, and wide potential window in different buffers.¹⁸ Multiwalled CNTs (MWCNTs) possess these interesting characteristics with the added advantage of lower relative costs, and have found extensive applications in printed pseudocapacitors and biosensors.^{18,20} Despite this, there are only a few studies on the development of conductive inks using only MWCNTs; most studies on carbon nanomaterial-based conductive inks have focused on the application of graphene or composites of MWCNTs as conductive fillers.^{21–24} Besides this, conductive inks are largely being explored for applications in supercapacitors, batteries, flexible electronics, *etc.*^{23–26} In this work, we sought to formulate an MWCNT-based conductive ink towards the fabrication of paper-based electrodes. These electrodes

were further utilized as biosensing substrates for the detection of *Neisseria gonorrhoeae*.

N. gonorrhoeae is the causative agent of the sexually transmitted infection (STI) gonorrhoea, which is presently one of the most prominent bacterial STIs around the world. According to a recent study, about 87 M cases of gonorrhoea were found worldwide among individuals aged 15–49 in 2016.²⁷ And it has been associated with many health problems in men, women, and children including high HIV infection risk, preterm birth, infertility, neonatal ophthalmia, *etc.*²⁸ Additionally, this STI remains highly under-reported and under-diagnosed in both high-income and low-income economies, which has hampered the efforts towards the world-wide decrease of this STI. Thus, a simple, cost-effective device that can be used for mass screening can significantly transform gonorrhoeal diagnostics and may aid in achieving the WHO goal of reducing the incidence of this disease by 90% by 2030.²⁹

There have been a few reports on DNA-based electrochemical biosensors for the detection of the *opa* gene (and its PCR amplicons) of *N. gonorrhoeae*.^{30–32} However, the *opa* gene is highly polymorphic and is also present in other commensal (harmless) *Neisseria* species, which may lead to cross reactivity and false positive results. On the other hand, the *porA* pseudogene is a non-functional gene in *N. gonorrhoeae* that has a highly conserved sequence and is not present in any of the commensal *Neisseria* species. Thus, this pseudogene can perhaps act as a promising detection target for *N. gonorrhoeae*.

In this work, we first formulated a carboxylated MWCNT (cMWCNT)-based conductive ink, which was subsequently utilized to fabricate paper-based biosensing electrodes. Oligonucleotide probes (one capture and one detector) specific to the *N. gonorrhoeae porA* pseudogene were designed. Furthermore, to impart specificity to the biosensing assay, a magnetic bead (MB)-based sandwich hybridization assay was designed, wherein the 5'-biotinylated capture probe (C) was immobilized onto the MBs using avidin (Av) to specifically bound to the target sequence (T) in a complex matrix. The detector probe (D) (tagged with methylene blue (MetB) at 3' end) was allowed to bind thereafter to form a capture-target-detector (C-T-D) sandwich hybridization complex at the MB surface. This assembly was thereafter drop cast onto the paper electrodes for electrochemical analysis. To the best of our knowledge, there is no report on the fabrication of a conductive ink-coated, paper-based biosensor for detection of the gonorrhoeal *porA* pseudogene.

2. Materials and methods

2.1. Materials and reagents

Carboxylated multi-walled carbon nanotubes (cMWCNT) and polysorbate 80 (PS80) were obtained from SRL Pvt. Ltd. (India). Carboxymethyl cellulose (CMC; high viscosity) and terpineol were procured from Central Drug House (P) Ltd. (CDH, India). All reagents were of analytical grade and were used without purification. Carboxylated magnetic beads (Dynabeads™

Table 1 DNA sequences of the biosensor oligonucleotide probes

Biosensor probes		
Probe type and name	Sequence	Melting temperature (T_m ; °C)
Capture probe (CP)	5' Biotin-CCT GCT ACT TTC ACG CTG GA 3'	62
Detector probe (DP)	5' AAG TAA TCA GAT GAA ACC AGT TC-Met Blue 3'	62
Target strand (T)	5' GAA CTG GTT TCA TCT GAT TAC TTT CCA GCG TGA AAG TAG CAG G 3'	65
Non-complementary probe (NC)	5' TTG ATT GAG CGT CAT AGA TCG GAC GGC ACT AGT CAG TAC TCG A 3'	63

MyOne™ Carboxylic Acid; MBs) were purchased from Thermo Fisher Scientific. Avidin (from egg white; lyophilized powder) was obtained from Sigma Aldrich (Merck, Germany). The oligonucleotide probes used in these studies were purchased from IDT (USA). The sequences of the oligonucleotide probes were self-designed (Table 1). All electrochemical studies were performed in phosphate buffered saline (PBS, 0.1 M) of pH 7 supplemented with 5 mM ferro-ferricyanide as the redox probes. PBS (pH 7) was prepared by first mixing 39 mL of monobasic sodium phosphate (NaH_2PO_4 , 0.2 M, Fisher Scientific) and 61 mL of dibasic sodium phosphate ($\text{Na}_2\text{HPO}_4 \cdot 2\text{H}_2\text{O}$, 0.2 M, Fisher Scientific), and thereafter diluting the resulting mixture to 200 mL with autoclaved MilliQ water. Sodium chloride (NaCl , 0.9%, Fisher Scientific) was added to this mixture to constitute the final buffer.

2.2. Conductive ink formulation

A conductive ink consists of four major components: (i) solvent, (ii) binder for proper adhesion to the desired substrate, (iii) rheology modifier for appropriate flow properties according to the application, and (iv) conductive filler that imparts conductivity. For ink formulation, CMC (1.5% w/v) was first dissolved in distilled water and was then mixed with terpineol and PS80 in the optimized ratio 2:1:1 (water:terpineol:PS80) (Fig. 1(A)). The resulting emulsion was stirred vigorously using a magnetic stirrer (~500 rpm, 2 h). Subsequently, cMWCNTs (1% w/v) were added to the desired emulsion with vigorous stirring (~1000 rpm, 1 h). The resulting conductive emulsion was probe ultrasonicated in an ice bath at a pulse of 0.5 s and 70% amplitude for 15 min. The ultrasonication was paused every 5 minutes to avoid overheating of the sample. The resulting conductive ink was stored in a closed container at low temperature (4–10 °C) to prevent evaporation of the solvent.

2.3. Design of biosensor oligonucleotide probes

The oligonucleotide probes were self-designed using open access software. In brief, the oligonucleotide probes specific to the gonococcal *porA* pseudogene were selected using the NCBI Nucleotide database and NCBI Primer-BLAST. For this purpose, the gonococcal *porA* pseudogene sequences from different strains of *N. gonorrhoeae* were aligned using Clustal Omega to confirm homology. Thereafter, the same sequence was aligned with *porA* pseudogene sequences from different strains of *N. meningitidis* to determine a sequence conserved only to *N. gonorrhoeae*. The selected capture (C) and detector (D) biosensor probes (Table 1) along with the complementary

target sequence (T) and non-complementary sequence (NC) were purchased from IDT, USA.

2.4. Fabrication of ink-coated paper bioelectrodes

For the fabrication of flexible paper electrodes, drawing paper (ivory paper, 200–300 gsm) was first cut into pieces of size $2 \times 2 \text{ cm}^2$. The choice of paper type was made based on the higher mechanical strength and lower porosity of ivory paper in relation to the traditionally used filter paper. Thereafter, 75 μL of the conductive ink was drop cast and coated uniformly over the paper using a paint brush (Faber Castell). The paper electrodes were annealed within the temperature range of 80–130 °C for a period of 5–15 min to optimize the annealing temperature and time and determine their effect on the conductivity. The coating process was repeated to determine the optimum number of coats (n) to obtain appreciable conductivity while maintaining adhesion on the paper substrate. The obtained cMWCNT@paper electrodes were cut into pieces of size $1 \times 1 \text{ cm}^2$ each and assessed for conductivity. After optimization of the number of coats, annealing temperature and time, cMWCNT@paper electrodes ($2 \times 1 \text{ cm}^2$) were fabricated for electrochemical studies and stored in dry, dark conditions until further use.

2.5. Electrochemical magnetic DNA hybridization assay

DNA complementary base pairing is currently a prominent method for DNA-based biosensors. In this study, a capture (C) and a detector probe (D) were designed to hybridize with the target DNA (T) at two adjacent sites. To enhance the specificity and the sensitivity of the assay, C was labelled with biotin at the 5' end and D was labelled with MetB at the 3' end. Furthermore, an MB-based assay was designed for the specific detection of gonorrhoeal DNA. The primary role of MB was sample enrichment: to isolate the target DNA from a mixture of interferents. The MetB labelling on the DP resulted in the amplification of the redox signal at the electrode surface.

For the electrochemical DNA assay, Av was first immobilized onto the carboxylated MBs *via* EDC/NHS-mediated covalent bond formation (detailed protocol given in the ESI†). Thereafter, the biotinylated C (1800 pmol mg^{-1} beads) was immobilized onto the Av/MBs *via* affinity interactions. Different concentrations of the T strand were then added to the C/Av/MB probes and incubated at 60 °C for 15 min with tilt rotation. This was followed by the addition of D and incubation at 60 °C for 15 min with tilt rotation. This resulted in the formation of a sandwich hybridization complex at the MB surface. Washing with double distilled water ($3\text{--}5 \times$) was conducted after every

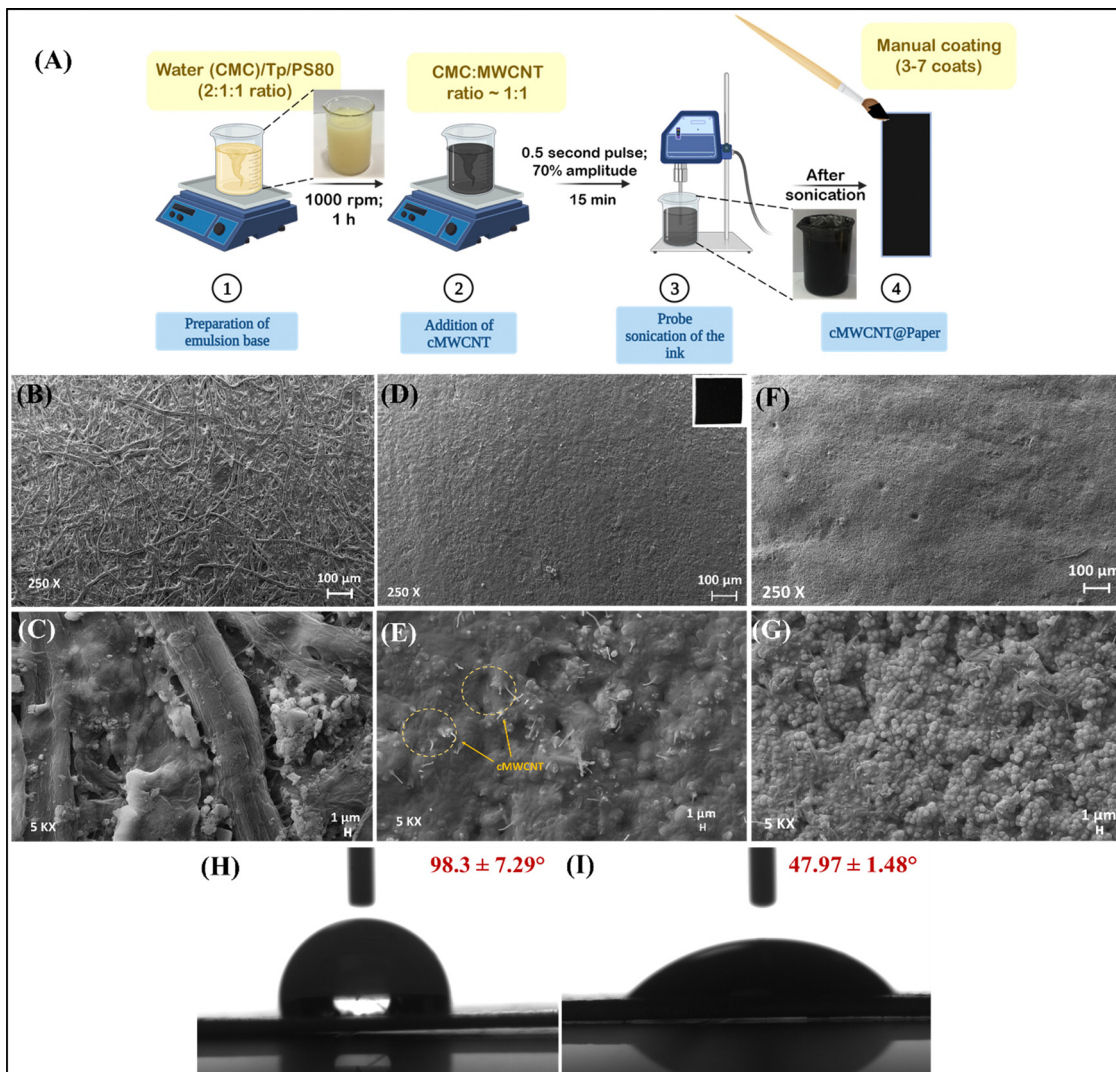


Fig. 1 (A) Schematic depicting the preparation of the conductive ink and subsequent fabrication of the cMWCNT@paper electrodes. SEM micrographs of (B) and (C) bare paper; (D) and (E) cMWCNT ink-coated paper (cMWCNT@paper) (inset of (D) shows the photograph of the cMWCNT@paper electrode ($2 \times 2 \text{ cm}^2$)); and (E) and (F) Avidin-modified MB/cMWCNT@paper electrode. Contact angle measurements for (H) bare paper, and (I) the cMWCNT@paper electrode.

modification step to remove non-specifically bound and unbound probes. Thus formed C-T-D/Av/MB complexes were redispersed in $30 \mu\text{L}$ deionized water and drop cast onto the cMWCNT@paper electrodes ($1 \times 1 \text{ cm}^2$). These modified electrodes were dried at $60 \text{ }^\circ\text{C}$ for 15 min and analyzed for electrochemical response *via* cyclic voltammetry (CV). The CV studies were conducted in PBS buffer supplemented with ferro-ferricyanide as the redox couple (Section 2.1) at a scan rate of 50 mV s^{-1} unless otherwise specified.

2.6. Real sample analysis

In order to check the applicability of the designed electrochemical biosensing assay in clinical settings, DNA from *N. gonorrhoeae* bacterial culture was first extracted using commercial QIAGEN DNA extraction kits. Thereafter, the DNA samples were diluted to different concentrations and denatured by incubation at

$95 \text{ }^\circ\text{C}$ for 5 min. This was followed by ultrasonication in a water bath for 10 min. These steps facilitated the denaturation and shortening of the DNA molecules, respectively. Thereafter, the procedure as described in Section 2.5 was repeated to determine the concentration of the gonococcal DNA sequences in the samples. The results were compared to those obtained by using the synthetic T probe.

Clinical samples (cervical/urethral swabs) are known to consist of a large amount of human DNA and DNA from non-pathogenic commensal bacteria that may significantly interfere with the detection of pathogenic DNA. Protein contamination can also occur sometimes during DNA extraction (especially when crude extraction methods are used, *e.g.* the boiling method). To determine the effect of interfering DNA and proteins on the detection of gonococcal DNA, non-gonococcal DNA from different bacteria was extracted and mixed with the

gonococcal DNA in the ratio of 50:1. The response of the electrochemical biosensing assay was then recorded for these DNA mixtures using the aforementioned procedure.

3. Results and discussion

3.1. Characterization and optimization studies

Fig. S1(A) and (B) (ESI[†]) show the XRD spectrum and the TEM image of the cMWCNT used in this study. The XRD spectrum reveals a sharp, high intensity peak at 26.2° corresponding to the (002) reflection plane of the crystalline carbon nanotubes. Smaller peaks are also observed centred at about 43.4° and 54.2° corresponding to the exposed (100) and (004) planes of the carbon nanotubes. The average diameter of the nanotubes, as seen in the TEM image, has been found to be 117.12 nm.

3.1.1. SEM and contact angle studies. The cMWCNT-based conductive ink was formulated by dispersing cMWCNT in an emulsion of CMC (dispersed in water) and terpineol stabilized by PS80. Fig. 1(A) depicts the various steps followed in the formulation of the conductive ink and subsequent coating on paper substrates. SEM analysis was conducted to analyse the surface morphology of the cMWCNT@paper electrodes and further modifications with MBs (Fig. 1(B–G)). The SEM micrographs of bare paper (Fig. 1(B) and (C)) show rough surface of the paper consisting of cellulose fibres. An additive/modifying agent can also be seen in the image (Fig. 1(C)) that probably has been used to bleach or modify the porosity of cellulose fibres. In contrast, the coating of the MWCNT ink appears smooth and evenly distributed along the paper surface indicating the homogeneity of the ink formulation (Fig. 1(D)). The inset in Fig. 1(D) shows the optical photograph of the cMWCNT@paper electrode. cMWCNTs can be seen protruding out of the ink matrix

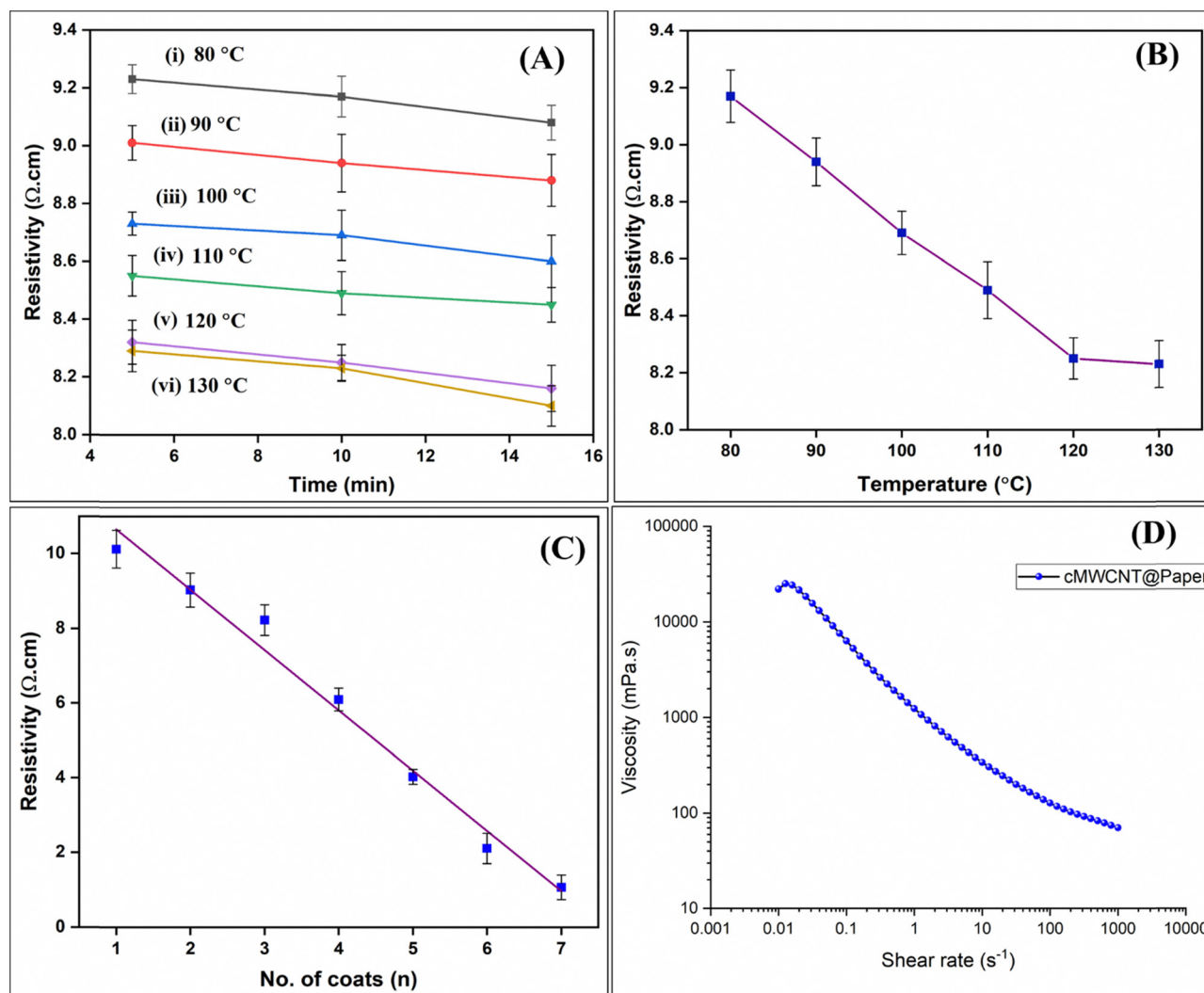


Fig. 2 (A) The change in resistivity of the cMWCNT@paper electrodes with annealing temperature and time, (B) the corresponding curve depicting the relationship between the resistivity of the cMWCNT@paper electrodes with temperature at a fixed annealing time of 10 min, (C) the change in the resistivity of the cMWCNT@paper electrodes with number of coats of the conductive ink, and (D) change in the viscosity of the cMWCNT ink with shear rate displaying shear thinning behaviour.

held together by CMC and residual PS80 remaining after annealing (Fig. 1(E)). For comparison, we modified the paper with cMWCNTs dispersed in PS80 *via* dip coating (3 \times) and analysed it *via* SEM (Fig. S2, ESI \dagger) (dip coating was utilized because the dispersion was not viscous enough to be coated/printed). In Fig. S2 (ESI \dagger), cMWCNTs are clearly visible and scattered over the paper surface. Cellulose fibres are also visible beneath the cMWCNTs. This is in contrast with the MWCNT@paper as shown in Fig. 1(D). Furthermore, Fig. 1(F) shows the impregnation of the ink matrix by Av/MBs (5 mg beads were adsorbed on 1 \times 1 cm² ink-coated paper). On further magnification, spherical Av/MBs can be clearly seen on the cMWCNT@paper electrodes (Fig. 1(G)). It appears that the Av/MBs have covered the surface evenly without any aggregation in a particular area.

The wettability of the cMWCNT ink coating on the paper substrate was assessed by contact angle measurements (Fig. 1(H) and (I)). The contact angle of the paper used in the study (ivory drawing paper, 250–300 gsm) was found to be 98.3 \pm 7.29 $^\circ$ (mean \pm error) (Fig. 1(H)), which decreased to 47.97 \pm 1.48 $^\circ$ for the cMWCNT@paper electrode (3 ink coats, 75 μ L for one coat) (Fig. 1(I)). The observed high contact angle of the bare paper indicates the presence of additional modifying agents in the paper matrix, as indicated by the SEM studies. Furthermore, the decrease in the contact angle after ink coating may be due to the presence of CMC in the ink, which is hydrophilic in nature. The presence of a low surface tension solvent (terpineol) and PS80 may also contribute to the observed lower contact angle of the ink.³³

3.1.2. Conductivity studies. The effect of annealing temperature, annealing time, and number of ink coatings (n) on the conductivity of the cMWCNT@paper electrodes was investigated. First, the paper substrates (2 \times 2 cm²) were coated thrice (75 μ L per coat) and annealed within the temperature range of 80–130 $^\circ$ C (Fig. 2(A)). The resistivities of the annealed cMWCNT@paper electrodes were subsequently determined. It was found that the resistivity decreased with annealing temperature and time, with the minimum value at 120 $^\circ$ C for 10 min. Keeping the annealing time fixed at 10 min, it was seen that the resistivity decreased until 120 $^\circ$ C, after which there was only a slight (non-significant) change (Fig. 2(B)). Hence, 120 $^\circ$ C for 10 min was considered as the optimum annealing

temperature and time, respectively, for further studies. This decrease in resistivity with annealing temperature and time is attributed to the evaporation and degradation of terpineol and PS80 at temperature $>$ 100 $^\circ$ C. Additionally, the mean (\pm SD) resistivity of the cMWCNT@paper at $n = 7$ decreased to 1.066 (\pm 0.31) Ω cm from 9.89 (\pm 1.2) Ω cm at $n = 1$ (Fig. 2(C)). The corresponding conductivity ($n = 7$) was found to be 1.48 S cm⁻¹. The resistivity was not measured beyond seven coatings as the MWCNTs leached out when the cMWCNT@paper electrode was immersed in aqueous solution. The following equations were utilized to determine the resistivity of the cMWCNT@paper electrodes:

$$\rho = \frac{\rho_o}{G'} \quad (1)$$

where ρ is the final resistivity corrected for the thickness of the coating, and ρ_o is the resistivity given by the following equation:

$$\rho_o = \left(\frac{V}{I} \times 2\pi S \right) \quad (2)$$

where V is the potential, I is the current and S is the distance between the probes of the conductivity meter (0.2 cm), and G' is the error introduced when the thickness of the conductive layer, $t \ll S$ and is given by:

$$G' = \frac{2S}{t} \ln 2 \quad (3)$$

The decrease in resistivity with n may be assigned to higher loading of cMWCNTs onto the paper that perhaps created a highly inter-networked matrix. Table 2 compares the resistivities of some MWCNT-based screen-printing inks with the present work. Section S2 (ESI \dagger) presents a video that shows the use of the cMWCNT@paper electrodes to complete a circuit and light a red LED, demonstrating their conductivity.

Another important factor in determining the application of paper-based biosensors is scalability in the fabrication process. Printing of the prepared cMWCNT conductive ink *via* an established printing technology may ensure the scalability of the fabrication of the paper electrodes. Hence, the prepared cMWCNT ink was analysed for rheology (flow behaviour) to determine whether it can be used for screen printing. The flow behaviour of the cMWCNT ink was analysed at different shear

Table 2 Comparison among different MWCNT-based ink formulations

S. No.	Nanomaterial	Binder	Resistivity	Applications	Ref.
1.	MWCNT			All-in-one fabric-based supercapacitors	25
2.	MWCNT/PEDOT:PSS	PEDOT:PSS	51.31 \pm 0.25 Ω sq ⁻¹	Flexible heating	21
3.	Graphene/MWCNT/Carbon black	Water-based acrylic resins	4 Ω sq ⁻¹	Electrothermal films	22
4.	Dihydroxyphenyl-functionalized multi-walled carbon nanotubes (MWNT-f-OH)/carbon black/graphite	waterborne acrylic resins	up to 29 Ω sq ⁻¹	Electrochemiluminescent devices	34
5.	Functionalized MWCNT	Hydroxyethyl cellulose	—	Humidity sensing	35
6.	MWCNT	PVP	0.5–13 Ω sq ⁻¹	Patch antennas	26
7.	Carboxyl-functionalized MWCNT	Carboxymethyl cellulose	1.066 \pm 0.31 Ω sq ⁻¹	DNA Biosensor	Present work

rates ($0.1\text{--}1000\text{ s}^{-1}$) using a parallel plate of 40 mm in diameter. It was found that the apparent viscosity of the ink decreased with the increase in shear rate, indicating a shear thinning and thixotropic behaviour (Fig. 2(D)), with an initial apparent viscosity of 22 Pa s, which is an ideal condition for screen printing. The presence of CMC may account for the high initial viscosity; however, the carbon nanomaterials are also known to increase the viscosity of inks. Thus, while both CMC and cMWCNT can together contribute to the high initial viscosity, the shear thinning behaviour of the ink is, mostly due to CMC, which is a well-known rheology modifier and a thixotropic agent. These results indicate the suitability of the formulated ink for screen printing suggesting that the formulated ink can be used for the batch production of low cost, screen-printed electrodes (SPEs).

3.1.3. Raman and XPS analyses. Raman and XPS analyses were conducted to verify the presence of cMWCNTs in the formulated conductive ink. For this purpose, the ink was dried at $120\text{ }^{\circ}\text{C}$ overnight and then kept at $350\text{ }^{\circ}\text{C}$ for 2 h to degrade the residual CMC. The obtained dried ink powder was analysed *via* Raman and XPS studies. The Raman spectrum of the dried ink reveals the two characteristic bands of graphitic

carbon-containing materials—the G band and the D band (Fig. 3(A)). The G band seen at 1582.53 cm^{-1} is a first order Raman process corresponding to the tangential mode vibrations of the C atoms. The presence of a single, sharp graphitic peak at $\sim 1582\text{ cm}^{-1}$ indicates the multiwalled nature (and the large diameter) of the carbon nanotubes. The D and 2D (G') bands observed at 1353.69 cm^{-1} and 2705.54 cm^{-1} , respectively, are assigned to the double resonance Raman processes. The D band indicates the presence of disorder induced by amorphous carbon, structural defects, *etc.*, while the 2D (G') band is an overtone of the D band that is dispersive in nature (its frequency is dependent on the excitation laser wavelength). Together with the G band, the G' band is the Raman signature of materials consisting of graphitic sp^2 carbon. The $I_{\text{D}}/I_{\text{G}}$ ratio is known to indicate the degree of defects, which may either be already present or induced by some physicochemical interaction, in the MWCNT structure. The $I_{\text{D}}/I_{\text{G}}$ ratio was found to be 0.66 for the dried ink powder indicating the presence of less defects in the chemical structure.

XPS studies were conducted to investigate the surface elemental composition of the as prepared conductive ink. Fig. 3(B) shows the survey scan spectra consisting of major peaks that

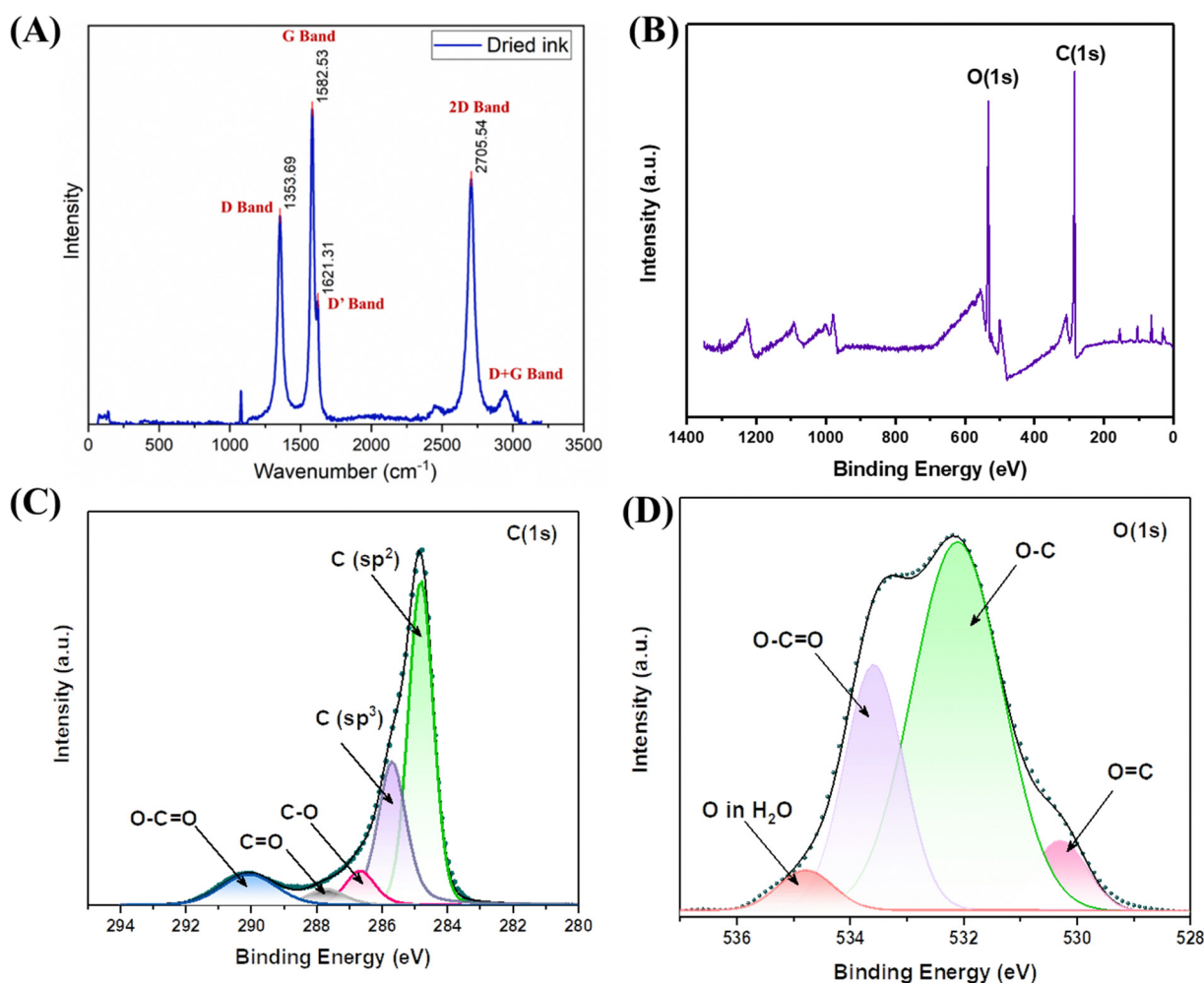


Fig. 3 (A). Raman spectrum, (B) XPS survey scan, and deconvoluted peaks of (C) C(1s), and (D) O(1s).

are attributed to C1s (284.5 eV) and O1s (530.5 eV), confirming the presence of cMWCNTs in the dried ink. The deconvoluted spectra for C1s in Fig. 3(C) exhibit five characteristic peaks and that for O1s (Fig. 3(D)) shows four characteristic peaks. The C1s main peak located at 284.5 eV corresponds to sp^2 hybridization (C=C). The peak observed at 285.1 eV is attributed to the sp^3 hybridization of C-C bonds. The peaks seen at 286.3 eV, 287.2 eV and 289.6 eV are assigned to the epoxy/hydroxy (–C–O), carbonyl groups (C=O), and carboxyl groups (O–C=O) of the cMWCNTs, respectively. In case of O1s, the deconvoluted peaks seen at 530.5 eV and 531.3 eV correspond to the oxygen double bonded to carbon (O=C) and single bonded to carbon (C–O), respectively. The peak at 533.5 eV corresponds to the oxygen atoms in carboxyl groups and those at 534.5 eV indicate the presence of oxygen in water at the surface.^{36–39} These results clearly reveal the presence of the cMWCNTs in the intact form in the as-prepared dried ink.

3.2. Electrochemical characterization studies

The continuous use stability is an essential consideration for a biosensing electrode. In simple terms, the electrochemical response of a biosensing electrode should be stable enough to

disallow any significant fluctuations with time provided that there are no changes in the system (*e.g.*, buffer composition). The cMWCNT@paper electrodes were analysed for continuous use stability in terms of their electrochemical response *via* cyclic voltammetry (CV). Fig. 4(A) shows the electrochemical response of the same electrode in the first and the 20th CV scan. There is no significant change in the peak current of both the scans indicating the stability of the cMWCNT@paper biosensing electrodes. It may be noted that the electrodes take about 20 minutes to stabilize (time taken by a biosensing electrode to be in dynamic equilibrium with the surrounding buffer to yield a stable response). The swelling nature of CMC present in the ink matrix may partially account for the stabilization time of the electrode. However, the eventual (and continued) stability of the electrode response suggests that the hydrophilic nature of the CMC perhaps does not interfere with the electrochemical response of the electrodes.

Batch reproducibility is another important consideration for paper-based electrodes. To assess the batch reproducibility of the fabricated cMWCNT@paper electrodes, 10 electrodes were randomly selected from different batches and analysed *via* CV

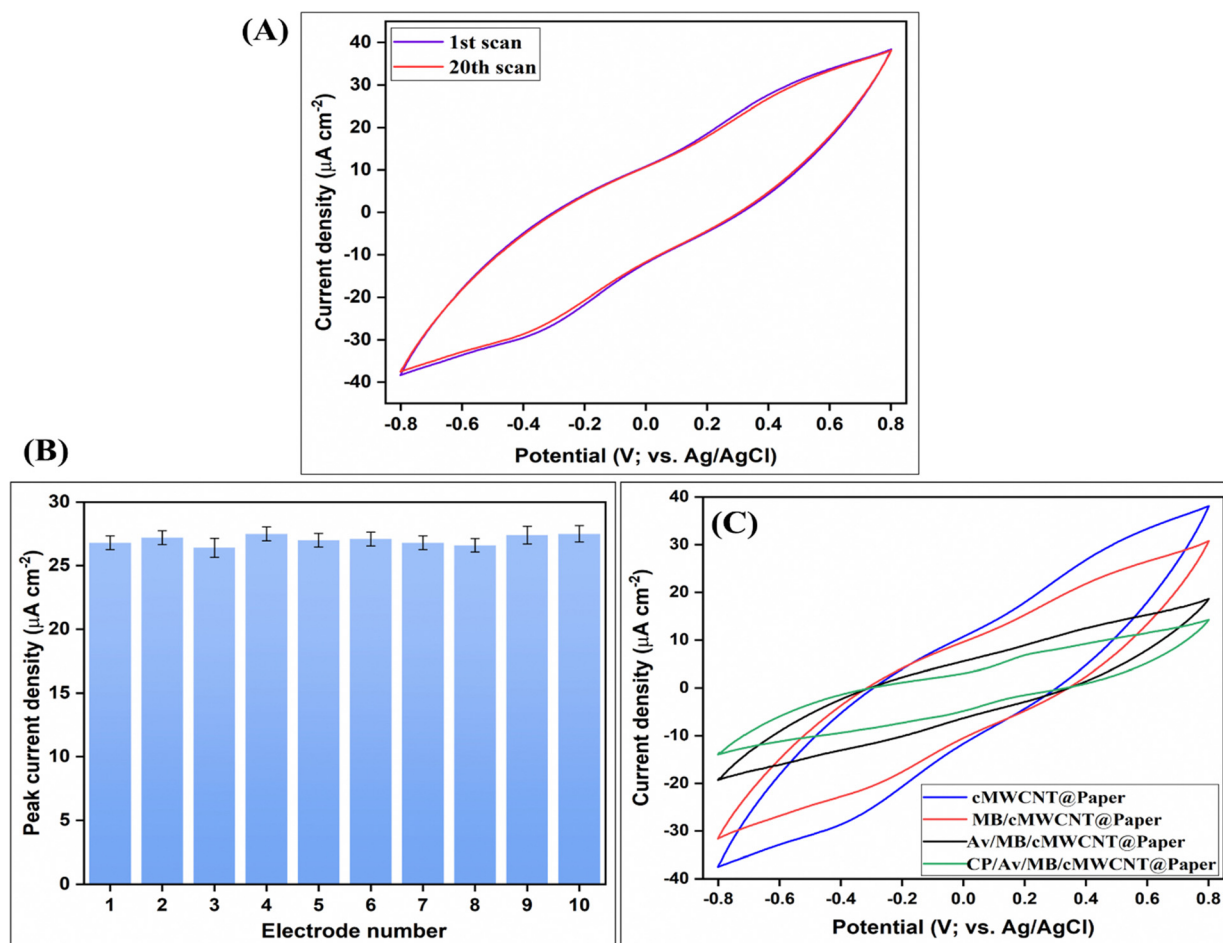


Fig. 4 (A) Current density vs. potential scans of the cMWCNT@paper showing continuous use stability, (B) peak current density (J) of different cMWCNT@paper electrodes indicating batch reproducibility, and (C) change in the current density curves of the cMWCNT@paper electrodes after modification with MBs and modified MBs.

(Fig. 4(B)). The current density (J) of a working electrode in an electrochemical system is given by,

$$J = I/A \quad (4)$$

where I is the current and A is the surface area. Since the surface area of the electrodes used in the study for electrochemical analysis was 1 cm^2 , the J and I values were equivalent. The peak J value of the cMWCNT@paper electrode was found to be $27.03 \pm 0.38 \mu\text{A cm}^{-2}$ (mean \pm SD). This indicates that despite the manual nature of the coating process, the ink coatings on the electrodes are uniform enough to obtain a similar electrochemical response. This further suggests that the cMWCNTs are homogeneously dispersed in the ink leading up to a stable electrochemical response across different batches of electrodes.

The change in the electrochemical response of the cMWCNT@paper electrodes after adsorption of the unmodified and modified MBs was also recorded. As shown in Fig. 4(C), the electrochemical peak response of the MB/cMWCNT@paper is slightly lower than that of the cMWCNT@paper electrode. This may be attributed to the repulsion of the negatively charged redox probes by the carboxylated MBs. The electrochemical response was found to be further decreased significantly for the Av/MB/cMWCNT@paper and CP/Av/MB/cMWCNT@paper electrodes due to the insulating nature of Av, which is a bulky glycoprotein, and DNA molecules. This also confirms, indirectly, the modification of MBs with avidin and subsequent immobilization of CP onto the Av/MBs *via* biotin-avidin interactions.

3.3. Electrochemical response studies

An electrochemical MB-assisted sandwich hybridization assay was designed for the detection of gonorrhoeal *porA* pseudogene (Fig. 5(A) and (B)). Prior to the response studies, the amount of MB required to yield a significant response at the cMWCNT@paper electrodes was optimized (Fig. S3, ESI†). A response time analysis was also conducted to determine the minimum time required for saturation of the CV response after drop casting of the C-T-D/Av/MB assembly. It was found that the response of the C-T-D/Av/MB/cMWCNT@paper electrode(s) saturated after 20 min for 1 pM target concentration (Fig. S4(A), ESI†). Hereinafter, the response was recorded after 20 min of immersion of the C-T-D/Av/MB/cMWCNT@paper electrodes in the buffer for biosensing measurements. For the electrochemical response studies, 0.5 mg MBs were adsorbed on the cMWCNT@paper electrodes for every concentration of the target DNA. Since temperature is an important factor controlling the DNA hybridization process, the annealing (DNA hybridization) was allowed to occur at $60 \text{ }^\circ\text{C}$ for 10 min. The temperature was selected with respect to the melting temperature of the oligonucleotide probes; normally the ideal annealing temperature is within $\pm 5 \text{ }^\circ\text{C}$ of the melting temperature of a particular DNA sequence. Fig. 5(C) shows the CV response of the cMWCNT@paper with change in the concentration of the target DNA sequence within the range 100 fM–100 nM. The corresponding calibration curve

was plotted between the net change in current density (ΔJ) and the concentration of the target DNA sequence, wherein the ΔJ values were calculated as:

$$\Delta J = J_c - J_0 \quad (5)$$

where J_c is the peak current density for a particular concentration of target DNA, and J_0 is the peak current density of the C/Av/MB/cMWCNT@paper electrode (blank). As shown in Fig. 5(D), a linear correlation was found between ΔJ and the log of the concentration of the target DNA, given by the equation:

$$\Delta J = 5.09 \times \log[\text{concentration}] + 12.59, R^2 = 0.98 \quad (6)$$

The observed increase in the current density can be attributed to the participation of MetB, attached at the 3' end of D, in the electron transfer process at the electrode surface. In fact, the redox peak of MetB is visible in the CV scans at higher concentrations of the target DNA sequence (Fig. 5(C)). The detection limit and sensitivity of the biosensing assay were found to be 0.13 pM and $5.09 \mu\text{A} (\log[\text{concentration}])^{-1}$, respectively. Furthermore, to ascertain the clinical applicability of the electrochemical biosensing assay, the response of the biosensing electrode was recorded against genomic DNA isolated from *N. gonorrhoeae*. The protocol followed was the same as that for the response studies with one minor modification—the genomic DNA was subjected to denaturation by heating at $95 \text{ }^\circ\text{C}$ for 10 min followed by shearing by ultrasonication for 10 min. Fig. 5(E) compares the response of the biosensing electrode to the genomic DNA and the same concentration of synthetic target DNA strand used in the response studies. The recovery rate was found to be 98–99% for the genomic samples for three different concentrations.

DNA isolated from clinical specimens consists of a small amount of pathogenic DNA mixed with human DNA and DNA from other commensal bacteria. In some cases, proteins or other cellular components may also be mixed in (in the case where DNA is isolated by the boiling method), which can act as interferents. Fig. 5(F) shows the results relating to the studies conducted to determine the effect of DNA/protein interferents on the biosensing assay response. The peak response of the biosensing electrode to gonorrhoeal genomic DNA was recorded in the presence of DNA from different bacterial species including *Neisseria meningitidis* (NM), *Chlamydia trachomatis* (Ch), *Streptococcus aureus* (SA), *Ureaplasma urealyticum* (U), *Enterococcus faecalis* (EF), and a cocktail of all these bacterial DNA (M). The response in the presence of excess BSA alone and along with non-gonorrhoeal DNA was also recorded. For this study, a fixed quantity of gonorrhoeal genomic DNA (1 pM) was mixed with either 50 \times concentration of DNA of other bacteria or BSA (as a protein interferent). No significant difference was found in the peak response of the C-T-D/Av/MB/cMWCNT@paper biosensing electrodes in the presence of the interfering DNA and proteins, indicating not only the specificity of the designed probes but also the significance of sample enrichment *via* MBs before biosensing. Table 3 summarizes the

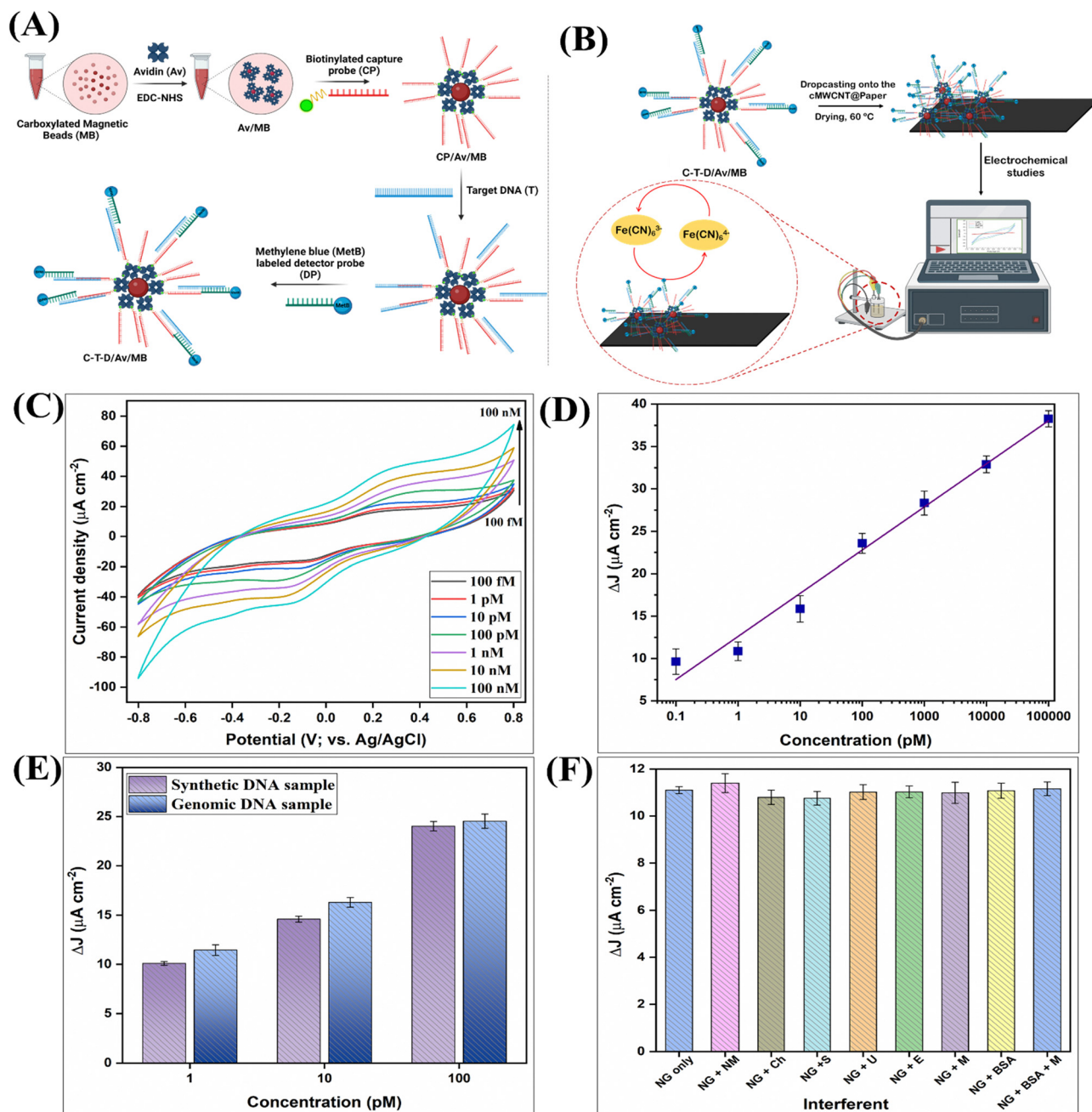


Fig. 5 Schematic displaying the (A) steps involved in the magnetic bead-assisted sandwich hybridization assay, and (B) subsequent drop casting on the cMWCNT@paper electrodes for electrochemical analysis. (C) Current density vs. potential curves of the cMWCNT@paper electrodes with increasing concentration of the C-T-D hybridization complex, (D) the corresponding calibration curve showing a linear correlation between the change in peak current density (ΔJ) and the log of target sequence concentration, (E) comparison between the ΔJ values obtained for the synthetic target DNA sequence and gonorrhoeal genomic DNA in different concentrations, and (F) the ΔJ response of the electrochemical biosensing electrodes to genomic DNA mixed with non-gonorrhoeal DNA and proteins.

results of the recent studies involving fabrication of paper-based electrochemical biosensors (printed either by inhouse prepared or commercial ink) for the detection of pathogenic DNA, and compares it to the present work. The storage stability of the cMWCNT@paper electrodes was also analysed by recording their CV response for 7–90 days, wherein the electrodes were stored at room temperature in dark, dry conditions (Fig.

S4(B), ESI†). The value of current density of the bioelectrode did not change significantly until 30 days (99.7% of response on 7 days). Thereafter, the response fell to 97.78% and 94.8% of the initial response at 60 and 90 days, respectively, indicating excellent storage stability of the fabricated cMWCNT@paper electrodes. This further eliminates the need for special storage conditions for the electrodes.

Table 3 Table comparing the recent studies on paper based electrochemical biosensors for pathogenic DNA detection

S. No.	Ink formulation/Nanomaterial	Target pathogen	Linear range	Sensitivity (LOD)	Ref.
1.	Graphene oxide-modified carbon ink screen printed on paper	<i>Orientia tsutsugamushi</i> (single stranded DNA)	$0.05 \times 10^2 \text{ pg } \mu\text{L}^{-1}$ to $6.3 \times 10^2 \text{ pg } \mu\text{L}^{-1}$	$1228.4 \text{ } \mu\text{A cm}^{-2} \text{ ng}^{-1}$ ($20 \text{ pg } \mu\text{L}^{-1}$)	40
2.	Ni-Au/CNT/PVA (vacuum filtration and drop casting)	HIV DNA	10 nM–1 μM	—(0.13 nM)	41
3.	Graphene nanosheets	—(dsDNA)	0.2–5 pg mL^{-1}	$0.00656 \text{ mA pg}^{-1} \text{ cm}^{-2}$	42
4.	Carbon graphene ink (commercial)	Hepatitis B virus	50 pM–100 nM	—(1.45 pM)	43
5.	Ag nanoprisms electrodeposited on graphene quantum dots (GQDs)	<i>Leishmania infantum</i>	1 zM–1 nM	1 zM (LOQ*)	44
6.	cMWCNT	<i>Neisseria gonorrhoeae</i>	100 fM–100 nM	$5.09 \text{ } \mu\text{A} (\log[\text{concentration}])^{-1}$ (0.13 pM)	Present work

4. Conclusions

We have fabricated a conductive ink-coated paper biosensing electrode for magnetic bead-assisted electrochemical detection of *porA*, a pseudogene specifically present in *N. gonorrhoeae*. The conductive ink consists of cMWCNTs homogeneously dispersed in an emulsion consisting of terpineol and CMC dispersed in distilled water stabilized by PS80. The ink-coated paper electrodes have displayed excellent continuous use stability and batch reproducibility, despite the manual coating of the paper substrates by the cMWCNT ink. The electrochemical DNA biosensing assay has been shown to be highly sensitive and specific to the *porA* gene sequence in a wide linear range spanning 10^5 orders of magnitude. The biosensing assay has been used to detect genomic gonorrhoeal DNA with excellent recovery. The addition of magnetic beads has imparted high selectivity to the biosensing assay as it was shown to detect gonorrhoeal genomic DNA even in the presence of other non-gonorrhoeal DNA present in concentrations as high as 50 times that of gonorrhoeal DNA. Furthermore, the formulated ink has been shown to be thixotropic, which signifies its ability to be screen printed. This study demonstrates the fabrication of efficient paper-based electrodes for electrochemical biosensing using a highly homogenous, conductive ink. Further studies should focus on modifications in the conductive ink formulation for conductivity enhancement and adherence to different substrates. And it should be interesting to investigate the effect of different conductive ink formulations on the electrochemical performance of the resulting electrodes.

Author contributions

BDM, NG: conceptualization; NG: investigation, formal analysis, writing – original draft; DK, AD, BDM: writing – review and editing, supervision, project administration; SS: resources, writing – review and editing.

Conflicts of interest

The authors declare no conflict of interest.

Acknowledgements

NG acknowledges the Vice Chancellor, Delhi Technological University (DTU), Delhi. NG also thanks Dr Suveen Kumar,

DST-INSPIRE Faculty, Department of Chemistry, Delhi University, Delhi, India, and Dr Shine Augustine, Postdoctoral Fellow, Sungkyunkwan University, Suwon, South Korea, for help in XPS and Raman spectroscopic analyses. The Central Research Facility (CRF), IIT Delhi, New Delhi (Hauz Khas and Sonipat campus) is acknowledged for the SEM and XPS analyses. BDM acknowledges the Science and Engineering Board (DST-SERB, Govt. of India) for award of the Distinguished Fellowship (SB/DF/011/2019) and partially funding this study.


References

- 1 T. Pinheiro, A. C. Marques, P. Carvalho, R. Martins and E. Fortunato, *ACS Appl. Mater. Interfaces*, 2021, **13**, 3576–3590.
- 2 J. P. Devadhasan and J. Kim, *Sens. Actuators, B*, 2018, **273**, 18–24.
- 3 H. Li and A. J. Steckl, *Anal. Chem.*, 2019, **91**, 352–371.
- 4 Q. H. Nguyen and M. I. Kim, *Trends Anal. Chem.*, 2020, **132**, 116038.
- 5 K. Ratajczak and M. Stobiecka, *Carbohydr. Polym.*, 2020, **229**, 115463.
- 6 S. Khaliliazar, A. Toldrà, G. Chondrogiannis and M. M. Hamed, *Anal. Chem.*, 2021, **93**, 14187–14195.
- 7 S. Kumar, S. Kumar, S. Srivastava, B. K. Yadav, S. H. Lee, J. G. Sharma, D. C. Doval and B. D. Malhotra, *Biosens. Bioelectron.*, 2015, **73**, 114–122.
- 8 H. Yan, F. Huo, Y. Yue, J. Chao and C. Yin, *J. Am. Chem. Soc.*, 2020, **143**, 318–325.
- 9 Y. Huang, Y. Zhang, F. Huo, J. Chao, F. Cheng and C. Yin, *J. Am. Chem. Soc.*, 2020, **142**, 18706–18714.
- 10 X. Chen, X. Zhang and F.-G. Wu, *Chin. Chem. Lett.*, 2021, **32**, 3048–3052.
- 11 B. Feng, Y. Zhu, J. Wu, X. Huang, R. Song, L. Huang, X. Feng and W. Zeng, *Chin. Chem. Lett.*, 2021, **32**, 3057–3060.
- 12 J. Li, M. Zhang, L. Yang, Y. Han, X. Luo, X. Qian and Y. Yang, *Chin. Chem. Lett.*, 2021, **32**, 3865–3869.
- 13 H. Yan, Y. Wang, F. Huo and C. Yin, *J. Am. Chem. Soc.*, 2023, **145**, 3229–3237.
- 14 E. Solhi, M. Hasanzadeh and P. Babaie, *Anal. Methods*, 2020, **12**, 1398–1414.
- 15 B. Yao, J. Zhang, T. Kou, Y. Song, T. Liu and Y. Li, *Adv. Sci.*, 2017, **4**, 1700107.

- 16 C. Zhao, J. Wang, Z.-Q. Zhang, Z. Sun and Z. Maimaitimin, *ChemElectroChem*, 2022, **9**, e202200948.
- 17 T. S. Tran, N. K. Dutta and N. R. Choudhury, *Adv. Colloid Interface Sci.*, 2018, **261**, 41–61.
- 18 J. R. Camargo, L. O. Orzari, D. A. G. Araujo, P. R. de Oliveira, C. Kalinke, D. P. Rocha, A. L. dos Santos, R. M. Takeuchi, R. A. A. Munoz and J. A. Bonacin, *Microchem. J.*, 2021, **164**, 105998.
- 19 W. T. Fonseca, K. R. Castro, T. R. de Oliveira and R. C. Faria, *Electroanalysis*, 2021, **33**, 1520–1527.
- 20 M. Mass, L. S. Veiga, O. Garate, G. Longinotti, A. Moya, E. Ramón, R. Villa, G. Ybarra and G. Gabriel, *Nanomaterials*, 2021, **11**, 1645.
- 21 A. S. Pillai, A. Chandran and S. K. Peethambharan, *Appl. Mater. Today*, 2021, **23**, 100987.
- 22 Y. Liao, Y. Tian, X. Ma, M. Zhao, J. Qian and X. Wang, *ACS Appl. Mater. Interfaces*, 2020, **12**, 48077–48083.
- 23 W. Yang and C. Wang, *J. Mater. Chem. C*, 2016, **4**, 7193–7207.
- 24 Y. Htwe and M. Mariatti, *J. Taiwan Inst. Chem. Eng.*, 2021, **125**, 402–412.
- 25 L. Jiang, H. Hong, J. Hu and X. Yan, *ACS Appl. Mater. Interfaces*, 2022, **14**, 12214–12222.
- 26 H. Menon, R. Aiswarya and K. P. Surendran, *RSC Adv.*, 2017, **7**, 44076–44081.
- 27 J. Whelan, V. Abbing-Karahagopian, L. Serino and M. Unemo, *BMC Infect. Dis.*, 2021, **21**, 1–23.
- 28 J. Whelan, J. Eeuwijk, E. Bunge and E. Beck, *Infect. Dis. Ther.*, 2021, **10**, 1887–1905.
- 29 W. H. Organization, Global health sector strategy on sexually transmitted infections 2016–2021: toward ending STIs, World Health Organization, 2016.
- 30 R. Verma, S. Sood, R. Singh, G. Sumana, M. Bala, V. K. Sharma, J. C. Samantaray, R. M. Pandey and B. D. Malhotra, *Diagn. Microbiol. Infect. Dis.*, 2014, **78**, 16–23.
- 31 R. Singh, R. Verma, A. Kaushik, G. Sumana, S. Sood, R. K. Gupta and B. Malhotra, *Biosens. Bioelectron.*, 2011, **26**, 2967–2974.
- 32 A. Soni, C. M. Pandey, S. Solanki and G. Sumana, *RSC Adv.*, 2015, **5**, 45767–45774.
- 33 R. P. Tortorich, H. Shamkhalichenar and J.-W. Choi, *Appl. Sci.*, 2018, **8**, 288.
- 34 Y. Liao, R. Zhang, H. Wang, S. Ye, Y. Zhou, T. Ma, J. Zhu, L. D. Pfefferle and J. Qian, *RSC Adv.*, 2019, **9**, 15184–15189.
- 35 V. S. Turkani, D. Maddipatla, B. B. Narakathu, T. S. Saeed, S. O. Obare, B. J. Bazuin and M. Z. Atashbar, *Nanoscale Adv.*, 2019, **1**, 2311–2322.
- 36 F. G. Pacheco, A. A. Cotta, H. F. Gorgulho, A. P. Santos, W. A. Macedo and C. A. Furtado, *Appl. Surf. Sci.*, 2015, **357**, 1015–1023.
- 37 S. Augustine, P. Kumar and B. D. Malhotra, *ACS Appl. Bio Mater.*, 2019, **2**, 5366–5378.
- 38 V. Duc Chinh, G. Speranza, C. Migliaresi, N. Van Chuc, V. Minh Tan and N.-T. Phuong, *Sci. Rep.*, 2019, **9**, 1–9.
- 39 G. Stando, S. Han, B. Kumanek, D. Łukowiec and D. Janas, *Sci. Rep.*, 2022, **12**, 1–13.
- 40 D. Kala, T. K. Sharma, S. Gupta, V. Verma, A. Thakur, A. Kaushal, A. V. Trukhanov and S. V. Trukhanov, *Sensors*, 2021, **21**, 4366.
- 41 Q. Lu, T. Su, Z. Shang, D. Jin, Y. Shu, Q. Xu and X. Hu, *Biosens. Bioelectron.*, 2021, **184**, 113229.
- 42 J. Mohanraj, D. Durgalakshmi, R. A. Rakkesh, S. Balakumar, S. Rajendran and H. Karimi-Maleh, *J. Colloid Interface Sci.*, 2020, **566**, 463–472.
- 43 C. Srisomwat, P. Teengam, N. Chuaypen, P. Tangkijvanich, T. Vilaivan and O. Chailapakul, *Sens. Actuators, B*, 2020, **316**, 128077.
- 44 F. Farshchi, A. Saadati and M. Hasanzadeh, *Anal. Methods*, 2020, **12**, 4759–4768.

Article

Conductive Ink-Coated Paper-Based Supersandwich DNA Biosensor for Ultrasensitive Detection of *Neisseria gonorrhoeae*

Niharika Gupta ¹, D. Kumar ², Asmita Das ¹, Seema Sood ³ and Bansi D. Malhotra ^{1,*} ¹ Department of Biotechnology, Delhi Technological University, Delhi 110042, India² Department of Applied Chemistry, Delhi Technological University, Delhi 110042, India³ Department of Microbiology, All India Institute of Medical Sciences, Ansari Nagar, New Delhi 110016, India

* Correspondence: bansi.malhotra@gmail.com

Abstract: Herein, we report results of the studies relating to the development of an impedimetric, magnetic bead-assisted supersandwich DNA hybridization assay for ultrasensitive detection of *Neisseria gonorrhoeae*, the causative agent of a sexually transmitted infection (STI), gonorrhoea. First, a conductive ink was formulated by homogeneously dispersing carboxylated multiwalled carbon nanotubes (cMWCNTs) in a stable emulsion of terpineol and an aqueous suspension of carboxymethyl cellulose (CMC). The ink, labeled C5, was coated onto paper substrates to fabricate C5@paper conductive electrodes. Thereafter, a magnetic bead (MB)-assisted supersandwich DNA hybridization assay was optimized against the *porA* pseudogene of *N. gonorrhoeae*. For this purpose, a pair of specific 5' aminated capture probes (SCP) and supersandwich detector probes (SDP) was designed, which allowed the enrichment of target gonorrhoeal DNA sequence from a milieu of substances. The SD probe was designed such that instead of 1:1 binding, it allowed the binding of more than one T strand, leading to a 'ladder-like' DNA supersandwich structure. The MB-assisted supersandwich assay was integrated into the C5@paper electrodes for electrochemical analysis. The C5@paper electrodes were found to be highly conductive by a four-probe conductivity method (maximum conductivity of 10.1 S·cm⁻¹). Further, the biosensing assay displayed a wide linear range of 100 aM–100 nM (10⁹ orders of magnitude) with an excellent sensitivity of 22.6 kΩ·(log[concentration])⁻¹. The clinical applicability of the biosensing assay was assessed by detecting genomic DNA extracted from *N. gonorrhoeae* in the presence of DNA from different non-gonorrhoeal bacterial species. In conclusion, this study demonstrates a highly sensitive, cost-effective, and label-free paper-based device for STI diagnostics. The ink formulation prepared for the study was found to be highly thixotropic, which indicates that the paper electrodes can be screen-printed in a reproducible and scalable manner.

Keywords: DNA biosensor; *Neisseria gonorrhoeae*; conductive ink; electrochemical; infectious diseases



Citation: Gupta, N.; Kumar, D.; Das, A.; Sood, S.; Malhotra, B.D.

Conductive Ink-Coated Paper-Based Supersandwich DNA Biosensor for Ultrasensitive Detection of *Neisseria gonorrhoeae*. *Biosensors* **2023**, *13*, 486.

<https://doi.org/10.3390/bios13040486>

Received: 28 February 2023

Revised: 13 April 2023

Accepted: 14 April 2023

Published: 18 April 2023



Copyright: © 2023 by the authors. Licensee MDPI, Basel, Switzerland. This article is an open access article distributed under the terms and conditions of the Creative Commons Attribution (CC BY) license (<https://creativecommons.org/licenses/by/4.0/>).

1. Introduction

Sexually transmitted infections (STIs) remain one of the major medical problems, with more than 1M infections being acquired every day worldwide [1]. Gonorrhoea, caused by the bacteria *Neisseria gonorrhoeae* (NG), is a curable STI having a very high incidence rate. The World Health Organization (WHO) has considered it as one of three STIs of global concern and has estimated eighty-two million new cases of gonorrhoea in 2020 worldwide [2]. Factors that contribute to the high prevalence of gonorrhoea include lack of access to testing and treatment, inadequate prevention efforts, and stigma surrounding STIs. Untreated gonorrhoea can lead to serious complications, including pelvic inflammatory disease, infertility, neonatal blindness, ectopic pregnancy, and an increased risk of HIV transmission [1,3,4]. Another crucial factor to consider is the alarmingly increasing cases of antimicrobial-resistant (AMR) gonorrhoea worldwide [2]. Thus, timely diagnosis and proper intervention is required to decrease the incidence of this STI.

The conventional detection strategies for *Neisseria gonorrhoeae* (NG) presently include culture techniques, microscopy, and the polymerase chain reaction (PCR). These techniques, though sensitive, are expensive, time-consuming, laborious, and cannot be performed outside of the laboratory [1,5]. Biosensors can prove to be essential for improving access to timely and accurate diagnosis, particularly in resource-limited settings where traditional laboratory-based testing may not be readily available. They can allow for the rapid detection of infections including gonorrhea at the point of care (POC), often providing results within minutes, which may help to expedite the treatment and reduce the risk of transmission [3,6,7]. In addition, biosensors can reduce the need for expensive and time-consuming laboratory testing, making them an attractive option for both healthcare providers and patients. Different kinds of DNA biosensors have been developed in recent years for the detection of various pathogens, such as *Vibrio cholerae* [8], *Haemophilus influenzae* [9], SARS-CoV-2 [10,11], Zika virus [12,13], etc. The high fidelity of DNA base pairing allows for the design and development of different kinds of DNA-based sensing mechanisms [3,6,10].

A few attempts to detect gonorrheal DNA have been made in the recent past. These studies have mostly focused on the development of amplification-based approaches for the visual detection of NG [3,6]. We have also previously reported the electrochemical detection of PCR amplicons of NG [14]. Visual detection is often semi-quantitative and amplification-based approaches suffer from limitations similar to those of other nucleic acid amplification assays (NAATs), e.g., the use of expensive reagents and the requirement of specific conditions (high temperature, etc.). In this context, supersandwich DNA hybridization is an attractive technique that alleviates the limitations associated with amplification-based assays and provides exceptionally high sensitivity as compared to traditional hybridization-based biosensors [15–17]. This method provides an enzyme-free signal amplification, can be operated at room temperature, and can be integrated into different biosensing modalities [15,16,18]. Supersandwich amplification-based biosensors have been applied for many applications including pathogen detection [19], and miRNA detection [16] among others.

The paper-based biosensors can prove to be advantageous for screening, monitoring, and detection of gonorrhea, as they are cost-effective, can be miniaturized, and can be used in low-resource settings. Different kinds of paper-based analytical devices have been reported in literature for the detection of pathogenic DNA [9,20–22]. Electrochemical paper-based devices have gained interest owing to their high accuracy, quantitative nature, ease of use, and applicability at the PoC [23,24]. Nanomaterial-enhanced, paper-based screen-printed electrodes (SPEs) have recently gained popularity as a low-cost and sensitive option to traditional diagnostic methodologies [23,25,26]. With the advent of papertronics, new-age paper-based devices have emerged that can be utilized for various electrochemical applications including biosensors. The development of conductive inks has further driven the growth of paper-based devices and vice versa. Conductive inks are materials that can be printed or applied in a thin layer to a substrate and can be used to create electronic circuits and devices. Conductive inks have emerged as low-cost options for the fabrication of paper-based biosensors [27,28]. These inks can be utilized for the fabrication of biosensors towards the detection of several different analytes, including DNA, hormones, metal ions, etc. [27,28].

In this work, we have fabricated a conductive ink-coated, paper-based impedimetric DNA supersandwich hybridization assay for highly sensitive and label-free detection of *N. gonorrhoeae*. For the conductive ink (named C5), multiwalled carbon nanotubes (MWCNTs) have been used as the conductive filler. MWCNTs possess a high aspect ratio and high surface area, making them highly conductive and suitable for many applications. In addition, MWCNTs have good adhesion to various substrates, including plastics and paper, which makes them well-suited for use in flexible and lightweight devices. MWCNTs have good mechanical strength and can withstand high temperatures, which makes them suitable for use in different electrochemical applications. The C5 ink was chosen from

a series of inks for its optimum rheological behavior and coated onto paper substrates manually (C5@paper). Further, a magnetic bead (MB)-assisted DNA supersandwich assay was optimized against the *porA* pseudogene sequence of NG. The use of magnetic beads offers several advantages, including simplification of the sample enrichment process, the ability to be used in high-throughput assays, and automation. They can separate a target analyte from a milieu of substances owing to magnetic separation and greatly ease the purification process. The MB-assisted supersandwich assay was integrated with the C5@paper electrode for label-free detection of NG using electrochemical impedance spectroscopy (EIS).

2. Materials and Methods

2.1. Materials and Instrumentation

Carboxylated MWCNT (cMWCNT) and polysorbate 80 (PS80) were procured from SRL Pvt. Ltd. (Mumbai, India). Carboxymethyl cellulose (CMC; high viscosity) and terpineol were purchased from Central Drug House (P) Ltd. (CDH, New Delhi, India). The oligonucleotide probes were procured from IDT (Coralville, IA, USA) (Table 1). Carboxylated magnetic beads (MBs; Dynabeads Carboxylic Acid™ MyOne™) were purchased from Thermo Fisher (Waltham, MA, USA). Freshly prepared phosphate-buffered saline (PBS, 0.1 M) of pH 7 supplemented with 5 mM ferro-ferricyanide as redox probes was utilized in the electrochemical studies, unless otherwise specified. All experiments were conducted in triplicates (n = 3) unless otherwise specified.

Table 1. Oligonucleotide probes used in the study.

S. No.	Probe Type	Probe Name	Sequence (5'-3')	Melting Temperature (°C)
1.	Capture probe	SCP	5' NH ₂ -TTT TTT CCT GCT ACT TTC ACG CTG GA 3' (26 bases) (5' amino C6 modification)	59
2.	Detector probe (supersandwich)	SDP	5' AAG TAA TCA GAT GAA ACC AGT TCC CTG CTA CTT TCA CGC TGG A 3' (43 bases)	50.8
3.	Target strand	TP	5' GAA CTG GTT TCA TCT GAT TAC TTT CCA GCG TGA AAG TAG CAG G 3' (43 bases)	66.2
4.	Non-complementary probe	NC	5' TTG ATT GAG CGT CAT AGA TCG GAC GGC ACT AGT CAG TAC TCG A 3' (43 bases)	67

The ink formulations were analyzed for viscosity and thixotropy on an Anton Paar rheometer by the parallel plate (PP40, diameter 40 mm) method. All rheology experiments were conducted at 25 °C. The C5@paper electrodes (1 × 1 cm²) were characterized for surface morphology via different techniques, including scanning electron microscopy (SEM), field emission SEM (FESEM), and atomic force microscopy (AFM). For SEM and FESEM analysis, the samples were dried under an infrared lamp for 30 min to eliminate any adsorbed moisture and sputter coated with Au for electrical conductivity. SEM was conducted on a ZEISS EVO 18 instrument at 10 kV acceleration voltage. FESEM was performed on a JEOL JSM-7800F Prime instrument. AFM studies were conducted on an Asylum Research MFP3D-BIO instrument in intermittent contact (tapping) mode. The conductivity of the C5@paper electrodes was analyzed via a four-probe conductivity meter (SES Instruments, India) (probe distance = 2 mm) at room temperature (25 °C). Cyclic voltammetry (CV) and EIS studies were performed on a single-channel Autolab potentiostat/galvanostat (Metrohm AG, Herisau, Switzerland). All CV studies were conducted at scan rate of 50 mV·s⁻¹ and EIS studies were conducted at 0.01 V within the frequency range of 0.1–10⁵ Hz.

2.2. Design of Oligonucleotide Probes

The supersandwich oligonucleotide probes were designed using NCBI-Primer BLAST, NCBI Nucleotide BLAST, and Clustal Omega. Briefly, a library of different sets of primers was prepared using NCBI-Primer BLAST, and their specificity was determined by aligning them with gonorrhoeal and non-gonorrhoeal genomic DNA sequences using NCBI Nucleotide BLAST. The non-gonorrhoeal DNA sequences used for alignment included those from *N. meningitidis*, commensal *Neisseria* species (*N. sicca*, *N. lactamica*, *N. mucosa*), *Chlamydia trachomatis*, *Ureaplasma urealyticum*, *Enterococcus faecalis*, *Escherichia coli*, *Staphylococcus aureus*, *Klebsiella pneumoniae*, *Mycoplasma genitalium*, and *Lactobacillus fermentum*. The forward primer from the set of probes having 100% similarity with gonorrhoeal DNA and having no or little similarity with non-gonorrhoeal DNA was selected as the capture probe (SCP), and an adjacent specific sequence was selected as the conventional detector probe (DP). For the supersandwich assay, the detector probe (SDP) sequence consisted of the DP sequence ligated to the SCP sequence in 5'-3' direction. The details of all the probes utilized in the study are given in Table 1. The alignment of the probes with the target DNA sequence is given in Section S1 of the Supplementary Information. Gel electrophoresis studies were conducted to determine the probe efficiency in forming a supersandwich duplex with the target DNA sequence.

2.3. Formulation of the Conductive Ink

For ink formulation, different amounts of CMC (1, 2.5, and 5% *w/v*) were dissolved in deionized (DI) water. These CMC dispersions were then mixed with terpineol (2:1 ratio) separately. Polysorbate 80 (PS80) was used as the stabilizer, as terpineol has limited solubility in water and CMC does not interact with organic solvents. The resulting emulsions, designated as CMC₁, CMC_{2.5}, and CMC₅, respectively, were stirred vigorously on a magnetic stirrer (~1000 rpm, 2 h). CMC₅ was chosen as the base for the conductive ink after rheological assessment. cMWCNTs were added to CMC₅ (cMWCNT:CMC ratio of 1:1) with vigorous stirring (~1000 rpm, overnight). The resulting conductive emulsion was probe ultrasonicated in an ice bath at a pulse of 1 s and 70% amplitude for 20 min, with pauses at every 5 min to prevent overheating. The resulting conductive ink, designated as C5, was stored in a closed container at low temperature (4 °C–10 °C) to prevent evaporation of the solvent.

2.4. Rheological Studies

The fluid properties of ink are imperative in understanding its behavior during the coating/printing process. The emulsion bases (CMC₁, CMC_{2.5}, and C₅) for the conductive ink, prepared with different amounts of CMC, were assessed for rheology by a plate-plate rheometer at 25 °C. The change in the shear viscosity of the emulsion bases was analyzed within the shear rate range of 0.1–100 s⁻¹. Further, a 3-interval thixotropy test (3iTT) was utilized for analyzing the recovery of the viscosities of the 3 emulsion bases after stress removal. This test can be used to simulate screen printing and other coating processes, wherein an abrupt increase in stress is observed during the printing/coating process. The emulsion bases were pre-sheared at 0.1 s⁻¹ for 20 s before the 3iTT. Thereafter, three intervals of different shear rates were applied: 0.1 s⁻¹ for 30 s (first interval), 200 s⁻¹ for 15 s (second interval; simulation of the printing process), and recovery at 0.1 s⁻¹ for 120 s.

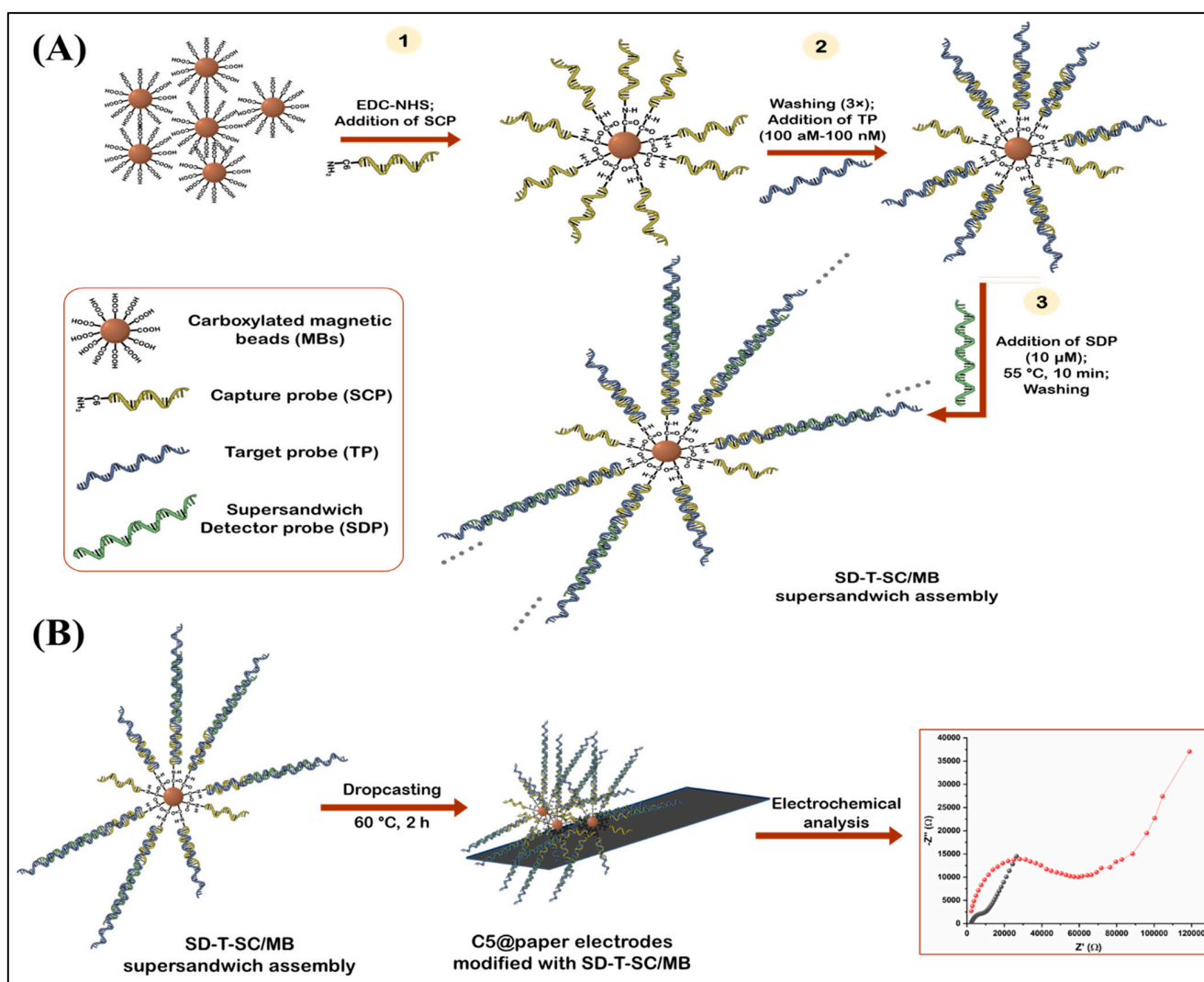
2.5. Fabrication of C5@paper Electrodes

The C5-coated paper electrodes (C5@paper) were fabricated by first coating drawing paper (200–300 gsm, 6 × 6 cm²) with the C5 ink using a commercially available paint brush (Faber-Castell). This C5-coated paper was then cut into strips having dimensions of 2 × 2 cm², which were then annealed at 120 °C for 10 min to allow evaporation of the solvent (terpineol and water). The effect of the number of coats (*n*) on the conductivity of the C5-coated paper was assessed by measuring the conductivity after each coat with

the 4-probe conductivity meter. For conductivity studies, the C5-coated paper strips were cut into pieces of size $1 \times 1 \text{ cm}^2$ each. The conductivity values of 4 strips ($1 \times 1 \text{ cm}^2$; 12 readings in total) were recorded at $25 \text{ }^\circ\text{C}$ and their mean value was reported for each coat. For electrochemical studies, the strips were cut into strips with dimensions of $2 \times 1 \text{ cm}^2$ to fabricate the C5@paper electrodes. All electrodes were stored in dark, dry conditions until further use.

2.6. Electrochemical Magnetic DNA Supersandwich Assay

The detailed protocol for the immobilization of SCP onto the MBs is provided in Section S2 of the Supplementary Information. Scheme 1 depicts the various steps involved in the electrochemical, MB-assisted biosensing assay.



Scheme 1. Schematic diagram depicting (A) the MB-assisted supersandwich hybridization assay for *N. gonorrhoeae* detection, and (B) subsequent integration with the C5@paper electrodes for electrochemical analysis via EIS.

2.6.1. Supersandwich Assay

Five milligrams of SCP/MBs were washed with DI water (3x) and dispersed in 500 μL of DI water, making the final concentration $10 \text{ mg}\cdot\text{mL}^{-1}$. Aliquots of 50 μL were made in different test tubes and 50 μL of TP was added to each tube in the concentration range of 100 aM–100 nM (5 zmol–5 pmol). Thereafter, 50 μL of SDP (10 μM) was added to each reaction tube and incubated at $55 \text{ }^\circ\text{C}$ for 10 min with mixing. This SD-T-SC/MB

supersandwich assembly was washed with DI water (3×) to remove unbound probes, and redispersed in 30 µL PBS buffer for electrochemical analysis.

2.6.2. Electrochemical Analysis

For the electrochemical studies, the SD-T-SC/MB assembly dispersed in 30 µL of PBS was drop cast onto the C5@paper electrodes. These modified electrodes were slowly dried at 60 °C for 2 h. Thereafter, impedance measurements for every electrode were recorded in PBS (pH 7) supplemented with 5 mM ferro-ferricyanide. The measurements were made in the range of 0.1–10⁵ Hz at 0.01 V. A calibration curve was plotted between the net change in charge transfer resistance (R_{ct}) of the C5@paper electrodes in the presence of different concentrations of TP (as compared to negative control) and the concentration of TP.

2.7. Real Sample Analysis

For practical applications, it is imperative that the electrochemical biosensing assay works in clinical settings and can specifically detect gonorrheal DNA from among a mixture of different substances. To assess this, the biosensing assay was first tested against gonorrheal genomic DNA. For this, DNA from *N. gonorrhoeae* bacterial culture was extracted using the boiling method. Briefly, a few colonies from the culture plate were dispersed in autoclaved, double distilled water (1 mL) and incubated at 90 °C for 1 h for inducing cell lysis. Then, the heat-lysed cell suspension was taken and centrifuged at 1200 rpm for 5 min to separate cell debris. The pellet was discarded and the remaining supernatant was stored at −20 °C until further use. The DNA was quantified using nanospectrophotometer (Nanodrop). It should be noted that DNA extracted using this method is often contaminated with RNA and other cellular components such as proteins. Hence, the purity level of such samples is often lower than the ideal values. This method was chosen for DNA extraction as it is quicker than the buffer-based commercial methods, requires fewer reagents, and is widely used in clinical labs for isolating DNA from cervical/urethral swabs—the samples utilized in gonorrhea testing.

Different dilutions of the extracted DNA were prepared, which were then sheared into smaller fragments by bath ultrasonication for 10 min, and denatured by incubation at 95 °C for 5 min. This ensured the denaturation of any residual, contaminating RNA and proteins in the samples. Thereafter, the protocol mentioned in the previous section was repeated to determine the concentration of gonorrheal DNA.

As clinical samples (particularly from female subjects) are known to contain DNA from different bacterial species, the specificity of the biosensing assay was further assessed by testing it against a mixture of gonococcal DNA with non-gonococcal DNA extracted from different bacteria. The DNA samples were extracted by the boiling method discussed above; hence, they also contained interfering RNA and proteins. The details of the bacterial species used in the study are given in Section S3. The response of the electrochemical biosensing assay to these mixed DNA samples was recorded in a similar manner as mentioned in Section 2.6.

3. Results and Discussion

3.1. Optimization and Characterization of the Ink Formulation

The ink formulation was optimized and characterized for flow properties by rheometry. The aim of this study was to prepare a homogenous ink with thixotropic properties, which pertain to a linear decrease in a liquid's viscosity with an increase in shear force followed by recovery of viscosity once the shear force is removed. Thixotropy allows for the smooth application of the ink on a particular substrate (in this case, paper) [29]. Most commercial paints and screen-printing inks are thixotropic in nature [29]. CMC is a known thixotropic agent and is prominently used as a rheological modifier [30]. To determine the effect of the amount of CMC on the ink rheology, three different solvent bases were prepared—CMC₁, CMC_{2.5}, and CMC₅—corresponding to 1%, 2.5%, and 5% CMC. Figure 1A shows the log plot of the change in viscosity with the shear rate in the range of 0.1–100 s^{−1}. The

viscosity varies linearly with the shear rate suggesting the shear thinning property of the three emulsion bases. The initial viscosities for CMC₁, CMC_{2.5}, and CMC₅ at 0.1 s⁻¹ were found to be 3.48 Pa.s, 14.42 Pa.s, and 18.9 Pa.s, respectively. This increase in initial viscosity is due to the increase in CMC content in the solvent bases. The thixotropic behavior was further assessed by the 3-interval thixotropy test (3iTT) (Figure 1B). This test can simulate processes such as painting, screen printing, etc., by applying a sudden high shear stress to ink and then analyzing the percentage recovery in the viscosity of the ink after the stress is removed abruptly. CMC₅ displayed the highest viscosity of 18.4 Pa.s at 0.1 s⁻¹ (30 s), while CMC₁ had the lowest viscosity (Figure 1B). In accordance with the shear thinning behavior, the viscosity of the emulsion bases decreased significantly at 200 s⁻¹. After the removal of the stress, the viscosity of the three emulsions recovered to different degrees. For CMC₁ and CMC_{2.5}, the viscosities decreased to 0.68 Pa.s and 0.76 Pa.s at 45 s (10% and 4.78%, respectively, of their initial viscosities at 30 s). While for CMC₅, the viscosity decreased to 1.08 Pa.s at 45 s (5.8% of initial viscosity at 30 s) indicating its higher viscosity in relation to the other two emulsion bases. This further suggests that CMC₁ would perhaps flow the fastest and CMC₅ would flow the slowest through the screen mesh while printing. After recovery of the shear rate from 200 s⁻¹ to 0.1 s⁻¹, the viscosity of CMC₁ recovered to 62.5% of its original initial viscosity after 75 s. At the same time, CMC_{2.5} and CMC₅ recovered 59.3% and 98.4% of their initial viscosities, respectively. Recovery of viscosity is crucial to determine the screen printability of inks as it indicates less seepage and dripping issues. For an efficient screen-printing ink, it is imperative that the ink should neither possess a very low viscosity (as it allows the creation of air bubbles) nor should it be too viscous, which leads to non-uniform printed patterns [29]. Since CMC₅ displayed an appreciable decrease in viscosity and the highest recovery, it was chosen as the emulsion base for the formulation of the ink.

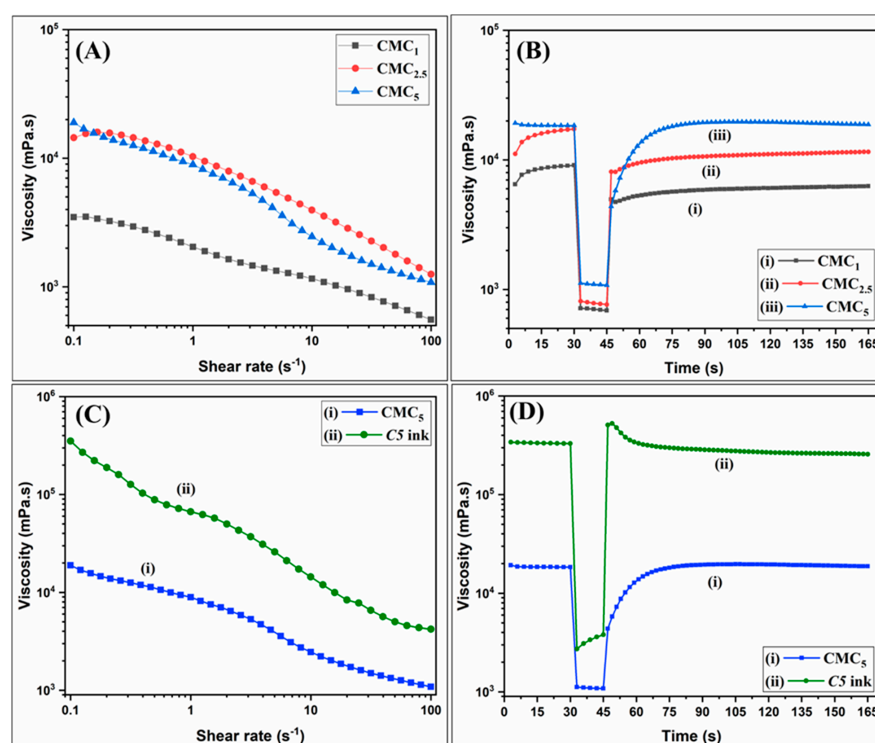


Figure 1. (A) Viscosity flow curves showing the change in viscosity of the CMC₁, CMC_{2.5}, and CMC₅ base emulsions with shear rate in the range of 0.1–100 s⁻¹, (B) Change in viscosity of the CMC₁, CMC_{2.5}, and CMC₅ base emulsions with time when subject to sudden change in the shear rate, (C) Viscosity flow curves of the CMC₅ base emulsion and the C5 ink with shear rate in the range of 0.1–100 s⁻¹, and (D) Change in viscosity of the CMC₅ base emulsion and C5 ink with time when subject to sudden change in shear rate.

The C5 ink was prepared by dispersing cMWCNT into the CMC₅ emulsion base uniformly, and the effect of cMWCNT on the flow properties of the final ink was observed (Figure 1C,D). As shown in Figure 1C, the initial viscosity of the C5 ink at 0.1 s⁻¹ was found to be significantly higher (352.1 Pa.s) than the CMC₅ emulsion. However, the ink retained its shear thinning property as the viscosity decreased linearly with the shear rate. It is also interesting to note that, during the thixotropy test (3iTT), the initial viscosity of the C5 ink (329.8 Pa. s at 0.1 s⁻¹ at 30 s) decreased by ~100 times to 3.79 Pa.s (~1% of the initial viscosity) at 200 s⁻¹ at 45 s. The viscosity further recovered to 90% of its initial value at 75 s after the removal of the stress. This indicated that the addition of cMWCNTs did not affect the thixotropic behavior of the ink and hence the C5 ink can potentially be used in screen printing of high-resolution patterns. Similar rheological behavior has been observed in other studies wherein MWCNT and other nanomaterials, such as silver, graphene, etc., were used as conductive fillers [29,31,32]. It has been reported that the presence of carbon nanomaterials as fillers in an ink increases the structural strength of the ink, and hence it may lead to a faster recovery of the viscosity [32]. The high viscosity recovery suggests that the colloidal stability of the ink is maintained even at higher shear rates, which results from the balance between the *van der Waals* interactions and steric stabilization among cMWCNTs, CMC (binder), and other dispersants (PS80) [31]. This eventually leads to better leveling during printing.

3.2. Morphological and Functional Characterization of C5@paper Electrodes

The morphology of the C5@paper electrodes has been studied by SEM and FESEM analysis (Figure 2A–F). The cellulose fibers of bare paper used as substrate are clearly visible in Figure 2A,B). These fibers are completely covered by the C5 ink after coating, which appears uniform and has a granular appearance (Figure 2C,D). The cMWCNTs seem to be completely enveloped with CMC (and possibly PS80), though they are visible at some locations protruding out of the ink matrix (Figure 2D). Further, Figure 2E shows the magnified FESEM image of the tilted lateral side of the C5@paper electrode. The ink coats are clearly visible with cMWCNT dispersed over the entire surface. Upon further inspection of the lateral edge of the C5@paper electrode, it seems that the ink has not completely penetrated the entire thickness of the paper, as cellulose fibers are visible in between the ink coating (Figure S2). Figure 2F shows the magnified view of the C5@paper electrode with a cMWCNT protruding out of the ink matrix, having an apparent diameter of 67.6 nm. The surface roughness of bare paper and C5@paper electrodes was further analyzed by AFM studies (Figure 2G(i,ii), respectively). The RMS surface roughness of bare paper and the C5@paper electrode was found to be 168.2 nm and 41.6 nm, respectively. This reduction in the surface roughness upon coating may be contributed to the masking of cellulose fibers by the ink. This further suggests that, despite the grainy appearance, the ink coating is smooth and possesses lower friction force as compared to bare paper [33].

The conductivity of the C5@paper electrodes was measured by the 4-probe conductivity method. The calculations involved in the measurement of conductivity are given in Section S4. After coating, the electrodes were annealed at 120 °C for 10 min. The conductivity of the C5@paper electrodes was found to increase with the number of coats, with maximum value at four coats ($n = 4$), as shown in Figure 2H. This increase in conductivity can be attributed to the increase in the cMWCNT content after each coat. Interestingly, the conductivity was found to first reduce and then seemed to saturate gradually for 5–8 coats. The CMC concentration (% *w/v*) is equivalent to that of cMWCNT in the C5 ink. Perhaps, the insulating nature of CMC starts dominating the conductivity after four coats and beyond. The saturation of the conductivity points toward the presence of competing factors contributed by the presence of conductive cMWCNTs and non-conductive binders (CMC) and, to some extent, emulsifiers (PS80). This is in contrast with a recent study that reported an increase in conductivity until saturation of a graphene-based ink with an increase in the number of (printing) coats [34].

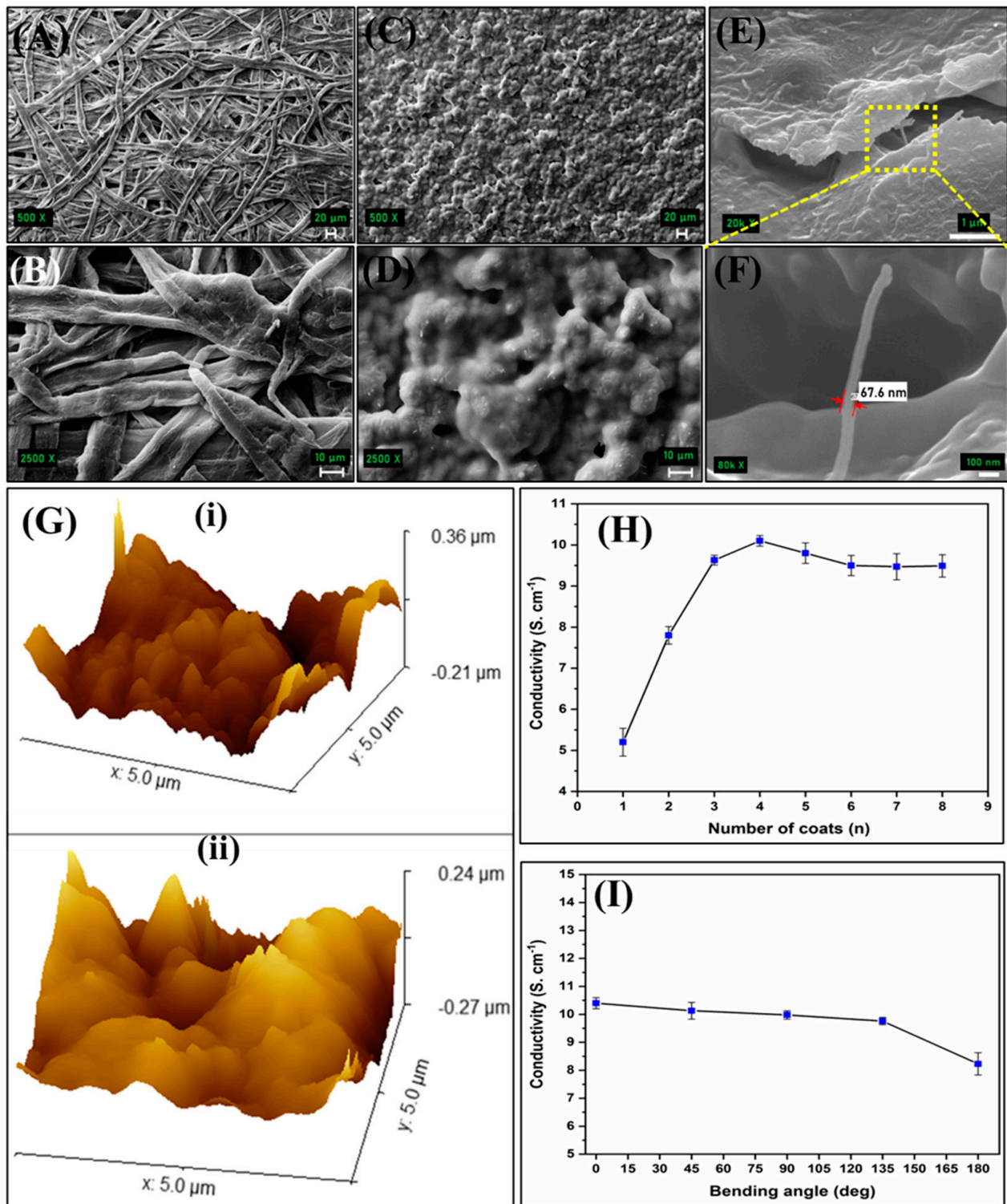


Figure 2. SEM images of (A,B) bare paper, and (C,D) C5@paper electrodes at different magnifications, (E) FESEM image of the C5@paper electrode, (F) High magnification FESEM image showing cMWCNT in the ink matrix, (G) AFM images of the (i) bare paper, and (ii) C5@paper electrode. Change in the conductivity of the C5@paper electrode with (H) number of coats, and (I) bending angle.

The maximum conductivity of the C5@paper electrode was found to be $10.1 \pm 0.24 \text{ S}\cdot\text{cm}^{-1}$ ($0.1 \pm 0.026 \text{ }\Omega\cdot\text{cm}$) after four coats of ink. A recent study has reported the conductivity of an MWCNT/PEDOT:PSS screen-printing ink to be $14.99 \text{ S}\cdot\text{cm}^{-1}$ for five printing passes [31].

It may be noted that the binder used in this study, PEDOT:PSS, is a conductive polymer, which played a significant role in the enhanced conductivity of the MWCNT ink. Another study reported the resistivity of an MWCNT ink in the range of $0.5\text{--}13\ \Omega\cdot\text{sq}^{-1}$ [35]. The study reported the use of PVP as a binder and 10% *w/v* MWCNT as a conductive filler. The results of these studies highlight the importance of the binder used in ink preparation. The use of a conductive binder may enhance the conductivity manifold, while an insulating polymer may compromise the conductivity of ink even if the conductive filler is used in excess. Keeping this in view, the high conductivity of the C5 ink, despite the use of a relatively smaller amount of MWCNT (5% *w/v*) and an insulating binder (CMC), alludes to the effectiveness of the method of ink preparation. Further, the change in conductivity of the C5@paper electrodes upon folding at different angles ($45\text{--}180^\circ$) was also estimated (Figure 2I). There was no significant change in the conductivity of the electrodes until 135° bending. However, the conductivity reduced drastically upon a 180° bend. The retention of conductivity until 135° suggests that cMWCNTs are well dispersed within the ink matrix [36]. However, the surface of the paper may crack at higher bending angles (180°) leading to cracks in the ink itself. This ultimately contributed to lower conductivity values at higher bend angles.

3.3. Electrochemical Studies

The electrochemical performance of the fabricated C5@paper electrodes and further modifications were characterized via CV and EIS. Multiple CV cycles were run to determine the stability of the fabricated electrodes upon continuous use in the buffer. As shown in Figure S2, the response of the electrode does not change significantly even after 50 cycles, indicating the stability of the electrodes in buffer conditions. It may be noted that the charging current was found to be too high in relation to the faradaic current in the CV curves, which could be due to the pseudocapacitance of the electrode. The swelling of CMC in aqueous conditions may also contribute to the high charging current. For this reason, EIS was chosen for further electrochemical studies. The batch reproducibility of the C5@paper electrodes was also assessed by randomly selecting 10 electrodes from different batches and measuring their charge transfer resistance (R_{ct}) values via EIS (Figure 3A). The R_{ct} values were determined by fitting the Nyquist plots by an equivalent model circuit given by $(R_s(Q_1[R_{ct}Q_2]))$, wherein R_s is the solution resistance, Q_1 is the constant phase element (CPE) associated with the (pseudo)capacitance of the electric double layer formed at the electrode surface, R_{ct} is the charge transfer resistance, and Q_2 is the CPE associated with the diffusion of redox species at the electrode surface (Figure S3A). The presence of Q_1 and Q_2 in the model circuit indicates the non-ideal behavior of the double-layer capacitance. This also indicates that the distribution of active sites over the electrode surface might be non-homogenous [37]. As shown in Figure 3A, no significant difference was found in the R_{ct} of the C5@paper electrodes, with the mean R_{ct} being $940.29 \pm 0.72\ \Omega$. These results suggest that the cMWCNTs were dispersed homogeneously in the C5 ink, which led to the uniform coating of the paper substrates. The change in the R_{ct} of the C5@paper electrodes with time (1–30 days) was also studied to determine the storage life of the electrodes (Figure S3B). It was found that the initial R_{ct} at Day 1 ($940\ \Omega$) reduced by a mere $\sim 0.5\%$ on Day 30 ($935.2\ \Omega$), suggesting that the electrodes can be stored for at least 30 days at room temperature in a dry environment.

Figure 3B shows the Nyquist plots of the C5@paper electrodes and subsequent modifications. It can be seen that the R_{ct} (which is generally correlated to the diameter of the semicircle in the Nyquist plot) increases after every modification. The R_{ct} of the C5@paper was found to be $940 \pm 4.2\ \Omega$, which further increased to $3.28 \pm 0.06\ \text{k}\Omega$ and $4.11 \pm 0.09\ \text{k}\Omega$, respectively, after modifications by SCP/MB and BSA/SCP/MB. This increase in R_{ct} indirectly indicates the immobilization of SCP and BSA onto the MB surface. The equivalent model circuit $(R_s(Q_1[R_{ct}Q_2]))$ fitted into the plots is given in Figure S3A. Prior to the electrochemical response studies, gel electrophoresis studies were conducted to confirm the formation of the supersandwich between the SCP, TP, and SDP probes. As shown

in Figure S4, DNA bands at ~100 bp and higher are observed at both 25 °C and 55 °C. Additionally, the supersandwich structures formed at both temperatures after a mere 5 min. Thus, 55 °C for 10 min was chosen as the optimal temperature and time for the DNA supersandwich hybridization studies. The higher temperature was chosen in order to avoid any non-specific interactions with non-gonorrhoeal DNA, which is often present in clinical samples. The time chosen was 10 min as the immobilization of SCP onto the MBs can significantly reduce their mobility in the aqueous phase. Steric hindrance can also hamper the rate of DNA hybridization. To compensate for such losses, the optimum incubation time was chosen as a bit higher than necessary.

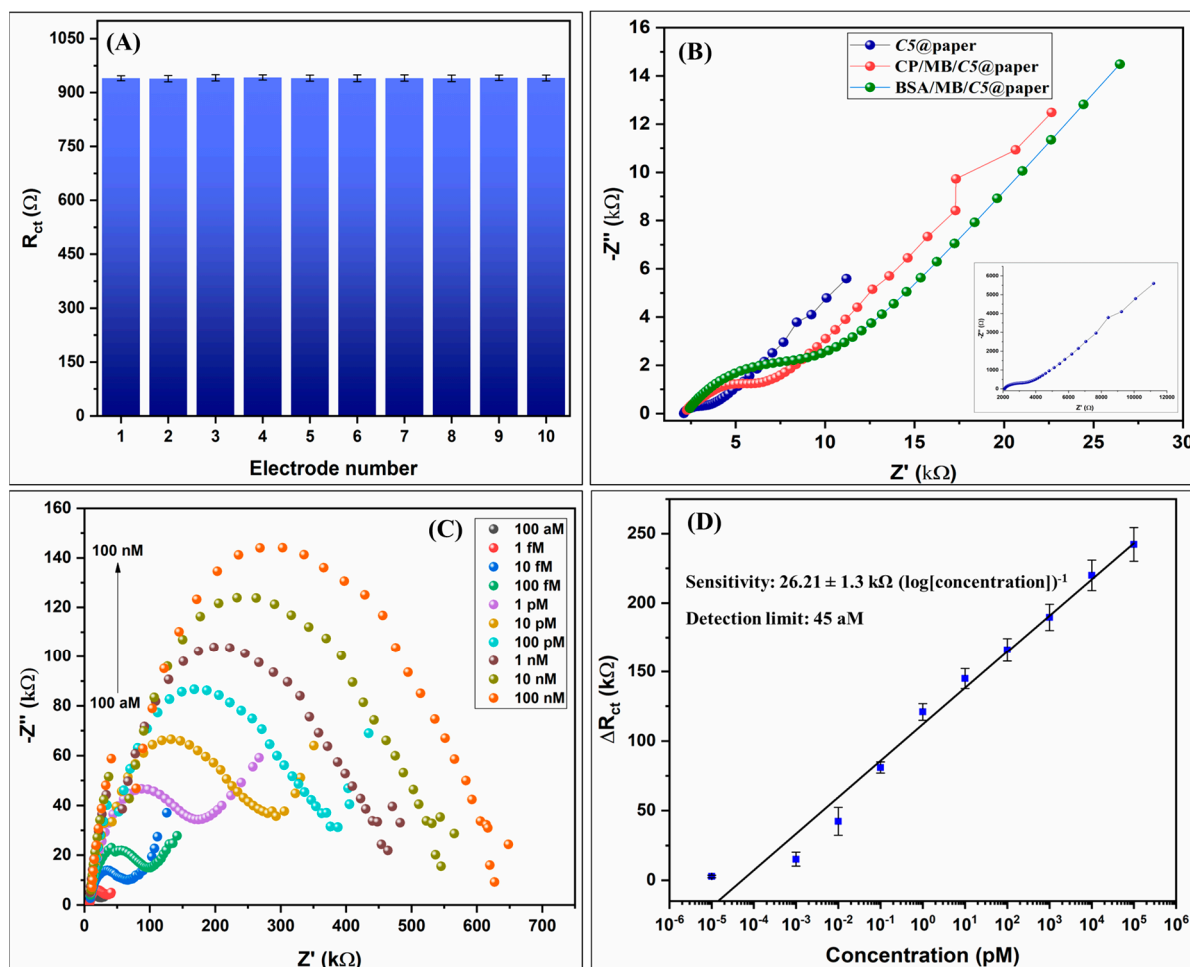


Figure 3. (A) Bar graph showing the R_{ct} values of C5@paper electrodes selected randomly from different batches. (B) Nyquist plots of the C5@paper, SCP/MB/C5@paper, and the BSA/SCP/MB/C5@paper electrodes. Inset shows the Nyquist plot of the C5@paper electrode. (C) Nyquist plots of the C5@paper after drop-casting of the SD-T-SC/MB for different concentrations of the TP. (D) Corresponding linear calibration curve showing ΔR_{ct} vs. log of the concentration of the TP.

The Nyquist plots of the C5@paper electrodes for different concentrations of the TP are given in Figure 3C. A significant rise in the impedance was observed with increasing concentration of the target DNA, as is evident by the increasing semicircle diameter. The change in the R_{ct} (ΔR_{ct}) was calculated by applying the following equation:

$$\Delta R_{ct} = R_m - R_0 \quad (1)$$

where R_m is the measured R_{ct} for a given concentration and R_0 is the R_{ct} of the negative control (electrode with no TP). The ΔR_{ct} values correlated linearly to the log of concentration of the *porA* target sequence (TP) (Figure 3D). The corresponding linear regression equation is:

$$\Delta R_{ct} = 26.21 \times \log[\text{concentration}] + 111.99, R^2 = 0.98 \quad (2)$$

The linear range of the assay was found to be 100 aM–100 nM (10^9 orders of magnitude) with an exceptional sensitivity of 26.21 k Ω ($\log[\text{concentration}]$)⁻¹ and a detection limit of 45 aM, as calculated by a previously reported method [37]. The enhanced sensitivity can be contributed to the formation of supersandwich structures at the surface of the MBs. As shown in Table 2, the biosensing assay proposed in this work possesses a better detection limit than most recent studies reported on the development of electrochemical DNA biosensors. Further, the value of the detection limit (45 aM) is equivalent to 10–22 copies μL^{-1} corresponding to the longest and the shortest supersandwich DNA duplex length of 150 bp and 69 bp, respectively (Figure S3). This detection limit range is superior to those reported by recent studies on visual detection of NG via a multiple cross displacement assay (20 copies/test) and loop-mediated isothermal amplification (LAMP) assay (50 copies/test) [3,6]. In these studies, gold nanoparticles were used as the colorimetric probe. Luo et al. reported a similar detection limit of 10 copies μL^{-1} for a Cas13a-based specific high-sensitivity enzymatic reporter unlocking (SHERLOCK) assay developed for NG *porA* and azithromycin resistance detection [38]. It may be noted that this assay was tested on only purified double-stranded DNA (dsDNA). This demonstrates the superiority of the proposed biosensing assay in terms of a relatively simpler detection strategy, the use of fewer reagents, and label-free electrochemical detection. PCR is currently the gold standard for the detection of NG in clinical samples. Comparison with commercial PCR assays in terms of detection limit indicates that there is a scope for improvement in the proposed supersandwich biosensing assay. GeneProof[®] claims the detection limit of its NG dual-target PCR kit to be 0.109 copies μL^{-1} [39]. While another study has reported the detection limit of the same assay being 1.5 copies μL^{-1} [40]. It is important to note here that PCR is an amplification-based assay, and, hence, in some instances, the detection limit is simply defined as being the lowest concentration returning amplification. Using this approach, a study reported the assay detection limit as being 1×10^{-7} dilution [41], while another reported a detection limit of 10^2 – 10^3 copies mL^{-1} (0.1–1 copy μL^{-1}) [42]. Thus, readers are advised to consider these factors while analyzing the differences between biosensing assays and PCR assays and their respective detection limits.

Table 2. Comparison of recent studies on paper-based biosensors for DNA detection.

S. No.	Ink Formulation/Nanomaterial	Type of DNA Assay	Target Pathogen	Linear Range	Sensitivity (LOD)	Reference
1.	Ni–Au composite/CNT/PVA	Traditional hybridization	HIV DNA	10 nM–1 μM	(0.13 nM)	[26]
2.	Tungsten disulfide quantum dots	Traditional hybridization	Specific meningitis	1 nM–100 μM	(1 nM)	[43]
3.	Oxidized graphitic carbon nitride	Traditional hybridization	Norovirus	10^{-7} – 10^2 μM	(100 fM)	[25]
3.	Graphene nanosheets	Direct analysis	(dsDNA)	0.2–5 pg mL^{-1}	0.00656 $\text{mA} \cdot \text{pg}^{-1} \text{cm}^{-2}$	[24]

Table 2. Cont.

S. No.	Ink Formulation/ Nanomaterial	Type of DNA Assay	Target Pathogen	Linear Range	Sensitivity (LOD)	Reference
4.	Carbon graphene ink (commercial)	Traditional hybridization (pyrrolidinyI peptide nucleic acid-mediated)	Hepatitis B virus	50 pM–100 nM	(1.45 pM)	[44]
5.	Ag nanoprisms electrode- posited on graphene quantum dots (GQDs)	Traditional hybridization	<i>Leishmania infantum</i>	1 zM–1 nM	1 zM (LOQ *)	[45]
6.	cMWCNT	Supersandwich hybridization	<i>Neisseria gonorrhoeae</i>	100 aM–100 nM (5 zmol–5 pmol)	$26.21 \text{ k}\Omega (\log[\text{concentration}])^{-1}$ (45 aM)	This work

3.4. Real Sample Analysis and Specificity Studies

To determine whether the electrochemical biosensing assay would perform in clinical conditions, its response was recorded against different concentrations of genomic DNA extracted from NG in the concentration range of 100 aM–1 pM. As shown in Figure 4A, there was no significant change in the ΔR_{ct} of the biosensing electrode for the same concentrations of the genomic DNA and synthetic TP used in the response studies. This indicates the applicability of the biosensing assay in real-life situations.

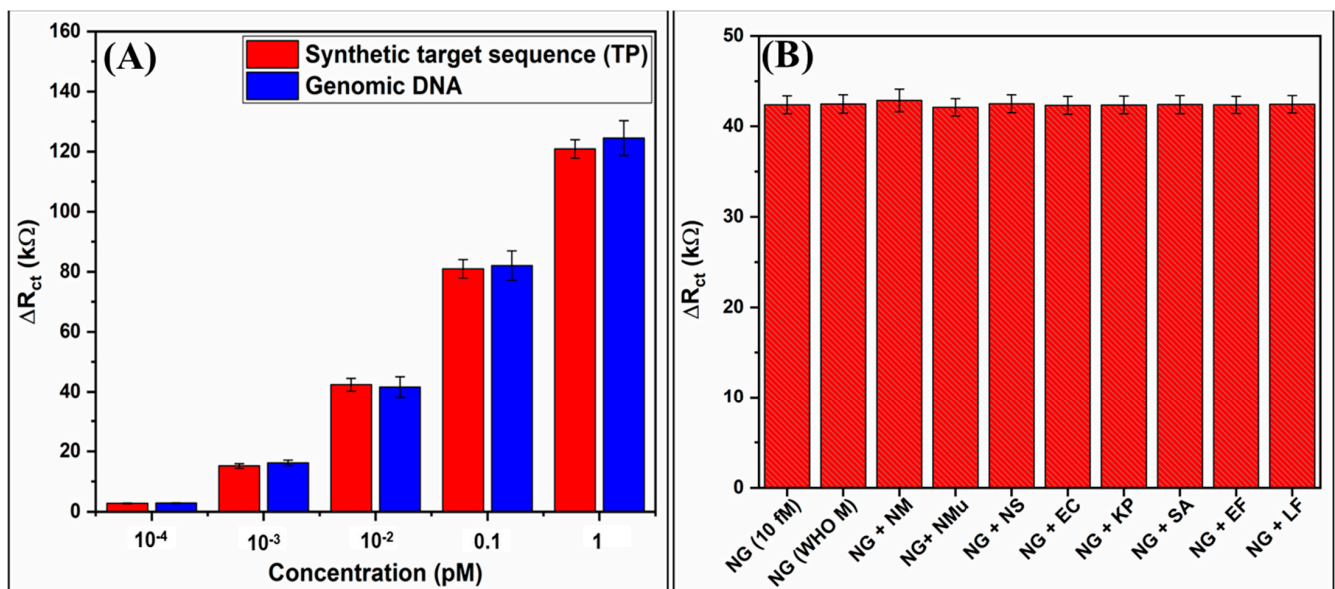


Figure 4. (A) Comparison between the biosensor response to synthetic TP and genomic DNA from NG for different concentrations (100 aM–1 pM). (B) Response of the biosensing assay to NG DNA mixed with DNA from other bacterial species. NM: *Neisseria meningitidis*, NMu: *Neisseria mucosa*, NS: *Neisseria sicca*, EC: *Escherichia coli*, KP: *Klebsiella pneumoniae*, SA: *Staphylococcus aureus*, EF: *Enterococcus faecalis*, LF: *Lactobacillus fermentum*.

The specificity of the biosensing assay was assessed by mixing the genomic DNA of NG with DNA from other bacteria (Section S3). The DNA was extracted using the boiling method; hence, all samples may contain protein and RNA as contaminants. The NG genomic DNA was mixed with DNA from other bacteria and subjected to the protocol mentioned in Section 2.7. As shown in Figure 4B, no significant change in ΔR_{ct} of the C5@paper biosensing electrode was observed when recorded in the presence of interfering DNA from different bacterial species. The ΔR_{ct} values for the different DNA mixtures are given in Table S1. These studies highlight the significance of sample enrichment via MBs before biosensing and hint at the high specificity of the designed oligonucleotide probes.

4. Conclusions

We have fabricated a conductive ink-coated, paper-based biosensing assay for the ultrasensitive detection of *Neisseria gonorrhoeae* using EIS. C5, the MWCNT-based conductive ink used in this study, was found to be highly conductive, with the maximum conductivity of the C5@paper electrodes being $10.1 \text{ S}\cdot\text{cm}^{-1}$. The ink formulation was optimized for thixotropy that can allow batch reproduction by screen printing. A magnetic bead-assisted supersandwich DNA hybridization assay was designed, which upon integration with the C5@paper electrodes, was found to be highly sensitive with an excellent detection limit (45 aM). The biosensing assay was further found to be highly specific for gonorrheal DNA when tested in a mixture of DNA from different non-gonorrheal species. This study not only reveals the utility of paper-based biosensors for DNA diagnostics but also highlights the potential of conductive inks in the fabrication of paper-based biosensors. It further attempts to bring gonorrhea to the forefront of scientific research as an important biosensing target. Further studies should focus on the modification of the conductive inks for obtaining improved electrochemical performance, which would further enhance biosensor sensitivity.

Supplementary Materials: The following supporting information can be downloaded at <https://www.mdpi.com/article/10.3390/bios13040486/s1>. Section S1: Alignment of the designed oligonucleotide probes with the target sequence (porA pseudogene); Section S2: Protocol followed for SCP immobilization on the MBs; Section S3: Bacterial species used in the specificity studies; Section S4: Calculation of resistivity of the C5@paper electrodes; Figure S1: FESEM image of the lateral edge of C5@paper electrode; Figure S2: CV curves of the C5@paper electrodes showing continuous use stability; Figure S3A: Equivalent circuit fitted into the Nyquist plots; Figure S3B: Bar graph showing the R_{ct} of C5@paper electrodes during 1-30 days of storage; Figure S4: Gel electrophoresis studies to ascertain the formation of DNA supersandwich structures; Table S1: R_{ct} values corresponding to 10 fM NG DNA mixed with DNA from different bacterial species.

Author Contributions: B.D.M. and N.G.: Conceptualization; N.G.: Experimentation, Writing; D.K.: Review and Editing, Supervision; A.D.: Resource Acquisition, Project administration, Supervision; S.S.: Review and Editing, Resource Acquisition; B.D.M.: Review and Editing, Supervision. All authors have read and agreed to the published version of the manuscript.

Funding: This research received no external funding.

Institutional Review Board Statement: Not applicable.

Informed Consent Statement: Not applicable.

Data Availability Statement: Data is contained within the articles and the supplementary information.

Acknowledgments: N.G. acknowledges the Central Research Facility (CRF), IIT Delhi, India for SEM, FESEM and AFM image acquisition. The CRF, Department of Applied Chemistry, DTU, Delhi, India is acknowledged for rheology analysis.

Conflicts of Interest: The authors declare no conflict of interest.

References

1. World Health Organization (WHO). Sexually Transmitted Infections (STIs). Available online: https://www.who.int/health-topics/sexually-transmitted-infections#tab=tab_1 (accessed on 24 February 2023).
2. World Health Organization (WHO). *Global Health Sector Strategies on, Respectively, HIV, Viral Hepatitis, and Sexually Transmitted Infections for the Period 2022–2030*; World Health Organization: Geneva, Switzerland, 2022; p. 9240053778.
3. Chen, X.; Zhou, Q.; Wu, X.; Wang, S.; Liu, R.; Dong, S.; Yuan, W. Visual and rapid diagnosis of *Neisseria gonorrhoeae* using Loop-mediated isothermal amplification combined with a polymer nanoparticle-based biosensor in clinical application. *Front. Mol. Biosci.* **2021**, *8*, 702134. [[CrossRef](#)]
4. Whelan, J.; Eeuwijk, J.; Bunge, E.; Beck, E. Systematic literature review and quantitative analysis of health problems associated with sexually transmitted *Neisseria gonorrhoeae* infection. *Infect. Dis. Ther.* **2021**, *10*, 1887–1905. [[CrossRef](#)]
5. Berus, S.M.; Adamczyk-Popławska, M.; Młynarczyk-Bonikowska, B.; Witkowska, E.; Szymborski, T.; Waluk, J.; Kamińska, A. SERS-based sensor for the detection of sexually transmitted pathogens in the male swab specimens: A new approach for clinical diagnosis. *Biosens. Bioelectron.* **2021**, *189*, 113358. [[CrossRef](#)] [[PubMed](#)]
6. Chen, X.; Huang, L.; Zhou, Q.; Tan, Y.; Tan, X.; Dong, S. A nanoparticle-based biosensor combined with multiple cross displacement amplification for the rapid and visual diagnosis of *Neisseria gonorrhoeae* in clinical application. *Front. Microbiol.* **2021**, *12*, 747140. [[CrossRef](#)]
7. Ma, J.; Du, M.; Wang, C.; Xie, X.; Wang, H.; Li, T.; Chen, S.; Zhang, L.; Mao, S.; Zhou, X. Rapid and sensitive detection of *Mycobacterium tuberculosis* by an enhanced nanobiosensor. *ACS Sens.* **2021**, *6*, 3367–3376. [[CrossRef](#)]
8. Ali, M.; Bacchu, M.; Setu, M.; Akter, S.; Hasan, M.; Chowdhury, F.; Rahman, M.; Ahommed, M.; Khan, M. Development of an advanced DNA biosensor for pathogenic *Vibrio cholerae* detection in real sample. *Biosens. Bioelectron.* **2021**, *188*, 113338. [[CrossRef](#)] [[PubMed](#)]
9. Saadati, A.; Ehsani, M.; Hasanzadeh, M.; Seidi, F.; Shadjou, N. An innovative flexible and portable DNA based biodevice towards sensitive identification of *Haemophilus influenzae* bacterial genome: A new platform for the rapid and low cost recognition of pathogenic bacteria using point of care (POC) analysis. *Microchem. J.* **2021**, *169*, 106610. [[CrossRef](#)]
10. Yang, Y.; Liu, J.; Zhou, X. A CRISPR-based and post-amplification coupled SARS-CoV-2 detection with a portable evanescent wave biosensor. *Biosens. Bioelectron.* **2021**, *190*, 113418. [[CrossRef](#)]
11. Hwang, C.; Park, N.; Kim, E.S.; Kim, M.; Kim, S.D.; Park, S.; Kim, N.Y.; Kim, J.H. Ultra-fast and recyclable DNA biosensor for point-of-care detection of SARS-CoV-2 (COVID-19). *Biosens. Bioelectron.* **2021**, *185*, 113177. [[CrossRef](#)]
12. Khristunova, E.; Dorozhko, E.; Korotkova, E.; Kratochvil, B.; Vyskocil, V.; Barek, J. Label-free electrochemical biosensors for the determination of Flaviviruses: Dengue, Zika, and Japanese Encephalitis. *Sensors* **2020**, *20*, 4600. [[CrossRef](#)]
13. Bishoyi, A.; Alam, M.A.; Hasan, M.R.; Khanuja, M.; Pilloton, R.; Narang, J. Cyclic voltammetric-paper-based genosensor for detection of the target DNA of Zika virus. *Micromachines* **2022**, *13*, 2037. [[CrossRef](#)] [[PubMed](#)]
14. Verma, R.; Sood, S.; Singh, R.; Sumana, G.; Bala, M.; Sharma, V.K.; Samantaray, J.C.; Pandey, R.M.; Malhotra, B.D. Coupling electrochemical response of a DNA biosensor with PCR for *Neisseria gonorrhoeae* detection. *Diagn. Microbiol. Infect. Dis.* **2014**, *78*, 16–23. [[CrossRef](#)] [[PubMed](#)]
15. Wang, J.; Shi, A.; Fang, X.; Han, X.; Zhang, Y. Ultrasensitive electrochemical supersandwich DNA biosensor using a glassy carbon electrode modified with gold particle-decorated sheets of graphene oxide. *Microchim. Acta* **2014**, *181*, 935–940. [[CrossRef](#)]
16. Wang, L.; Shan, T.; Pu, L.; Zhang, J.; Hu, R.; Yang, Y.; Yang, J.; Zhao, Y. Glucometer-based electrochemical biosensor for determination of microRNA (let-7a) using magnetic-assisted extraction and supersandwich signal amplification. *Microchim. Acta* **2022**, *189*, 444. [[CrossRef](#)]
17. Xia, F.; White, R.J.; Zuo, X.; Patterson, A.; Xiao, Y.; Kang, D.; Gong, X.; Plaxco, K.W.; Heeger, A.J. An electrochemical supersandwich assay for sensitive and selective DNA detection in complex matrices. *J. Am. Chem. Soc.* **2010**, *132*, 14346–14348. [[CrossRef](#)] [[PubMed](#)]
18. Feng, Q.; Wang, M.; Qin, L.; Wang, P. Dual-signal readout of DNA methylation status based on the assembly of a supersandwich electrochemical biosensor without enzymatic reaction. *ACS Sens.* **2019**, *4*, 2615–2622. [[CrossRef](#)] [[PubMed](#)]
19. Li, J.; Jiang, J.; Su, Y.; Liang, Y.; Zhang, C. A novel cloth-based supersandwich electrochemical aptasensor for direct, sensitive detection of pathogens. *Anal. Chim. Acta* **2021**, *1188*, 339176. [[CrossRef](#)]
20. Liu, F.; Liu, H.; Liao, Y.; Wei, J.; Zhou, X.; Xing, D. Multiplex detection and genotyping of pathogenic bacteria on paper-based biosensor with a novel universal primer mediated asymmetric PCR. *Biosens. Bioelectron.* **2015**, *74*, 778–785. [[CrossRef](#)]
21. Colozza, N.; Caratelli, V.; Moscone, D.; Arduini, F. Origami paper-based electrochemical (bio) sensors: State of the art and perspective. *Biosensors* **2021**, *11*, 328. [[CrossRef](#)]
22. Nguyen, Q.H.; Kim, M.I. Nanomaterial-mediated paper-based biosensors for colorimetric pathogen detection. *Trends Anal. Chem.* **2020**, *132*, 116038. [[CrossRef](#)]
23. Solhi, E.; Hasanzadeh, M.; Babaie, P. Electrochemical paper-based analytical devices (ePADs) toward biosensing: Recent advances and challenges in bioanalysis. *Anal. Methods* **2020**, *12*, 1398–1414. [[CrossRef](#)]
24. Mohanraj, J.; Durgalakshmi, D.; Rakkesh, R.A.; Balakumar, S.; Rajendran, S.; Karimi-Maleh, H. Facile synthesis of paper based graphene electrodes for point of care devices: A double stranded DNA (dsDNA) biosensor. *J. Colloid Interface Sci.* **2020**, *566*, 463–472. [[CrossRef](#)]

25. Rana, A.; Killa, M.; Yadav, N.; Mishra, A.; Mathur, A.; Kumar, A.; Khanuja, M.; Narang, J.; Pilloton, R. Graphitic carbon nitride as an amplification platform on an electrochemical paper-based device for the detection of norovirus-specific DNA. *Sensors* **2020**, *20*, 2070. [CrossRef] [PubMed]
26. Lu, Q.; Su, T.; Shang, Z.; Jin, D.; Shu, Y.; Xu, Q.; Hu, X. Flexible paper-based Ni-MOF composite/AuNPs/CNTs film electrode for HIV DNA detection. *Biosens. Bioelectron.* **2021**, *184*, 113229. [CrossRef] [PubMed]
27. Camargo, J.R.; Orzari, L.O.; Araujo, D.A.G.; de Oliveira, P.R.; Kalinke, C.; Rocha, D.P.; dos Santos, A.L.; Takeuchi, R.M.; Munoz, R.A.A.; Bonacin, J.A. Development of conductive inks for electrochemical sensors and biosensors. *Microchem. J.* **2021**, *164*, 105998. [CrossRef]
28. de Araujo Andreotti, I.A.; Orzari, L.O.; Camargo, J.R.; Faria, R.C.; Marcolino-Junior, L.H.; Bergamini, M.F.; Gatti, A.; Janegitz, B.C. Disposable and flexible electrochemical sensor made by recyclable material and low cost conductive ink. *J. Electroanal. Chem.* **2019**, *840*, 109–116. [CrossRef]
29. Hong, H.; Jiyong, H.; Moon, K.-S.; Yan, X.; Wong, C.-P. Rheological properties and screen printability of UV curable conductive ink for flexible and washable E-textiles. *J. Mater. Sci. Technol.* **2021**, *67*, 145–155. [CrossRef]
30. Edali, M.; Esmail, M.N.; Vatistas, G.H. Rheological properties of high concentrations of carboxymethyl cellulose solutions. *J. Appl. Polym. Sci.* **2001**, *79*, 1787–1801. [CrossRef]
31. Pillai, A.S.; Chandran, A.; Peethambharan, S.K. MWCNT Ink with PEDOT:PSS as a multifunctional additive for energy efficient flexible heating applications. *Appl. Mater. Today* **2021**, *23*, 100987. [CrossRef]
32. Liu, L.; Shen, Z.; Zhang, X.; Ma, H. Highly conductive graphene/carbon black screen printing inks for flexible electronics. *J. Colloid Interface Sci.* **2021**, *582*, 12–21. [CrossRef]
33. Zheng, Y.; He, Z.; Gao, Y.; Liu, J. Direct desktop printed-circuits-on-paper flexible electronics. *Sci. Rep.* **2013**, *3*, 1786. [CrossRef]
34. He, P.; Cao, J.; Ding, H.; Liu, C.; Neilson, J.; Li, Z.; Kinloch, I.A.; Derby, B. Screen-printing of a highly conductive graphene ink for flexible printed electronics. *ACS Appl. Mater. Interfaces* **2019**, *11*, 32225–32234. [CrossRef] [PubMed]
35. Menon, H.; Aiswarya, R.; Surendran, K.P. Screen printable MWCNT inks for printed electronics. *RSC Adv.* **2017**, *7*, 44076–44081. [CrossRef]
36. Pekturk, H.Y.; Elitas, M.; Goktas, M.; Demir, B.; Birhanu, S. Evaluation of the effect of MWCNT amount and dispersion on bending fatigue properties of non-crimp CFRP composites. *Eng. Sci. Technol. Int. J.* **2022**, *34*, 101081. [CrossRef]
37. Kumar, S.; Gupta, N.; Malhotra, B.D. Ultrasensitive biosensing platform based on yttria doped zirconia-reduced graphene oxide nanocomposite for detection of salivary oral cancer biomarker. *Bioelectrochemistry* **2021**, *140*, 107799. [CrossRef] [PubMed]
38. Luo, H.; Chen, W.; Mai, Z.; Yang, J.; Lin, X.; Zeng, L.; Pan, Y.; Xie, Q.; Xu, Q.; Li, X. Development and application of Cas13a-based diagnostic assay for *Neisseria gonorrhoeae* detection and azithromycin resistance identification. *J. Antimicrob. Chemother.* **2022**, *77*, 656–664. [CrossRef]
39. GeneProof®. GeneProof *Neisseria gonorrhoeae* PCR Kit. Available online: <https://www.geneproof.com/geneproof-neisseria-gonorrhoeae-pcr-kit/p1069> (accessed on 4 October 2022).
40. Golparian, D.; Hellmark, B.; Unemo, M. Analytical specificity and sensitivity of the novel dual-target GeneProof *Neisseria gonorrhoeae* PCR kit for detection of *N. gonorrhoeae*. *Apmis* **2015**, *123*, 955–958. [CrossRef]
41. Goire, N.; Ohnishi, M.; Limnios, A.E.; Lahra, M.M.; Lambert, S.B.; Nimmo, G.R.; Nissen, M.D.; Sloots, T.P.; Whiley, D.M. Enhanced gonococcal antimicrobial surveillance in the era of ceftriaxone resistance: A real-time PCR assay for direct detection of the *Neisseria gonorrhoeae* H041 strain. *J. Antimicrob. Chemother.* **2012**, *67*, 902–905. [CrossRef]
42. Zhao, L.; Liu, A.; Li, R.; Zhao, S. Multiplex TaqMan real-time PCR platform for detection of *Neisseria gonorrhoeae* with decreased susceptibility to ceftriaxone. *Diagn. Microbiol. Infect. Dis.* **2019**, *93*, 299–304. [CrossRef]
43. Gupta, R.; Valappil, M.O.; Sakthivel, A.; Mathur, A.; Pundir, C.S.; Murugavel, K.; Narang, J.; Alwarappan, S. Tungsten disulfide quantum dots based disposable paper based lab on a chip for specific meningitis DNA detection. *J. Electrochem. Soc.* **2020**, *167*, 107501. [CrossRef]
44. Srisomwat, C.; Teengam, P.; Chuaypen, N.; Tangkijvanich, P.; Vilaivan, T.; Chailapakul, O. Pop-up paper electrochemical device for label-free hepatitis B virus DNA detection. *Sens. Actuators B Chem.* **2020**, *316*, 128077. [CrossRef]
45. Farshchi, F.; Saadati, A.; Hasanzadeh, M. Optimized DNA-based biosensor for monitoring *Leishmania infantum* in human plasma samples using biomacromolecular interaction: A novel platform for infectious disease diagnosis. *Anal. Methods* **2020**, *12*, 4759–4768. [CrossRef] [PubMed]

Disclaimer/Publisher's Note: The statements, opinions and data contained in all publications are solely those of the individual author(s) and contributor(s) and not of MDPI and/or the editor(s). MDPI and/or the editor(s) disclaim responsibility for any injury to people or property resulting from any ideas, methods, instructions or products referred to in the content.

NIHARIKA GUPTA

New Delhi, INDIA

niharika.gupta990@gmail.com

+91-8882104471



PROFILE SUMMARY

Submitted PhD thesis entitled “Nanomaterials modified conducting paper sensors for biomedical applications.” Hands on experience (>6 years) in synthesis, characterization, and functionalization of nanomaterials, conductive inks, biosensor development (immunosensors and DNA sensors), DNA assays, PCR development, etc.

(https://scholar.google.co.in/citations?user=uqPG7_oAAAAJ&hl=en).

Experienced in academic writing and content editing including grammar correction, structural changes, and proofreading.

CAREER OBJECTIVE

To work in a reputed institution that provides an excellent research environment and drives my passion towards the development of:

- (i) Cost-effective, reliable biosensing devices that can be applied at the PoC for detection of clinically relevant analytes.
- (ii) Sustainable and all-printed biosensing substrates.

EDUCATION

Certificate/Degree Awarded	Board/Institute	Duration	Marks Obtained (GPA/%)
Ph.D. (Biotechnology)	Delhi Technological University, Delhi (India)	2017-2023	Result awaited
M. Tech. (Biomedical Engineering)	Delhi Technological University, Delhi (India)	2014-16	8.7
B.Tech. (Biotechnology)	Banasthali University, Rajasthan (India)	2009-13	73%
Certificate in European Language (German)	Banasthali University, Rajasthan (India)	2010-11	72%
Senior Secondary (XII)	CBSE, India	2007-08	79.4%

Secondary School (X)	Central Board of Secondary Education (CBSE), India	2005-06	88%
----------------------	--	---------	-----

LIST OF PUBLICATIONS

- **Niharika Gupta**, D. Kumar, Asmita Das, Seema Sood, and Banshi D. Malhotra. “Conductive ink-coated paper-based supersandwich DNA biosensor for ultrasensitive detection of *Neisseria gonorrhoeae*.” *Biosensors* 13(2023), 486. (IF-5.4)
- Simran Kaur, **Niharika Gupta**, and Banshi D. Malhotra. “Recent developments in wearable & non-wearable point-of-care biosensors for cortisol detection.” *Expert Review of Molecular Diagnostics* 23(2023), 217-230. (IF-5.67; Citations - 1)
- **Niharika Gupta**, D. Kumar, Asmita Das, Seema Sood, and Banshi D. Malhotra. “Carbon nanotubes modified conductive ink for application to paper-based electrochemical biosensors for pathogenic DNA detection.” *New Journal of Chemistry* 47(2023), 10930-10941. (IF-3.9)
- **Niharika Gupta***, Keshav Todi*, Tarun Narayan, and Banshi D. Malhotra. “Graphitic carbon nitride-based nanoplatfoms for biosensors: Design strategies and applications.” *Materials Today Chemistry* 24(2022), 100770. (IF-7.6; Citations - 29) *Equal authors
- **Niharika Gupta**, Shine Augustine, Tarun Narayan, Alan O’Riordan, Asmita Das, D. Kumar, John H.T. Luong, and Banshi D. Malhotra. “Point-of-care PCR assays for COVID-19 detection.” *Biosensors* 11(2021), 141. (IF-5.4; Citations - 86)
- Suveen Kumar*, **Niharika Gupta***, and Banshi D. Malhotra. “Ultrasensitive biosensing platform based on yttria doped zirconia-reduced graphene oxide nanocomposite for detection of salivary oral cancer biomarker.” *Bioelectrochemistry* 140 (2021), 107799. (IF-5.76; Citations - 21) *Equal authors
- **Niharika Gupta**, Venkatesan Renugopalakrishnan, Dorian Liepmann, Ramasamy Paulmurugan, and Banshi D. Malhotra. “Cell-based biosensors: Recent trends, challenges and future perspectives.” *Biosensors and Bioelectronics* 141 (2019), 111435. (IF-12.54; Citations - 210)
- Sushil K. Tripathi, **Niharika Gupta**, Manohar Mahato, Kailash C. Gupta, and Pradeep Kumar. “Selective blocking of primary amines in branched polyethylenimine with biocompatible ligand alleviates cytotoxicity and augments gene delivery efficacy in mammalian cells.” *Colloids and Surfaces B: Biointerfaces* 115(2014), 79-85. (IF-5.26; Citations - 35)

RESEARCH AND ACADEMIC EXPERIENCE

- **2022-till date:** Guest Faculty
Department of Biotechnology, Delhi Technological University, New Delhi, India
- ✓ Took up teaching of the subjects Immunotherapeutics and Molecular Virology (M.Sc. III Sem, 2022-23 session) and Instrumentation in Biotechnology (B. Tech. V and VII Sem, 2023-24 session).

- **2019-21:** Teaching Assistant
Department of Biotechnology, Delhi Technological University, New Delhi, India
 - ✓ Supervised teaching lab experiments (B. Tech. III and V Sem, and M. Sc. II Sem) for the subjects Molecular Biology, Immunology, and Analytical Instrumentation.
- **August 2017–July 2023: PhD Research Scholar**
Department of Biotechnology, Delhi Technological University, New Delhi, India
 - ✓ **Developed nanomaterial-based printable, conductive inks (and other strategies) for paper modification, and their subsequent application in electrochemical DNA biosensors (detection of *Neisseria gonorrhoeae*).**
 - ✓ **Developed magnetic bead-based DNA assays (sandwich and supersandwich) for integration with conductive paper-based electrodes.**
 - ✓ **Work responsibilities also included general lab management and monitoring of student project work (Bachelor/Master thesis).**
- **November 2016–July 2017: Junior Research Fellow (JRF)**
Department of Microbiology, All India Institute of Medical Sciences (AIIMS), New Delhi, India
 - ✓ DBT (Govt. of India)-sponsored project entitled “Nanoenabled biosensor for detection of *Neisseria gonorrhoeae*.”
 - ✓ Responsibilities included optimization and validation of conventional duplex PCR against *porA* pseudogene and *opa* gene of *N. gonorrhoeae*. (This PCR is currently in use at AIIMS New Delhi for patient sample analysis.)

RESEARCH SKILLS

Hands-on experience on the following:

- **Instrumentation:** Electrochemical analyzer (potentiostat/galvanostat), PCR thermocycler, UV-Vis/NIR spectrophotometer, 4-probe conductivity meter, Nanodrop spectrophotometer, and other common lab equipment (probe ultrasonicators, muffle furnace, laminar flow hood, magnetic stirrers, etc.).
- **Techniques: synthesis** of inorganic (Au NPs, Cu NPs, Ag nanostructures, etc.), organic (PANI, etc.), and organic-inorganic hybrid nanomaterials (Au-PANI, etc.) (hydrothermal, *in situ* synthesis on substrates, other chemical methods), **functionalization with chemical groups** (APTES modification, capping by functional groups, hydrophobization of paper, etc.), **formulation of conductive, printable inks, DNA assays, PCR** (conventional), magnetic bead-based assays, **electroanalytical techniques** (Cyclic voltammetry, electrochemical impedance spectroscopy, differential pulse voltammetry, etc.).
- **Data analysis/interpretation and software:** XRD, FT-IR, Raman spectrometry, AFM, SEM & TEM, rheological analysis, Origin data analysis software, NOVA for electrochemical data analysis.

RESEARCH PROJECTS & INTERNSHIPS

- **April 2015–June 2016** – Completed Master’s thesis work entitled “Development of biofunctionalized nanocomposite-based biosensor for oral cancer detection” under the guidance of Prof. Bansi D. Malhotra, Nanobioelectronics Lab, Delhi Technological University, New Delhi, India. (**This work was published in the journal *Bioelectrochemistry* in 2021**).
- **July–December 2012** – Completed Bachelor thesis work entitled “Chemical Vectors for Gene Delivery” under the guidance of Dr. Pradeep Kumar, Scientist, NAR Lab, CSIR- Institute of Genomics and Integrative Biology (CSIR-IGIB), Delhi, India. (**This work was published in the journal *Colloids and Surfaces B: Biointerfaces* in 2014**)

OTHER WORK EXPERIENCE

- **2019:** Worked as a Market Research Executive (secondary data and content editing) for Goldstein Research Intelligence Pvt. Ltd. (Noida, UP, India) on freelance basis.
- **August–October 2016:** Copyeditor
Aptara Corp., Noida (UP), India
 - ✓ Responsibilities included copyediting of book chapters (Pearson) and grammar correction (if any).
- **October 2013–March 2014:** Associate-Indexing & Abstracting
IDS Infotech Ltd., Noida (UP), India
 - ✓ Responsibilities included abstracting and indexing of journal and scientific articles enlisted in the EBSCO database.

AWARDS AND ACHIEVEMENTS

- Awarded “Commendable Research Award” and a cash prize of Rs. 50,000/- (distributed equally among all authors) for publication in SCI/SCIE-indexed journals (IF > 5) (2020, 2022, 2023).
- Qualified the **Graduate Aptitude Test in Engineering (GATE-Biotech)** in 2016 with a score of 562 (All India Rank-223).
- Named the overall best performance winner (Biotechnology) at the annual interuniversity technical fest “Mayukh” held at Banasthali University, Rajasthan (2011-12).
- Won many awards for speech, debates and poetry recitation in English, Hindi, and Sanskrit throughout secondary and higher secondary schooling (inter-school and inter-zonal level).

SOFT SKILLS

- Excellent communication and presentation skills.
- Excellent written communication skills.
- Good time management and multi-tasking skills.
- Languages:
 - ✓ English (Proficient)
 - ✓ Hindi (Proficient)

✓ German (Basic)

PERSONAL INFORMATION

Date of Birth: 28 September 1990

Marital Status: Unmarried

Gender: Female

Nationality: Indian

I hereby declare that all the above particulars are true and correct to the best of my knowledge.

PLACE: New Delhi

Niharika Gupta